THE SELECTION OF OPERATING CONDITIONS AND THE DESIGN OF TOOLING FOR ELECTROCHEMICAL MACHINING

A Thesis submitted in partial fulfilment for the Degree of

Doctor of Philosophy

of the University of Strathclyde

Department of Production Engineering

by

W. GORDON CLARK, B.Sc.

July, 1974

PAGE NUMBERING AS ORIGINAL

ABSTRACT

Electrochemical machining has found numerous applications in recent years. The process offers significant economic advantages over conventional machining methods where complex shapes are required in high performance metals. However, a general lack of information on the design of a machining operation has resulted in an unacceptable amount of trial and error development work in many instances.

This thesis is concerned with the selection of operating conditions and the design of tooling for electrochemical machining. An introduction to this aspect of the process is followed by a review of current literature on the subject. A model is adopted for the prediction of the one-dimensional equilibrium gap. The model utilises two parameters which require experimental determination. The model also predicts an upper bound to the electrolyte velocity in the electrode gap which corresponds to a limiting value of the tool feedrate. Various other apparent limitations on the metal removal rate are discussed.

Preliminary experimental work was carried out to test the applicability of the theoretical model with particular reference to the pressure drop across the electrode gap. The results verify the model but the model parameters show dependence on the operating conditions of machining.

The experimental work was extended, using a production electrochemical machine, to cover operating conditions used in practice. Sodium chloride and sodium nitrate solutions were the electrolytes in the machining tests. The anode workpieces were manufactured from mild steel and were initially plane and parallel to the cathode. The

machining characteristics of the two electrolytes with mild steel are discussed. Anode profiles are presented at various operating conditions with the model parameters required to match the experimental test data. Phenomena other than the electrolyte conductivity appear to influence the anode profile in tests with sodium nitrate electrolyte.

The theoretical model is not verified with respect to the upper bound to the electrolyte velocity. Tool feedrates and electrolyte flow velocities are used which exceed those predicted theoretically. The upper bound to the electrolyte velocity is the performance limit of the electrolyte pump.

A separate investigation was required to determine the cause of machining failure. Miniature bead thermistors were inserted through the cathode into the electrode gap to measure the temperature of the electrolyte close to the cathode. Temperatures in this region are found to be greater than those measured at outlet. Machining failure is shown to be the result of boiling of the electrolyte around the gas bubbles evolved at the cathode. The conductivity of the electrolyte becomes less due to the formation of steam bubbles and the anode converges towards outlet so that sparking or arcing occurs across the gap.

A correlation is introduced to allow prediction of this condition. The operating characteristics of electrochemical machining are discussed in relation to the correlation and other limitations. An optimum outlet pressure exists which allows an increase in feedrate particularly at low machining voltages. A procedure for the selection of operating conditions is proposed.

CONTENTS

NOMENCLATURE

SYMBOL	QUANTITY	UNITS
A	Density function $(\rho_o \lambda_g / \sigma \varepsilon \lambda_a \rho_g)$	None
B	Temperature constant $(\gamma V / c_f \varepsilon \lambda_a)$	None
C	State constant $(2 \lambda_g R_g T_o / \sigma \varepsilon \lambda_a V_o^2)$	None
c	Specific heat	$kJ\ kg^{-1} K^{-1}$
E	Applied Voltage	volts
E_{pol}	Polarisation potential	volts
E_{rev}	Reversible potential	volts
$f(\frac{\gamma}{g}\alpha)$	Heterogeneous conduction function	None
f	Friction factor $\left(\frac{8\tau}{\rho_f V_f^2}\right)$	None
k	Electrolyte conductivity	$ohm^{-1}\ cm^{-1}$
K_c	Inlet loss coefficient $(f_o L / y_o)$	None
L	Length of machining gap	m
M	Frictional multiplier (f/f_o)	None
M_a	Mach number	None
$\dot{m}$	Mass flux	$kg\ s^{-1}\ m^{-2}$
n	Void function exponent	None
p	Static pressure	$kN\ m^{-2}$
Q	Volume flowrate	$m^3\ s^{-1}$
R	Electrical resistancexarea	$ohm\ cm^2$
Re_o	Reynolds number $(2 y_o V_o / \nu_o)$	None
R_g	Gas constant	$m\ K^{-1}$
r	Electrical resistivity	ohm cm

T	Temperature	K
T_r	Reference temperature $(V/c_f \varepsilon \lambda a)$	K
t	Time	s
V	Velocity	m s^{-1}
V	Voltage	volts
V_c	Feedrate	mm min^{-1}
x	Position variable	m
y	Electrode gap width	mm
α	Void fraction	None
γ	Conductivity coefficient	K^{-1}
δ	Bubble layer thickness	m
ε	Current efficiency	None
ϱ	Constant $(\rho_o y_o V_o / \rho_a L V_c)$	None
η	Constant $(1 - \lambda_g/\lambda_a)$	None
λ	Electrochemical equivalent	g F^{-1}
ν	Kinematic viscosity	m^2 s^{-1}
ρ	Density	kg m^{-3}
σ	Gas slip ratio (V_g/V_f)	None
τ	Shear stress	N m^{-2}
ϕ	Current density	A cm^{-2}

Subscripts

a	Anode
b	Boiling
c	Cathode

e	Exit
f	Electrolyte
g	Gas
l	Bubble-electrolyte layer
o	Inlet

Superscripts

o	Dimensionless variable
*	Intrinsic variable

1.0 INTRODUCTION

1.1 General

The development of electrochemical machining is a result of the need for a method of machining high strength metals which are difficult and expensive to machine conventionally. The process is capable of machining complex forms at high metal removal rates in a single tool pass. The machined surface is such that finishing processes may not be required.

Electrochemical machining has been used with particular success in the production of turbine blades and drop forge dies and has been applied in various metal removal modes such as drilling, turning, broaching and trepanning.

However a limited amount of information is available on the selection of operating conditions and the design of tooling. For this reason the advantages of the process are not fully realised in many applications and extensive development work and high costs are associated with the introduction of the process to new manufacturing areas.

1.2 Principles of Electrochemical Machining

Electrochemical machining is based on the process of electrolysis. In principle the application of a potential difference across metal electrodes immersed in an electrolyte causes negative ions to move towards the anode and positive ions to move towards the cathode.

The anode dissolves in the form of ions and electrons go into the external circuit, e.g. for an iron anode:

$$Fe \rightarrow Fe^{++} + 2e$$

At the cathode water molecules receive electrons from the external circuit resulting in the release of hydrogen gas:

$$2\,H_2O + 2e \rightarrow H_2 + 2O\,H^-$$

The metal ions combine with the hydroxyl ions to form a precipitate. Other reactions may occur (1) depending on the metal, the type of electrolyte and the potential across the cell.

From Faraday's laws of electrolysis, the weight of metallic element removed from the anode is proportional to the current, the time and the chemical equivalent weight of the anode metal:

$$m = \frac{A\,It}{z\,F} \qquad (1)$$

where m is the mass of metal removed,

A is the atomic weight of the metal,

I is the current,

t is the time,

z is the metal valency,

and F is Faraday's constant.

For alloy metals the reciprocal of the average of the reciprocals of A/z of the constituent metals is used. The equation shows the inherent advantage of electrochemical machining over conventional machining methods in that metal removal rate is independent of the mechanical properties of the metal.

To achieve metal removal rates acceptable in a production process, current densities of from 50 to 300 A cm^{-2} are required. A potential difference of 10-25 V is applied across the anode and cathode. The electrolyte is pumped through a small gap between the electrodes to remove the products of electrolysis.

The cathode (tool) is fed towards the anode (workpiece) to compensate for dissolution and form the tool shape on the workpiece such that complex shapes can be formed by a linear movement. The smaller the gap between the electrodes the greater is the current density and, hence, metal removal rate. Thus at a constant feedrate the process becomes self-regulating and the dissolution rate equals the tool feedrate. The gap becomes constant under these conditions and is known as the equilibrium gap.

As the current flows between the electrodes various phenomena oppose the current such as the difference in electrode potentials and the activation and concentration over voltages at both electrode surfaces. Under normal conditions, the voltage drop at the electrodes is small. The main voltage loss occurs in the electrolyte and is described by Ohm's law. Thus the operating conditions of machining, which control the gap width between the electrodes, are the voltage, the current density, which is proportional to feedrate, and the electrolyte resistance.

The operating conditions are governed by certain limitations on the process and are critical in relation to the economics of the process and to the accuracy and surface integrity of the work.

In addition, the large capital investment required for electrochemical machining plant makes necessary an accurate assessment of future costs and production rates which are, to some extent, determined by the operating conditions of machining.

1.3 The Selection of Operating Conditions

For known work material and dimensions the operating conditions of electrochemical machining are the tool feedrate, the applied potential or voltage, the electrolyte flowrate and the inlet and outlet pressure of flow in the tooling fixture. The electrolyte type, concentration and temperature should also be specified.

The choice of operating conditions is related to their effect on the equilibrium gap between the electrodes which is determined from:

$$y_e = \frac{V\,k\,C}{V_c} \qquad (2)$$

where y_e is the equilibrium gap,

V is the machining voltage,

k is the electrolyte conductivity,

V_c is the tool feedrate,

and C is a constant relating to the workpiece material.

It is convenient to discuss each of the conditions controlling the gap width.

(a) Tool Feedrate

Electrochemical machining becomes economic, relative to

conventional machining methods, when the workpiece or component is required in sufficient quantities such that considerable investment in large plant is justified. The absence of tool wear also makes the process attractive to large batch and mass production. To reduce the resultant high machine time cost on each component the tool feedrate, which is proportional to current density, should be as rapid as possible within the limitations of available power supplies.

(b) Machining Voltage

A small part of the machining voltage is required for the electrode reactions and the remainder is dissipated as heat in the electrolyte. Thus low machining voltages reduce the power loss during machining. In addition the degree of damage to the tool if sparking occurs is increased at high voltages.

(c) Electrolyte Conductivity

The most economic means of increasing the electrode gap width is to use an electrolyte with high conductivity. The conductivity is determined by the type, concentration and temperature of the electrolyte. The type of electrolyte is important in relation to the dimensional control and surface integrity of the work; this has resulted in a considerable amount of research (2, 3, 4, 5) into this aspect of electrochemical machining.

Acid electrolytes are attractive due to their high conductivities but are not often used in production machines due to their corrosive activity. In industrial practice solutions of sodium chloride and sodium nitrate, or mixtures of both, are normally employed. The addition of other salts to these electrolytes is required, in some cases, to remove oxide films from the workpiece. The concentration of the electrolytes ranges from 50 to 400 g/litre and temperatures are normally between 30 and 40^{o}C; higher electrolyte temperatures increase the conductivity but cause excessive evaporation losses from the working tank and the concentration has to be continually corrected if repeatable machining accuracy is required. This factor, in conjunction with the saturation concentration of the salt, places an upper limit on the electrolyte conductivity.

From consideration of the tool feedrate, the machining voltage and the electrolyte conductivity in relation to equation (2), small electrode gaps are a result of economic use of the process. However, other factors influence the choice of gap size. A small equilibrium gap reduces the size of machining inaccuracies due to process fluctuations and allows improved tool reproduction on the workpiece (9). In addition, Wilson (6) has shown that an allowance should be left on the workpiece prior to machining. The allowance depends on the gap width, the tool shape and the tolerance on the workpiece and is normally a few gap widths. As casting and forming techniques become more accurate, electrochemical machining may be required to remove a relatively small allowance on the workpiece and consequently a small

gap is necessary.

The operating condition which restricts the use of small equilibrium gaps is the electrolyte flowrate. If the flowrate is not sufficient machining failure or sparking will occur which can cause damage to the tool. Machining failure can also result in inaccuracies in the finished work (10). High delivery pressures are required to force sufficient electrolyte flow through small electrode gaps. These pressures, which are limited by the capacity of suitable pumps, can cause deflection of the tool fixture and ram and consequent loss of accuracy in the work.

One of the main advantages of electrochemical machining is the high metal removal rates obtainable in hard and tough metals. Providing the electrolyte flowrate is adequate, no upper limit to the metal removal rate is apparent. However, no satisfactory method of prediction of the minimum flowrate required for given operating conditions has been developed.

An objective of the present work is to examine the causes of machining failure or sparking and establish a basis for the optimum selection of operating conditions.

1.4 Tool Design

The operating conditions of machining should be determined prior to the design of the cathode or tool. The degree of control of these conditions is the main factor affecting the repeatable accuracy of the work. However, the accuracy within specific tolerances is dependent

on the design of the cathode or tool.

Tool design has been described (6) as the key to electro-chemical machining and consists of:

(a) design of fixtures for workpiece and tool location and alignment, the situation of power connections and the use of suitable materials. The position of electrolyte entry and exit slots in complex tools requires careful consideration and experimental work may be required. Wilson (6) has developed guidelines in this respect although experience in the use of the process is an advantage.

(b) determination of the shape and size of the tool to give the required component dimensions.

As the tool is fed towards the workpiece the shape of the workpiece becomes approximately complementary to the shape of the tool; the two surfaces differ by the thickness of the gap. For accurate reproduction the tool shape must allow for the gap width.

In generating or two dimensional machining operations, the difference between the tool size and the hole or shaft size is termed the overcut. Various investigators (9, 11, 12, 13) have developed empirical and theoretical equations, in terms of the forward gap, for calculating the overcut. The exact overcut required may be obtained in machine trials by small adjustment of the machining voltage or the electrolyte conductivity.

In die sinking operations (the machining of three dimensional shapes) the gap width varies with the angle which the tool face makes

with the feed direction. A 'cos θ' method has been developed (7) in relation to this but does not apply to regions of the gap with inclination to the feed direction approaching 90^{o} or with appreciable curvature. In this instance the current distribution can be described by Laplace's equation and an analogue or mathematical solution is required to allow prediction of the gap width. Tipton (11) has developed computer programs for the solution of Laplace's equation, to allow calculation of the tool shape required for a given work shape and vice versa. The programs can be extended to deal with two dimensional surfaces.

The methods for the prediction of overcut and tool shape assume a constant electrolyte conductivity within the electrode gap although the programs developed by Tipton (11) can be readily modified to incorporate empirical corrections for conductivity variations. However, the voltage drop across the electrodes causes resistance heating of the electrolyte which increases the conductivity of the electrolyte. Gas bubbles evolved at the electrodes reduce the conductivity. The combined effect of these factors result in deviations, between the tool and work form, which are influenced by the machining voltage, current density, electrolyte flowrate and the inlet and outlet pressure from the tooling. The flowrate and pressure at a point within the gap cannot be assessed without difficulty even for simple shaped tools. As a result the approach to tool design at present is to make the tool shape close to that required and modify it by trial and error until accurate work is obtained. The cost of development work of this nature and the risk and delay involved have prevented

the use of electrochemical machining in many potentially economic applications. The initial tooling cost is high so that the process is not competitive for other than mass or large batch production and where alternative methods are very expensive.

One of the purposes of this work is to develop a simple method of prediction of the gap width variation due to conductivity effects. In conjunction with the existing methods of tool shape calculation this will reduce or eliminate the need for trial and error tool development.

1.5 Scope of Work

The prediction of the equilibrium electrode gap in electrochemical machining, in relation to non-uniform electrolyte conductivity, was investigated initially by Tipton (7). To reduce the complexity of the problem the effect of temperature dependent electrolyte conductivity was considered. However, Thorpe (14) carried out an order of magnitude analysis which showed that the effects of gas bubbles and ohmic resistance heating are of the same order of magnitude. Hopenfield and Cole (15) derived a system of coupled, non-linear, differential equations which describe the equilibrium gap. The one dimensional equations of mass, continuity of momentum, energy and charge, subject to certain assumptions and simplifications, were solved simultaneously by a numerical method suitable for a digital computer. The predicted electrode gaps show reasonable qualitative agreement with corresponding experimental data. Thorpe and

Zerkle (16) used a similar approach to that of Hopenfield and Cole. The describing system of equations was solved to obtain algebraic expressions for the gap width variation and the distribution of gas bubbles, electrolyte temperature, velocity and pressure within the gap. The analysis was further developed (17) for radial flow with axially symmetric, curved electrodes. The value of the approach taken by Thorpe and Zerkle is that the algebraic expressions allow quantitative determination of the main features of the process which serve as convenient rules for the tool and production engineers concerned with electrochemical machining. The analysis is also more general than that formulated by Hopenfield and Cole (15) in that it includes the possibility of non-homogeneous flow and incorporates a generalised heterogeneous conduction relation.

1.5.1 The Theoretical Model

The derivation of the equations developed by Thorpe and Zerkle (16) is presented in Appendix 1. The equations are:

$$\alpha = \frac{Ax^*}{1 + A\ x^*} \tag{45}$$

$$y^o = \frac{y}{y_o} = \frac{1 + Bx^*}{(1 + Ax^*)^n} \tag{46}$$

$$V_f^o = \frac{V_f}{V_o} = \frac{(1 + Ax^*)^{n+1}}{1 + Bx^*} \tag{47}$$

$$T^o = \frac{T}{T_o} = 1 + T_r{}^o\ x^* \tag{48}$$

$$p^{o} = \frac{p}{\rho_o V_o^2/2} = \frac{C\,T^{o}}{A} \tag{49}$$

$$\frac{dp^{o}}{dx^{*}} = -\frac{2}{y^{o}} \left[\frac{dV_f^{o}}{dx^{*}} + \beta \frac{M k_o}{4} V_f^{o\,2} \right] \tag{50}$$

The quantities in the equations are in non-dimensional form.

The dependent variables are the pressure p^{o}, the temperature T^{o}, the gap thickness y^{o}, the void fraction of gas bubbles, α, the electrolyte velocity V^{o} and the gas density function A; x^{*} is a position variable along the electrode gap. Thorpe and Zerkle considered the gas density function to be constant at low pressure drops and obtained good agreement with the experimental results of Hopenfield and Cole. This experimental work was carried out with short electrodes at pressure drops an order of magnitude smaller than those in industrial practice and for a limited number of tests. At high pressure drops across the electrode gap the gas density varies appreciably and the equations (45) to (50) must be solved simultaneously. In this instance a numerical solution to the equations, suitable for a digital computer, is required. Thorpe and Zerkle have stated (16) that a computer program has been developed for this purpose. The author is very grateful to Thorpe and Zerkle for the use of this computer program. The program is listed, with input instructions, in Appendix II.

The model parameters, to be determined experimentally, are the frictional multiplier, M, and the void function exponent, n. In equation (50) the two components of pressure drop are the acceleration of the electrolyte and the frictional pressure loss. Thorpe and Zerkle

use the concept of the two phase frictional multiplier, M, to account for increase in shear stress at the surfaces of the electrodes due to the evolution of gas bubbles at the cathode and the dissolution of the anode. Frictional multipliers are commonly employed in the analysis of two phase flow systems (19). Martinelli and Nelson (20) have developed an empirical method of determining the frictional multiplier in steam-water flow. However, no theoretical prediction of friction factor in flow with bubble nucleation has been developed.

The void function exponent, n, is a generalisation of possible heterogeneous conduction mechanisms to account for the effect of hydrogen gas bubbles on the electrolyte conductivity. For a random dispersion of non-conducting spheres in a conducting medium Bruggeman (21) derived the relation

$$r = r_o \ (1 - \alpha)^{-1.5}$$

where r is the resistivity of the mixture,

r_o is the resistivity of the conducting medium

and α is the volume fraction of spheres.

De la Rue and Tobias (21) have shown experimentally that up to a void fraction of 40% this relation adequately describes the resistivity variation due to the uniform dispersion of non-conducting particles in an electrolyte. However, optical studies of gas evolution in electrochemical machining have shown (22) that the bubbles are concentrated in a layer close to the cathode surface. In addition the void function exponent takes into account the assumptions of no

relative motion between bubbles and electrolyte and that the gas bubble layer, δ, is equal to the gap width. Thus the void function exponent may only be determined experimentally.

Values are required for the frictional multiplier, M, and the void function exponent, n, under conditions similar to those in electrochemical machining in industry, to allow prediction of the pressure requirements and gap width variation for a machining operation.

1.5.2 Feedrate Limitation due to Flow Choking

The equations derived by Thorpe and Zerkle (16,17,18) were also developed to allow determination of limits on the process. This provides a basis for the selection of operating conditions.

The equation for the pressure gradient becomes (Appendix I):-

$$\frac{dp^o}{dx^*} = \frac{-2\,(1+Ax^*)^{2n}}{(1+Bx^*)^2}\left[(n+1)\left(A + \frac{C\,Tr^o}{p^o}x^*\right) - \frac{B(1+Ax^*)}{1+Bx^*} + \frac{\delta M k_o}{4}\,\frac{(1+Ax^*)^{n+2}}{1+Bx^*}\right] + \left[1 - 2(n+1)\,\frac{(1+Ax^*)^{2n}}{(1+Bx^*)^2}\,(1+Tr^o x^*)\,\frac{C}{p^{o2}}\,x^*\right] \qquad (59)$$

This equation is a form of that derived by Wallis (19) due to the assumption of two phase homogeneous flow. The equation has a singularity i.e. machining conditions may be such that the

denominator becomes zero:

$$2(n+1)\ \frac{(1 + Ax^*)^{2n}}{(1 + Bx^*)^2}\ (1 + T_r{}^o\, x^*)\ \frac{C}{p^o 2}\ x^* = 1 \qquad (60)$$

Thorpe and Zerkle consider that this corresponds to a choking condition similar to that occurring in compressible flow through convergent nozzles. The situation cannot be tolerated if machining failure and sparking across the gap is to be avoided. If the tool feedrate is maintained then the flowrate must be reduced. The highest temperature and the lowest pressure will occur at outlet from the electrode gap so that choking will occur in the exit plane. Inspection of equation (60) shows that choking and machining failure, will occur at high tool feedrates and small electrode gaps and that an upper limit of electrolyte inlet flow velocity exists for given machining conditions. Machining breakdown has been observed (23) due to an increase in electrolyte flowrate. Thus the proposed choking condition represents a severe limitation on the metal removal rate in electrochemical machining.

1.5.3 Alternative Failure Modes in Electrochemical Machining

Thorpe and Zerkle develop theoretically an upper bound to the electrolyte velocity in the electrode gap. However, various other limitations on the process affecting the selection of operating conditions may be discussed.

In an early assessment of the factors affecting the choice of operating conditions, Tipton (7) suggests that the lower bound to the electrolyte flow velocity in a machining operation is that where boiling

of the electrolyte occurs within the gap at outlet. For typical conditions of machining the choking and boiling bounds, derived from equations (60) and (48) respectively, to the electrolyte velocity are shown in Fig. 1.1. Acceptable values of the tool feedrate lie to the left of each curve. Feedrates greater than about 3 mm. min^{-1} may not be used if both limitations are valid. However Baldwin (24) found that, at the minimum flowrate required for equilibrium machining, the temperature increase was less than 30 K under all test conditions. This condition would further restrict the feedrates obtainable for the conditions in Fig. 1.1.

Cavitation may occur in the flow between the electrodes and produce a poor surface finish on the workpiece (25). Cavitation is the vapourisation of a liquid due to decrease in pressure whereas boiling is the vapourisation of a liquid due to heat addition. Cavitation ensues if the velocity head of electrolyte flow increases to a point where the static pressure of flow falls below the vapourisation pressure of the electrolyte at that temperature in the electrode gap. This is most likely to arise at a point in the gap where an abrupt change in flow direction occurs such as at inlet to the gap or in a complex three-dimensional tool. Cavitation in electrochemical machining has been investigated by Kawa fune (25), Chikamori (26) and Ito (27). It was found that cavitation close to the inlet in forward flow drilling could be prevented by reducing the flowrate or by application of a sufficiently high outlet pressure. The outlet pressure required for a rounded inlet was lower than that for a sharp inlet particularly where the inlet diameter of the drill approached the

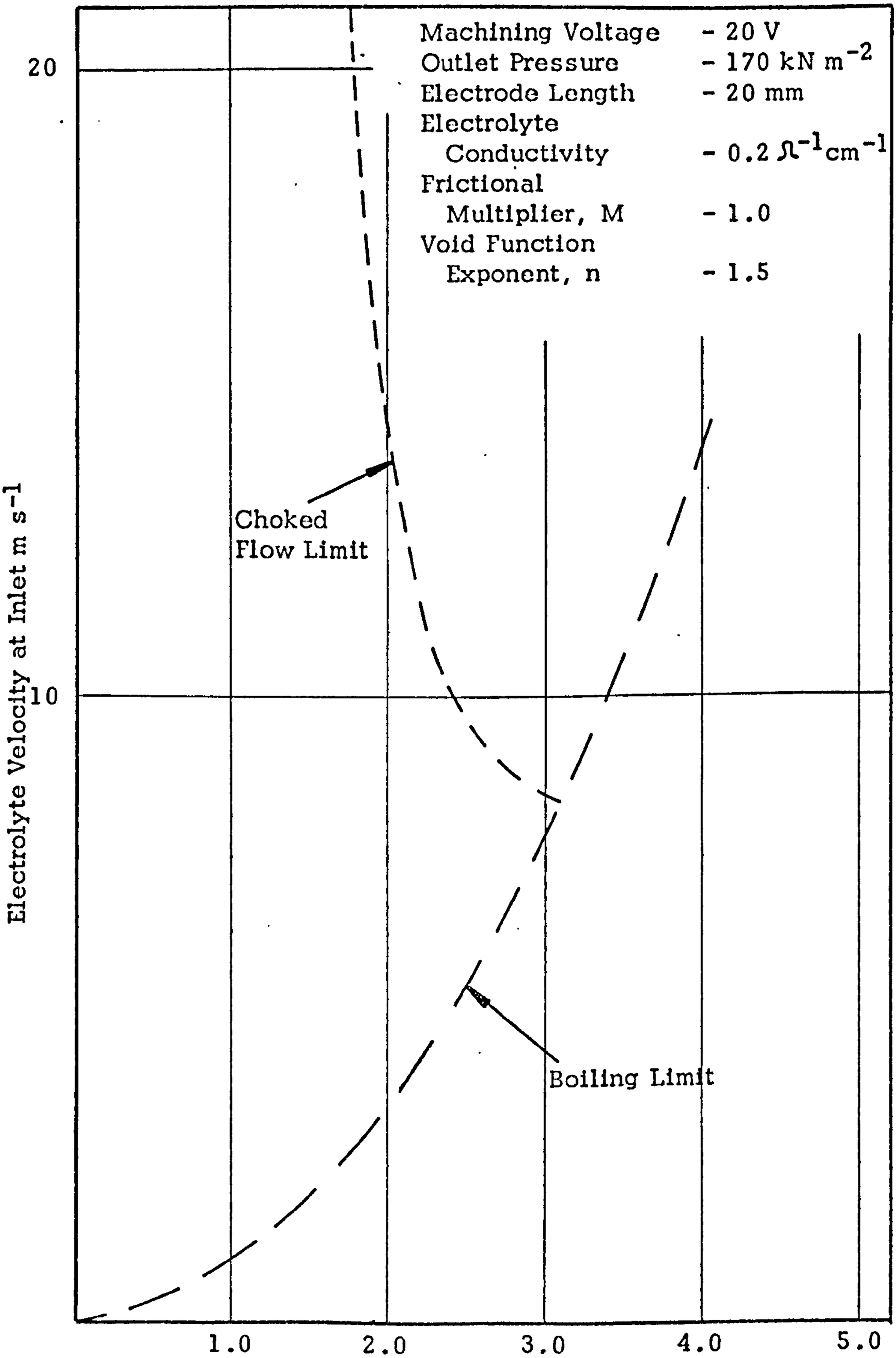

FIG. 1.1 CHOKED FLOW AND BOILING LIMITS TO THE TOOL FEEDRATE

outlet diameter. Cavitation was not observed in reverse flow drilling. Wilson (6) has outlined some methods for the prevention of cavitation in three dimensional tooling such as smoothly blended electrolyte supply ducts and the use of flow restrictors.

In an investigation of the current voltage characteristics of electrochemical machining, Baxter (28) found a maximum current density, or metal removal rate, for each set of test conditions. From measurements of the potential distribution across the electrode gap, the maximum current density was found to be to a crisis of cathodic hydrogen evolution. The current density distribution over the electrodes was uniform under equilibrium conditions; as the maximum current density was approached, the current density towards outlet became less. From consideration of the experimental relationship between bubble diameter and pressure, the maximum current density was attributed to a limitation on the velocity of hydrogen bubble departure from the cathode surface.

The mechanism proposed by Baxter (28) and the theoretical choked flow condition developed by Thorpe and Zerkle (16) are both closely related to the evolution of hydrogen gas bubbles at the cathode. Landolt et al (22) have carried out a photographic study of hydrogen bubbles between the electrodes. It was observed that bubble size decreased strongly with increase in electrolyte flow velocity and increased with increase in current density. At flow velocities greater than 1000 cm. s^{-1} the bubbles were either smaller than 20μm (the limit of resolution of the optical arrangement) or were dissolved in the electrolyte. The bubbles were concentrated in a region close to the

cathode. No attempt was made to analyse the complex case of multiple bubble dynamics in turbulent flow. At low electrolyte flowrates large voltage oscillations, of cathodic origin, and eventual sparking occurred. The onset of the fluctuations coincided with the appearance of a different type of bubble of large size and odd shape. Although sparking could not be photographed, it was proposed that machining breakdown was caused by instantaneous complete coverage of the cathode by hydrogen bubbles.

The causes of machining failure, proposed by Baxter and Landolt et al, are similar but were not related to a method of prediction of a lower bound to the electrolyte velocity. The limitations on the process discussed above relate mainly to hydrogen bubble evolution at the cathode. However, the selection of operating conditions is also affected by the electrochemical processes at the anode surface.

1.5.4 Anodic Processes

The surface integrity of the workpiece in electrochemical machining has been found (29) to depend on the workpiece material, the electrolyte and, of particular interest in this context, the current density, which is proportional to tool feedrate, and the electrolyte flowrate. These factors determine the type of process which may occur at the anode surface. The processes are related (30) to regions on the idealised current density-anode potential curve (Fig. 1.2). The anode potential is the potential difference between the metal surface and the electrolyte.

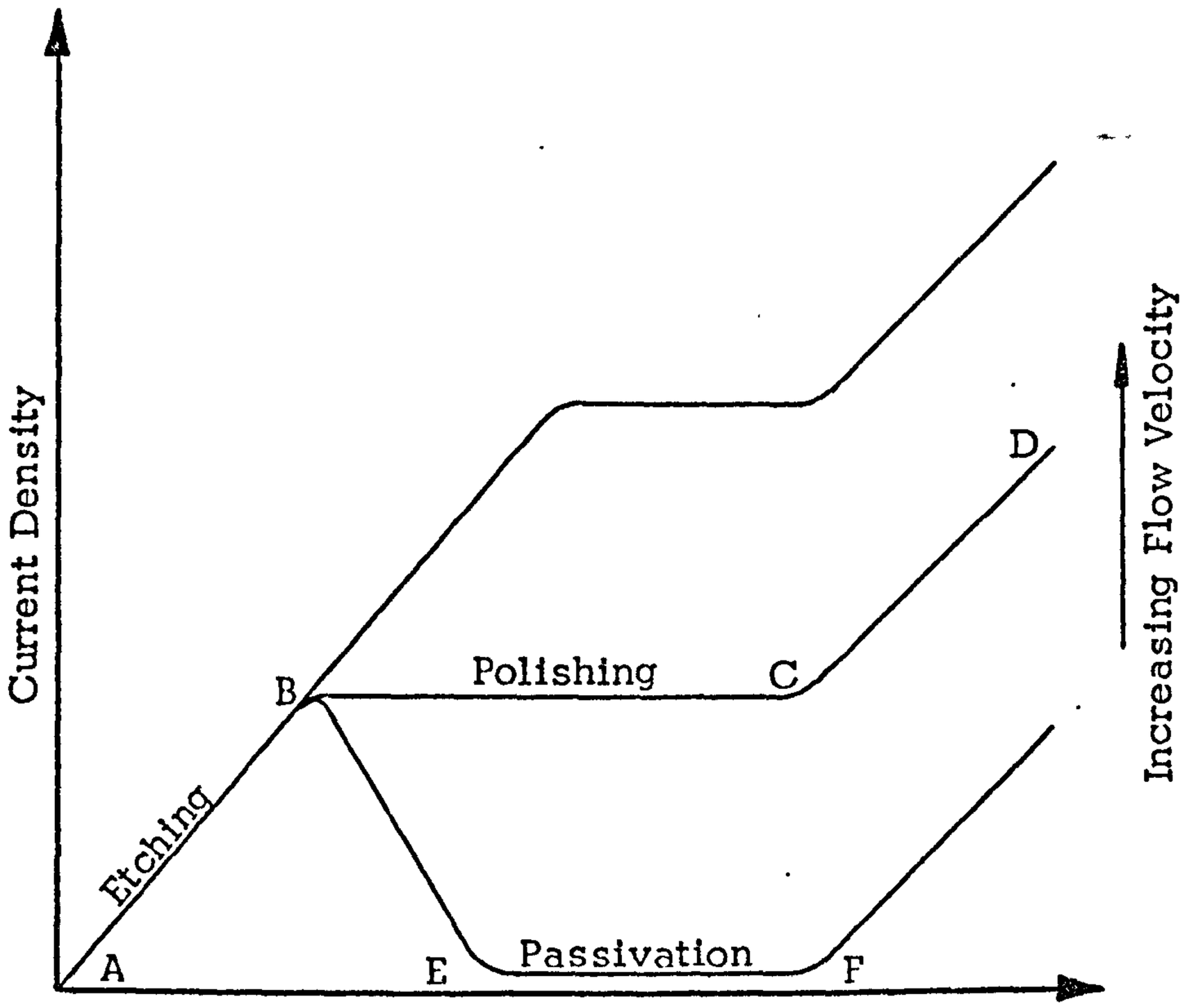

FIG. 1.2 IDEALISED POLARISATION CURVES SHOWING CHANGE OF REGIME WITH INCREASING FLOW VELOCITY

Etching takes place on the initial part AB of the curve. No anodic films are formed and dissolution is under activation control. Small variations in the metal dissolution rate result in an etched finish which may be quite acceptable. The flat portion of the curve BC corresponds to polishing which occurs due to the influence of a solid film on the anode surface. Various types of film may be formed and are described by Hoar (31). The rate of dissolution is controlled by diffusion of ions through the solid film. Gas is evolved at the anode in the region CD of the curve; the gas may be oxygen or chlorine. At higher anode potentials a smooth but not polished surface is produced. Passivation is the strong inhibition of dissolution in the region EF of the curve. The process is similar to polishing except that the solid film allows little or no diffusion of metal ions. In some instances the film may not be electronically conducting.

The idealised polarisation curve is considerably more complex in practice and increase in electrolyte flow velocity raises the curve to a higher current density and transition points may be sensitive to small flow variations. Various investigators (5, 29, 30, 32) have studied polarisation curves to establish suitable electrolytes to produce a satisfactory surface finish, with good dimensional, control on a given workpiece metal.

Faust (33) and Turner (34) suggest that the lower bound to the electrolyte velocity is related to the polarisation curves and is caused by a limiting current density or passivation. In a static electrolyte a limiting current density may occur at the anode surface above which

dissolution is controlled by the formation of a diffusion layer on the surface. The high electrolyte velocities used in electrochemical machining reduce the thickness of the diffusion layer. Faust and Turner suggest that the film thickness is rate determining but calculations of the flow velocity required to prevent a limiting thickness (and a limiting current density) are regarded as order of magnitude estimates. Landolt et al (35) found that the onset of passivation is determined by flowrate and current density. From known mass transfer equations, which relate to the diffusion layer, they obtained order of magnitude agreement, in a semi-quantitative test, with experimentally observed passivation current densities.

Larsson (29) plotted machining characteristics, for various metal-electrolyte combinations, in a form of polarisation curve which showed the transition from activation to diffusion control. The form of polarisation curve was also used to determine the shaping performance or throwing power of electrolytes. It was found that, for accurate reproduction of sharp detail, the machining gap should be small and machining should be at the highest current density before diffusion control sets in. For tools without appreciable curvature or sharp detail, advantage should be taken of the faster cutting rates which result from the high current densities in the diffusion region. In this region the current density for a given flowrate was found to be considerably elevated by increasing the electrolyte flowrate. This may be an important factor in determining the flow requirements for machining. The dependence of current density on flowrate may be

determined empirically from the above form of polarisation curve for a range of flow velocities. However, hydrodynamic mass transfer relations, similar to those used by Landolt et al (35), did not predict the onset of diffusion control for a machining cell which was similar to those used in practice. Thus the detailed mechanism of the diffusion layer and the requirement of a minimum electrolyte flowrate, in this respect, is not clear.

Passivation may cause machining breakdown and sparking in electrochemical machining (6, 36). Baldwin (24) observed heavy pitting of the surface of stainless steel anodes towards outlet under machining failure conditions. It was suggested that failure was related to anodic phenomena. A minimum flowrate of 6×10^{-4} m^3 s^{-1} per 155 A cm^{-2} was required for satisfactory machining. However, flowrates of this order have been observed (37) at current densities an order of magnitude greater.

1.6 Objects of Work

The objects of the work are:

(a) To establish the cause or causes of machining failure. The conflicting reports as to the limitations on metal removal rate and its importance in practice indicate that a detailed investigation is required.

(b) To develop a method of prediction of the maximum reliable feed-rate at minimum power requirements for known electrolyte pump

characteristics and workpiece dimensions. The prediction of operating conditions is fundamental to the economics of the process and to the design of the cathode or tool.

(c) The theoretical model formulated by Thorpe and Zerkle (16, 17), for the prediction of the equilibrium gap width between the electrodes, requires verification. The model is dependent on two empirical parameters i.e. the frictional multiplier, M, and the void function exponent, n. An object of the work is to determine values for these parameters for conditions similar to those in electrochemical machining in industry.

(d) To investigate the theoretical choked flow condition, which is an upper bound to the electrolyte velocity, as it appears to occur at the high feedrates and small electrode gaps most favourable to economic and accurate machining.

2.0 PRELIMINARY EXPERIMENTAL WORK

2.1 Introduction

Experimental work was required to accomplish the stated objectives. The experimental facilities were a 10,000 A Anocut 'Shaped Electrode' machine, installed in the Production Engineering Laboratory under a Department of Trade and Industry contract, and a small machine frame and power supply bought from Rolls-Royce Limited.

Preliminary experimental work was carried out on the small machine to develop experimental methods and instrumentation and to establish the approach to the work.

The algebraic relations, formulated by Thorpe and Zerklé (16), apply under condition of low pressure drop and the gas density is assumed constant along the electrode length. The further development of the model accounts for the variation in gas density at high pressure drops such as occur in practice. A direct approach to this would be the measurement of the volume of gas at locations along the gap. Various techniques, described by Wallis (19), were considered in this respect but none were found suitable to the conditions encountered in electrochemical machining. The gas density function can be determined from:

$$A = \frac{CT^{o}}{p^{o}} \qquad (49)$$

Since the temperature increase is linear (equation (48)) the measurement of pressure distribution, which is non-linear (equation (50)), is an alternative

method of defining the gas density variation along the electrode length. A brief investigation was also carried out on (a) the dependence of machined surface finish and metal removal rate on electrolyte flowrate and (b) the effect of the main operating conditions on the gap width variation along the electrode length. This formed the preliminary experimental work.

The time available on the Anocut machine was necessarily limited. The experimental work using this machine was intended to extend the preliminary work to operating conditions similar to those in practice. In particular values of the model parameters, the frictional multiplier, M, and the void function exponent, n, were required for these conditions. This machine was provided with a sophisticated spark detect system so that an investigation of the process limitations, the upper and lower bounds to the electrolyte velocity, could also be carried out. It was intended that the investigation would provide a basis for the selection of operating conditions.

The work was concerned with tool design and operating conditions for a given anode metal-electrolyte combination. For the results to be directly applicable to the combinations used in practice an idealised metal and electrolyte were required. However, no such combination or even a universal electrolyte has become established.

Electrochemical machining is the accepted method of manufacture of turbine and compressor blades and has numerous other applications in the aero-space industry. Thus early research work was carried out, and continues, on nimonic alloys (29), titanium

alloys (38) and stainless steels (24).

The electrochemical machining of carbon steels is being investigated by research workers (5, 39, 40, 41) in General Motors Corporation, U.S.A. in relation to the manufacture of forging dies. The success of the process in this application has been reported (42) by a Continental car manufacturer. Mao et al (41) found, from polarisation and electrochemical machining studies, that similar behaviour is obtained on both mild steel (1020) and fully-hardened steel (5160 H). The effects of the microstructure of carbon steels on machinability have been established by Freer et al (30). For these reasons, and cost considerations, mild steel anodes were used throughout the experimental work.

Sodium chloride and sodium nitrate solutions were used in the machining tests. These salts are inexpensive and the choice of electrolyte in most production applications appears to be restricted to them (6). The polarisation characteristics of mild steel with these electrolytes have been reported by Chikamori (43). With the sodium chloride solution dissolution was under activation control and the current efficiency was close to 100%. With sodium nitrate solution passivation occurred at low electrode potential, and current density and dissolution rate were low. Above an electrode potential of 1.5 V dissolution was in the transpassive region and dissolution rate and current efficiency increased. However, the current efficiency was always lower than that for sodium chloride due to the evolution of oxygen at the anode surface.

Sodium chlorate electrolyte produces smooth bright surfaces with good dimensional control on steel anodes (5). However, this electrolyte was not used as it is relatively expensive, a fire hazard and decomposes to sodium chloride during machining (44).

An initially plane and parallel electrode configuration was used in the experimental work to facilitate workpiece-tool alignment and the measurement of workpiece profile deviations. The theoretical model applies to this type of configuration and the electrolyte flow is not subject to rapid acceleration or deceleration due to the tool shape. This is idealisation of the situation as, in practice, each complex shaped tool has individual flow patterns. Thus the use of a complex tool geometry would produce results applicable only to that particular tool although work of this nature would be a logical extension of the present work.

2.2 The Machining System

2.2.1 The Basic Machine

The machine (Fig. 2.1) was a three-station, electrochemical drilling machine which had been used previously for production work at Rolls Royce Limited. A manual feed was operated by a handwheel for fitting and positioning of workpieces. The automatic feed was driven by an electric motor through a 1400:1 reduction gear box. A thyrotron speed control unit allowed an infinitely variable selection of feedrates between 0.1 and 8 mm min^{-1}. The machine was reconditioned prior to the experimental work and a small table was built

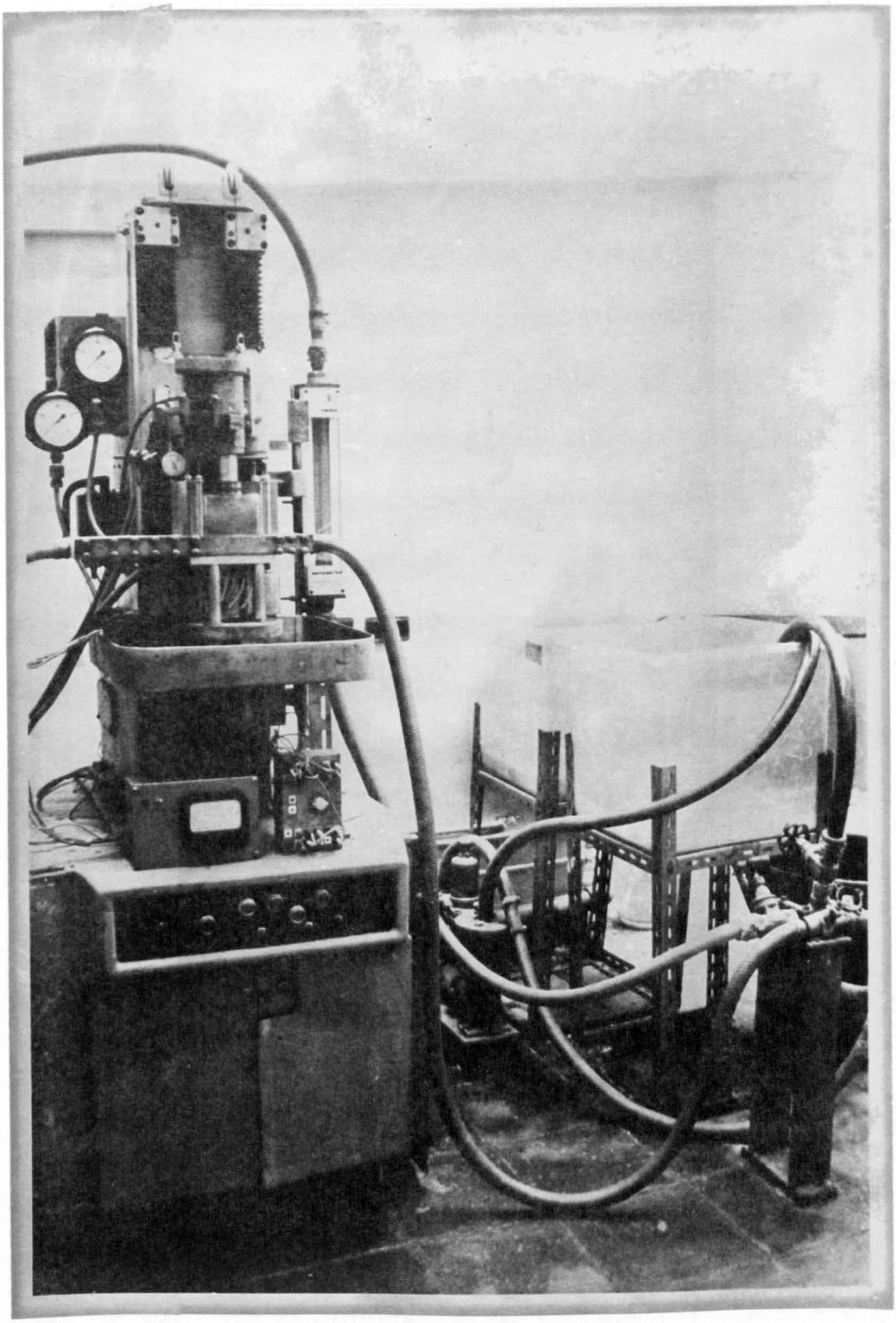

FIG. 2.1 ELECTROCHEMICAL MACHINE, ELECTROLYTE PUMP AND STORAGE TANKS

into the machine to provide support for the machining cell.

2.2.2 The Power Supply

The power supply was a low voltage, d.c. rectifier supplied from the three-phase, 440 V mains. The output voltage could be preset to a maximum of 32 V for currents up to 250 A or to 16 V for currents up to 500 A. The output voltage was stabilised manually against load current variation. To reduce damage to tooling due to sparking across the electrodes and to prevent overload, the machining current could be set, with a contact ammeter, to trip at any desired level to suit a particular machining operation.

2.2.3 The Electrolyte System

The electrolyte flow system is shown in Fig. 2.2. The electrolyte was stored in three polypropylene tanks with a total capacity of 0.25 m^3. A Mono pump (type SH32) was installed which was suitable for use with corrosive liquids. The pump was driven by a 1.1 kW motor and was capable of delivery pressures up to 600 kN m^{-2} and a maximum flowrate of 30×10^{-5} m^3 s^{-1}. A by-pass valve on the delivery side of the pump allowed variable electrolyte flowrate and a needle valve controlled the outlet pressure from the machining cell. The electrolyte was recirculated from one tank and a filter was installed in the circuit. The temperature of the electrolyte in the working tank was controlled by a heat exchanger operated from the cold water supply.

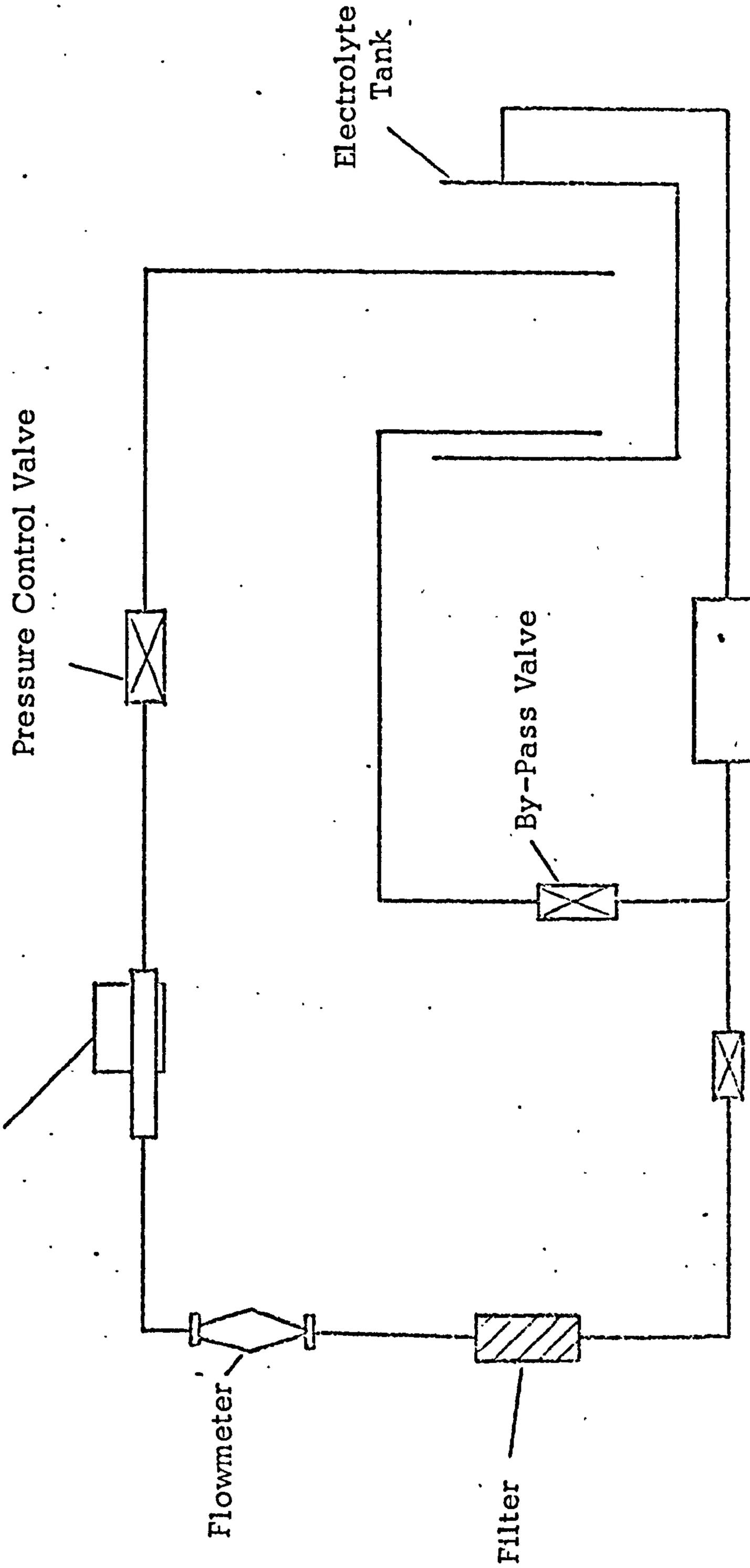

FIG. 2.2 ELECTROLYTE FLOW SYSTEM

2.2.4 The Machining Cell

The machining cell (Fig. 2.3) located the tool and workpiece and confined the electrolyte flow to the gap between the electrodes. The flow channel was made from perspex plate which was considered to have suitable properties of strength, electrical insulation and machinability. The channel had an entrance length of 50 hydraulic diameters to provide a fully established velocity profile at the inlet to the electrode gap. A similar arrangement has been used by Landolt et al (22) and in many investigations of fluid flow in pipes and channels.

The flow channel groove was machined on one plate and the two plates bolted together. A slot, 100 mm long in the direction of flow and 12.6 mm wide was machined through the plates to give a sliding fit to the workpiece and tool. Sealing was effected by 'O' rings at all interfaces.

The stainless steel workpiece fixture was attached to the feed drive platen. The workpiece was press-fitted in a slot in the fixture and clamped with two fitted bolts. Access for the removal of the workpiece was made with the manual feed drive and by sliding the perspex sealing chamber up the shaft of the workpiece fixture. Prior to final assembly shims were positioned such that the tool face was parallel to the anode face.

2.3 Instrumentation

A 0 - 32 V voltmeter, built into the power supply, measured the output voltage. The voltage at the machining cell could also be

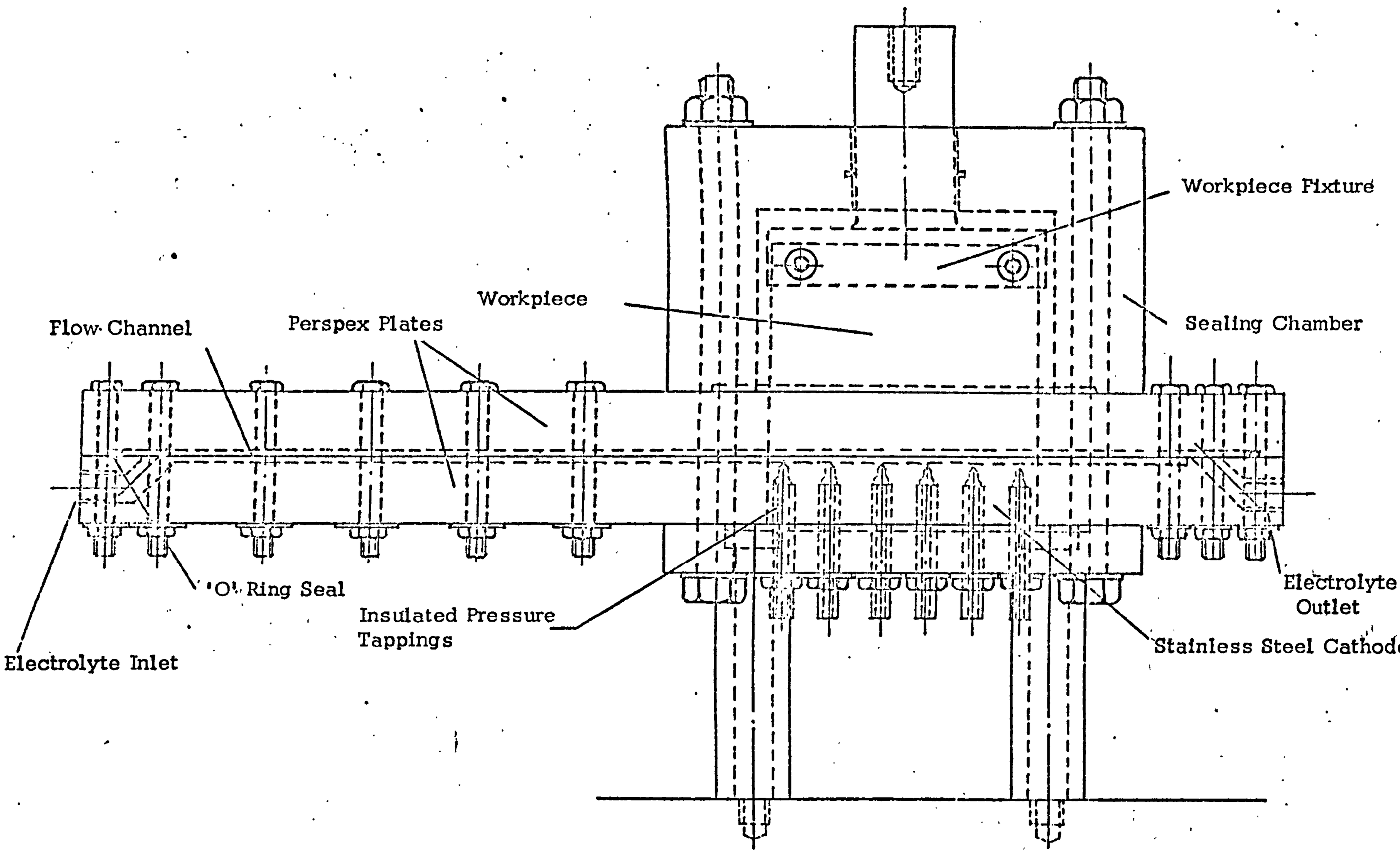

FIG. 2.3(a) MACHINING CELL

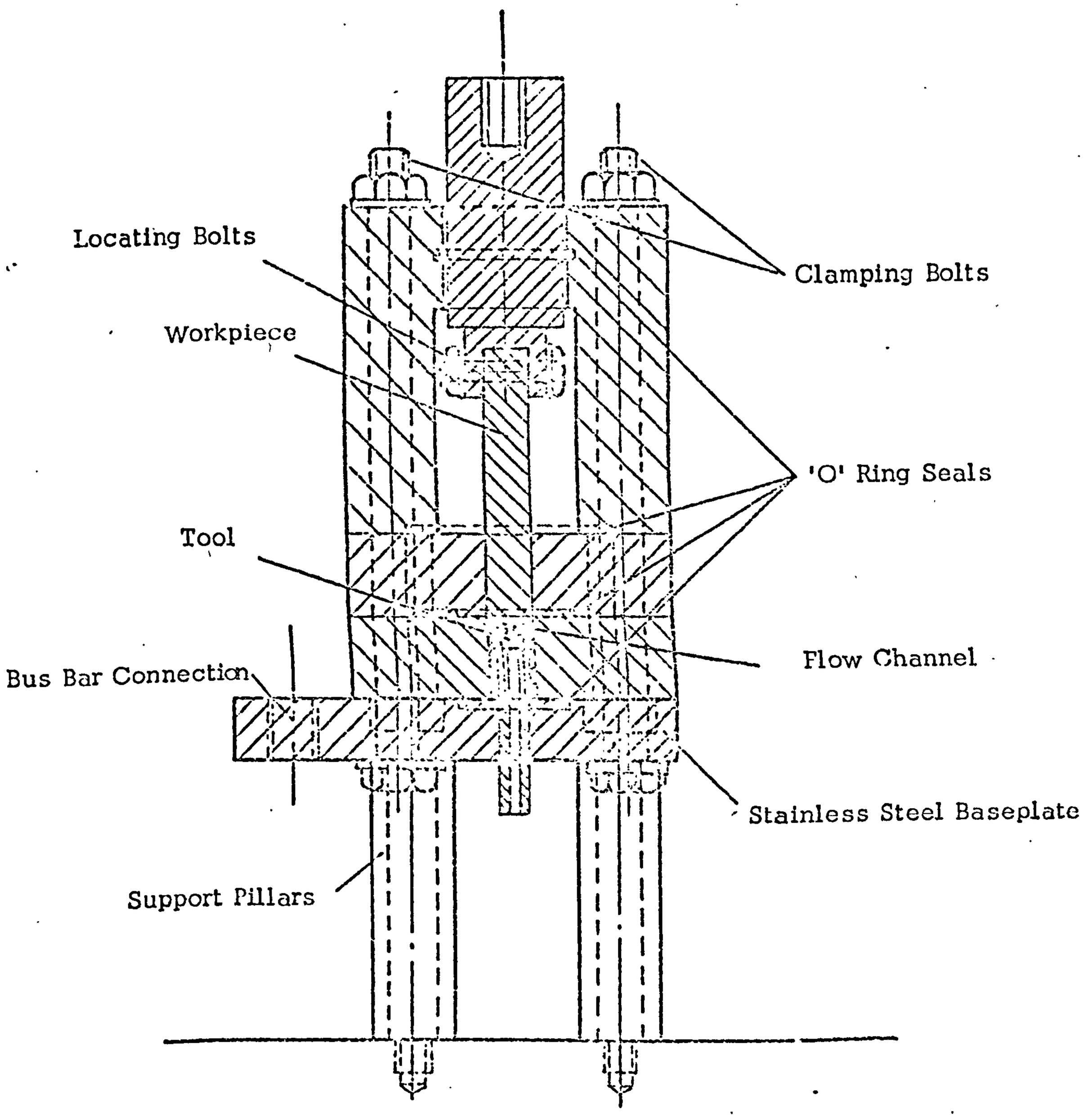

FIG. 2.3(b) SECTION OF MACHINING CELL

measured with a 20 k Ω per volt meter. Machining current readings were taken directly from the ammeter on the power supply unit.

Workpiece feed measurement was made from the drive platen with a 0.01 mm dial gauge. The gap width before and after machining was measured, with the dial gauge, by an electric contact method of determining the tool datum. An impulse tachometer was mounted on the feed-drive spindle to permit feedrate setting from a calibration.

The electrolyte flowrate was measured with a Rotameter (24 X) flowmeter, which was supplied with a theoretical calibration for liquids of different viscosity and density, and which was also calibrated experimentally with the electrolyte used in the tests. Inlet and outlet pressures at the machining cell were measured with stainless steel tube Bourdon gauges. Thermometers measured the inlet and outlet electrolyte temperatures.

To determine the pressure distribution along the electrolyte length, five, 1.5 m differential manometers were installed in series adjacent to the machine. The pressure was measured at six equally spaced locations along the electrode length. Ideally the tappings, which were made in the cathode, had to be as small as practicable but this would cause a poor response in the manometers. The most suitable diameter of the tappings was found to 0.6 mm. The tappings did not affect the machined surface of the anode. Coloured carbon tetrachloride of specific gravity 1.63 was used as an indicating liquid in the manometers.

The conductivity and other electrolyte properties were determined

from measurement of the density and temperature and from reference data presented in Appendix III.

The workpiece profile deviation was measured with the jig shown in Fig. 2.4. The workpiece was moved under the dial gauge and readings were taken relative to the gap inlet position. This position was taken to be 3 mm from the side due to inlet rounding.

2.4 Experimental Procedure

The workpiece was ground, so that the datum faces were parallel, to ± .005 mm. measured and weighed. The workpiece was fitted into the fixture and the gap set with the manual feed and the dial gauge. The electrolyte temperature and specific gravity were adjusted to the required values. The pump was switched on and flow conditions were allowed to stabilise. The manometer bleed valves were opened to remove air bubbles from the pressure tapping leads. The feed drive motor was started and the speed set to the feedrate required. The machining power was switched on and the feed drive clutch engaged. The electrolyte flowrate, inlet and outlet pressures and temperatures, and the manometer deflections were noted continuously throughout the test. After each test, which lasted from six to eight minutes, the manometer deflections were noted at the same flowrate as that during the test. The workpiece was then removed, measured and weighed and the profile deviation recorded.

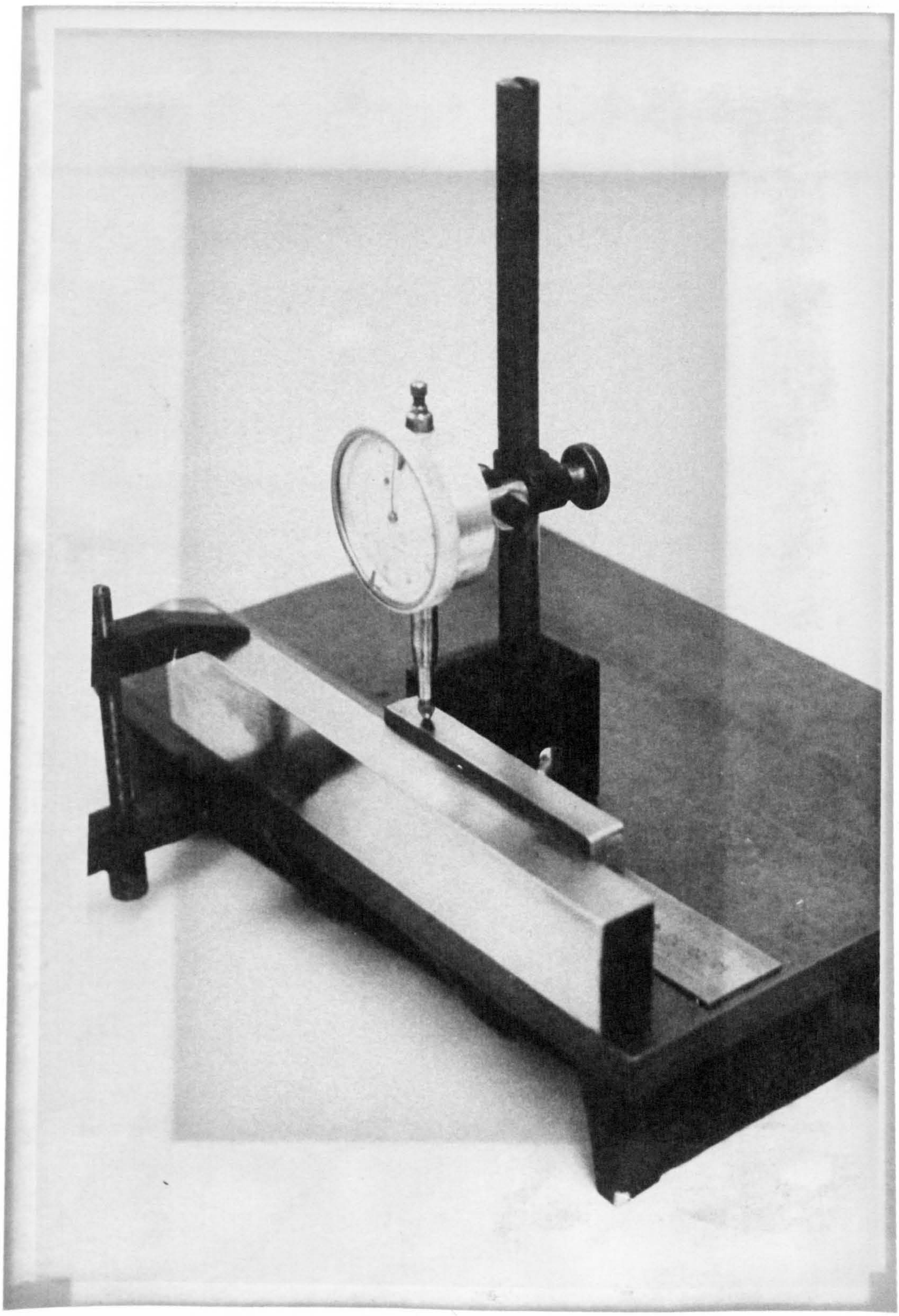

FIG. 2.4 WORKPIECE PROFILE MEASUREMENT JIG

2.5 Experimental Results

The test series was carried out at machining voltages of 12 and 24 V. Feedrates were calculated to give a machining gap of 3.18 mm which was the thickness of the inlet flow channel. The electrolyte was a 10% sodium chloride solution at an inlet temperature of 20°C. A range of flowrates was used at each machining condition and at outlet pressures of 170 and 450 kN m^{-2}.

The total pressure drop across the electrode gap for the tests is shown in Fig. 2.5. An increase in pressure drop for flow with machining was observed relative to flow without machining. Increase in outlet pressure reduced the pressure drop at a given flowrate whereas increase in current density produced a small increase in pressure drop. This suggests that the increase in pressure drop is closely associated with the evolution of hydrogen gas bubbles at the cathode surface. Within the accuracy of the measurements the pressure distribution within the gap was linear although this may have been due to the low current densities and relatively large gap width.

The ratio of the change in gap width in the direction of flow to the gap width at inlet is shown in Fig. 2.6. For an increase in gap width the workpiece profile was assumed positive. For the conditions of machining all the anode profiles were positive i.e. ohmic resistance heating of the electrolyte was predominant over the effect of gas bubbles in determining the electrolyte conductivity. This is contrary to the results of Hopenfield and Cole (15); their experimental conditions differed in that they used short electrodes and lower outlet

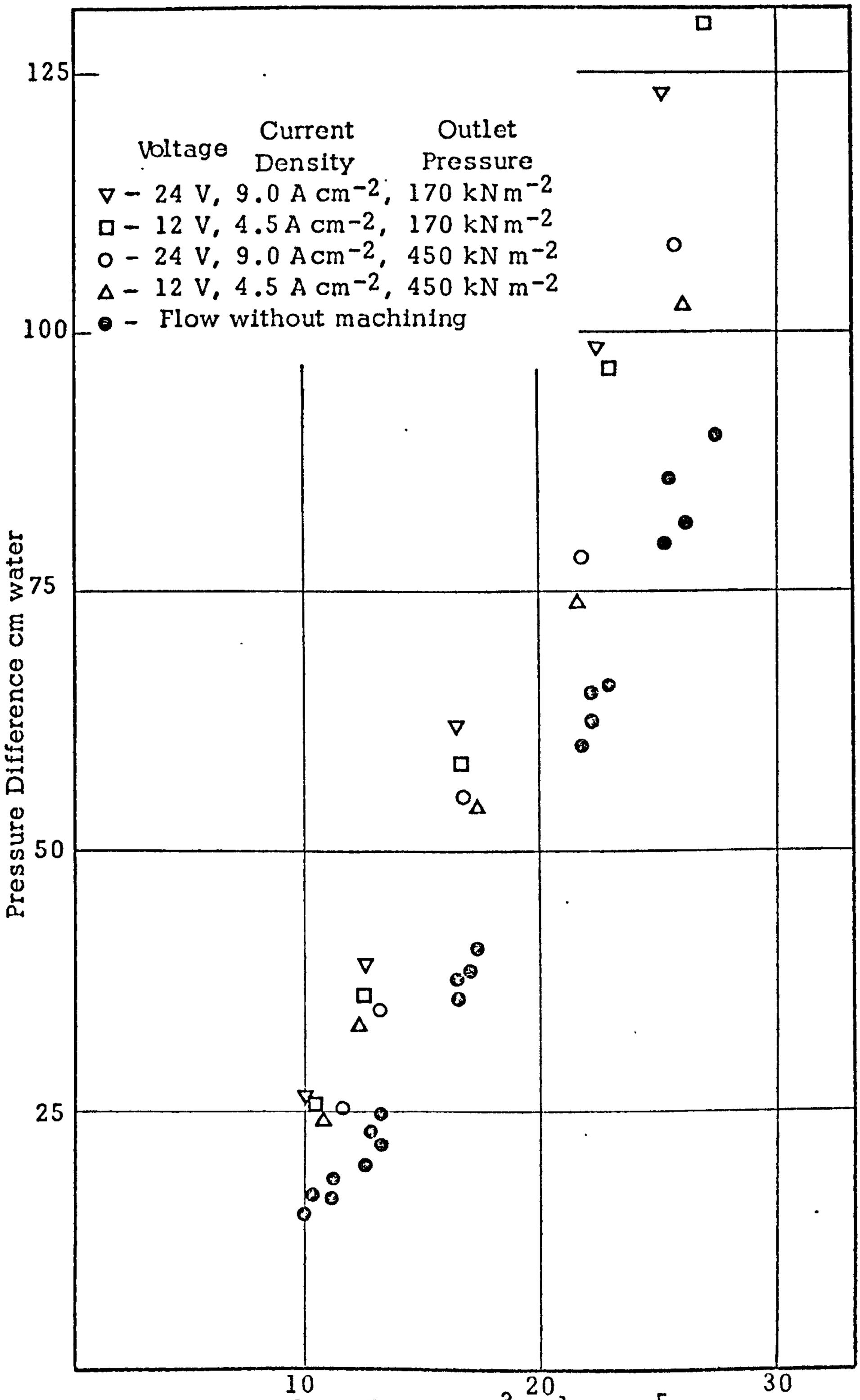

FIG. 2.5 PRESSURE DROP AS A FUNCTION OF FLOWRATE, OUTLET PRESSURE AND CURRENT DENSITY

Voltage - 24 V
Current Density - 9.0 A cm^{-2}
Outlet Pressure- 450 kN m^{-2}

Electrolyte Flowrates:
○ - 22 x 10^{-5} m^3 s^{-1}
△ - 17 x " "
□ - 12 " "

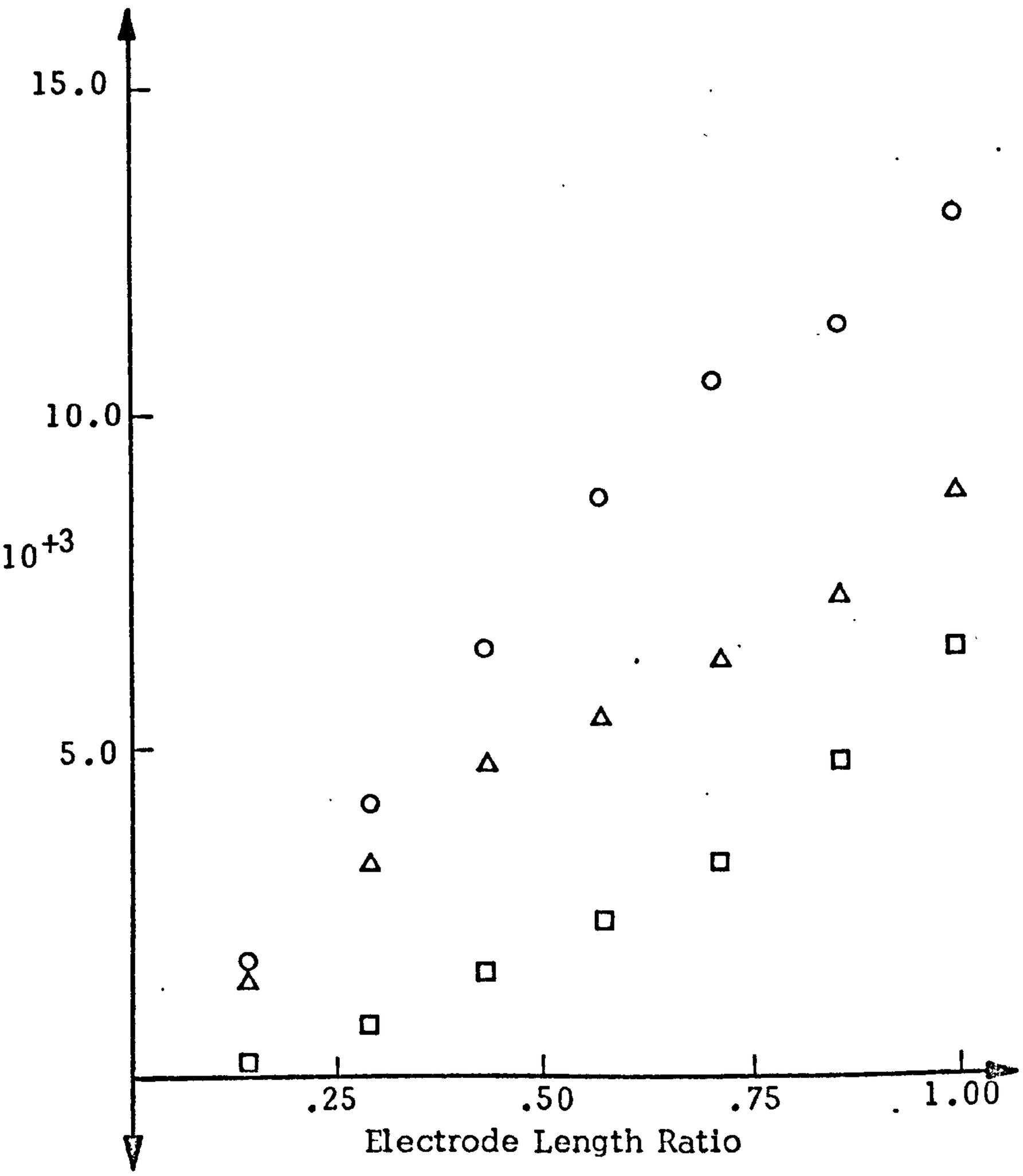

FIG. 2.6 VARIATION IN ELECTRODE GAP WIDTH WITH ELECTROLYTE FLOWRATE

pressures.

The metal removal rate for each test is plotted against electrolyte flowrate in Fig. 2.7. At each current density the metal removal rate was closely predicted from Faraday's laws of electrolysis based on a valency of dissolution of two for the mild steel anodes. The metal removal rate was virtually unaffected by electrolyte flowrate if a minimum flowrate was exceeded which was similar at both current densities. At flowrates below this minimum the metal removal rate was substantially reduced. The machined surface finish of the anode also deteriorated below the minimum flowrate.

In general the preliminary experimental work allowed experience to be developed in experimental procedures and design and enabled the specific objectives of the work, discussed in the previous chapter, to be formulated.

2.6 Modifications to Experimental Methods

The inlet length in the flow channel in the preliminary experimental work allowed the flow at inlet to the electrode gap to be fully established. However at small electrode gaps and high flow velocities such as occur in practice, the pressure drop along the inlet length would be high and outwith the capacity of suitable pumps. To carry out tests at small electrode gaps a flow channel was designed (Fig. 2.8) without an inlet length so that it could be used with the original workpiece fixture, sealing chamber and baseplate.

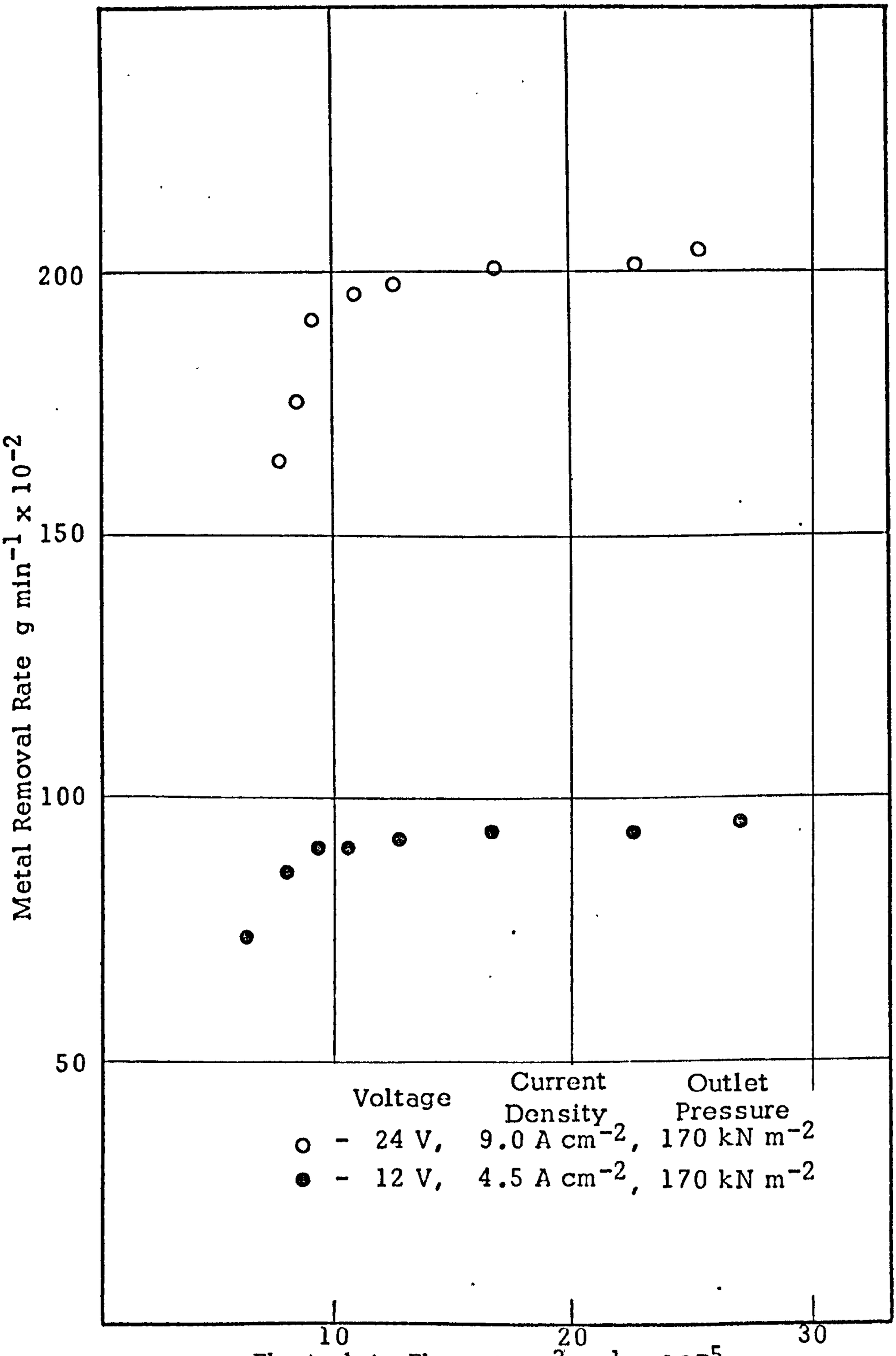

FIG. 2.7 INFLUENCE OF ELECTROLYTE FLOWRATE ON METAL REMOVAL RATE

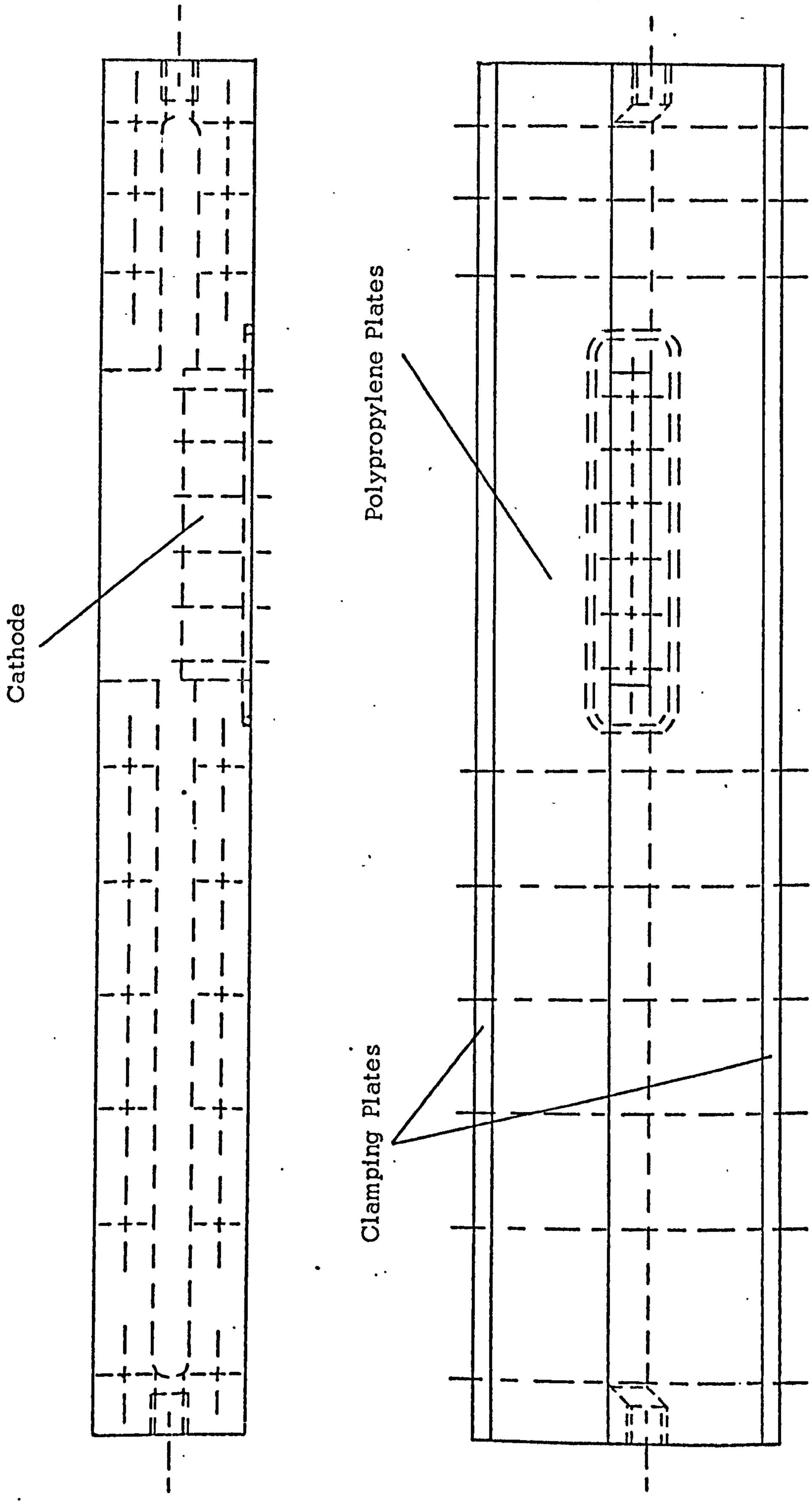

FIG. 2.8 FLOW CHANNEL

The flow channel was manufactured from two polypropylene plates; the side dimensions of the tool and workpiece were machined from one plate and the plates bolted together. Two steel plates were fitted to the sides of the channel to add rigidity and allow the polypropylene to be compressed onto the workpiece and tool and prevent side flow past the electrodes.

An additional manometer was installed, for the measurement of inlet pressure loss, with mercury as an indicating liquid. Bromoform of specific gravity 2.85 was used as an indicating liquid in the existing manometers. The outlet pressure tapping was made as close as practicable to the electrode gap at outlet such that the static pressure measured was that just at outlet and abrupt expansion losses were minimised.

To record the machining current a 50mV., 500 A shunt was placed in series with the power supply cables and the voltage drop across the shunt was displayed on a Rikadenki, three-pen, chart recorder. Miniature bead thermistors (type S.T.C. FS2) were used to record inlet and outlet electrolyte temperatures. The thermistors were calibrated against thermometers in a controlled temperature bath. The change in resistance of the thermistor beads, with temperature, was measured with a Wayne Kerr Universal Bridge and was also displayed on the pen-recorder chart.

The supply of electrolyte at constant temperature to the machining cell using a heat exchanger was troublesome. This system was replaced by discharging the electrolyte from the machining cell

to a separate tank. After the test the metal hydroxide was allowed to settle to the bottom of the tank and clean electrolyte was siphoned from the top of the tank back to the supply tank.

2.7 Experimental Results

Operating conditions were chosen to give a range of flowrates up to the maximum pump performance and at machining currents within the capacity of the power supply. The machining voltage was 16 V and the feedrate was nominally 0.55 mm min^{-1}. The electrolyte was a 10% sodium chloride solution at an inlet temperature of 20°C. The theoretical electrode gap width at inlet, at these conditions, was 0.70 mm. The test results are presented in Table 1.

In Fig. 2.9 the experimental anode profile is compared with

(a) the predicted profile from the algebraic relation, equation (46), in which the gas density is assumed constant along the electrode length;

(b) the predicted profile for the further development of the theory for which a computer solution is required. For the values of the frictional multiplier and void function exponent assumed in previous work (15, 16) the agreement is poor.

To match the experimental data the frictional multiplier was increased until the computed inlet pressure became close to the experimental value. The void function exponent was then adjusted by trial and error to give a best fit of the computed gap variation with the experimental anode profile.

Test No.	Feedrate mm min^{-1}	Machining Current A	Electrolyte Flowrate $m^3 s^{-1} \times 10^{-5}$	Inlet Pressure $kN m^{-2}$	Outlet Pressure $kN m^{-2}$	Pressure Drop after Test $kN m^{-2}$	Inlet Loss Coefficient Ko	Inlet Gap Width mm
1	.56	318	9.5	490	155	255	.36	.73
2	.54	308	8.8	425	140	220	.31	.69
3	.56	312	6.1	340	165	110	.34	.75
4	.55	316	5.0	300	165	70	.39	.73
5	.56		Machining Failure Conditions					.63
6	.55	317	5.3	340	230	76	.34	.68
7	.53	315	5.4	390	320	65	.36	.74
8	.80		Pips formed on anode surface					.53
9	.78	447	6.0	485	150	200	.38	.69
10	.75		Machining Failure Conditions					.58

Machining Voltage - 16 V

Sodium Chloride Solution at 20°C

Electrolyte Concentration - 10% in Tests 1 to 8
16% in Tests 9 and 10

TABLE I

Test 1

Experimental Data		Computed Data	
Voltage	- 16 V	Current Density	- 24.4 A cm^{-2}
Current	- 318 A	Electrode Gap at	-
Flowrate	- 9.5 $m^3 s^{-1} \times 10^{-5}$	Inlet	- .70 mm
Inlet Pressure	- 490 kN m^{-2}	Flow Velocity at	
Outlet Pressure	- 155 kN m^{-2}	Inlet	- 11.4 m s^{-1}
Temperature		Temperature	
Increase	- 12.8 K	Increase	- 12.1 K
Electrode Gap at		Void Fraction at	
Inlet	- .73 mm	Outlet	- .207

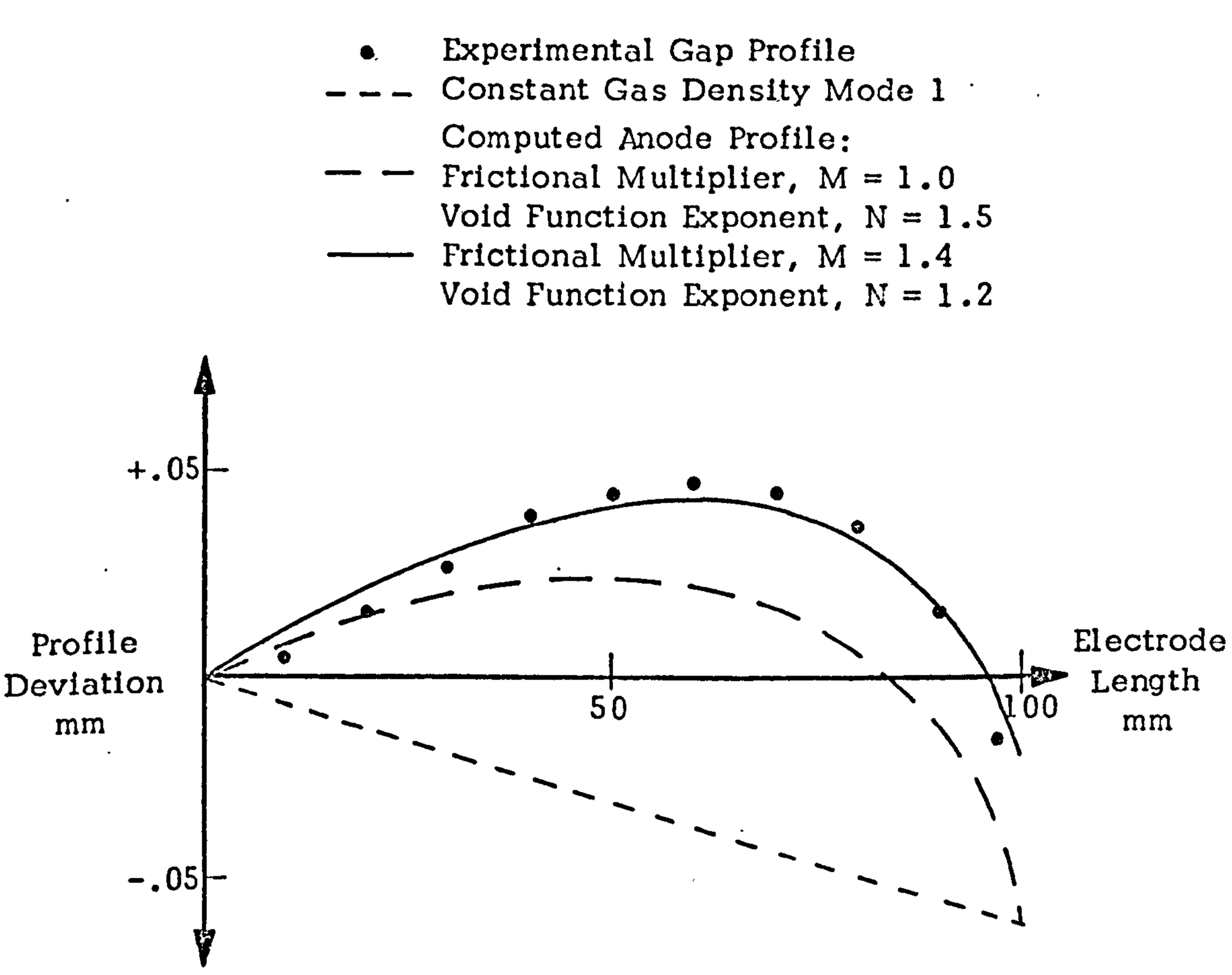

FIG. 2.9 COMPARISON OF EXPERIMENTAL AND THEORETICAL ANODE PROFILES

Some further matching was usually required since M and n are inter-dependent.

The matching procedure was also carried out for the tests at lower flowrates presented in Figs. 2.10 and 2.11. Reducing the flowrate did not markedly alter the anode profile. The experimental pressure distribution along the electrode length is also compared with the predicted distribution. The non-linearity of the pressure distribution particularly towards outlet is a significant factor in relation to the observed convergence of the anode profile towards outlet. The assumption of a linear pressure distribution as in previous analyses (8) would not allow accurate prediction of the anode profile.

The inlet pressure loss coefficients were obtained from measurement of the pressure distribution after each test at the same flowrate as that during the test. The measurements were then plotted and extrapolated to the gap inlet. The difference between the extrapolated value and the pressure upstream of the electrode gap was taken to be the inlet pressure loss. This procedure could not be adopted for the pressure distribution data for flow with machining due to the observed non-linearity. The inlet loss coefficients were considered to be unaffected by the evolution of hydrogen bubbles at the cathode. The loss coefficients were between 0.3 and 0.4; a coefficient of 0.5 is normally assumed (46) for an abrupt contraction although the area reduction ratio influences this value. The relatively low coefficients appear to be the result of inlet rounding of the workpiece which can be seen in Fig. 2.4.

The experimental friction factors for flow without machining were within ± 10% of those predicted from the empirical Blasius relation (46). For flow in rectangular ducts local friction factors

Test 2

Experimental Data		Computed Data	
Voltage	- 16 V	Current Density	- 24.0 A cm^{-2}
Current	- 308 A	Electrode Gap at Inlet	- .71 mm
Flowrate	- $8.8 \times 10^{-5} m^3 s^{-1}$	Flow Velocity at Inlet	- 10.5 m s^{-1}
Inlet Pressure	- 425 kN m^{-2}	Temperature Increase	- 13.0 K
Outlet Pressure	- 140 kN m^{-2}	Void Fraction at Outlet	- .236
Temperature Increase	- 14 K		
Electrode Gap at Inlet	- .69 mm		

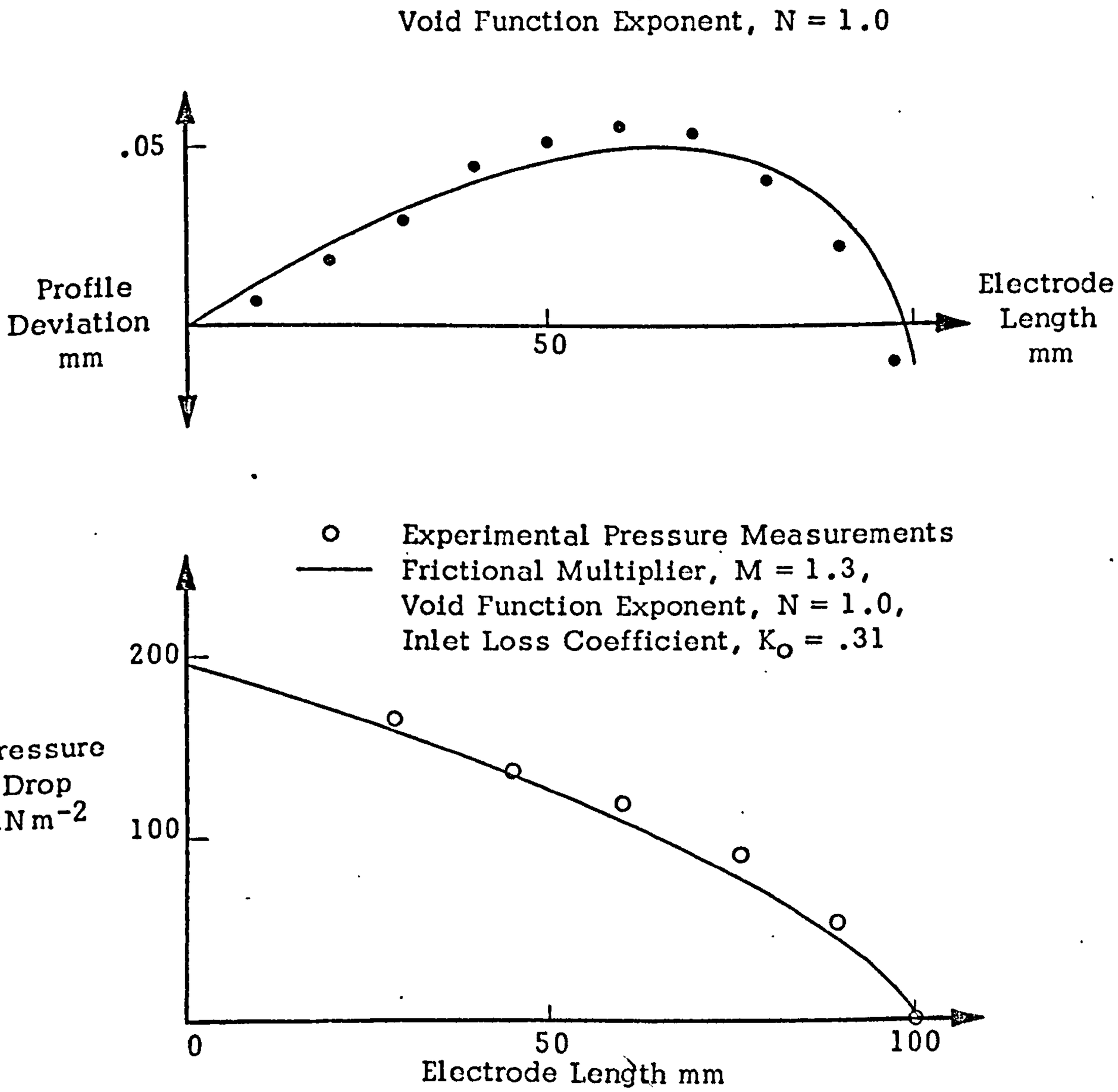

FIG. 2.10 COMPARISON OF THEORETICAL AND EXPERIMENTAL ANODE PROFILE AND PRESSURE DISTRIBUTION

Test 4

Experimental Data		Computed Data	
Voltage	- 16 A	Current Density	- 24.2 A cm^{-2}
Current	- 316 A	Electrode Gap at Inlet	- .70 mm
Flowrate	- $5.0 \times 10^{-5} m^3 s^{-1}$	Flow Velocity at Inlet	- 5.9 m s^{-1}
Inlet Pressure	- 300 kN m^{-2}	Temperature Increase	- 25.1 K
Outlet Pressure	- 165 kN m^{-2}	Void Fraction at Outlet	- .341
Temperature Increase	- 24 K		
Electrode Gap at Inlet	- .73 mm		

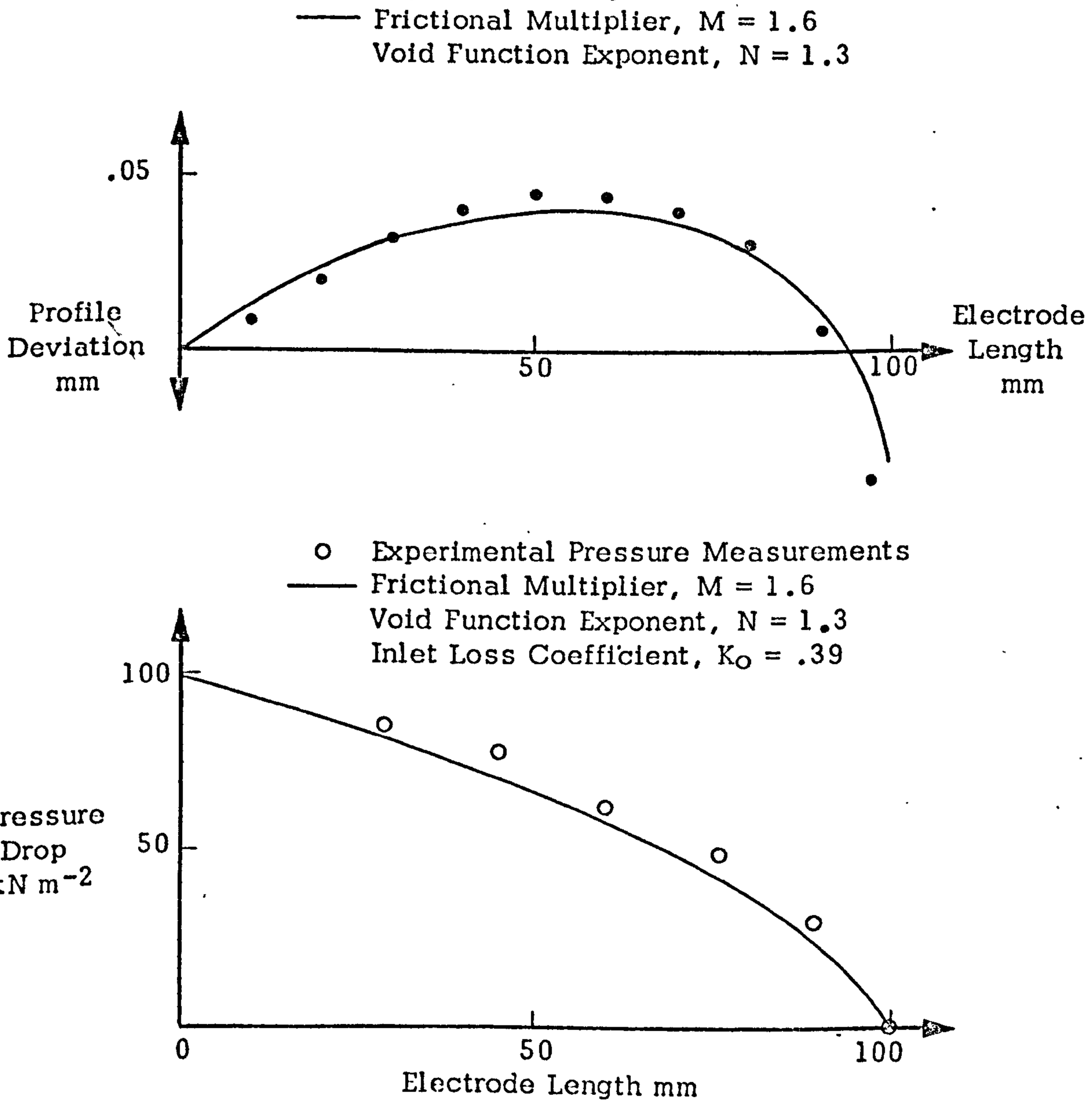

FIG. 2.11 COMPARISON OF THEORETICAL AND EXPERIMENTAL ANODE PROFILE AND PRESSURE DISTRIBUTION

attain fully developed values at about 10 hydraulic diameters from inlet (47) or 15 mm from inlet for the conditions used in these tests. Since the first pressure tapping was situated 28.5 mm from inlet, the high values of the friction factor in this region were taken into account by the inlet loss coefficient.

Insufficient electrolyte flowrate caused a substantial change in the machining characteristics (Fig. 2.12). The machining current fell from 290 to 270 A and equilibrium machining did not become established. The test was terminated after about one minute to prevent sparking across the electrode gap. Although the model developed by Thorpe and Zerkle (16, 17, 18) applies only to equilibrium machining, the model was used in an attempt to show characteristics peculiar to machining failure. The experimental anode profile could not be matched by a single value of the void function exponent. A value of 1.0 similar to that required in the previous tests gave good agreement over the first 50 mm of the electrode length whereas a value of 1.6 gave some agreement towards outlet. The electrolyte outlet temperature increased to a maximum of 45°C which was well below the boiling point of the electrolyte. Thus the assumption of electrolyte boiling in the exit plane as a lower bound to the electrolyte velocity, is not verified. The Reynolds Number at inlet in this test was about 7000 such that the flow was turbulent.

The effect of increase in outlet pressure to 320 kN m^{-2} is shown in Fig. 2.13. The pressure increase reduced the volume of gas bubbles in the gap such that the electrolyte conductivity was more dependent on ohmic resistance heating of the electrolyte. The void function exponent was similar to those in the tests at lower pressures but the frictional multiplier was less which may also be due to smaller

Test 5

Experimental Data		Computed Data	
Voltage	- 16 V	Current Density	- 24.4 A cm^{-2}
Current	- 290 to 270 A	Electrode Gap at Inlet	- .70 mm
Flowrate	- $4.0 \times 10^{-5} m^3 s^{-1}$	Flow Velocity at Inlet	- 4.8 m s^{-1}
Inlet Pressure	- 260 kN m^{-2}	Temperature Increase	- 30.2 K
Outlet Pressure	- 155 kN m^{-2}	Void Fraction at Outlet	- .399
Temperature Increase	- 25 K		
Electrode Gap at Inlet	- .63 mm		

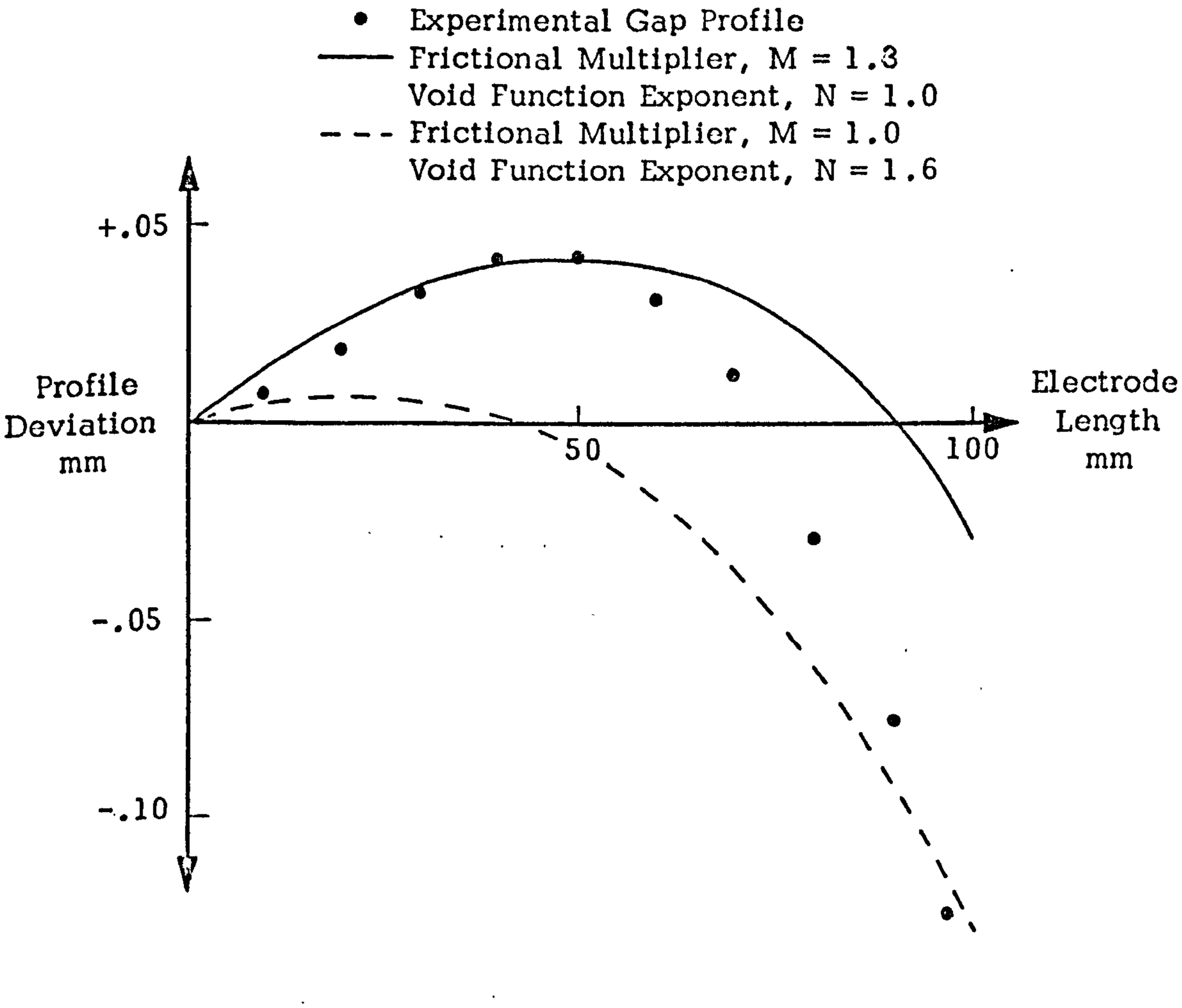

FIG. 2.12 COMPARISON OF THEORETICAL AND EXPERIMENTAL ANODE PROFILES AT MACHINING FAILURE CONDITIONS

Test 7

Experimental Data		Computed Data	
Voltage	- 16 V	Current Density	- 23.5 A cm^{-2}
Current	- 315 A.	Electrode Gap at Inlet	- .72 mm
Flowrate	- $5.4 \times 10^{-5} m^3 s^{-1}$	Flow Velocity at Inlet	- 6.38 m s^{-1}
Inlet Pressure	- 390 kN m^{-2}	Temperature Increase	- 24.1 K
Outlet Pressure	- 320 kN m^{-2}	Void Fraction at Outlet	- .187
Temperature Increase	- 22 K		
Electrode Gap at Inlet	- .74 mm		

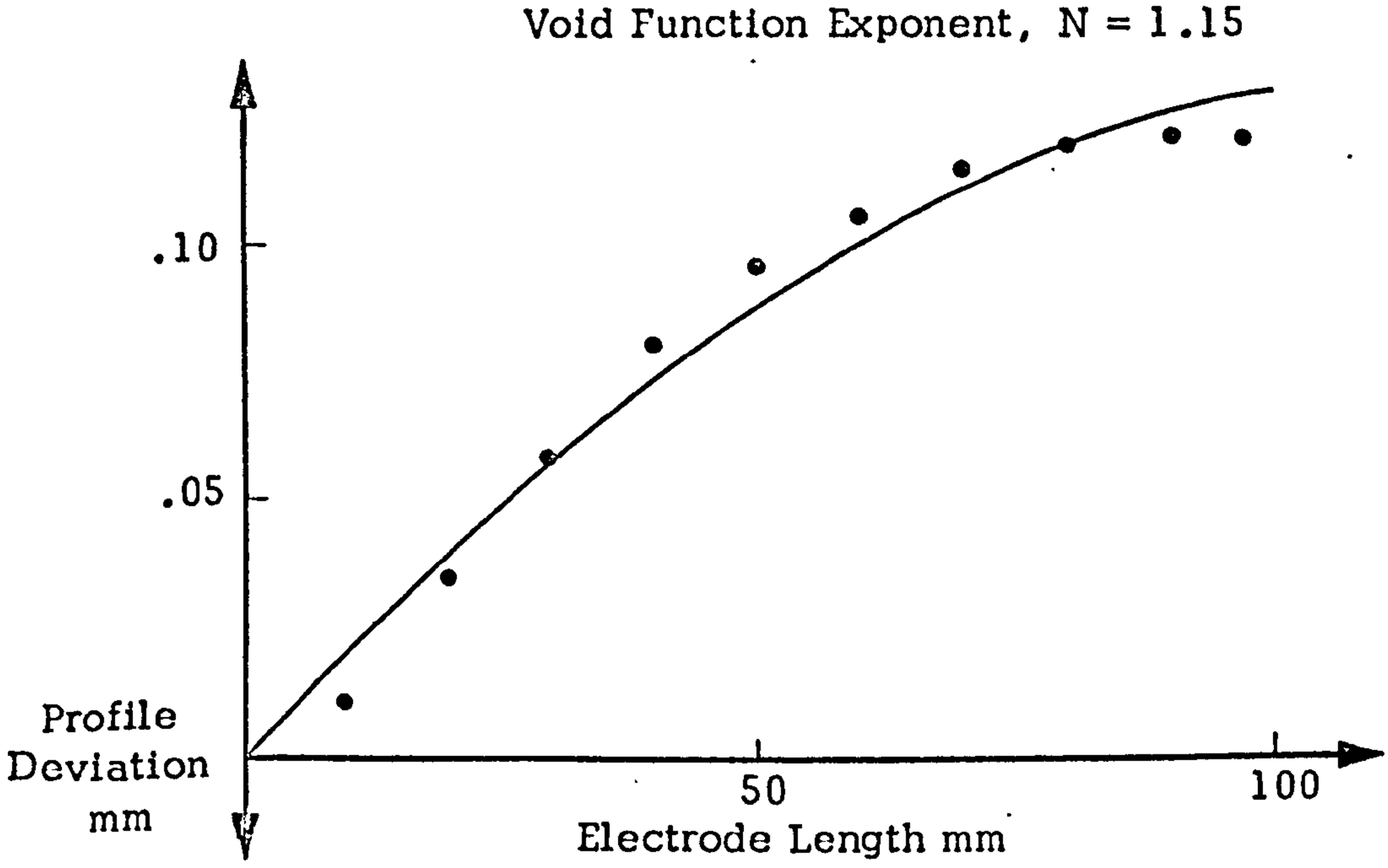

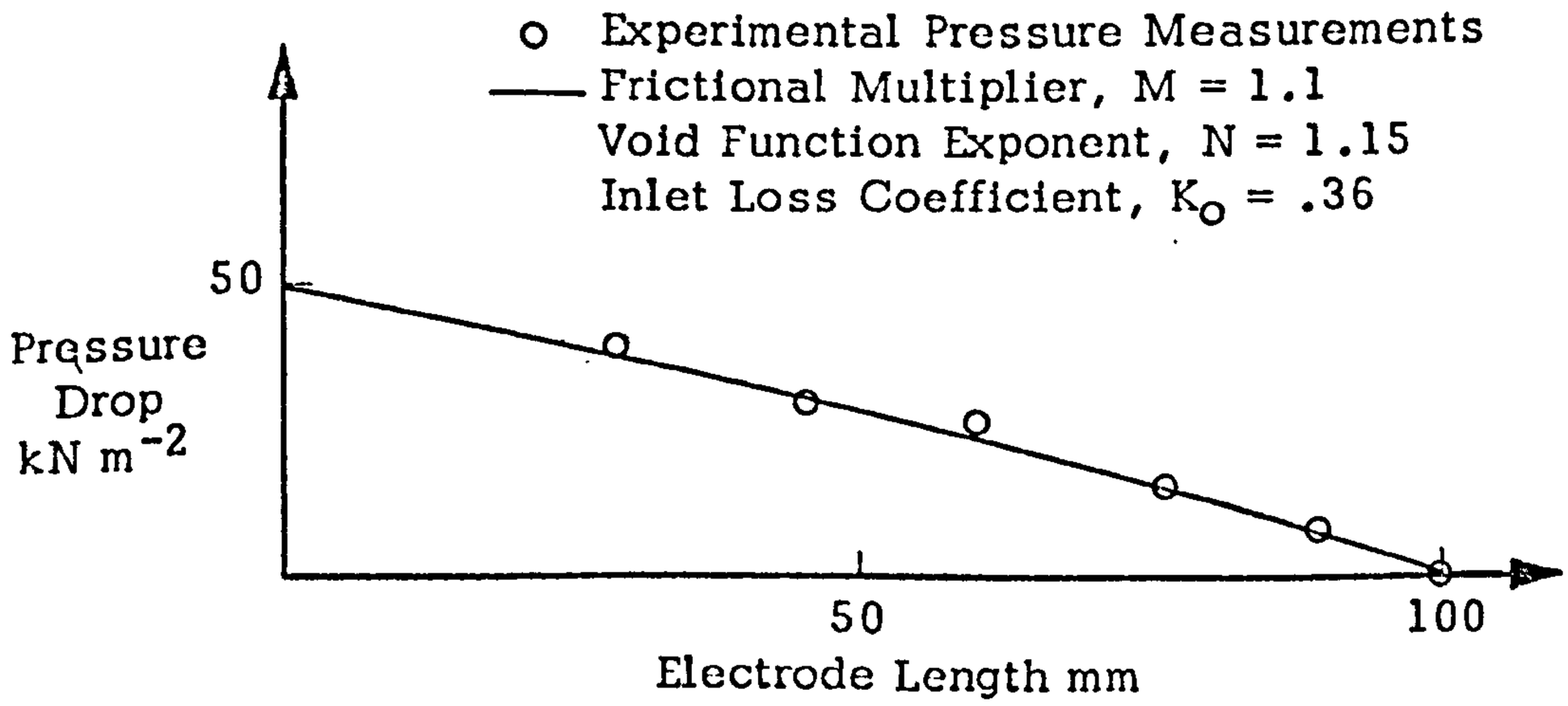

FIG. 2.13 COMPARISON OF THEORETICAL AND EXPERIMENTAL ANODE PROFILE AND PRESSURE DISTRIBUTION

bubbles. The pressure distribution in the gap was almost linear and the anode profile for this test would be predicted with fair accuracy from the algebraic relation, equation (46).

To assess the effect of increase in current density on the anode profile and pressure distribution, the feedrate was increased to 0.80 mm min^{-1}. This resulted in a machining current of 440 A which was close to the maximum available from the power supply. However, inspection of the machined surface of the anode showed small pips at locations corresponding to the pressure tappings. The pips, caused by the smaller electrode gap, resulted in errors in the pressure measurements. To avoid this the electrolyte concentration was increased to 16% such that the electrode gap was similar to that in the previous tests.

The increase in current density accentuated the non-linearity of the anode profile (Fig. 2.14). The frictional multiplier was also greater than in the tests at the lower current density. Further reduction in flowrate from that in Test 9 produced machining failure characteristics similar to those in Test 5.

2.8 Summary

The results verified the theoretical model. However, the assumption of constant gas density is not consistent with the results and a simultaneous solution to equations (45) to (50) is required particularly at high current densities and high pressure drops. The

Test 9

Experimental Data		Computed Data	
Voltage	- 16 V	Current Density	- 34.8 A cm^{-2}
Current	- 447 A	Electrode Gap at Inlet	- .67 mm
Flowrate	- $6.0 \times 10^{-5} m^3 s^{-1}$	Flow Velocity at Inlet	- 7.4 m s^{-1}
Inlet Pressure	- 485 kN m^{-2}	Temperature Increase	- 28.2 K
Outlet Pressure	- 150 kN m^{-2}	Volume Fraction at Outlet	- .389
Temperature Increase	- 27 K		
Electrode Gap at Inlet	- .69 mm		

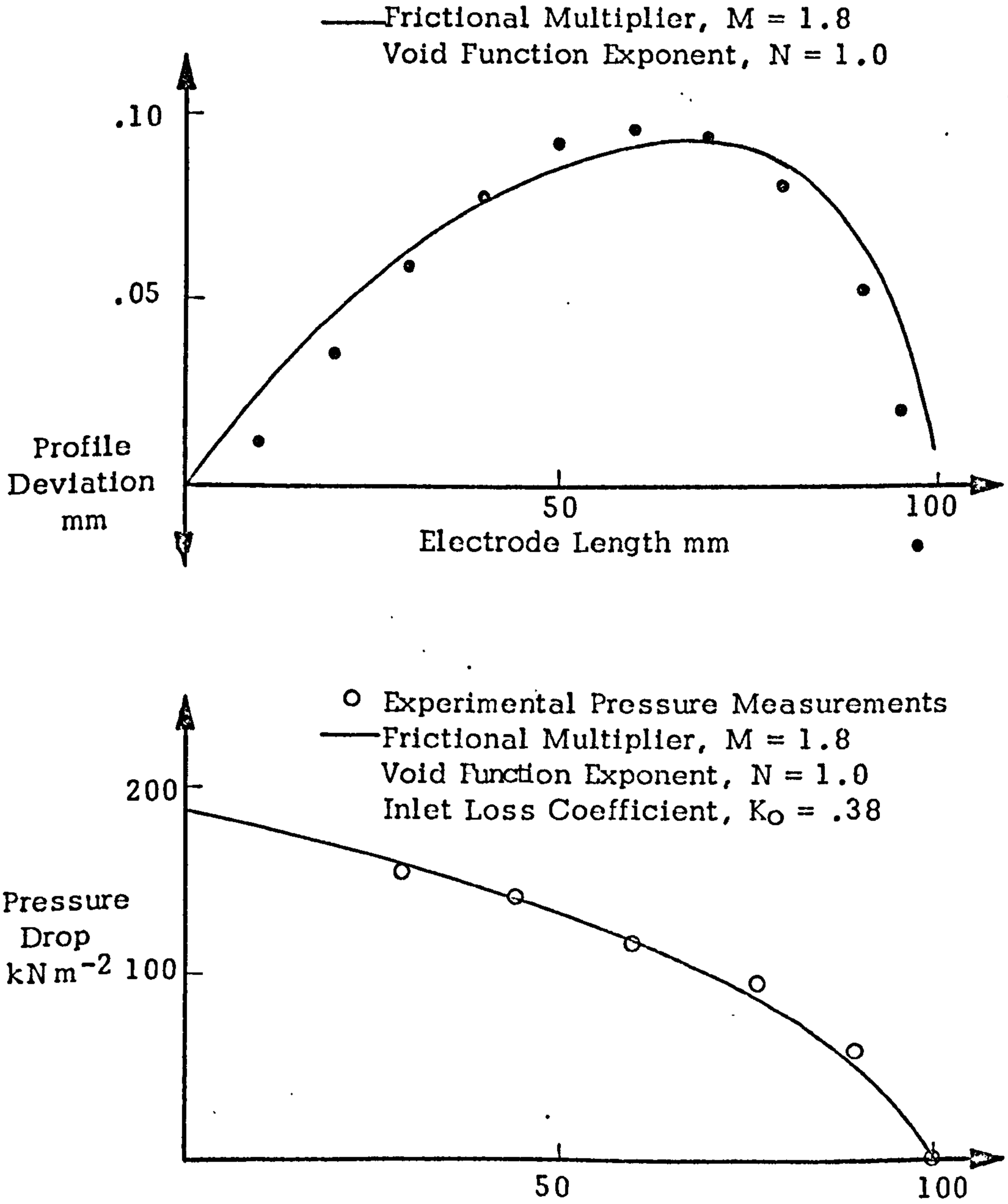

FIG. 2.14 COMPARISON OF THEORETICAL AND EXPERIMENTAL ANODE PROFILES AND PRESSURE DISTRIBUTION

model parameters differ from the previously assumed values (16, 17) and show some dependence on the operating conditions of machining. It was, therefore, considered important that results should be obtained for conditions similar to those in practice. The anode profile is strongly influenced by the current density and outlet pressure but not by the electrolyte flowrate.

A minimum electrolyte flowrate is required for equilibrium machining. Below the minimum flowrate the current becomes less and the electrode gap converges towards the cathode at outlet which would eventually cause sparking across the gap. The cause of machining failure is not apparent but was not investigated further since a fast spark detect system was not available on the small machine.

3.0 EXPERIMENTAL WORK WITH THE ANOCUT MACHINE

The Anocut machine, power supply and auxiliary plant was manufactured by Alfred Herbert Limited under licence from Anocut Engineering Company, U.S.A. A plan of the installation in the Production Engineering Laboratory is shown in Fig. 3.1. The plant also included a cooling system, electrolyte storage tanks and waste tanks.

3.1.1 The Anocut Machine

The machine was a general purpose, vertical 'A' frame type and supported a feed ram situated above a machine table. The feed ram, with 0.45 m stroke, was driven by normal feed and rapid traverse motors at feedrates of 0.3 to 8.0 mm min^{-1} and 600 mm min^{-1} respectively. A counterbalance weight minimised backlash in the ram drive. The ram platen was a 0.30 m square stainless steel plate with a pattern of tapped holes for tool location. The cables from the power supply were attached to the ram internally. Microswitches limited the ram stroke and allowed setting to a predetermined position.

The machine table below the ram was an 0.6 m square granite block with keyways for alignment of the workpiece fixture. The fixture may also be held in position from tapped holes around the granite blocks. The cables for connection to the workpiece entered through a sealing device in the side of the working enclosure. Vertical

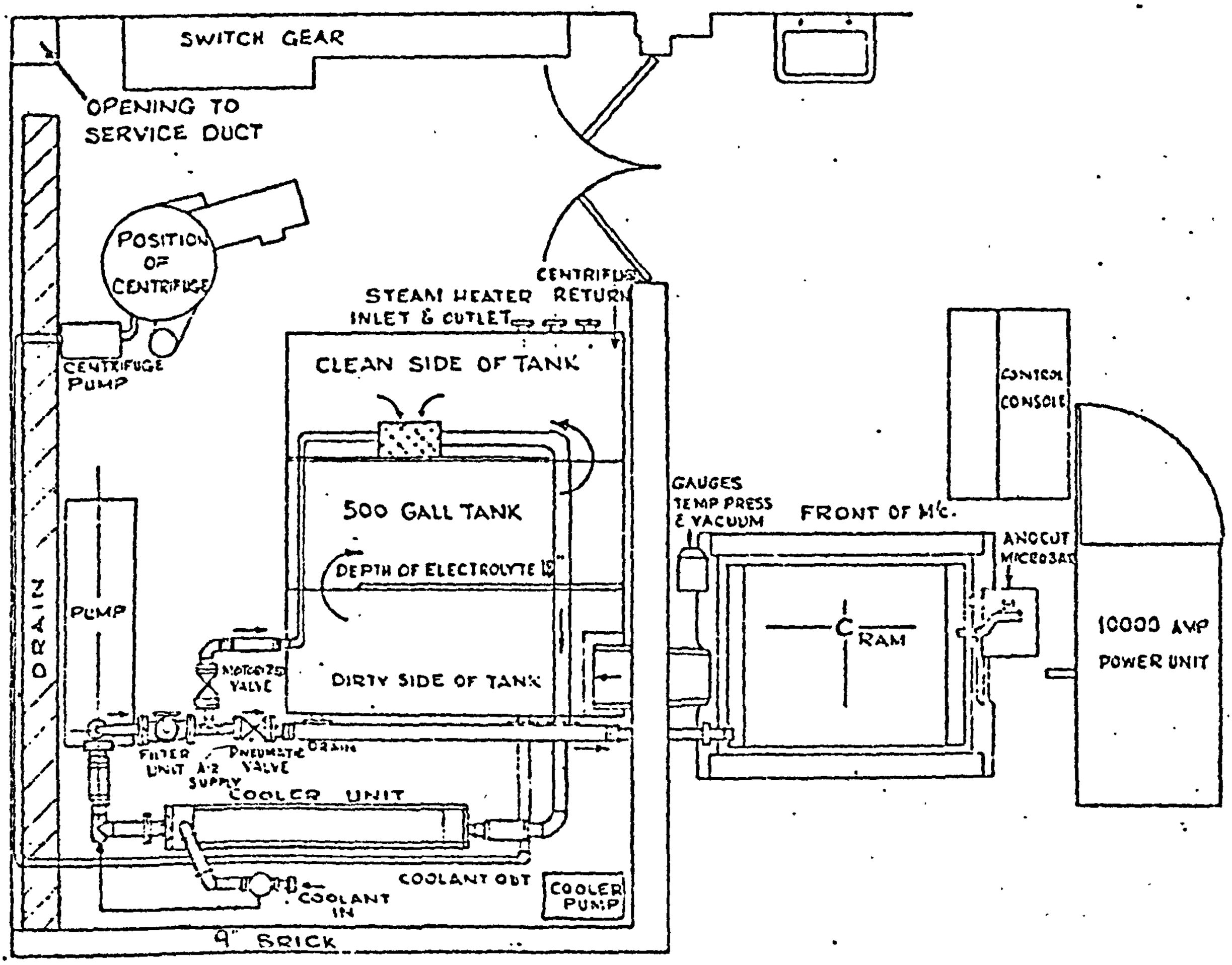

FIG. 3.1 PLAN OF THE ANOCUT INSTALLATION

sliding covers prevented electrolyte splash outwith the machine.

Hydrogen and other gases, produced by the machining process, were removed from the working enclosure and the electrolyte tank by an exhaust fan. The fan motor was interlocked with the power supply so that machining could not occur in the event of malfunction of the fan motor. The machine frame and all metal parts in the working area were at negative potential for corrosion protection.

3.1.2 The Power Supply

The power supply was a low voltage, direct current rectifier operating from a 550 A, 440 V, 3 phase supply. The output voltage, of from 0-24 V, was stabilised, against load current and mains voltage variation, within $\pm$ .05 V. by silicon controlled rectifiers. The maximum direct current capacity was 10,000 A.

Sparks can occur across the electrodes during machining and cause damage to the power supply and to the tool. To reduce or prevent damage the power supply had a 'Microbar' device connected across the positive and negative conductors leading to the machine. The device utilised a crow-bar circuit such that the supply of current to the work was cut off by a short circuit across the power cables. The short circuit was accomplished by a bank of silicon controlled rectifiers which became conductive very rapidly when a spark was detected. The sensitivity of the 'Microbar' unit was adjustable and in the course of the experimental work a sensitivity of 75% was used.

This prevented visible damage to the workpiece and tool.

The power supply was also provided with a fault-finding system which indicated the type of fault on the control console. Rising current and falling current trip units may be used to detect rapid change in machining current. These are controlled by variable resistors on the console such that trip sensitivity was adjustable. A red pointer on the ammeter could be set to trip the machining current at any required value. The control console also indicated contact between the work and tool. The detection of one of these faults short-circuited the power supply, stopped the ram drive and the nature of the fault was indicated on the console.

The power supply was interlocked with the electrolyte pump and the spark protection system was only energised when normal feed was engaged. Various other safety devices protected the power supply and safeguarded the operator.

3.1.3 The Electrolyte System

The electrolyte was contained in a 2.3 m^3 stainless steel tank fitted with covers to minimise evaporation losses. Baffles in the tank reduced mixing between the electrolyte returning to the tank and the clean electrolyte. The electrolyte was drawn from the clean side of the tank and supplied to a manifold in the working enclosure by a 56 kW centrifugal pump with a nominal capacity of 15×10^{-4} m^3 s^{-1} at 1400 kN m^{-2}. With the pneumatic valve (shown in Fig. 3.1) open, the delivery pressure of electrolyte to the machine

was controlled, by a by-pass valve, from the control console.

During the machining process, heat is generated in the electrolyte by the power loss in the electrode gap and by the pump. To control the electrolyte temperature, the electrolyte was drawn from the tank through a heat exchanger. A thermostat valve regulated the flowrate of cooling water to the heat exchanger. The valve was adjustable to allow selection of electrolyte temperature. Steam heaters immersed in the tank allowed the temperature to be increased at the beginning of a shift.

A drain at the side of the working enclosure returned the electrolyte to the tank. A pump drew the electrolyte from this side of the tank and delivered it to a centrifuge which removed the metal hydroxides from the electrolyte. The sludge from the centrifuge was discharged, at pre-set time intervals, to tanks in the basement. Filters in the tank and on the delivery side of the pump prevented small particles in the electrolyte from entering the workpiece-tool fixture.

3.2 Operation and Instrumentation of the Anocut Machine

The operator console provided for the control of the ram drive, the electrolyte system and the power supply.

The ram position was indicated by a pointer on a scale and by an 0.01 mm dial gauge adjacent to the working enclosure. The feedrate was set prior to machining with a variable speed control and was displayed on a meter on the console.

The electrolyte pump was operated at the console; the supply pressure was regulated by a bar knob which actuated the by-pass valve. The electrolyte supply temperature was measured in the inlet manifold and displayed close to the working enclosure.

Machining voltage was measured from voltage sensing leads attached to the workpiece and tool. The output voltage from the power supply was also measured. The machining current was displayed on the console by an ammeter.

3.2.1 Additional Instrumentation

To allow feedrate setting with accuracy, the feedrate was calibrated with respect to the position indicator of the multi-turn control knob of the variable speed drive. The electrolyte flowrate was measured with an orifice plate in conjunction with mercury and bromoform manometers. The orifice plate was made to the specifications in B.S. 1042 and calibrated with a weighing tank. Valves at inlet and outlet to the workpiece-tool fixture allowed control of flowrate and outlet pressure.

In the initial tests, the electrolyte inlet and outlet temperatures were measured with thermometers. However, thermistors were used for most of the work to provide a continuous record of temperatures. The thermistors also facilitated the control of electrolyte inlet temperature. The machining current was also displayed on the Rikadenki pen recorder using a 50 mV, 5000 A shunt in series with the power supply. An integrating milli-voltmeter measured the product of machining current and time.

The specific gravity of the electrolyte was measured with a hydrometer. The electrolyte properties could then be determined from reference data in Appendix III.

3.3 The Machining Cell

The workpiece-tool fixture (Fig. 3.2) was designed and manufactured by the Manufacturing Methods Development Department of Rolls-Royce (Hillington) Limited.

The machining cell was machined from Tufnol grade GF/45 which has high strength and low moisture absorption. This material is used extensively for insulation purposes in tooling fixtures in industrial electrochemical machining. The cell was made in two halves with the side dimensions machined from the halves and with provision for electrolyte inlet and outlet. The halves were located with two dowel pins. Six bolts, clamped the halves onto the workpiece and tool. The cell was a force fit on the tool to minimise sideflow past the electrodes.

The brass tool was brazed to the shaft and located in a flange bolted to the ram platen. A recess was machined in the stainless steel baseplate to give lateral location to the workpiece which was clamped with two socket cap screws. The base plate was bolted to a machine square set onto the granite machine table.

Provision was made in the cell for the measurement of inlet and outlet pressures using Bourdon gauges. The thermistors were set into stainless steel tubes with an insulating grade of Araldite. The stainless

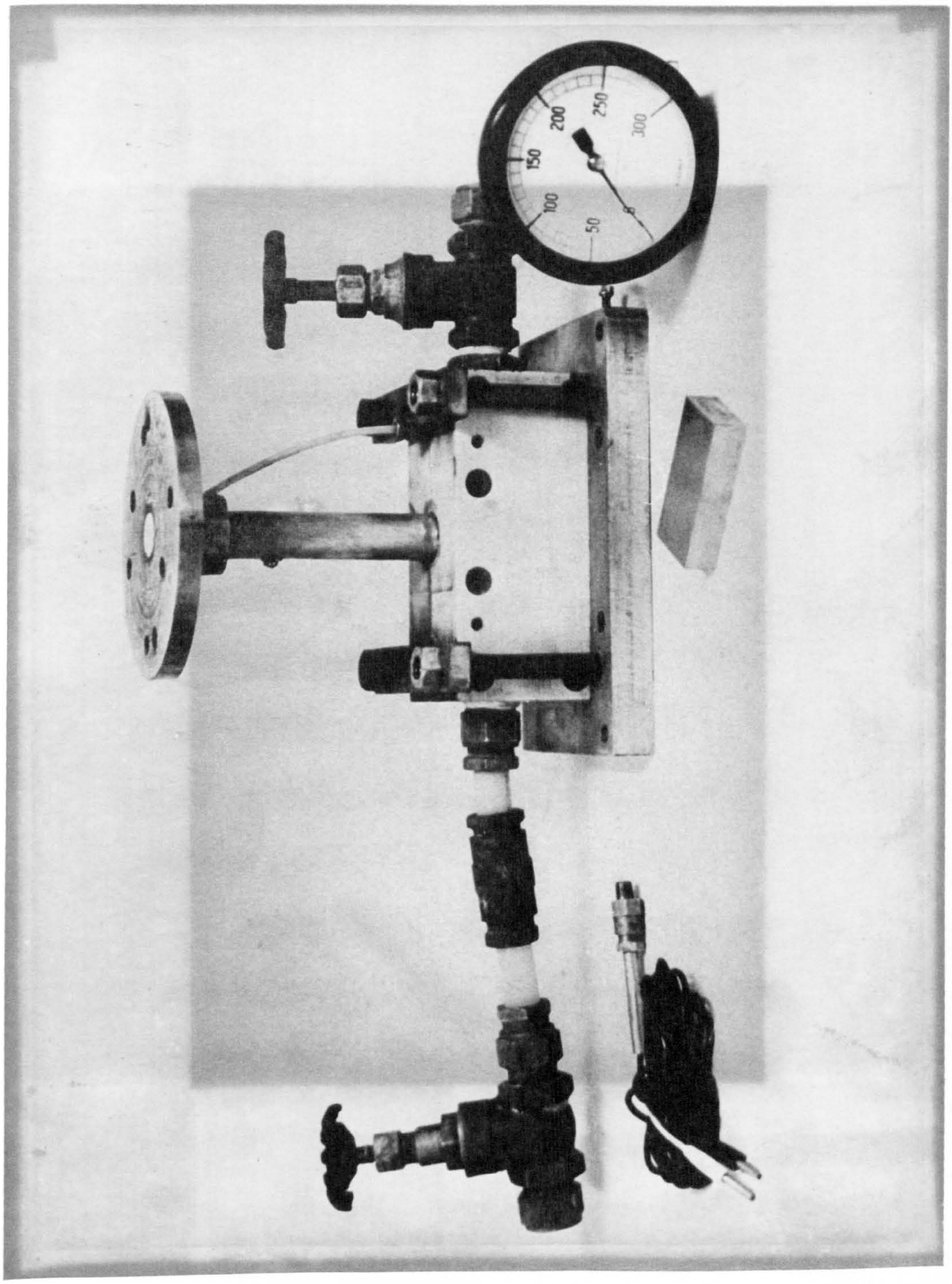

FIG. 3.2 THE MACHINING CELL

steel tubes were inserted into parallel fittings in the nylon piping at inlet and outlet to the cell such that the thermistors tips were exposed to the electrolyte flow.

3.4 Experimental Procedures

An initial series of tests was carried out to gain experience in the use of the machine and ancillary plant and to establish suitable operating conditions.

The machining cell was assembled on the machine table and the tool shaft flange bolted to the ram platen. The baseplate of the machining cell was aligned by traversing the ram until the tool fitted exactly into the baseplate recess. A surface ground workpiece was fitted into the recess and identical slip gauges placed at each end. The tool was jogged down until contact with the slips was indicated on on the control console. The workpiece was clamped in position. The parallelism of the tool and workpiece faces was assessed with feeler gauges and shims could be inserted beneath the baseplate.

To reduce the time taken for machining to attain equilibrium conditions, the initial gap was set close to that theoretically required. The machining cell was then clamped to the baseplate.

The electrolyte pump was started and the pneumatic valve opened. The inlet pressure was set by controlling the by-pass valve. The electrolyte temperature at inlet was monitored from the pen recorder. The thermostat valve, regulating the cooling water flow, was not

particularly effective. A sudden reduction in flowrate, such as at the beginning of a test, could produce quite a large change in the electrolyte supply temperature. To prevent this the flowrate, prior to a test, was restricted with the outlet pressure valve and the valve opened in the initial period of the test. Experience in the use of the plant and the relatively short test times allowed temperature control within $\pm 1^{o}C$ throughout each test. The electrolyte specific gravity also required frequent checks as evaporation from the tank increased the concentration. Water was added to the tanks to offset evaporation losses. The centrifuge was kept in operation throughout the tests to maintain a reasonable degree of electrolyte purity.

The feedmotor was switched on and the feedrate set with the drive clutch disengaged. The machining power and ram drive were started simultaneously. An assistant timed the test and checked the feedrate from the dial gauge. The voltage was set to the required value. When the machining current reached equilibrium the inlet and outlet pressures and electrolyte flowrate were noted at intervals for a further two to four minutes. The inlet and outlet temperatures were displayed alternately on the recorder with a switchbox.

The machining power and ram drive were switched off at the same time. The tool downfeed, test time and the reading from the integrating millivoltmeter were recorded. The electrolyte pump was switched off.

The machining cell was raised onto the tool shaft. The electrode gap at inlet was measured with feeler gauges. The dial gauge was set

to zero and the tool moved slowly down onto the workpiece until contact was indicated on the control console. The minimum electrode gap width was taken to be the distance traversed by the tool. The use of optical methods of gap measurement were impracticable due to the limited space available and the severe corrosion conditions in the working enclosure.

A black film was observed on the cathode after machining. The film was easily removed by rubbing with a damp cloth. The formation of such films may be the result of electro-phoresis (6) and can cause a potential loss at the cathode surface.

The weight, dimensions and profile deviation of the workpiece were measured. Tests at constant operating conditions gave anode profiles which were repeatable within $\pm$ 0.025 mm along the electrode length. The surface finish, at 10 mm from inlet, the centre and 10 mm from outlet, was measured with a Rank Taylor Hobson Talysurf machine.

3.5 The Selection of Operating Conditions

An initially plane and parallel electrode configuration was used for the reasons discussed in Chapter 2. The electrode dimensions were specified in the design of the machining cell by Rolls-Royce (Hillington) Limited and were 76.0 mm in the direction of flow and 38.0 mm wide.

Sodium nitrate and sodium chloride solution were the electrolytes. A concentration of 32% was chosen for the sodium nitrate solution. Further increase in concentration gives small increase in conductivity

(Appendix III, Fig. A8) and complete dissolution of the salt in the tank is difficult. A 14% concentration of sodium chloride was required to give a similar conductivity to that of the sodium nitrate solution. The electrolyte supply temperature was 40°C. The cooling systems of production machines are designed to operate at temperatures in this range and evaporation losses are minimised.

The remaining operating conditions to be specified were the tool feedrate, machining voltage, electrolyte flowrate and outlet pressure. A large number of tests would be required to assess the effect of varying one operating condition while maintaining the others at constant values. As an alternative, the tool feedrate, the most important operating condition, was kept constant and two levels of the outlet pressure and machining voltage were established. A range of flowrates was required at each combination to investigate the upper and lower bounds to the electrolyte velocity. From the initial series of tests a base feedrate of 1 mm min^{-1} allowed a range of flowrates to be used at machining voltages of 10 and 20 V. At the same feedrate and at the upper voltage level, outlet pressures of 170 and 800 kN m^{-2} were found to be suitable. The feedrate was then increased at each voltage level to determine the maximum feedrate. These operating conditions cover the range used in practice for die sinking or forming operations.

The results are presented in sections on metal removal rates, workpiece profile deviations and limitations on the metal removal rate.

3.6 Experimental Results

3.6.1 Metal Removal Rates

Metal removal rates were investigated under equilibrium machining conditions with sodium chloride and sodium nitrate electrolytes. In Fig. 3.3 the metal removal rate is shown against current density. The current density was calculated from the product of machining current and time, recorded by the integrating millivoltmeter, divided by the electrode area and test time. A sample of readings from the millivoltmeter was checked by measuring the area under the current time chart with a planimeter and good agreement was observed. The variation in current density for a given feedrate was due mainly to the time taken to reach equilibrium conditions.

The theoretical metal removal rates predicted from Faradays laws for valencies of dissolution of two and three are shown. For machining tests with the sodium chloride solution, the metal removal rate was in agreement with a valency of two. Current efficiencies, based on weight loss measurements, were within $\pm$ 3% of 100%. Current density or feedrate applied voltage and electrolyte flowrate had no effect on the current efficiency. For tests using the sodium nitrate electrolyte metal removal rates showed relatively poor agreement with a valency of three. Current efficiencies at the higher current densities were of the order of 110 to 120% for a valency of three, or 73 to 80% for a valency of two. At the lowest current density the current efficiencies ranged from 76 to 89% for a valency of three or 50 to 59% for a valency of two and became less with decrease in flowrate.

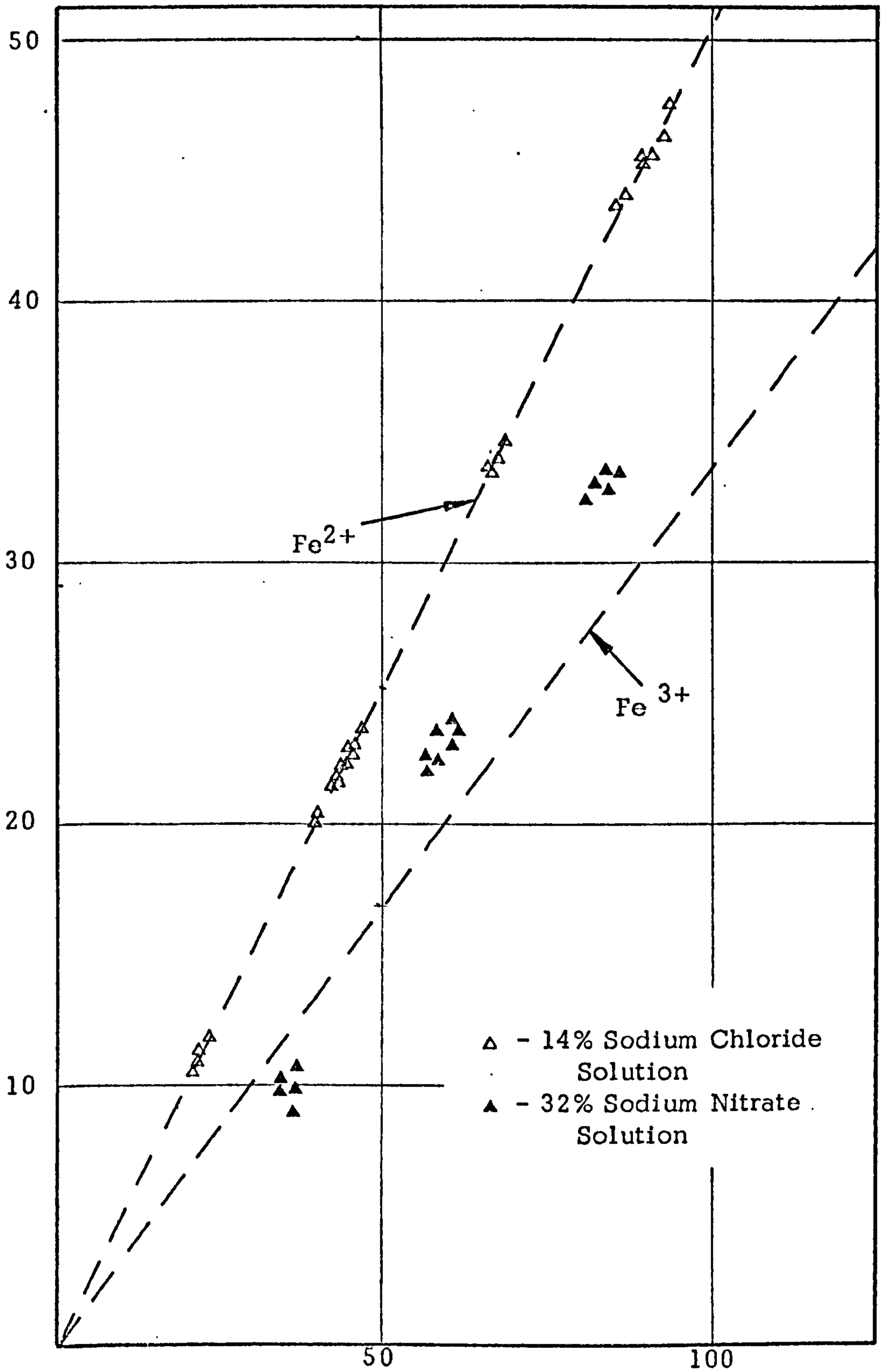

FIG. 3.3 METAL REMOVAL RATE AGAINST CURRENT DENSITY

A greenish-black precipitate formed in the sodium chloride solution indicating the presence of ferrous hydroxide ($Fe(OH)_2$) whereas a reddish-brown precipitate in the nitrate electrolyte indicated ferric hydroxide ($Fe(OH)_3$). A similar result has been obtained by Mao (48).

The appearance of the machined surfaces was quite different for the two electrolytes. The sodium chloride electrolyte produced surfaces which were smooth but not polished and were the colour of conventionally machined mild steel. This type of finish suggests activation control. In contrast the test specimens machined using sodium nitrate were dark brown and became darker in the direction of flow. The edge definition was sharper. These factors indicate the formation of a thin, electronically conducting, oxide film on the surface (30) and that machining is in the transpassive mode (39). The low current efficiencies for the nitrate solution relative to those for the chloride solution, for a valency of two, may be the result of some iron being dissolved as ferric ions or that part of the current was consumed in generating oxygen at the anode surface. The ferrous hydroxide may react with the oxygen to form ferric hydroxide:

$$4\ Fe(OH)_2 + 2\ H_2O + O_2 \rightarrow 4\ Fe(OH)_3$$

The averaged surface finish measurements for the workpieces is shown (Fig. 3.4). Very little variation was evident with current density, machining voltage and electrolyte flowrate. The finish of the workpieces machined with sodium nitrate solution was slightly better than those with sodium chloride solution.

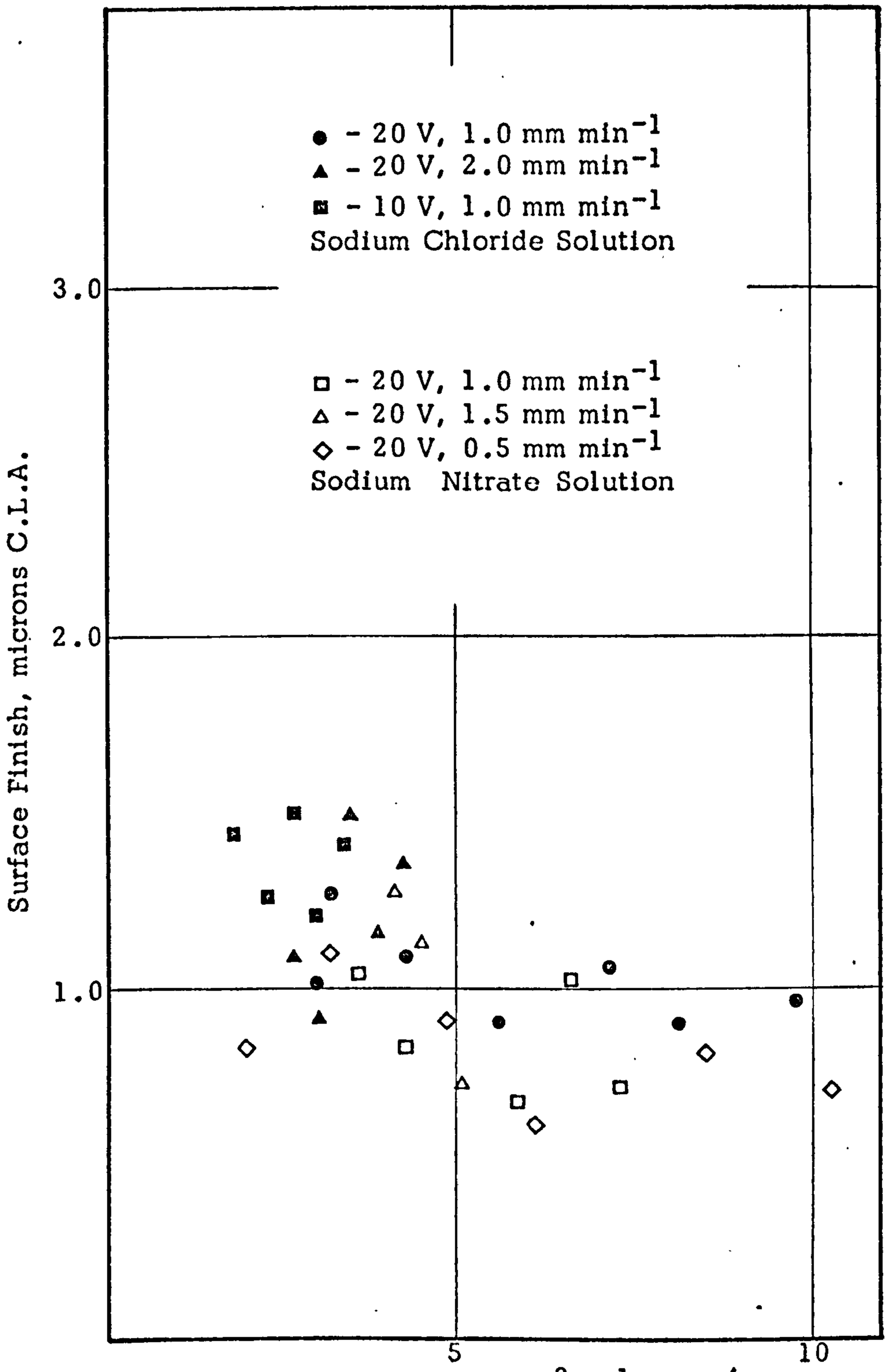

FIG. 3.4 MACHINED SURFACE FINISH

3.6.2 Workpiece Profile Deviations

At equilibrium conditions of machining the tool feedrate is equalled by the anode dissolution rate and the electrode gap becomes constant. Equilibrium conditions in tests were indicated by a constant machining current, electrolyte flowrate and outlet temperature. Workpiece profile deviations from that of the tool are caused by variation in electrolyte conductivity along the electrode length. For the purposes of presentation an increase in gap width in the direction of flow is assumed positive and a decrease as negative.

The first test series at constant operating conditions is presented in Table 2. The corresponding profile deviations are shown in Figs. 3.5 and 3.6. An initial test was required for any series of given operating conditions to set the machining voltage and tool feedrate. The machining currents were within $\pm$ 4% of the theoretical value of 1295 A for a feedrate of 1.0 mm min^{-1}. The measured inlet gap widths for most of the tests were greater than the theoretical value of 0.883 mm. This may be due to the method of determining the activation overpotential (Appendix I). However, the accuracy of gap measurement was not considered sufficient to justify experimentally determined overpotentials.

The matching procedure for the model parameters was carried out to fit the experimental anode profiles. An inlet loss coefficient of 0.35 was assumed, consistent with the loss coefficients determined experimentally in Chapter 2. In general the gap width increased along

Test No.	Machining Current A	Electrolyte Flowrate $m^3s^{-1} \times 10^{-4}$	Inlet Pressure $kN\ m^{-2}$	Outlet Pressure $kN\ m^{-2}$	Temperature Increase K	Inlet Gap Width $m \times 10^{-3}$	Computed Current A
1-02	1250	9.8	1620	300	7.0	0.87	1295
1-03	1280	8.1	1350	250	9.0	0.93	1295
1-04	1280	7.1	1050	230	9.8	0.94	1295
1-05	1310	5.6	830	200	13.2	0.86	1295
1-06	1330	4.3	580	180	15.8	0.90	1295
1-07	1300	3.2	480	165	19.5	0.92	1295
1-08	1290	3.0	460	170	23.2	0.96	1295
1-09			Machining Failure Conditions				

Operating Conditions: Machining Voltage - 20 V
Tool Feedrate - 1.0 mm min^{-1}
Sodium Chloride Solution at 14% Concentration
Electrolyte Inlet Temperature - 40°C

TABLE 2

Test 1-02

Computed Data

Current Density - 44.9 A cm^{-2}
Electrode Gap at Inlet - .883 mm
Flow Velocity at Inlet - 29.2 m s^{-1}
Temperature Increase - 6.55 K
Void Fraction at Outlet - .056

• Experimental Gap Profile
—— Frictional Multiplier, M = 2.1,
Void Function Exponent, N = 0.3.

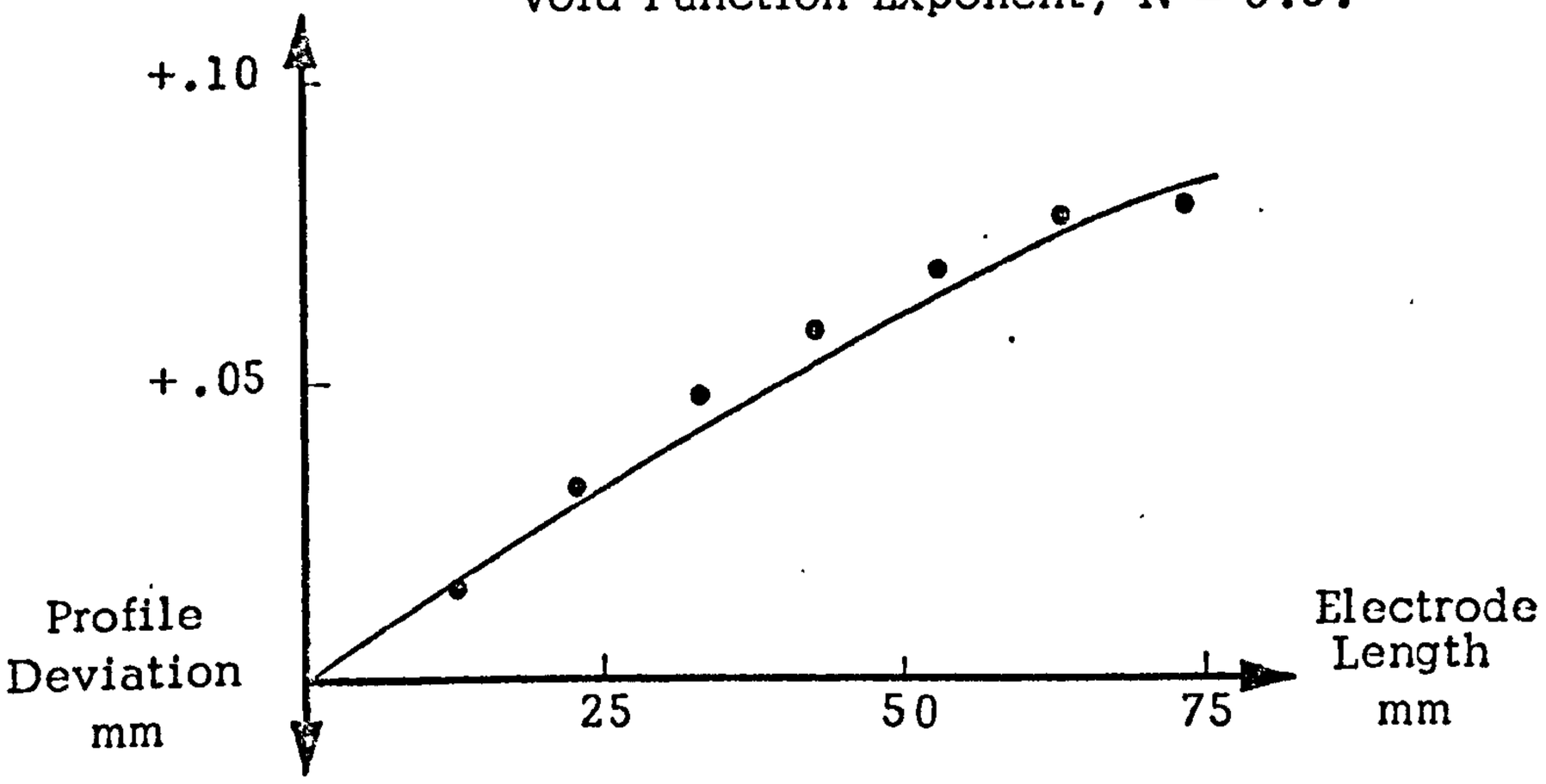

Test 1-03

Computed Data

Current Density - 44.9 A cm^{-2}
Electrode Gap at Inlet - .883 mm
Flow Velocity at Inlet - 23.97 m s^{-1}
Temperature Increase - 7.9 K
Void Fraction at Outlet - .079

• Experimental Gap Profile
—— Frictional Multiplier, M = 2.6
Void Function Exponent, N = 0.5

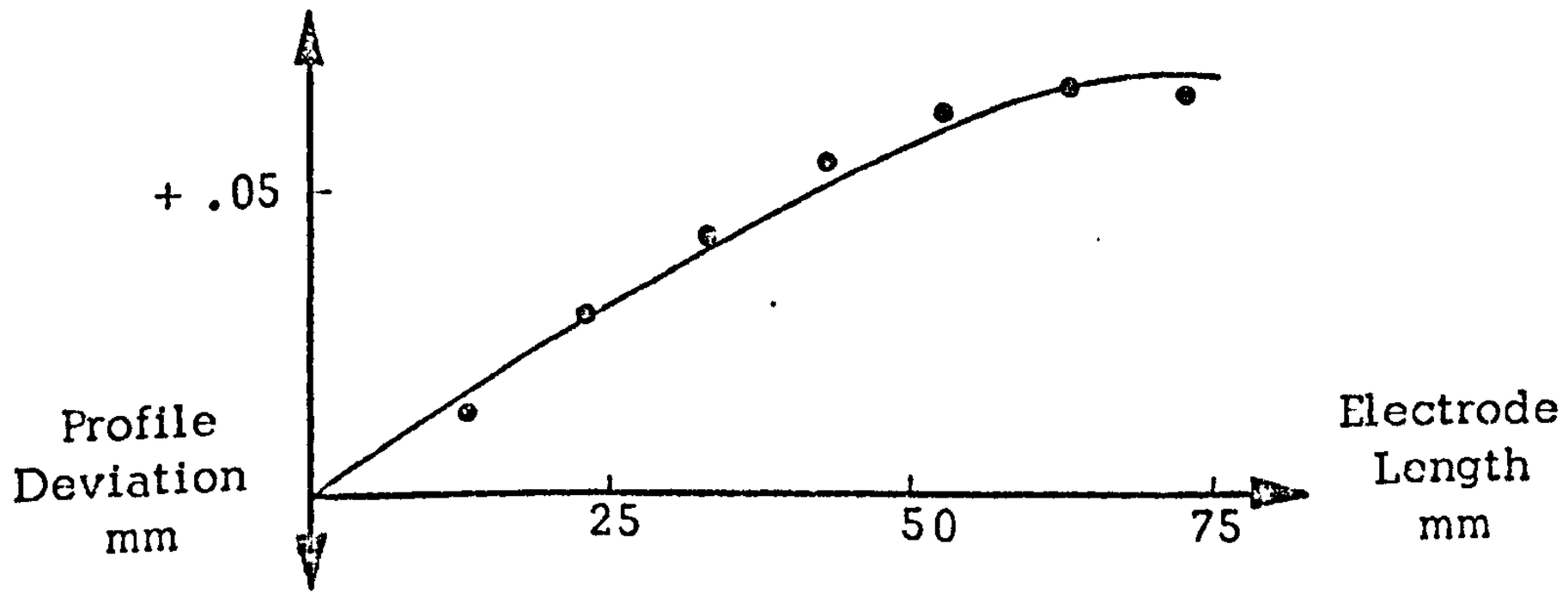

FIG. 3.5 COMPARISON OF THEORETICAL AND EXPERIMENTAL ANODE PROFILES

Test 1-05
Computed Data

Current Density - 44.9 A cm^{-2}
Electrode Gap at Inlet - .883 mm
Flow Velocity at Inlet - 16.7 m^{-1}
Temperature Increase - 11.9 K
Void Fraction at Outlet - .141

• Experimental Gap Profile
—— Frictional Multiplier, M = 2.5
Void Function Exponent, N = 0.9

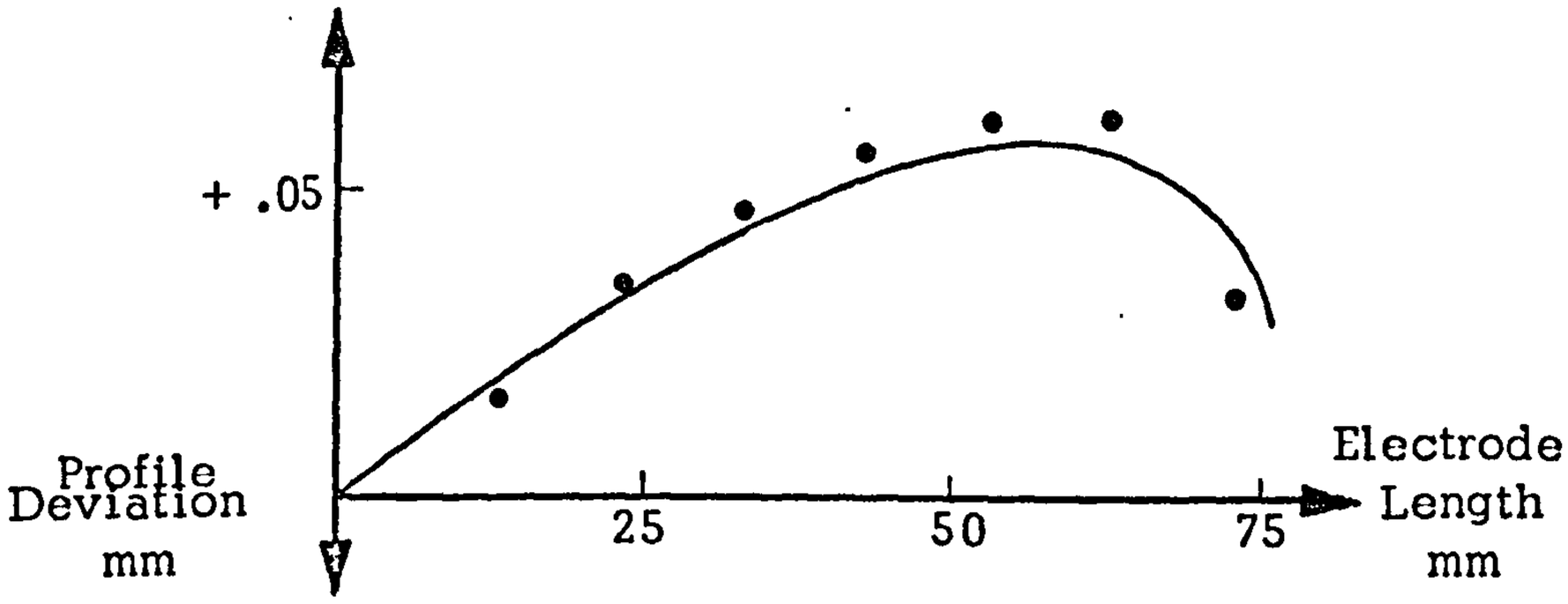

Test 1-07
Computed Data

Current Density - 44.8 A cm^{-2}
Electrode Gap at Inlet - .883 mm
Flow Velocity at Inlet - 9.54 m s^{-1}
Temperature Increase - 21.0 K
Void Fraction at Outlet - .262

• Experimental Gap Profile
—— Frictional Multiplier, M = 2.8,
Void Function Exponent, N = 1.2.

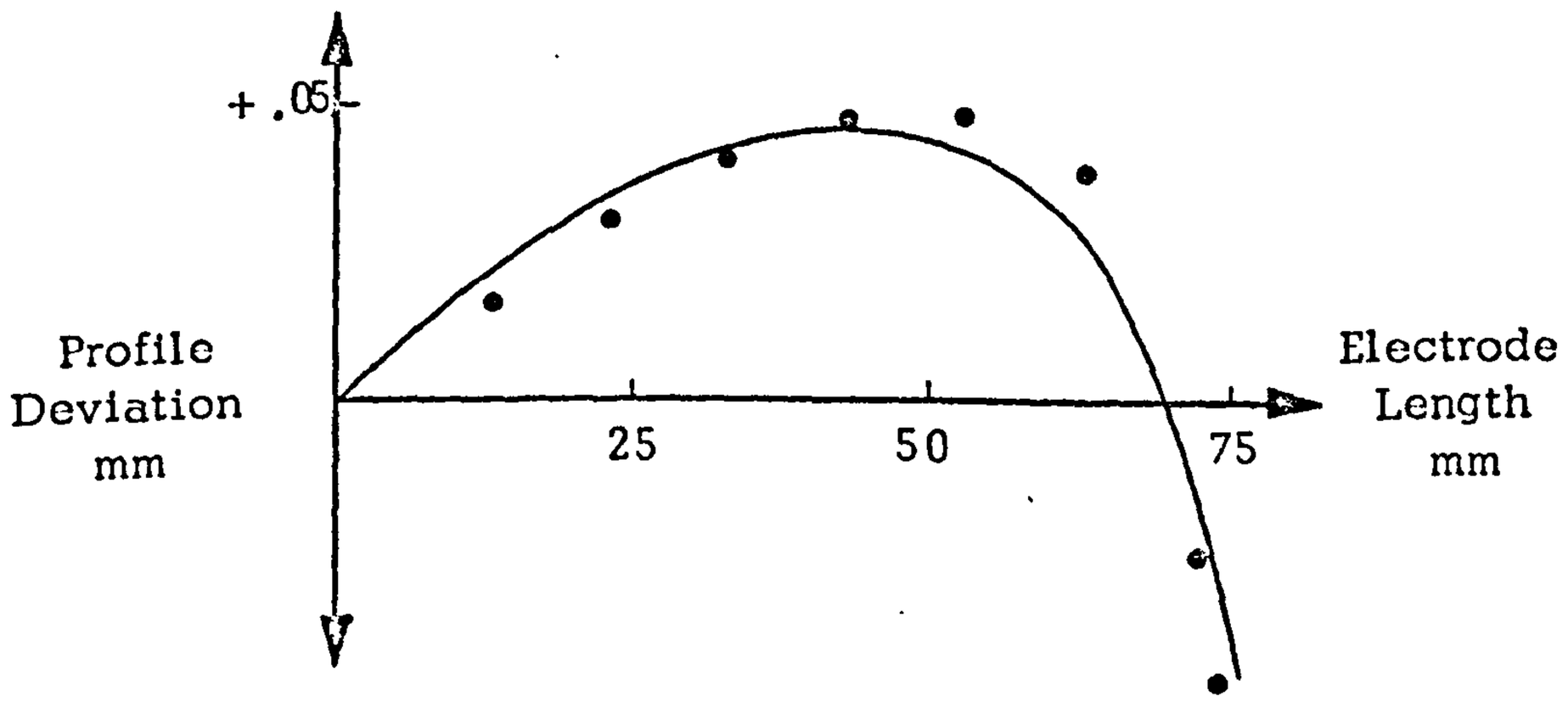

FIG. 3.6 COMPARISON OF THEORETICAL AND EXPERIMENTAL ANODE PROFILES

the electrode length. The effect of flowrate variation was small over the first 50 mm of the electrodes. The temperature gradient along the electrode length is inversely proportional to flow velocity whereas the pressure at inlet increases with the square of velocity. Thus reducing the flowrate increased the electrolyte temperature at a point in the gap but the effect on electrolyte conductivity was balanced by the increased volume of gas bubbles. At the lower flowrates the anode profile became distinctly non-linear towards outlet.

The model parameters required to fit the experimental anode profiles, showed dependence on the electrolyte flowrate. The frictional multiplier increased from 2.1 to 2.8 over the range of flowrates and the void function exponent increased from 0.3 to 1.2.

A series of tests at an outlet pressure of 800 kN m^{-2} is presented in Table 3 with corresponding anode profiles in Figs. 3.7 and 3.8. The machining current and inlet gap width were independent of outlet pressure. However, the volume of gas bubbles was significantly less than at the lower pressure such that the effect of gas bubbles on the electrolyte conductivity was small. At the lowest flowrate, the electrode gap increased by almost half from inlet to outlet. The anode profiles were linear and would be predicted accurately from the constant gas density model. The model parameters were lower than those in Figs. 3.5 and 3.6 and showed less dependence on the electrolyte flowrate.

Tests at a machining voltage of 20 V and a feedrate of 2.0 mm min^{-1} are presented in Table 4 and in Fig. 3.9. Increase in feedrate or current

Test No.	Machining Current A	Electrolyte Flowrate $m^3 s^{-1} \times 10^{-4}$	Inlet Pressure $kN\ m^{-2}$	Outlet Pressure $kN\ m^{-2}$	Temperature Increase K	Inlet Gap Width $m \times 10^{-3}$
1-11	1320	7.5	1620	800	8.5	0.88
1-12	1320	6.8	1480	800	9,5	0.91
1-13	1390	5.7	1150	800	12.7	0.94
1-14	1350	4.3	1050	800	18.5	0.94
1-15	1310	2.5	890	800	32.5	0.90
1-16	1370	1.8	860	800	43.0	0.92
1-17		Machining Failure Conditions				

Operating Conditions: Machining Voltage - 20 V
Tool Feedrate - 1.0 mm min^{-1}
Sodium Chloride Solution at 14% Concentration
Electrolyte Temperature at Inlet - 40°C

TABLE 3

Test 1-11
Computed Data

Current Density - 44.9 A cm^{-2}
Electrode Gap at Inlet - .883 mm
Flow Velocity at Inlet - 22.23 m s^{-1}
Temperature Increase - 8.51 K
Void Fraction at Outlet - .029

• Experimental Gap Profile
—— Frictional Multiplier, M = 1.2
Void Function Exponent, N = 0.0

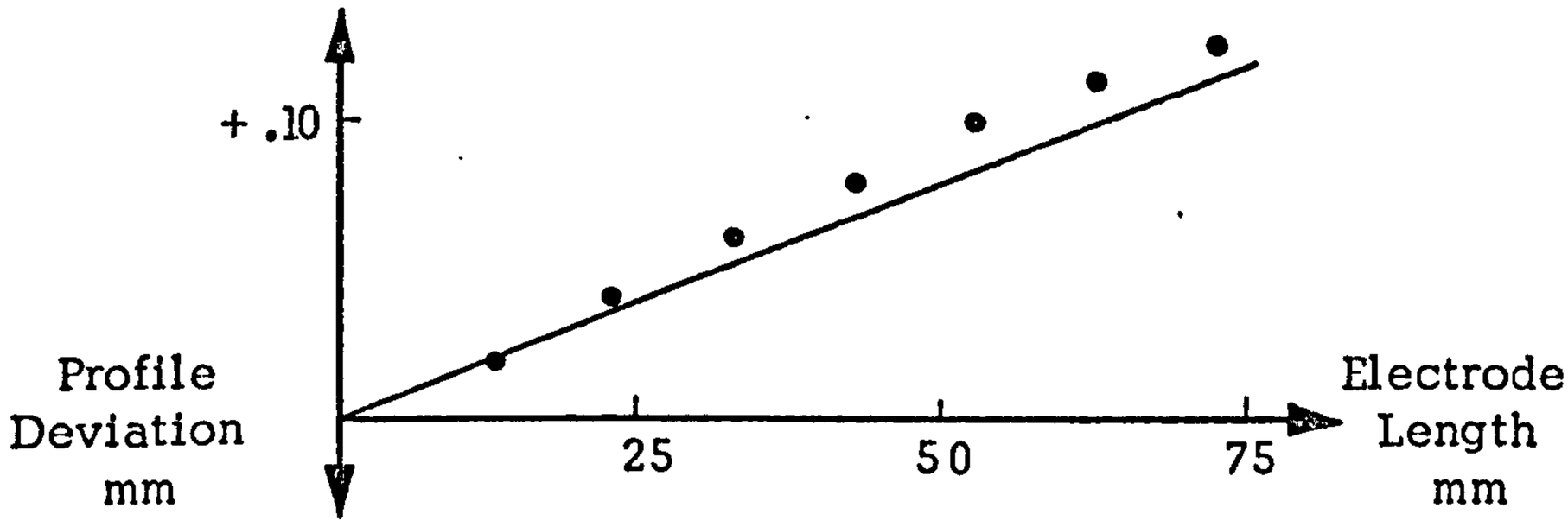

Test 1-13
Computed Data

Current Density - 44.9 A cm^{-2}
Electrode Gap at Inlet - .883 mm
Flow Velocity at Inlet - 16.95 m s^{-1}
Temperature Increase - 11.8 K
Void Fraction at Outlet - .039

• Experimental Gap Profile
—— Frictional Multiplier, M = 1.2
Void Function Exponent, N = 0.3

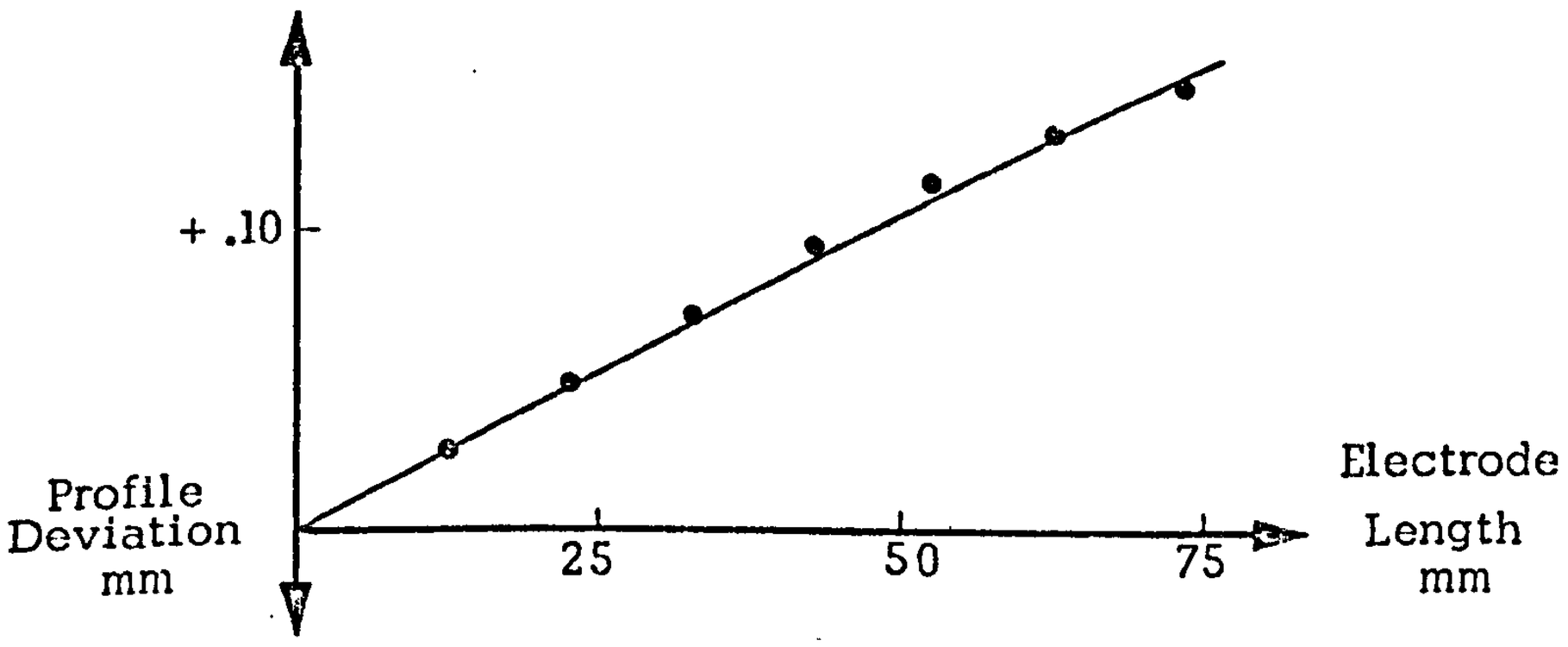

FIG. 3.7 COMPARISON OF THEORETICAL AND EXPERIMENTAL ANODE PROFILES

Test 1-15
Computed Data

Current Density - 44.9 A cm^{-2}
Electrode Gap at Inlet - .883 mm
Flow Velocity at Inlet - 7.42 m s^{-1}
Temperature Increase - 26.4 K
Void Fraction at Outlet - .087

• Experimental Gap Profile
—— Frictional Multiplier, M = 1.8
Void Function Exponent, N = 0.3

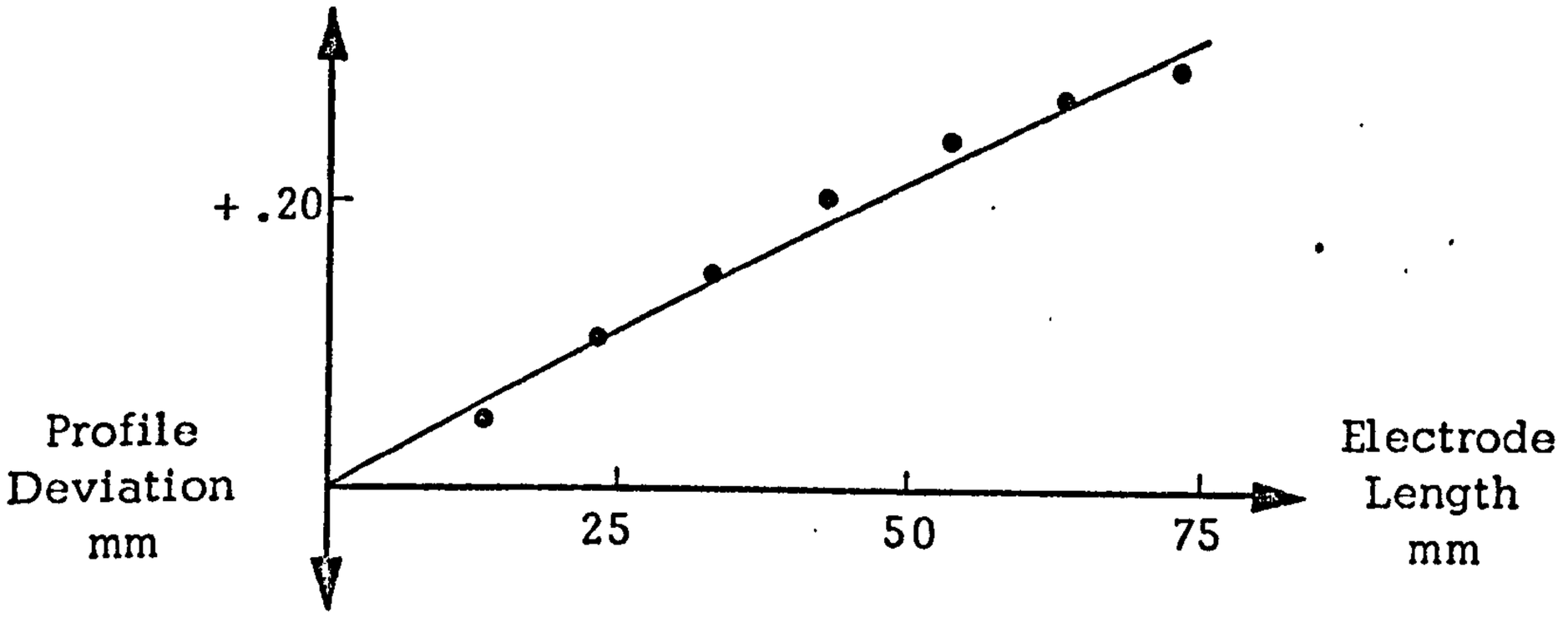

Test 1-16
Computed Data

Current Density - 44.9 A cm^{-2}
Electrode Gap at Inlet - .883 mm
Flow Velocity at Inlet - 5.34 m s^{-1}
Temperature Increase - 37.8 K
Void Fraction at Outlet - .121

• Experimental Gap Profile
—— Frictional Multiplier, M = 2.1
Void Function Exponent, N = 0.4

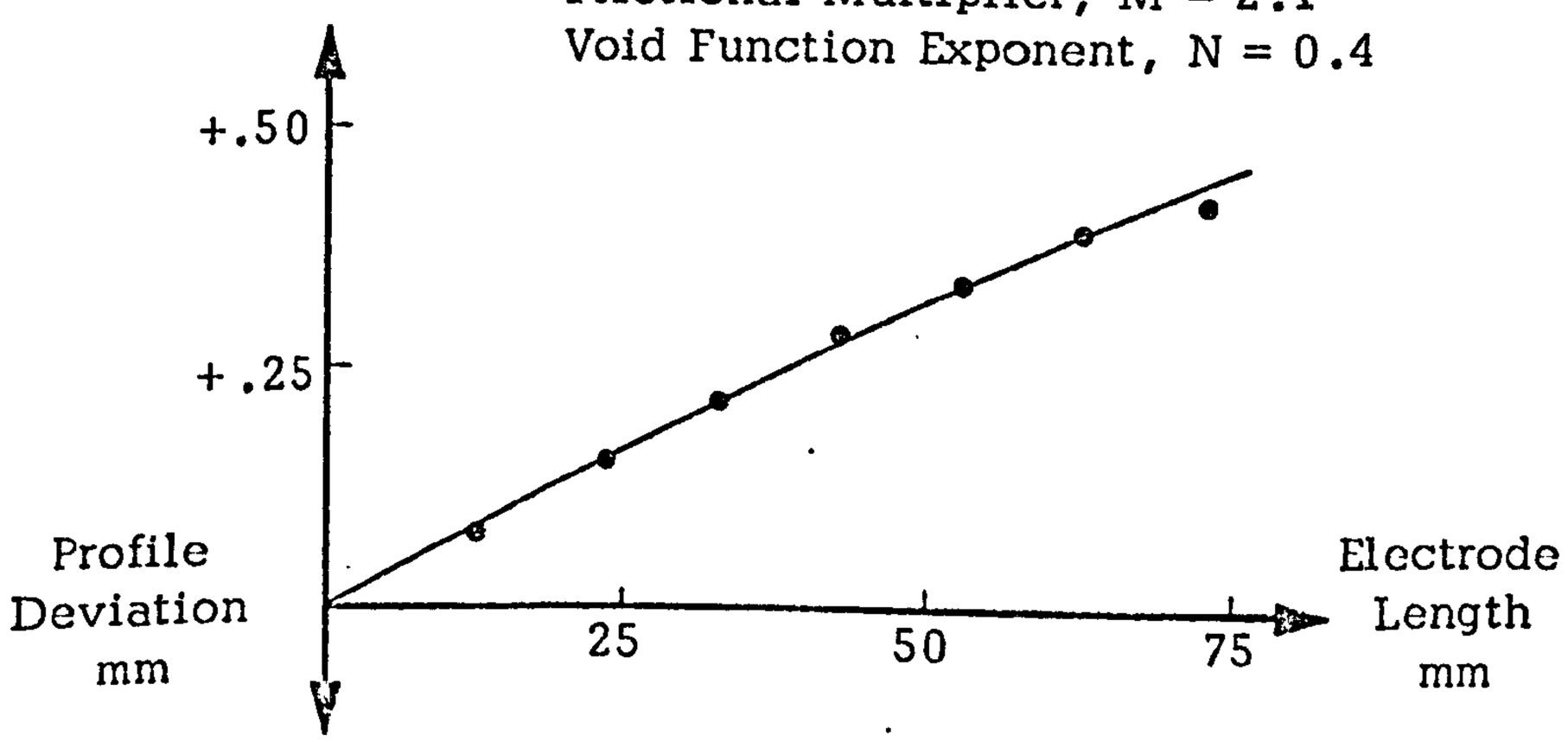

FIG. 3.8 COMPARISON OF THEORETICAL AND EXPERIMENTAL ANODE PROFILES

Test No.	Machining Current A	Electrolyte Flowrate $m^3s^{-1} \times 10^{-4}$	Inlet Pressure $kN\ m^{-2}$	Outlet Pressure $kN\ m^{-2}$	Temperature Increase K	Inlet Gap Width $m \times 10^{-3}$
1-18	2740	4.2	1720	210	31.0	.51
1-19	1650	3.9	1420	190	36.0	.46
1-20	2530	3.5	1350	180	39.0	.44
1-23	2680	3.0	1270	160	46.0	.47
1-24	2650	2.7	1150	170	49.0	.45
1-25		Machining Failure Conditions				

Operating Conditions: Machining Voltage - 20 V
Tool Feedrate - 2.0 mm min^{-1}
Sodium Chloride Solution at 14% Concentration
Electrolyte Inlet Temperature - 40°C

TABLE 4

Test 1-18
Computed Data

Current Density - 89.7 A cm^{-2}
Electrode Gap at Inlet - .439 mm
Flow Velocity at Inlet - 24.9 m s^{-1}
Temperature Increase - 33.7 K
Void Fraction at Outlet - .297

• Experimental Gap Profile
—— Frictional Multiplier, M = 2.4,
Void Function Exponent, N = 0.5

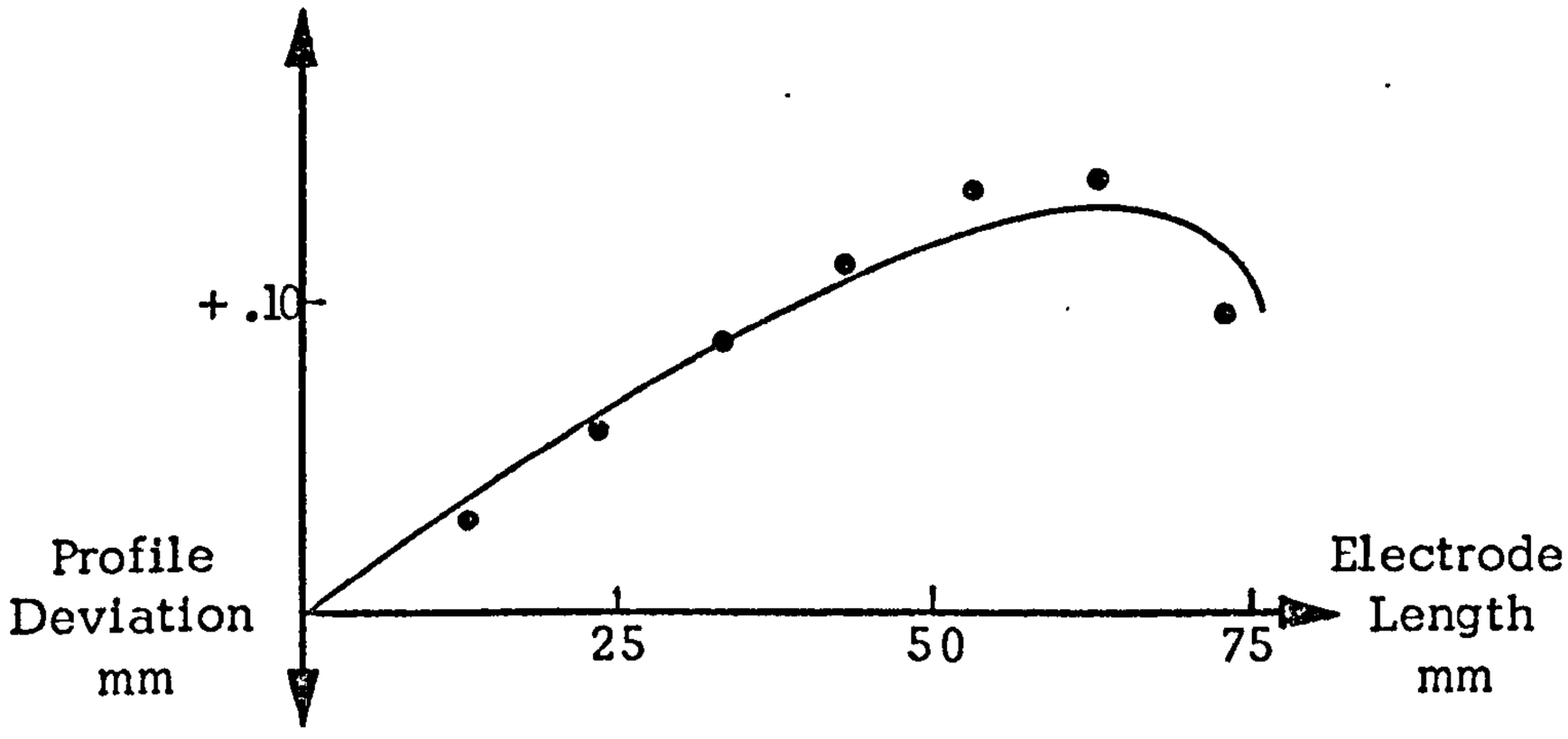

Test 1-24
Computed Data

Current Density - 89.7 A cm^{-2}
Electrode Gap at Inlet - .439 mm
Flow Velocity at Inlet - 16.1 m s^{-1}
Temperature Increase - 47.4 K
Void Fraction at Outlet - .438

• Experimental Gap Profile
—— Frictional Multiplier, M = 2.9,
Void Function Exponent, N = 1.0

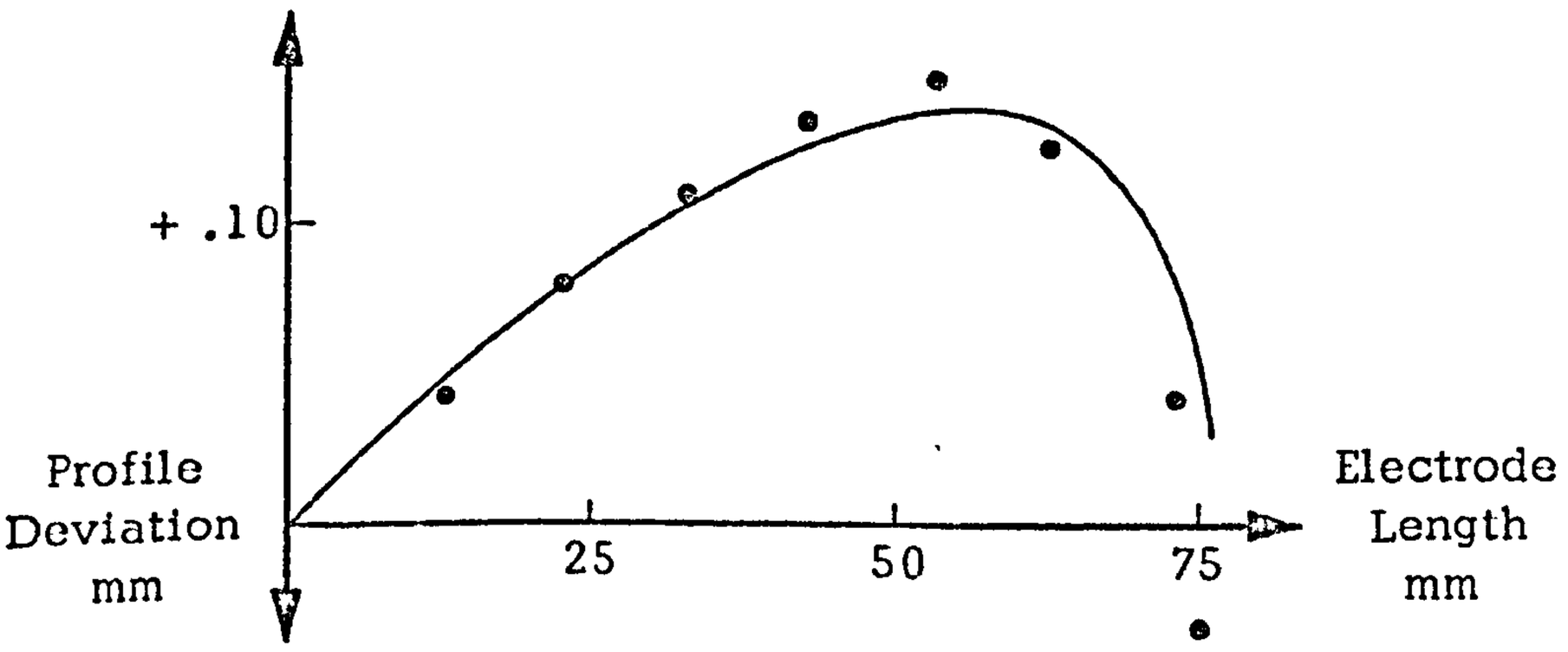

FIG. 3.9 COMPARISON OF THEORETICAL AND EXPERIMENTAL ANODE PROFILES

density at a given electrolyte flowrate results in an increase in ohmic resistance heating of the electrolyte and a greater mass of hydrogen bubbles evolved at the cathode. Thus the relative magnitude of these effects was increased. The increase in feedrate also reduced the inlet gap width such that a greater pressure was required for a given flow-rate. The overall effect of increase in feedrate was to cause substantial variation in the gap width, along the electrode length, relative to the inlet gap width. The model parameters (Fig. 3.9) were similar to those at the lower feedrate (Fig. 3.5 and 3.6).

Results for tests at a machining voltage of 10 V and a feedrate of 1.0 mm min^{-1} are shown in Table 5 and Fig. 3.10. The lower voltage reduced the gap width but also resulted in less resistance heating of the electrolyte. Thus the anode profiles in Fig. 3.10 showed less variation along the electrode gap than at the higher voltage. The model parameters are of the same order as those at the higher feedrate and machining voltage. The operating conditions which significantly affect the model parameters are the electrolyte flow velocity and the outlet pressure.

A test series, with sodium nitrate solution as the electrolyte, is presented in Table 6. As a result of the difference in experimental current efficiencies the comparison of sodium chloride and sodium nitrate solutions at similar current densities and electrode gap widths was not practicable. The inclusion of the current efficiency term in the calculation of machining current gave agreement within 8% of the observed machining currents but the calculated currents were, in

Test No.	Machining Current A	Electrolyte Flowrate $m^3s^{-1} \times 10^{-4}$	Inlet Pressure $kN\ m^{-2}$	Outlet Pressure $kN\ m^{-2}$	Temperature Increase K	Inlet Gap Width $m \times 10^{-3}$
1-33	1340	3.4	1650	180	11.2	.47
1-34	1270	3.0	1480	170	13.1	.41
1.35	1380	2.7	1200	160	14.7	.41
1-36	1360	2.3	1030	170	15.9	.48
1-37	1320	1.8	960	170	19.1	.43
1-38	Machining Failure Conditions					

Operating Conditions: Machining Voltage - 10 V
Tool Feedrate - 1.0 mm min^{-1}
Sodium Chloride Solution at 14% Concentration
Electrolyte Inlet Temperature - 40°C

TABLE 5

Test 1-27
Computed Data

Current Density - 44.9 A cm^{-2}
Electrode Gap at Inlet - .393 mm
Flow Velocity at Inlet - 22.7 m s^{-1}
Temperature Increase - 9.9 K
Void Fraction at Outlet - .234

• Experimental Gap Profile
—— Frictional Multiplier, M = 2.5,
Void Function Exponent, N = 0.4

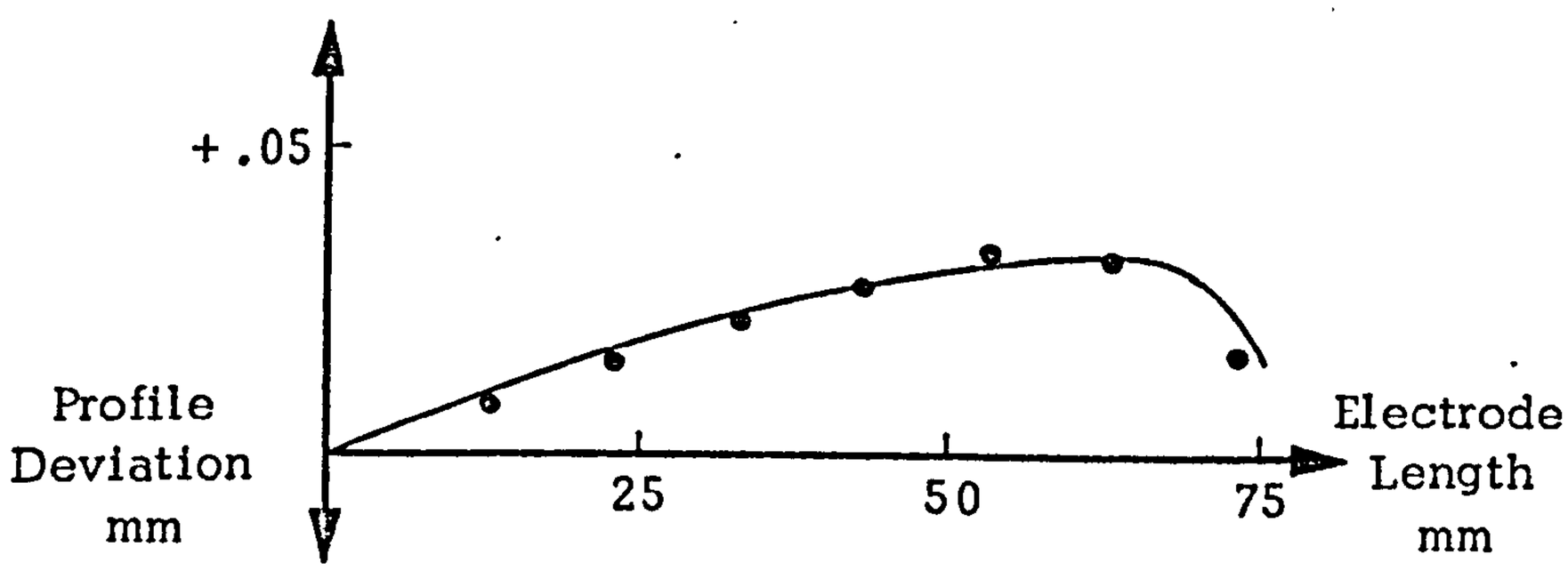

Test 1-24
Computed Data

Current Density - 44.9 A cm^{-2}
Electrode Gap at Inlet - ..393 mm
Flow Velocity at Inlet - 11.9 m s^{-1}
Temperature Increase - 18.9 K
Void Fraction at Outlet - .377

• Experimental Gap Profile
—— Frictional Multiplier, M = 3.2,
Void Function Exponent, N = 0.8

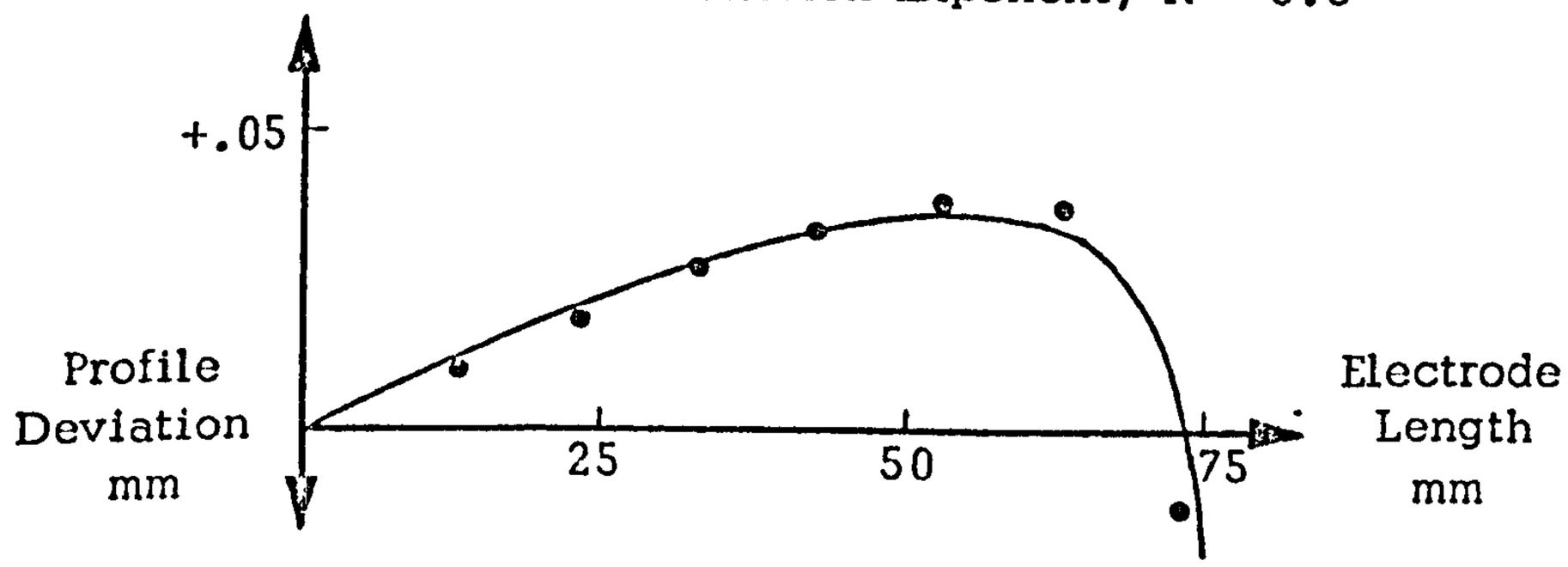

FIG. 3.10 COMPARISON OF THEORETICAL AND EXPERIMENTAL ANODE PROFILES

Test No.	Machining Current A	Electrolyte Flowrate $m^3 s^{-1} \times 10^{-4}$	Inlet Pressure $kN\ m^{-2}$	Outlet Pressure $kN\ m^{-2}$	Temperature Increase K	Inlet Gap Width $m \times 10^{-3}$	Current Efficiency %	Computed Current A	Computed Inlet Gap $m \times 10^{-3}$
2-13	1780	7.3	1830	240	12.8	.66	74	1752	.654
2-14	1690	6.6	1480	210	13.2	.69	73	1774	.645
2-15	1740	5.9	1290	190	13.6	.74	79	1648	.696
2-16	1750	4.3	1020	180	17.1	.77	79	1648	.696
2-17	1850	3.6	840	170	21.1	.75	75	1728	.662
2-18	Machining Failure Conditions								

Operating Conditions: Machining Voltage - 20 V
Tool Feedrate - 1.0 mm min^{-1}
Sodium Nitrate Solution at 32% Concentration
Electrolyte Inlet Temperature - 40°C

TABLE 6

Test 2-13

Computed Data

Current Density	- 60.6 A cm^{-2}
Electrode Gap at Inlet	- .654 mm
Flow Velocity at Inlet	- 29.3 m s^{-1}
Temperature Increase	- 11.9 K
Void Fraction at Outlet	- .123

• Experimental Gap Profile
—— Frictional Multiplier, M = 1.4
Void Function Exponent, N = 0.0

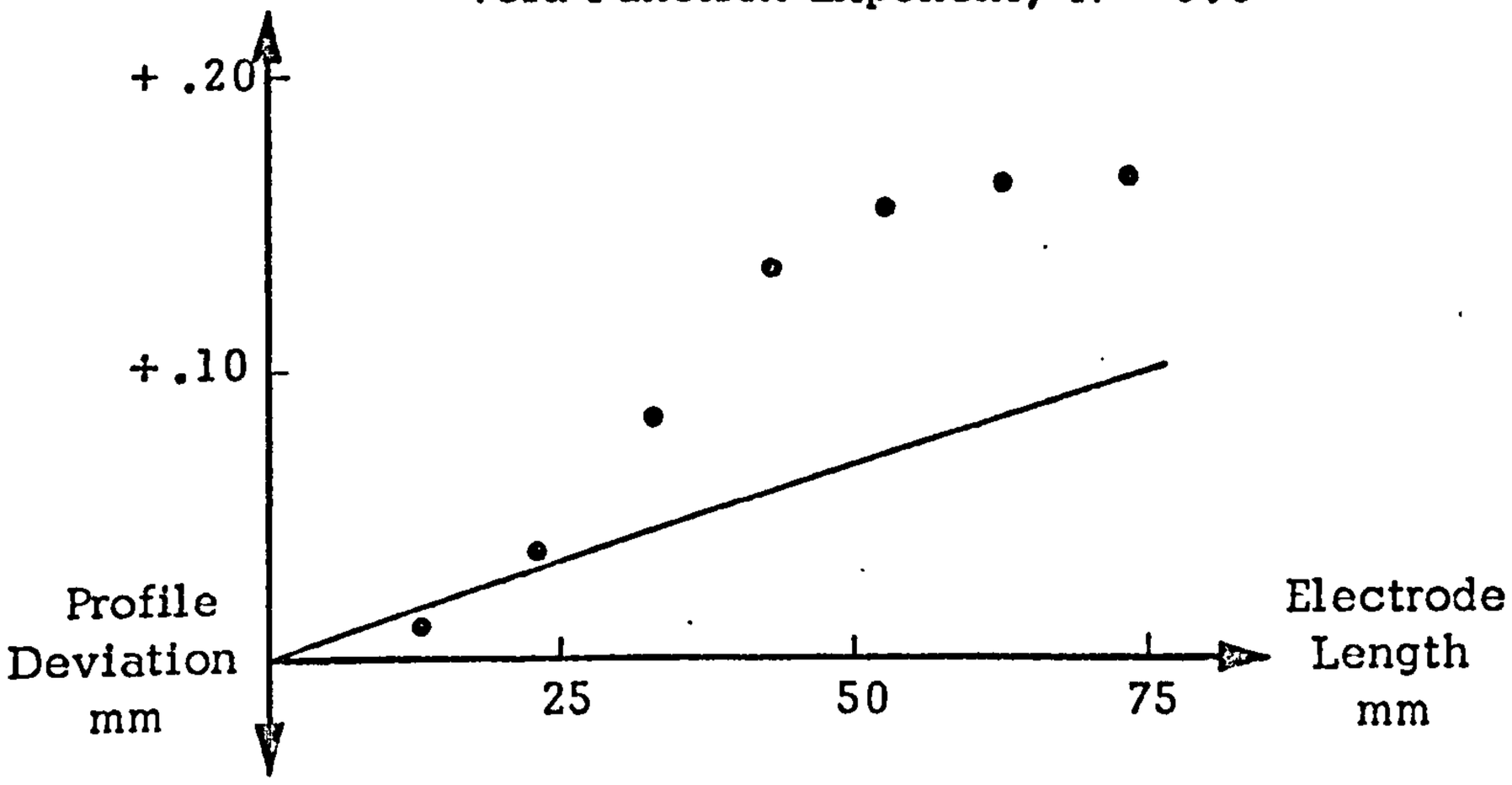

Test 2-15

Computed Data

Current Density	- 56.8 A cm^{-2}
Electrode Gap at Inlet	- .696 mm
Flow Velocity at Inlet	- 22.2 m s^{-1}
Temperature Increase	- 14.6 K
Void Fraction at Outlet	- .161

• Experimental Gap Profile
—— Frictional Multiplier, M = 1.8
Void Function Exponent, N = 0.0

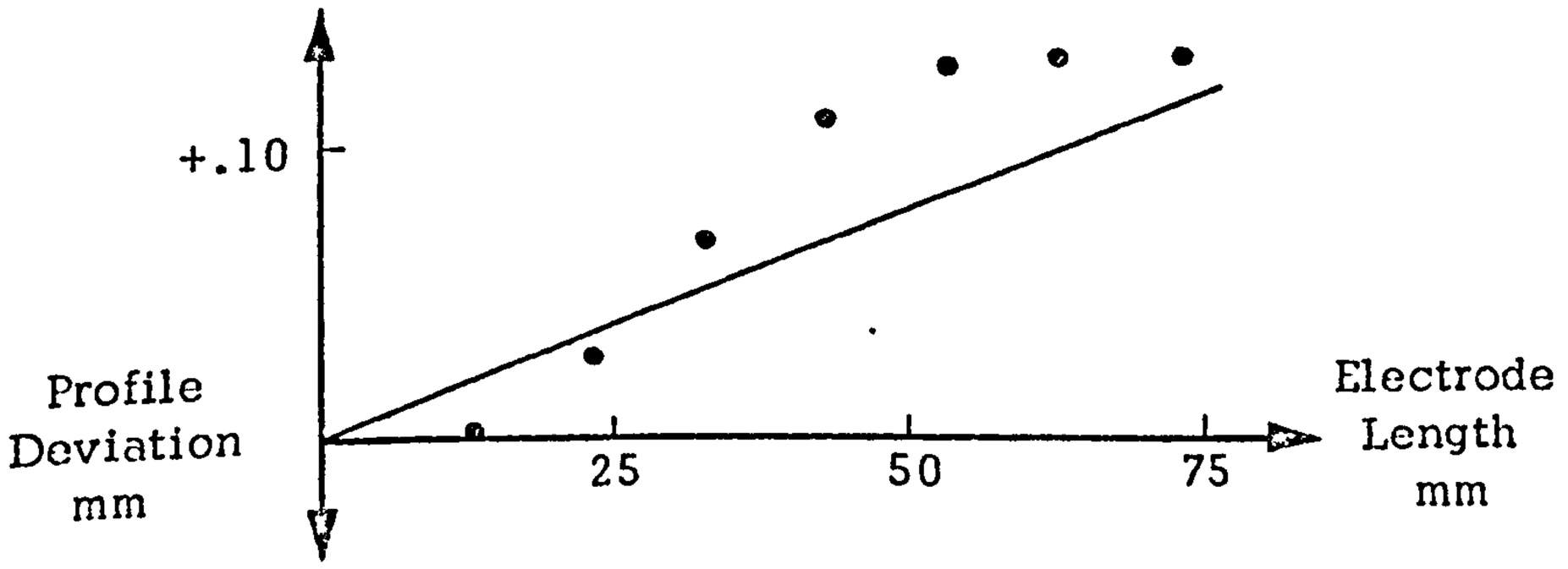

FIG. 3.11 COMPARISON OF THEORETICAL AND EXPERIMENTAL ANODE PROFILES

Test 2-16

Computed Data

Current Density - 56.8 A cm^{-2}
Electrode Gap at Inlet - .696 mm
Flow Velocity at Inlet - 16.2 m s^{-1}
Temperature Increase - 19.2 K
Void Fraction at Outlet - .223

• Experimental Gap Profile
—— Frictional Multiplier, M = 2.1
Void Function Exponent, N = 0.4

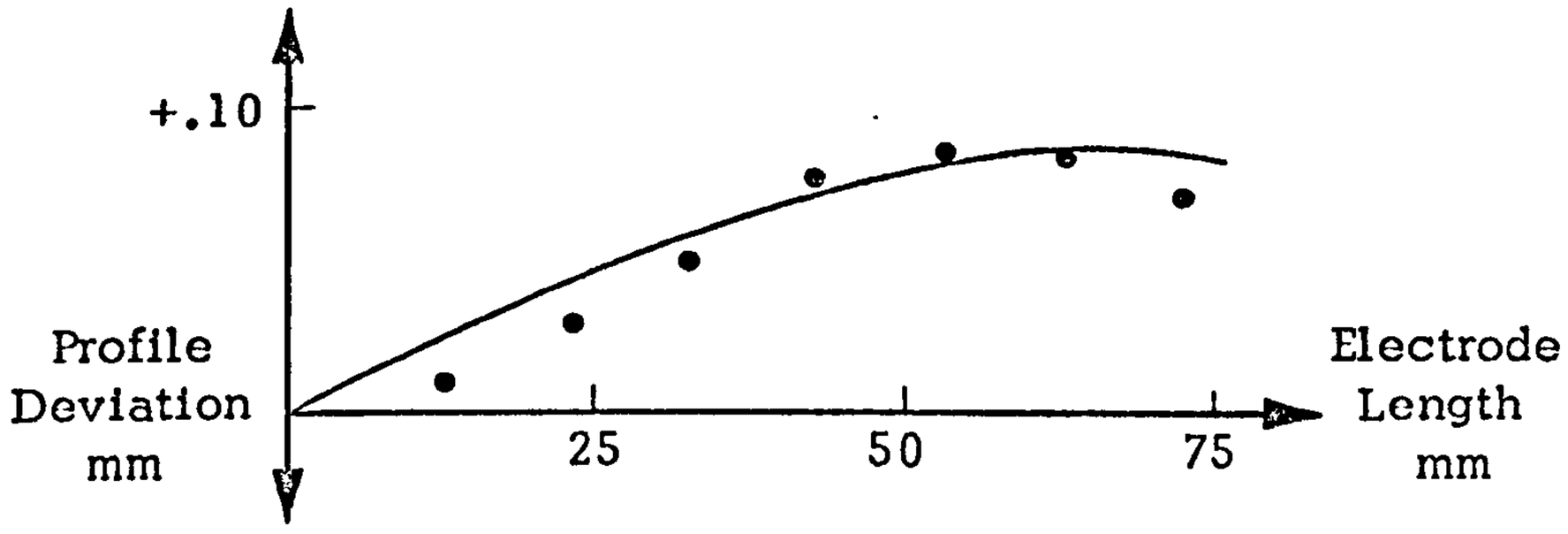

Test 2-17

Computed Data

Current Density - 59.8 A cm^{-2}
Electrode Gap at Inlet - .662 mm
Flow Velocity at Inlet - 14.2 m s^{-1}
Temperature Increase - 24.9 K
Void Fraction at Outlet - .290

• Experimental Gap Profile
—— Frictional Multiplier, M = 1.7
Void Function Exponent, N = 0.6

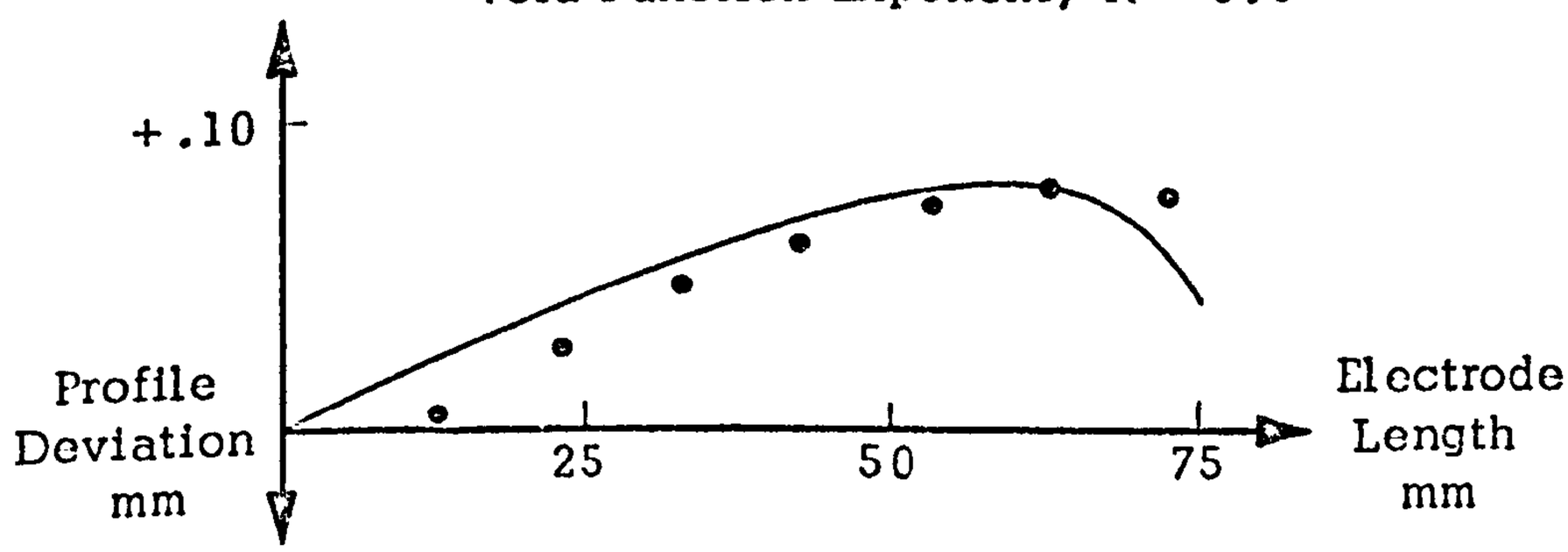

FIG. 3.12 COMPARISON OF THEORETICAL AND EXPERIMENTAL ANODE PROFILES

general, lower. However, the experimental currents were subject to errors in feedrate setting and in the shunt. Thus the introduction of the current efficiency for the determination of electrode gap and current, as suggested by Tipton (11), was in reasonable agreement with the results.

The anode profiles for the tests with sodium nitrate solution are shown in Figs. 3.11. The increase in gap width along the electrode length was greater than that predicted theoretically assuming a void function exponent of zero i.e. gas bubbles had no effect on the electrolyte conductivity. Further tests, at the conditions used in Test 2-13, gave a repeatability of $\pm$ .025 mm for the anode profile deviation. The profiles in Fig. 3.12 showed some agreement with theory but the values of the void function exponent were lower than those for the tests with sodium chloride solution at similar flow velocities. The results suggest that, with sodium nitrate solution, factors other than the electrolyte conductivity affect the anode profile deviation.

3.6.3 Limitations on the Metal Removal Rate

Metal removal rates greater than those in Fig. 3.3 could not be obtained. For example machining at a feedrate of 2.5 mm min^{-1}, corresponding to a current density of 101 A. cm^{-2}, at a voltage of 20 V with the sodium chloride electrolyte resulted in the breakdown of equilibrium conditions and a spark across the electrode gap. The electrolyte flowrate was not sufficient to maintain machining and this represents the limitation on metal removal rate.

An investigation of machining failure and sparking was possible since the Microbar device prevented damage to the tool and workpiece.

Tests were carried out at constant conditions of voltage, feedrate and outlet pressure (Table 2). The flowrate was reduced in successive tests until a spark occurred in Test 1.09. The characteristics of machining failure were similar to those at 20 V and 2.5 mm min^{-1}. No upper bound to the electrolyte flow velocity, due to the choked flow condition, was observed.

The machining current-time and outlet temperature-time characteristics of machining failure for Test 1-09 are shown in Fig. 3.13. (The output voltage from the power supply was stabilised against load current variation.) The initial machining current is low due to a high preset gap; the slight drop in current is caused by back-lash in the ram drive. Under normal conditions the machining current would attain an equilibrium value of about 1300 A and the flowrate and outlet temperature would also become constant. At machining failure small fluctuations in machining current were evident and the current fell slowly. Simultaneously, the electrolyte outlet temperature rose to a maximum of 92^{o}C and the flowrate became less. The test was terminated by a spark detected by the Microbar unit which cut-out the power supply and ram drive and indicated a spark on the control console.

The machined surface finish and appearance of the workpiece (Fig. 3.14 extreme right) was similar to that obtained under equilibrium conditions and the current efficiency was close to 100%. The anode profile

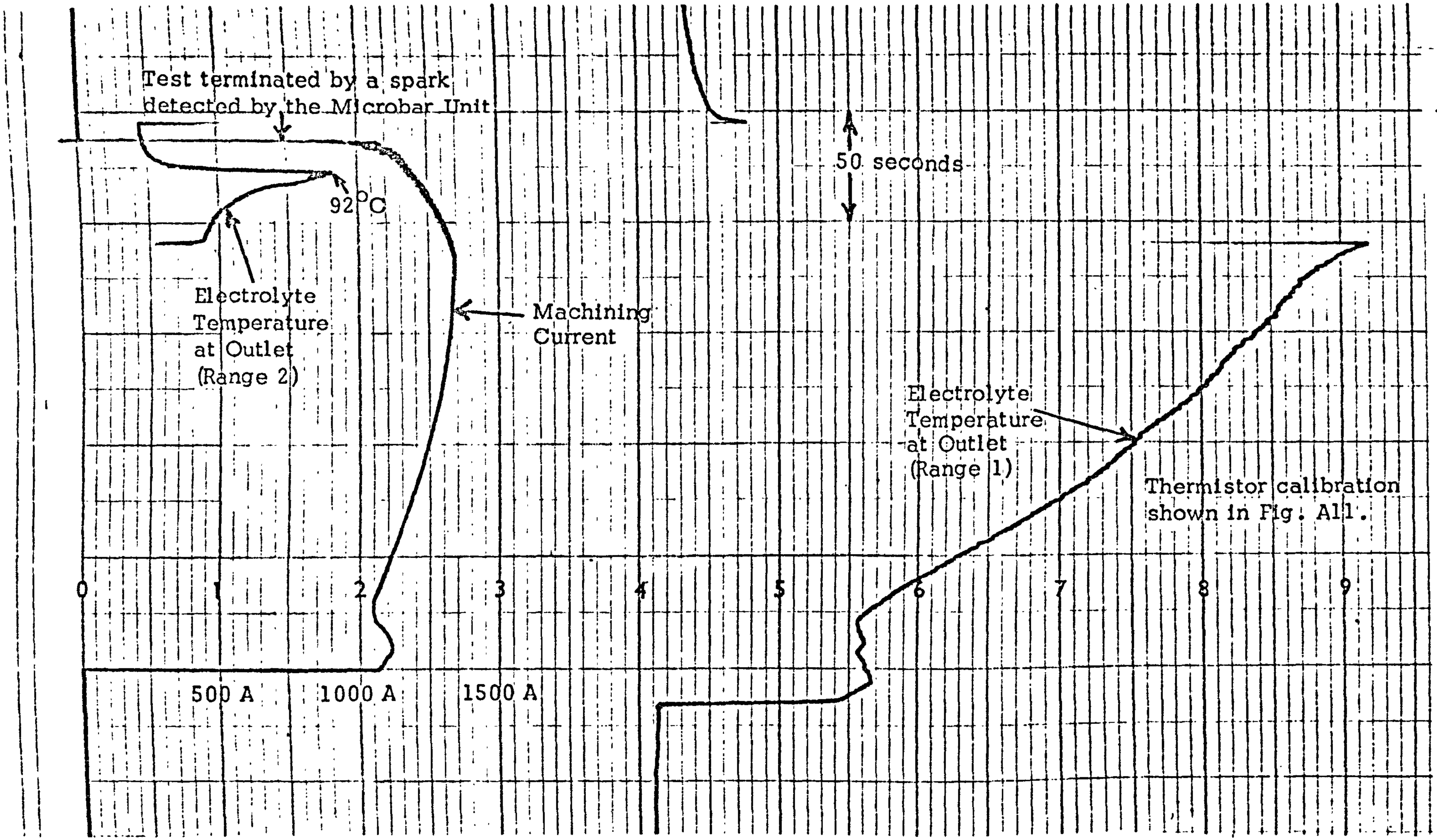

FIG. 3.13 CHART RECORDING FOR TEST 1-09 (TABLE 2)

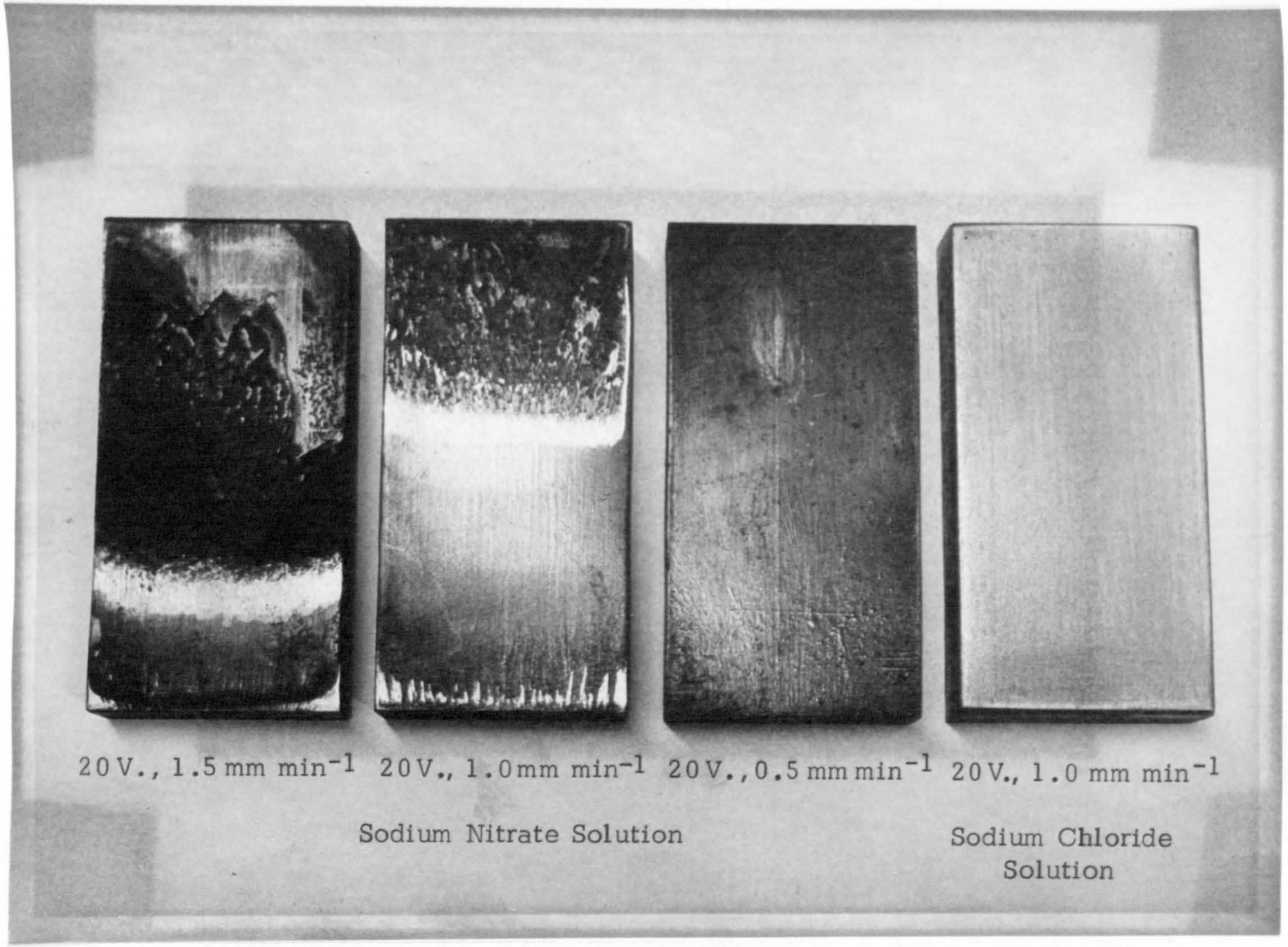

FIG. 3.14 MACHINED SURFACES FOR TESTS AT MACHINING FAILURE CONDITIONS

converged sharply at outlet towards the cathode as observed in Fig. 2.12. Machining breakdown was a dynamic condition; as the electrode gap towards outlet became smaller the electrolyte flow was restricted which resulted in an increase in outlet temperature. The fall in machining current and the convergence of the gap indicated that the current density or electrolyte conductivity towards outlet was less than over the remainder of the surface.

The electrolyte temperature increase, for the tests in Tables 2 and 3, is shown against flowrate in Fig. 3.15. Good agreement with ohmic resistance heating, equation (48), is observed. At an outlet pressure of 800 kN m^{-2} lower flowrates and pressure differentials were sufficient to maintain equilibrium machining conditions. In Test 1-17 the high temperature and pressure of the electrolyte, at outlet from the machining cell, burst the nylon piping and tests were discontinued although lower flowrates may have been possible.

For tests at a feedrate of 2 mm min^{-1} (Table 4) the characteristics of machining failure were similar to those in Test 1-09 but occurred more rapidly. The machining current rose to a peak below the theoretical equilibrium value and fell and a spark terminated the test. During the fall in current the cell vibrated and steam was evident in the working enclosure. However, under equilibrium conditions the highest temperature recorded was 89°C (Test 1-24) which is well below the boiling point of 120°C for the electrolyte. In Table 5, for tests at a machining voltage of 10 V, lower flowrates than at 20 V were sufficient to maintain equilibrium machining.

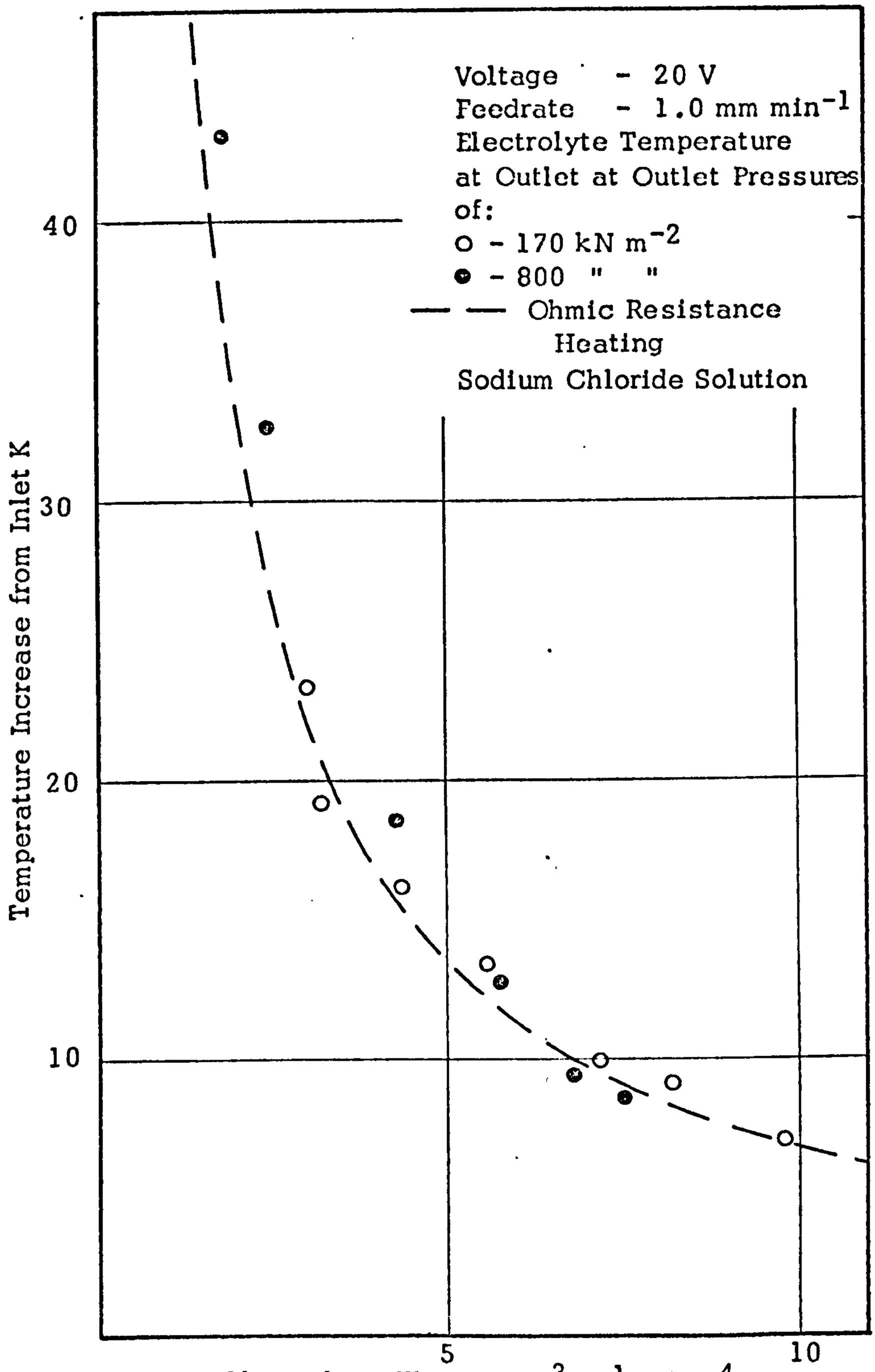

FIG.3.15 VARIATION IN TEMPERATURE INCREASE WITH OUTLET PRESSURE AND FLOWRATE

The characteristics of machining breakdown with the sodium nitrate solution are shown in Fig. 3.16. The machining current rose to a peak, above the equilibrium current for tests at this feedrate, and fell and a spark was indicated on the control console. The machined surfaces, for tests in which a spark occurred, are shown in Fig. 3.14. At the higher current densities the surface finish of the inlet region was similar, apart from some polished streaks just at inlet, to that obtained under normal conditions. The distinctive shiny strip, which was silver-gold in colour, was followed by a brown, rough surface extending to outlet. The electrode gap converged towards the cathode in this region similar to that in tests with sodium chloride solution at machining failure. At a feedrate of 0.5 mm min^{-1} in Fig. 3.14 a light coloured area indicated the position of the spark.

In tests with the sodium nitrate solution, in which machining failure occurred, there was a marked reduction in machining current efficiency (Table 7) based on a valency of two for the dissolution of steel. In tests 2-30 and 2-31 the machining current was set to trip at about 400 A. greater than the equilibrium current in tests 2-22 to 2-25. When the current rose above equilibrium, corresponding to the onset of machining failure, the test was terminated. The current efficiency of tests 2-30 and 2-31 compared with those for tests at equilibrium conditions. The appearance of the machined surfaces was also similar. The lower current efficiency in tests 2-27 and 2-28 may be due to low current densities towards outlet. Konig and Degenhardt (49) observed low current efficiencies and passivation at low current

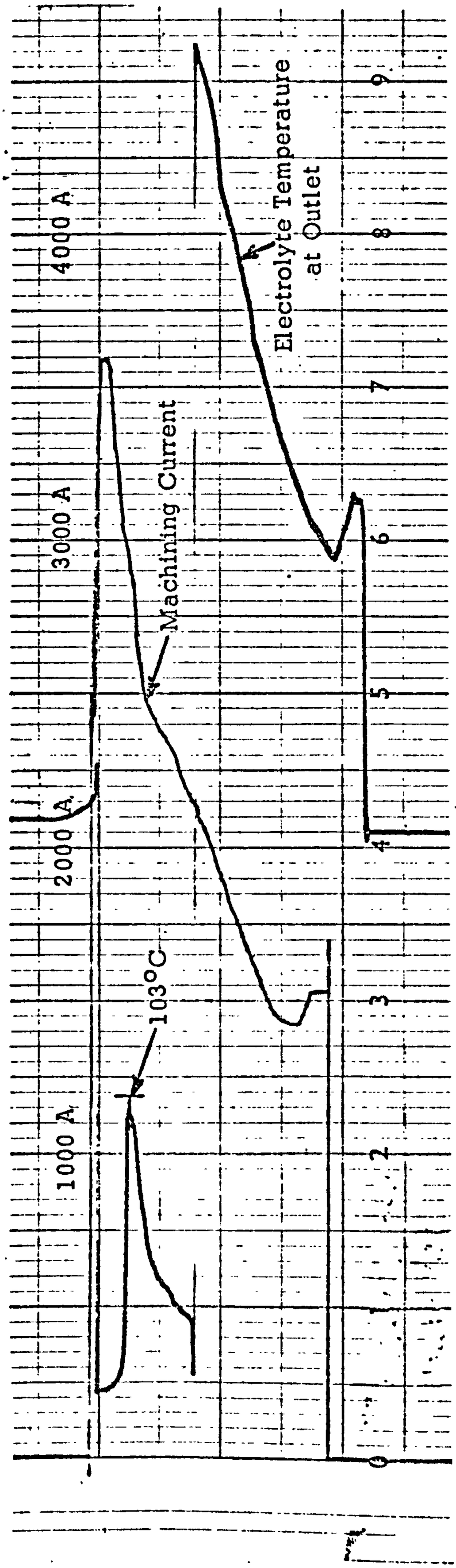

FIG. 3.16 CHART RECORDING FOR TEST 2-27 (TABLE 7)

Test No.	Machining Current A	Electrolyte Flowrate $m^3\ s^{-1} \times 10^{-4}$	Inlet Pressure $kN\ m^{-2}$	Outlet Pressure $kN\ m^{-2}$	Current Efficiency %
2-22	2450	5.2	1830	200	80
2-23	2500	4.6	1710	190	79
2-24	2700	4.2	1580	170	76
2-25	2630	3.7	1510	170	78
2-27	Machining failure, peak current 3600A				58
2-28	Machining failure, peak current 3300A				65
2-30	Machining failure, current tripped at 3000A				78
2-31	Machining failure, current tripped at 3000A				76

Operating Conditions: Machining Voltage - 20 V
Tool Feedrate - 1.5 mm min^{-1}
Sodium Nitrate Solution at 32% Concentration
Electrolyte Inlet Temperature - 40°C

TABLE 7

densities in tests with the same metal-electrolyte combination. The reduced current efficiency and surface marking may be the result of machining failure and not the cause.

4.0 FURTHER INVESTIGATION OF PROCESS LIMITATIONS

4.1 The Lower Bound to the Electrolyte Velocity

The previous experimental work was not conclusive in relation to the lower bound to the electrolyte velocity. Further work was required to determine the cause of machining failure. The dependence of the lower bound to the electrolyte velocity on outlet pressure related machining failure with the volume of hydrogen bubbles close to the cathode. The temperature of the electrolyte within the gap also appeared to be of significance. Thus experimental work was initiated in an attempt to measure the temperature of the electrolyte close to the cathode surface.

4.1.1 Experimental Technique

A conventional method of temperature measurement with thermocouples was considered due to their compact size. However, thermocouples in electrolytes are subject to errors due to an electrochemical e.m.f. at the junction (50). Miniature bead thermistors are an alternative method of temperature measurement suitable for recording purposes. Thermistor beads are made of thermally sensitive semi-conductor materials usually enclosed in a glass envelope and have negative logarithmic change in resistance with temperature. S.T.C. type FS 2 thermistors were selected, these being the smallest available from commercial sources.

The machine, power supply, flow system and machining cell,

described in 2.2.1, 2.2.2, 2.2.3 and 2.6 were used. The machining cell was modified to allow placement of the thermistors in the cathode (Fig. 4.1). The thermistors beads were approximately 1 mm in diameter and were inserted through the baseplate and cathode protruding 0.8 mm from the cathode surface. To achieve this the cathode was clamped to a surface table with the cathode face separated from the table by 0.8 mm shims. A layer of plasticene was squeezed between the respective faces and the thermistors pressed through the cathode into the plasticene to make contact with the surface table. An insulating grade of Araldite was poured around each thermistor and allowed to set. The plasticene prevented the Araldite from seeping onto the thermistor tips.

The thermistors were calibrated by immersing the cathode assembly in a pyrex beaker placed on a hot plate-stirrer unit. Steady temperatures, over the anticipated working range of the thermistors, were measured with thermometers. The conductance of each thermistor was measured with a Wayne Kerr Universal Bridge. The water in the beaker was replaced with a light oil to calibrate the thermistors at temperatures from 100 to 150^{o}C.

To investigate the thermistor response the cathode assembly was dipped into water at various temperatures. For each step change in temperature there was a sharp rise to about 75% of the difference followed by a delay of less than ten seconds to attain the observed temperature of the water. This compared well with the thermistor response prior to calibration. The proximity of the thermistor tips to

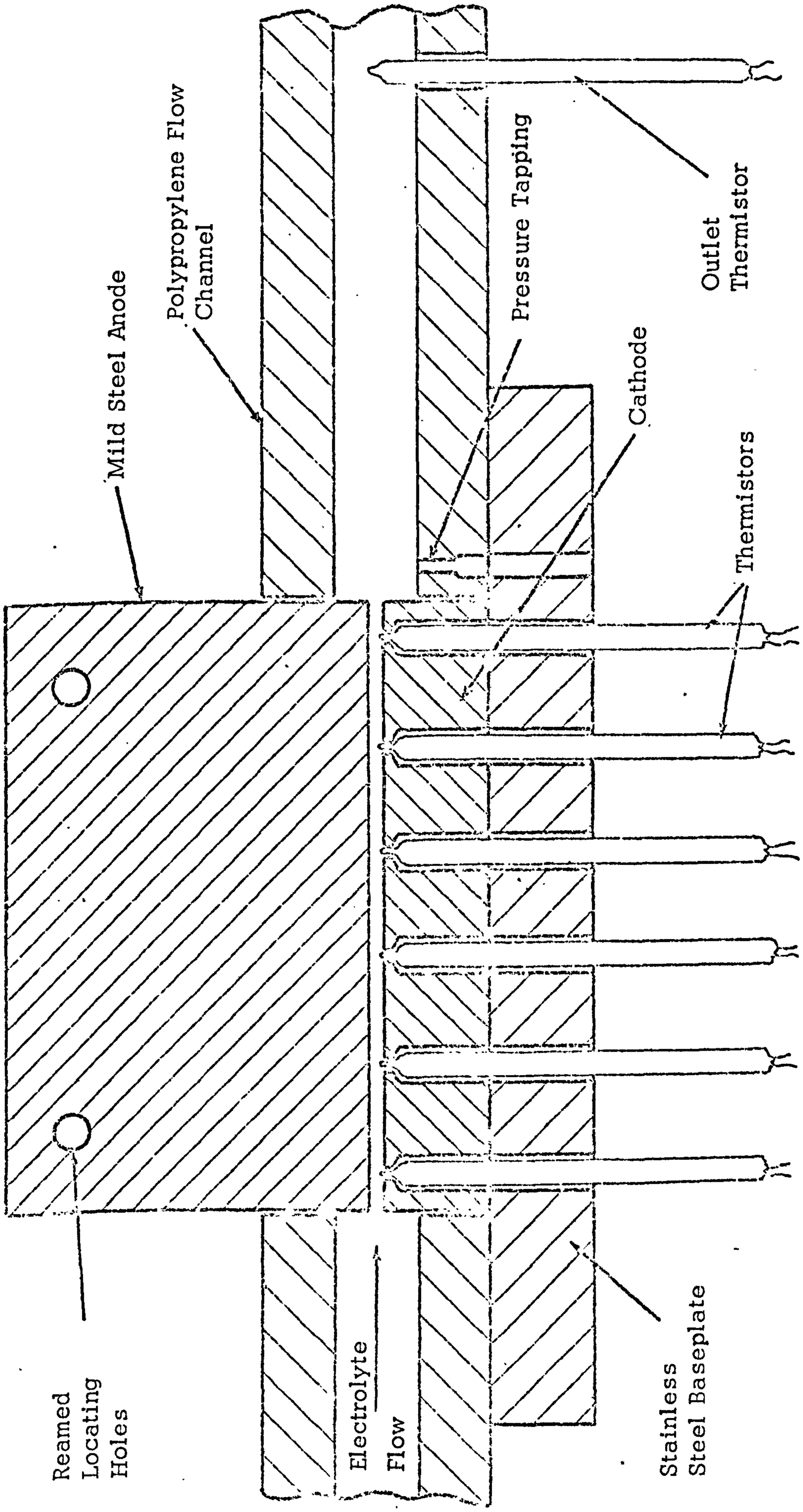

FIG. 4.1(a) SCHEMATIC CROSS SECTION OF MACHINING CELL

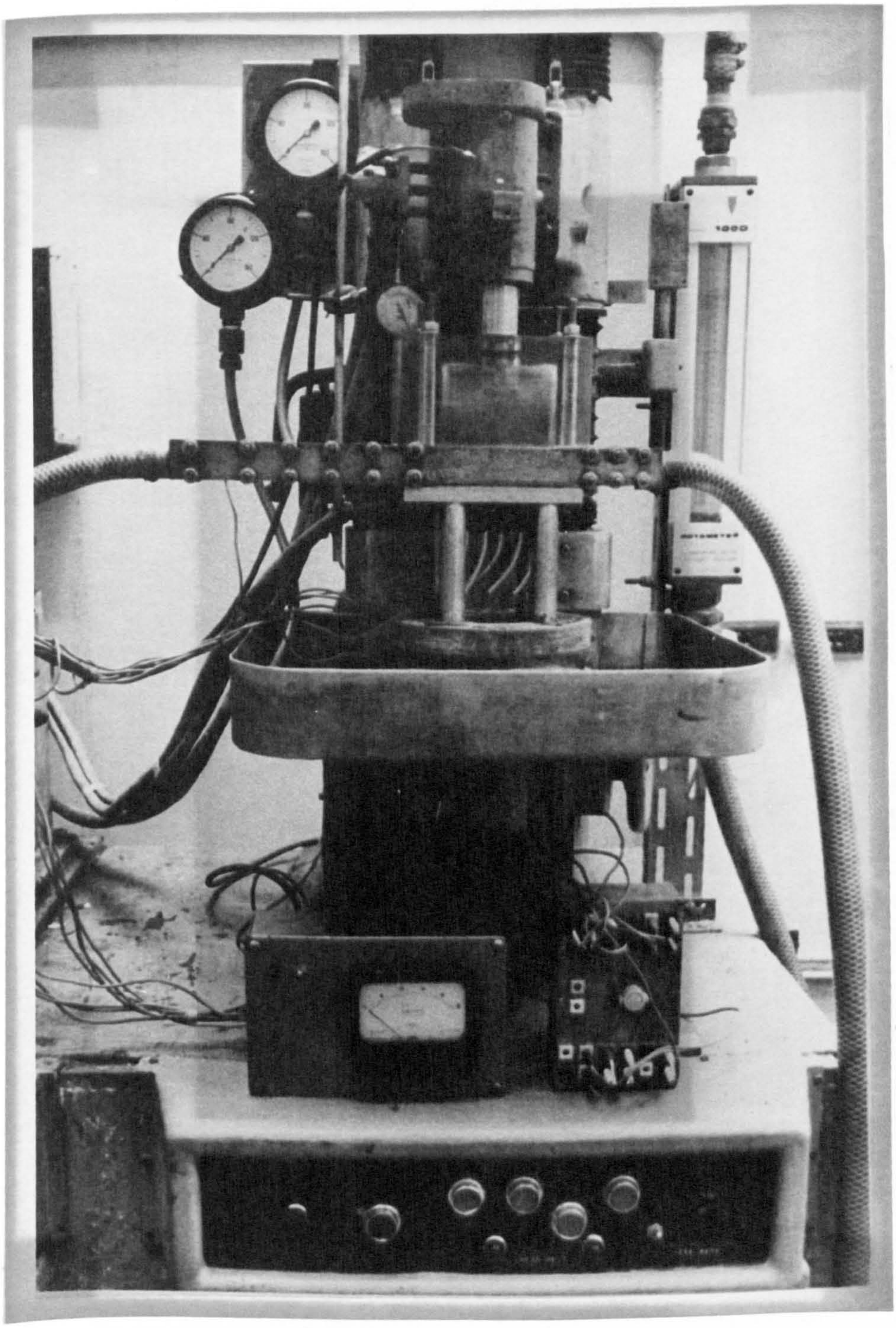

FIG. 4.1(b) MACHINING CELL ARRANGEMENT

the cathode appeared to have very little effect on the measurements.

The cathode assembly was fitted to the flow channel. The thermistor leads were connected to a multiple switch-box with one lead to a Wayne Kerr Universal Bridge and the output from the Bridge displayed on the pen recorder. A scan of all the thermistors could be made in about three minutes.

Test operating conditions were a machining voltage of 32 V and a feedrate of 0.35 mm min^{-1} to give a machining current of about 220 A. A 10% solution of sodium chloride, at an inlet temperature of 20°C, was used. The electrolyte from the machining cell was discharged to a separate tank to maintain a constant inlet temperature in each test. The calculated machining gap for these conditions was 2.35 mm which gave adequate clearance to the thermistor tips.

The initial gap was set by placing a slip, ground to the required size, on the cathode and bringing the workpiece face down to contact the slip. The position was noted from the dial gauge, the slip removed and the workpiece reset.

Electrolyte, at various tank temperatures, was pumped through the machining cell. The thermistor readings from the pen-recorder were checked from the calibrations at the appropriate temperatures and good agreement was observed.

To prevent electrolyte by-passing the electrodes, the polypropylene flow channel was compressed onto the electrodes with the fitted bolts. This appeared to be successful as no side flow effects were evident on the machined workpiece.

The experimental series consisted of tests at the operating conditions specified but with a small reduction in flowrate in successive tests to the machining failure conditions. Care was exercised to prevent sparks and damage to the thermistors.

4.1.2 Experimental Results

The increase in electrolyte temperature, measured at inlet and outlet points, is shown against electrolyte flowrate in Fig. 4.2. The theoretical temperature increase (equation 48) is also shown. The temperatures, measured by the thermistor 6 mm from outlet within the electrode gap, are greater than those measured downstream of the electrodes. At the lower flowrates the temperatures within the gap increase to a maximum which corresponds with the boiling point of the electrolyte at the outlet pressure of 170 kN m^{-2}.

The chart recording for a test in which boiling occurred is shown in Fig. 4.3. The appropriate thermistor calibrations are shown in Appendix 4. At a flowrate of 3.8×10^{-5} m^3 s^{-1} the temperature recorded within the gap is 116°C compared with the boiling point of 119°C (Fig. A.6). The electrolyte temperature at outlet from the gap is 60.5°C. Reducing the flowrate to 3.5×10^{-5} m^3 s^{-1} increased the outlet temperature to 64°C with no effect on the temperature measured within the gap. The fluctuations in machining current were evident at flowrates lower than 5.0×10^{-5} m^3 s^{-1}.

The greater temperatures within the gap are due to the hydrogen bubbles, evolved at the cathode, which reduce the area

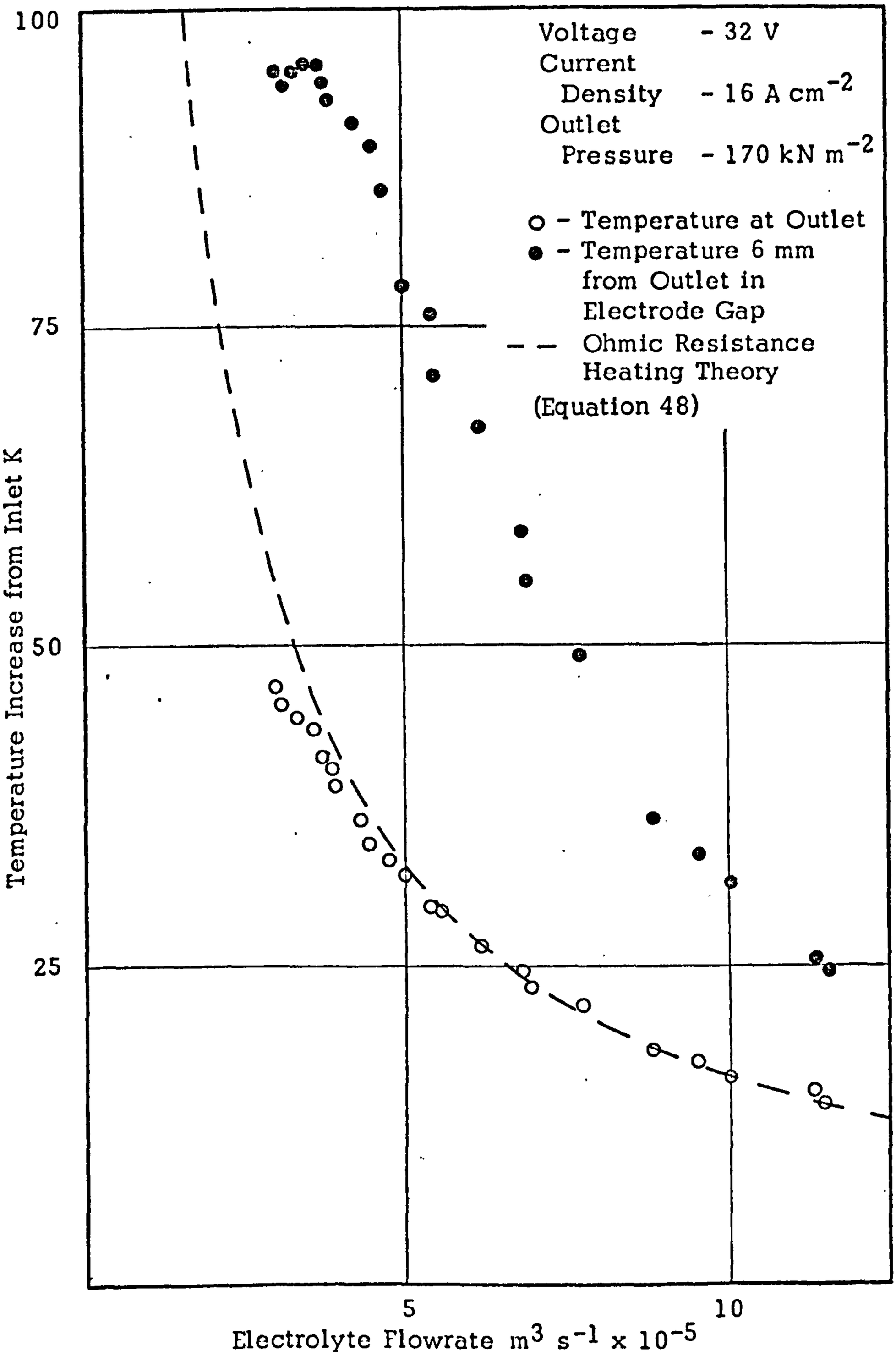

FIG. 4.2 VARIATION IN TEMPERATURE INCREASE WITH ELECTROLYTE FLOWRATE

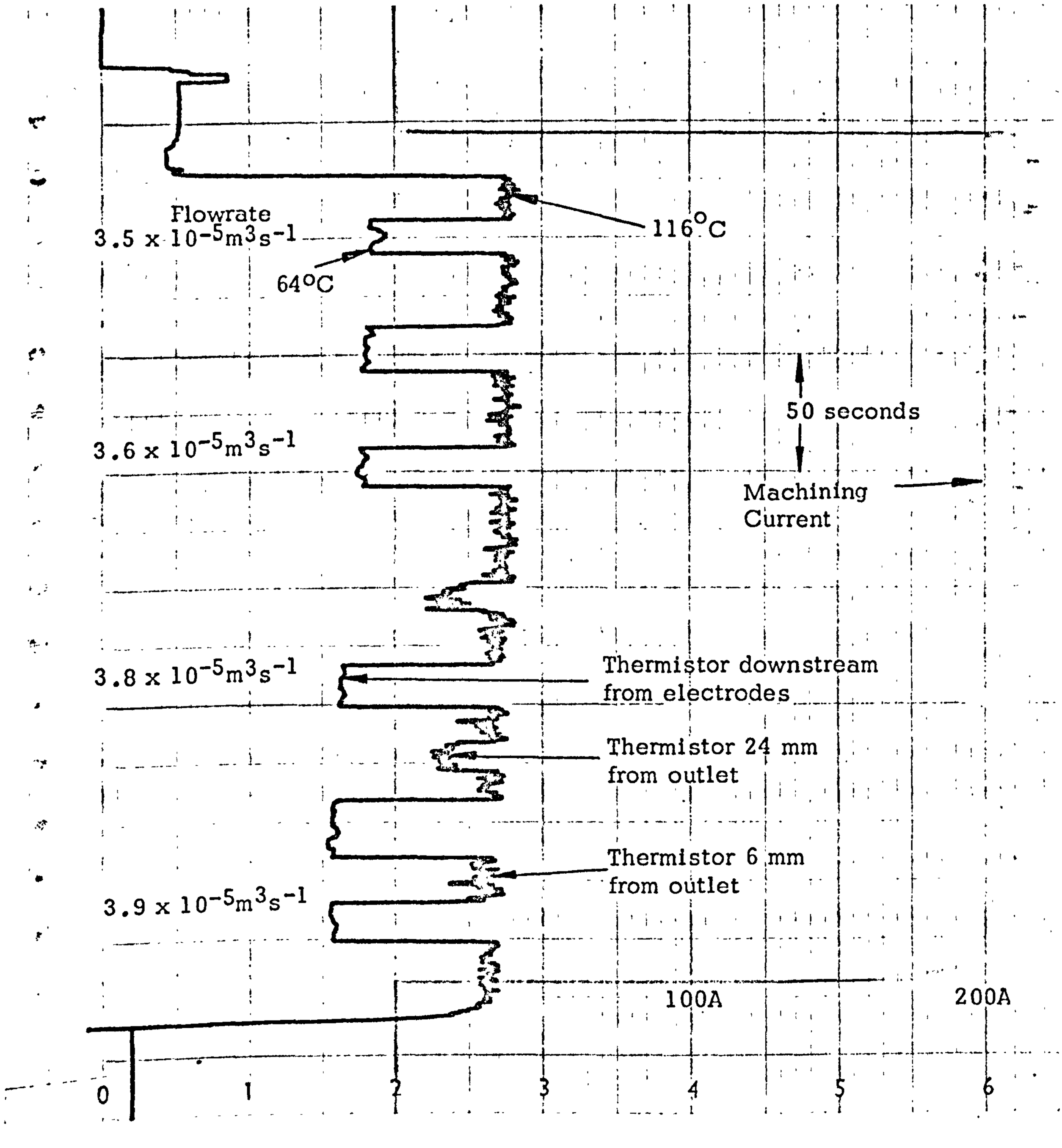

FIG. 4.3 CHART RECORDING

available for the passage of current. The high current flux in the electrolyte around the bubbles generates greater temperatures than in the bulk electrolyte flow. The thermistors in the gap measure the averaged temperature of the bubble-electrolyte layer. The abrupt enlargement of the channel, at outlet from the electrode gap, induces turbulence which mixes the electrolyte and a uniform temperature is recorded downstream of the electrodes. The temperatures measured at this point, 7 hydraulic diameters downstream of the gap, showed good agreement with the temperatures at the discharge point to the electrolyte tank.

In Fig. 4.4 the temperature increase, measured by the six thermistors within the gap, is plotted against electrode length. Apart from a sharp rise from inlet the temperature increase is linear. At the lowest flowrate boiling is observed to spread along the electrode gap towards inlet.

The variation in machining gap width along the electrode length, for various electrolyte flowrates, is shown in Fig. 4.5. An increase in gap width is assumed positive and a decrease as negative. The inlet gap width is assumed constant although the initial gap setting was reduced by up to 0.2 mm at the lower flowrates to maintain a similar equilibrium current in all tests. At the lowest flowrate, corresponding to boiling within the gap, the anode surface converges sharply towards the cathode. If the test were continued this would cause a spark across the gap as experienced in the tests using the Anocut machine. The convergence of the anode profile, at machining failure conditions, is caused by steam bubbles which increase

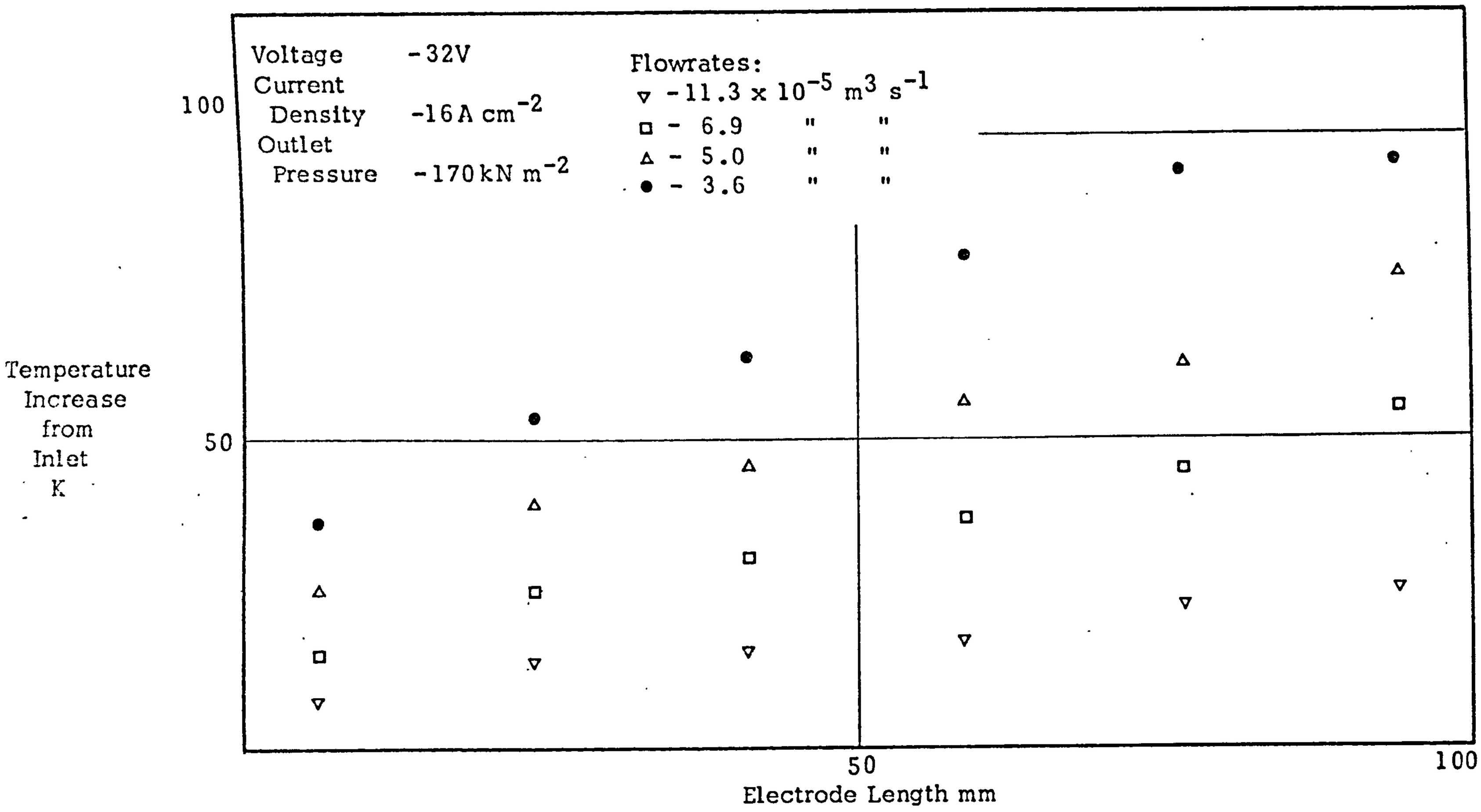

FIG. 4.4 TEMPERATURE INCREASE ALONG THE ELECTRODE LENGTH

Voltage - 32 V
Current
Density - 16 A cm^{-2}
Outlet
Pressure - 170 kN m^{-2}

Flowrates:
△ - 11.3 x 10^{-5} $m^3 s^{-1}$
▽ - 8.8 x " "
□ - 5.0 x " "
● - 3.6 x " "

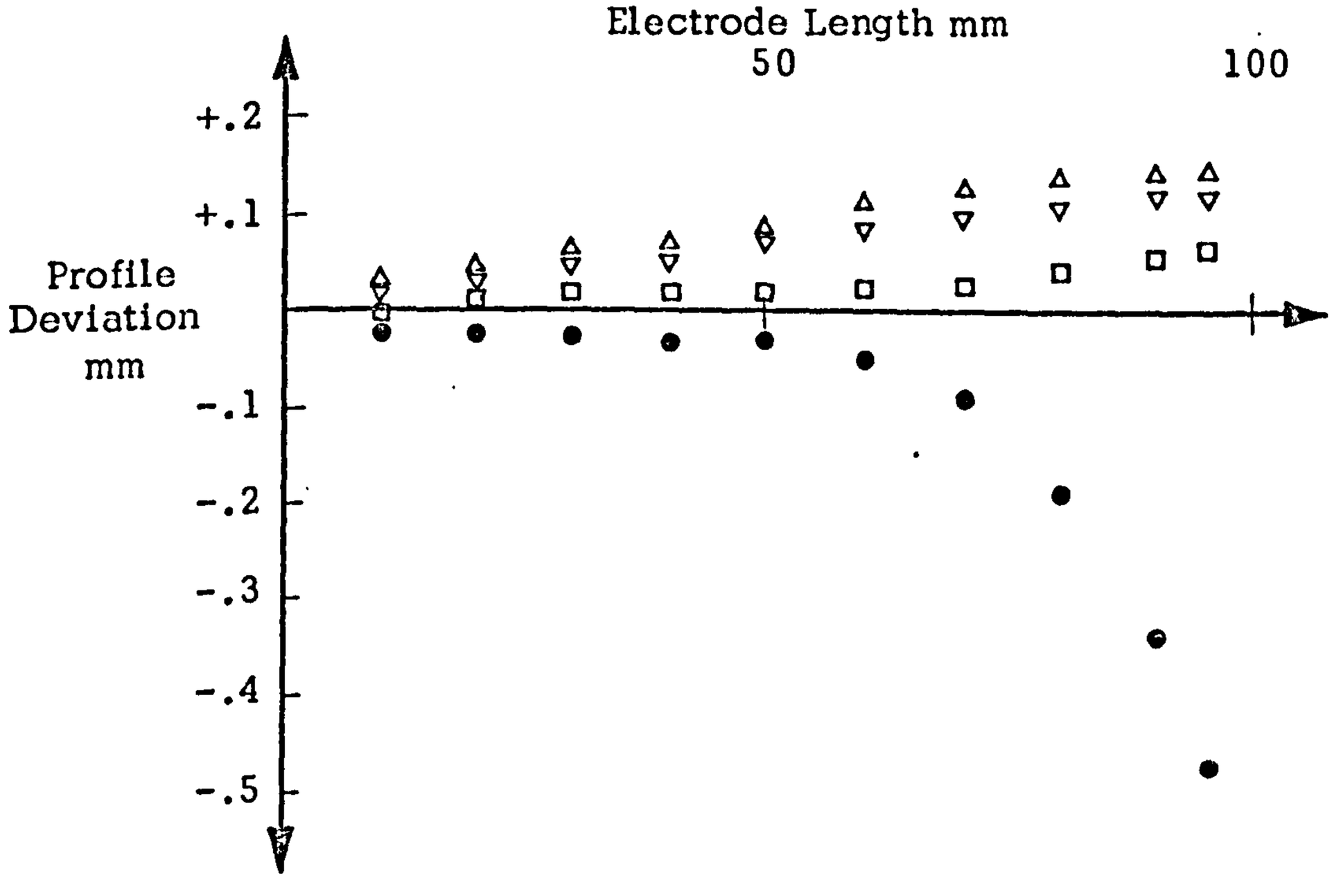

FIG. 4.5 INFLUENCE OF ELECTROLYTE FLOWRATE ON THE ANODE PROFILE

the resistance of the electrolyte.

In Fig. 4.6 the temperature increase from outlet is shown against electrolyte flowrate for three outlet pressures. At each pressure the temperatures measured 6 mm from outlet, within the gap, reach a maximum which corresponds with the boiling point of the electrolyte at that pressure. Below the electrolyte boiling point, the temperatures vary significantly with outlet pressure. Increase in pressure reduces the volume of the bubbles so that the current density in the electrolyte around the bubbles is less and lower temperatures are recorded.

A further test series was carried out at a machining voltage of 16 V which is more typical of electrochemical machining in practice. The current density was maintained at 16 A cm^{-2} and electrolyte concentration was increased to give a machining gap width of 1.60 mm. This was considered to be the smallest safe gap for tests. In Fig. 4.7 boiling occurred within the gap, as noted previously, but at a lower flowrate than at 32 V since less power is dissipated in the electrolyte. The highest temperatures measured downsteam of the electrodes are about 30% lower than at the higher voltage.

Some differences in the mode of machining failure, with sodium chloride and sodium nitrate electrolytes, were observed in Chapter 3. Further tests were carried out with a 17% sodium nitrate solution such that the conductivity was similar to that of the 10% sodium chloride solution. The feedrate was based on an apparent valency of three for the steel anodes and machining currents were similar to

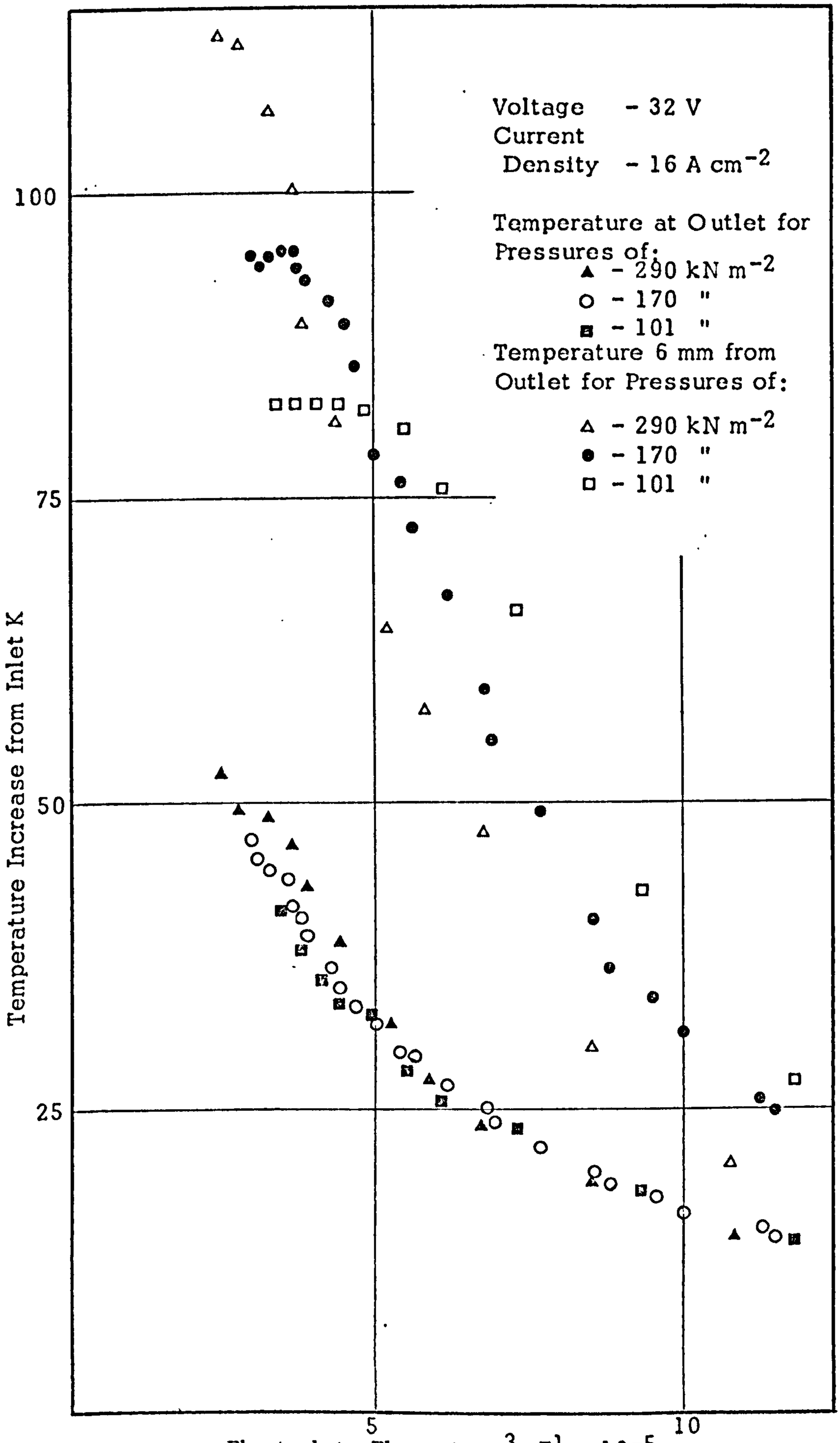

FIG. 4.6 VARIATION IN TEMPERATURE INCREASE WITH OUTLET PRESSURE AND FLOWRATE

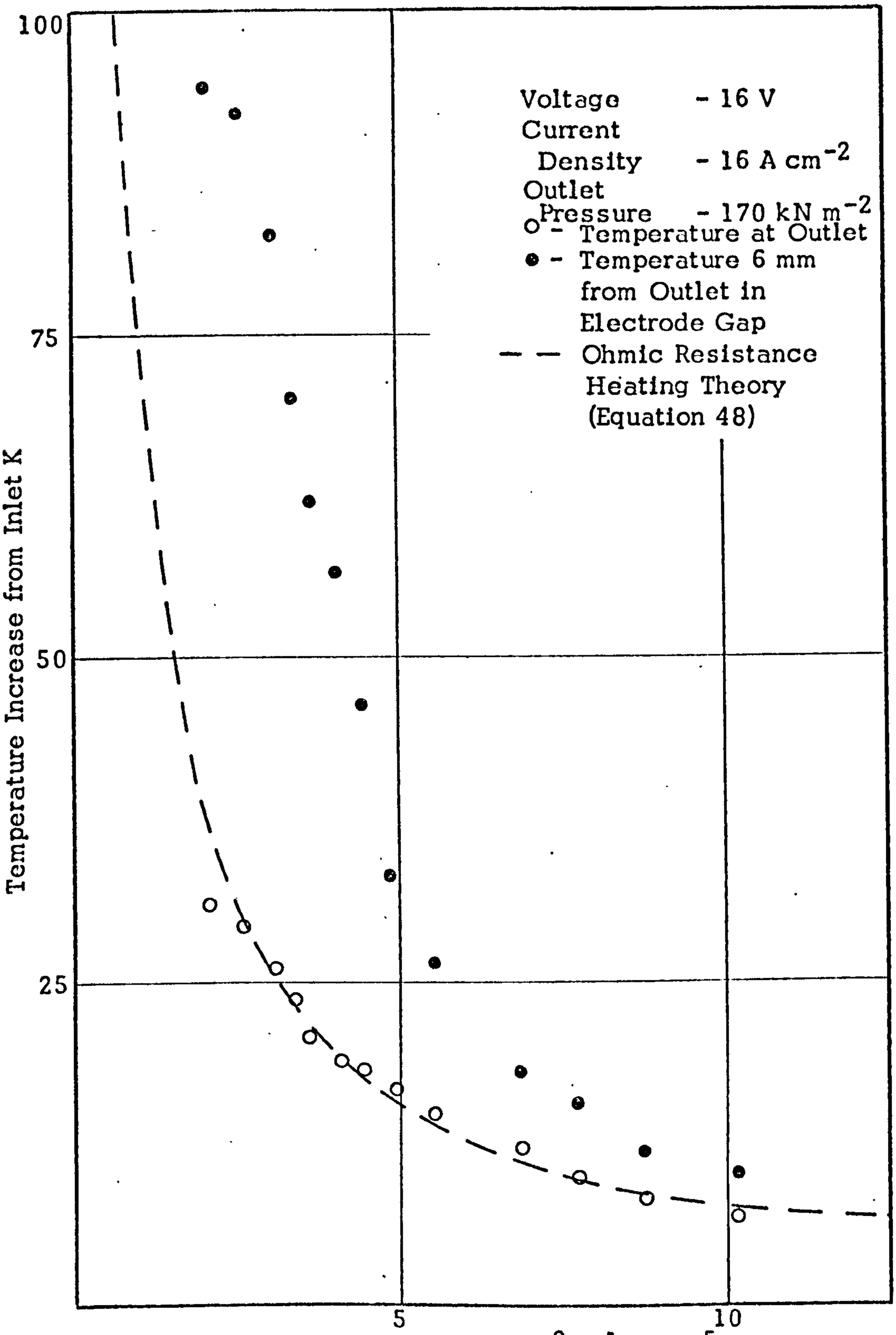

FIG. 4.7 VARIATION IN TEMPERATURE INCREASE WITH ELECTROLYTE FLOWRATE

those in tests with the sodium chloride solution. The colour of the precipitate in the electrolyte was reddish-brown typical of ferric hydroxide. However a valency of dissolution of two is more probable as indicated by the previous work with this electrolyte. Electrolyte flowrate has a marked effect on current efficiency (Fig. 4.8). Current efficiencies were calculated from weight loss measurements assuming a valency of two. At the lower values of efficiency a light grey powdery film formed on the anode surface indicating passivation. The machining current increased during the test as the anode approached the cathode and equilibrium conditions did not become established. In an attempt to prevent passivation the electrolyte temperature and concentration were increased to values similar to those used in tests with the Anocut machine but passivation again occurred in the same flowrate range.

In Fig. 4.9 the temperature increase from inlet is shown against electrolyte flowrate for the nitrate and chloride solutions. Temperatures measured downstream of the electrodes show fair agreement. However, the temperatures measured within the gap with the nitrate solution are lower than those for the chloride solution. This indicates that less gas is evolved at the cathode with the nitrate solution. A similar result has been observed photographically by Landolt et al (22). This clearly demonstrates that the higher temperatures, within the gap close to the cathode, than those at outlet are due to the presence of gas bubbles and not to any other effect.

The workpiece profile deviations for the tests with the nitrate solution are shown in Fig. 4.10. At the highest flowrate the electrode

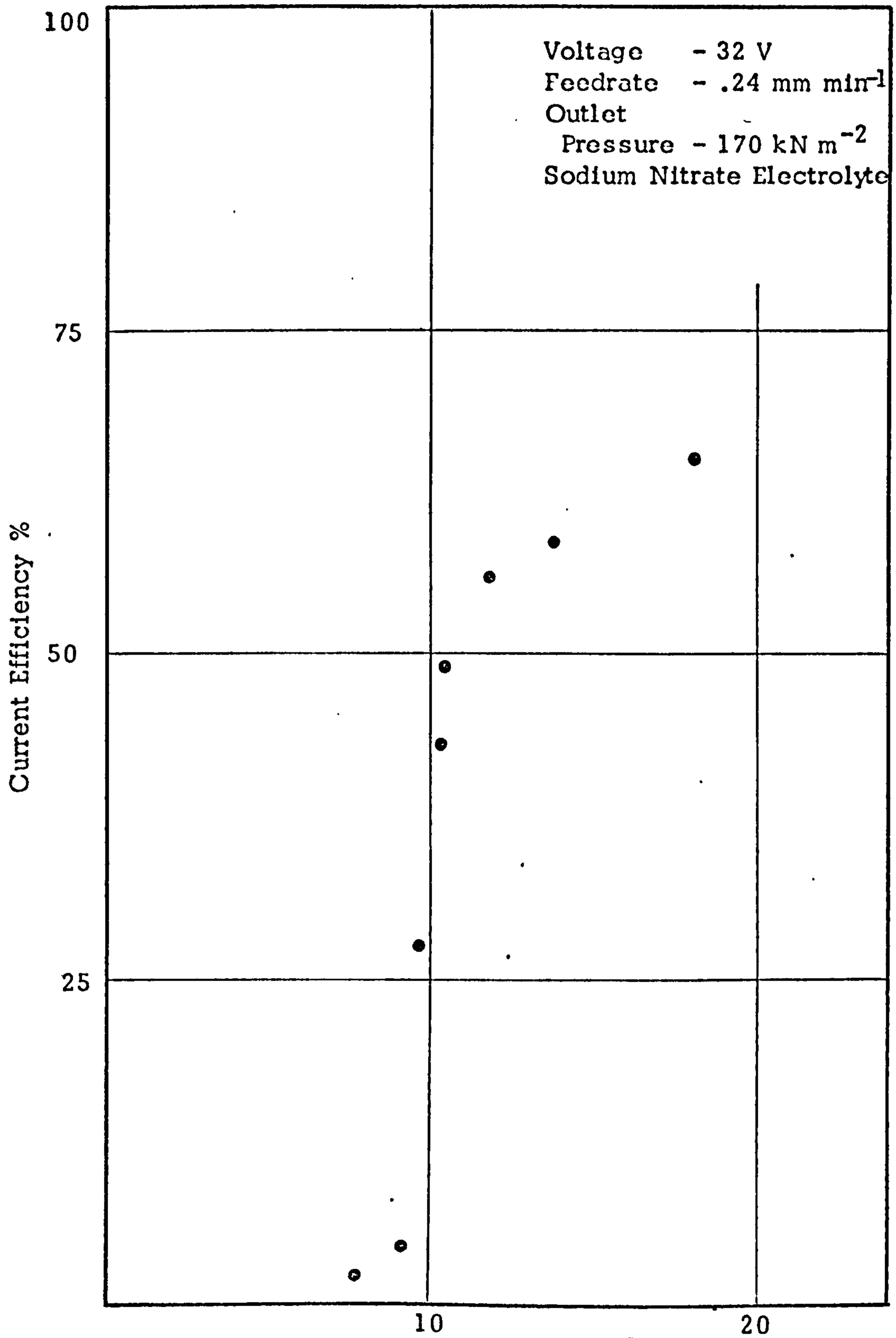

FIG. 4.8 DEPENDENCE OF CURRENT EFFICIENCY ON ELECTROLYTE FLOWRATE

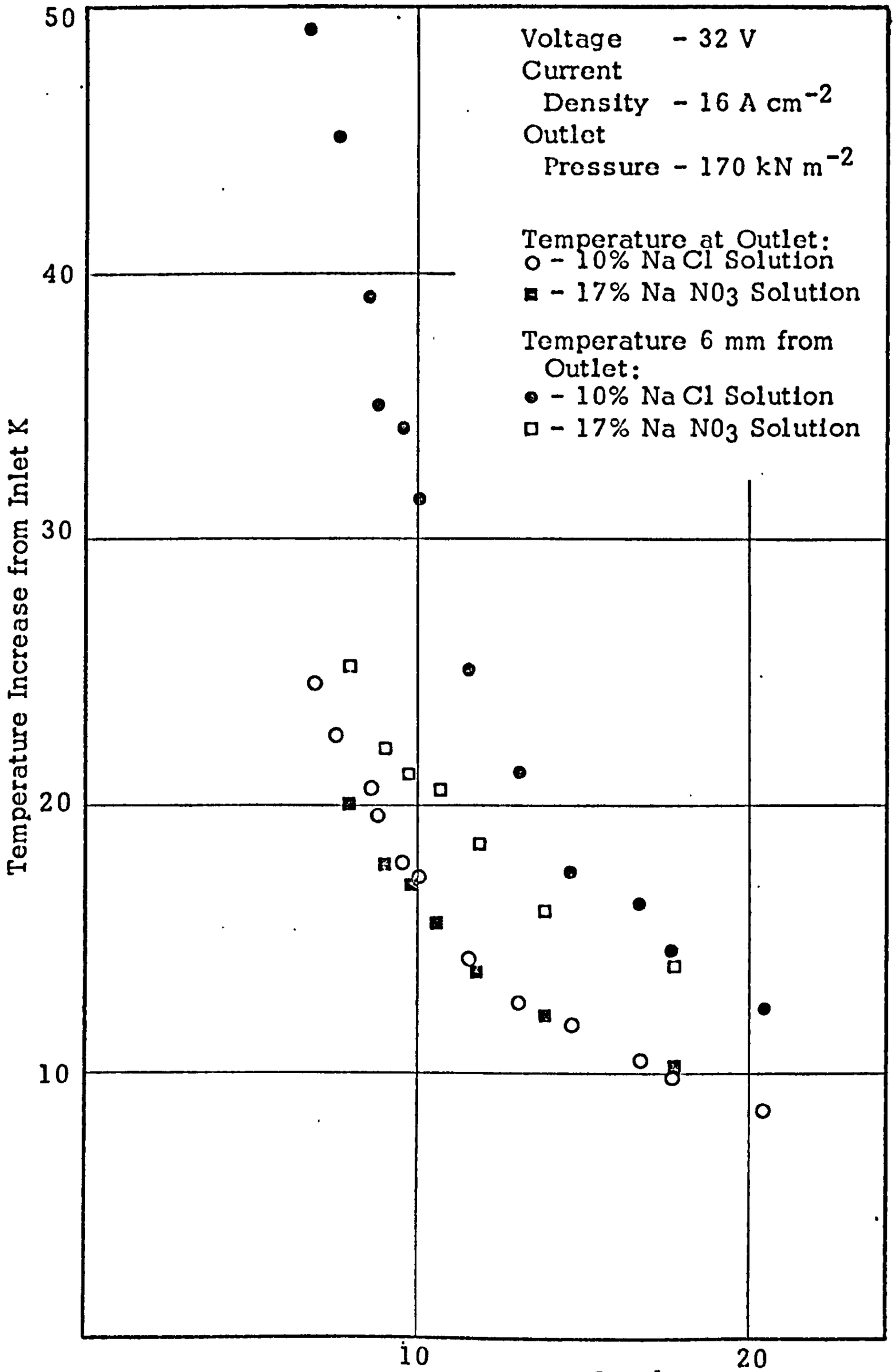

FIG. 4.9 COMPARISON OF TEMPERATURE INCREASE FOR SODIUM CHLORIDE AND SODIUM NITRATE ELECTROLYTES

Voltage - 32 V
Current
Density - 16 A cm^{-2}
Outlet
Pressure - 170 kN m^{-2}
Sodium Nitrate Solution

Flowrates:
○ - 18.0 x 10^{-5} m^3 s^{-1}
□ - 13.8 " "
△ - 11.8 " "
▼ - 10.5 " "
■ - 10.2 " "
● - 9.8 " "
▲ - 9.1 " "

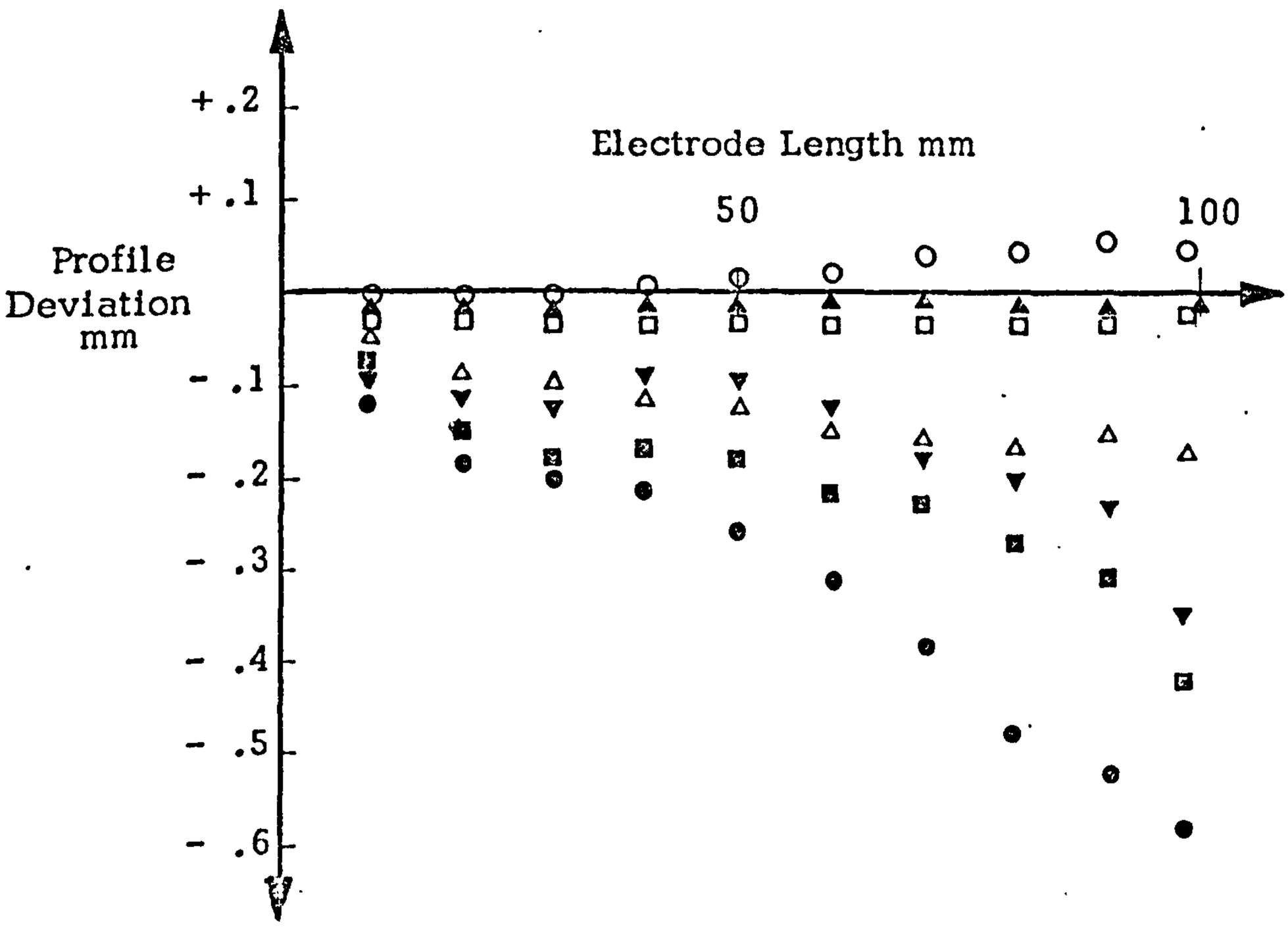

FIG. 4.10 INFLUENCE OF ELECTROLYTE FLOWRATE ON THE ANODE PROFILE

gap increases slightly along the electrode length. As the flowrate, and current efficiency, become less the anode surface slopes towards the cathode. For conditions of almost complete passivation the gap is constant along the electrode length. Comparison with the anode profiles in Fig. 4.5 shows that anodic phenomena have a considerable effect on the profiles for tests with sodium nitrate solution.

In the test at 9.8×10^{-5} in^3 s^{-1} in Fig. 4.10, which corresponds to the onset of passivation, the current efficiency appears to become less along the electrode length. Konig and Degenhardt (49) have found that the efficiency of machining steel with nitrate electrolyte decreases slowly with increase in electrolyte temperature. However, the marked change in efficiency along the electrode length indicates that electrode length in addition to current density and flow-rate, determines the onset of passivation.

For the special case of machining steel, at current densities much lower than those in practice and using sodium nitrate solution, the lower bound to the electrolyte velocity is where passivation of the anode surface occurs. For the tests using sodium nitrate solution, at high current densities, and for sodium chloride solution the lower bound to the electrolyte velocity appears to be due to boiling of the electrolyte in the bubble layer.

4.2 The Upper Bound to the Electrolyte Velocity

The object of this section of the experimental work was to determine the existence of the choked flow condition predicted theoretically. Choking represents an upper bound to the electrolyte velocity in the gap and cannot be tolerated if machining failure and sparking is to be avoided. The choked flow limitation, shown in Fig. 1.1 for typical machining conditions, indicates that choking places a severe restriction on the feedrate in electrochemical machining.

This condition was not encountered in the previous experimental work due to the relatively long electrode lengths and limited pump capability which limited the electrolyte flow velocity. Thus choking is most likely to occur where the flow path length is short and the electrode gap is small. From a practical point of view these conditions are applicable in machining operations such as drilling, broaching and blanking where high feedrates are essential if the process is to be competitive with alternative machining methods.

4.2.1 Design of Experiments

The use of the above machining modes in the experimental work was considered but it was concluded that the electrolyte flowrate and pressure would be subject to many variable effects such as the depth of the tool in the work, the overcut and the tool shape which would cause difficulty in the analysis of results. Plane parallel electrodes were used since the electrolyte flow at inlet is

uniform and the velocity can be easily established.

The experiments were designed on the maximum capabilities of available equipment. The small electrochemical drilling machine described in Chapter 2 had a maximum feedrate of 8 mm min^{-1} so that current densities of up to 360 A cm^{-2} could be obtained. The power supply operated within limits of 250 A at 32 V and 500 A at 16 V. Since a wide range of voltages was required the maximum current available was taken to be 250 A such that the electrode area was restricted to 0.7 cm^2.

The most suitable electrolyte pump was a 'D' type, .75 kW, Mono pump available at another station of the small machine. Previous work (51) indicated that this pump was capable of a flowrate of 3×10^{-5} m^3 s^{-1} at a delivery pressure of 3000 kN m^{-2}. To realise high flow velocities the electrode width had to be small and 3 mm was considered suitable and no mechanical failure of the electrodes was observed. In the main working range this gave electrode gap width to inter-electrode gap ratios of 10 to 60. The electrode length was, therefore, limited to about 20 mm to remain within the current available. However, calculations showed that, operating at maximum feedrate and pump capability, the electrolyte would boil at outlet. An electrode length of 10 mm was found to be more suitable. Since the electrolyte velocity is high the effect of electrode length on pressure loss (proportional to length and the square of velocity) is small in the range available.

4.2.2 The Machining System

The electrochemical machine and power supply are described in Chapter 2.

The machining cell is shown in Fig. 4.11. Since the object of the work was to determine the choked flow velocity it was essential that there was no side flow past the electrodes. The cell design allowed the tool and workpiece aperture to be adjusted by varying the torque on the clamping bolts and the polypropylene housing was compressed onto the electrodes. This proved to be effective as small razor sharp rags at the sides of the workpiece after machining indicated the absence of side flow. Since the feed drive was through a 1400:1 reduction gearbox the force required to drive the workpiece into the cell was not sufficient to overload the feed motor.

To prevent electrolyte spray in the event of an accident a perspex sealing chamber was situated above the flow channel and was self-locating on the workpiece fixture shaft. The tool was made removeable in the event of spark damage and was located in a slot in the base-plate and clamped with a lock-nut. The workpieces were accurately positioned on the drive shaft with vertically in line, fitted bolts. To align the workpiece with the tool aperture the base-plate shaft was made a clearance fit on the machine table location and clamped with the workpiece in contact with the tool.

The electrolyte flow system was built for previous experimental work. The electrolyte temperature in the working tank was controlled by a 2 kW, fused silica sheath heating element and an electric contact

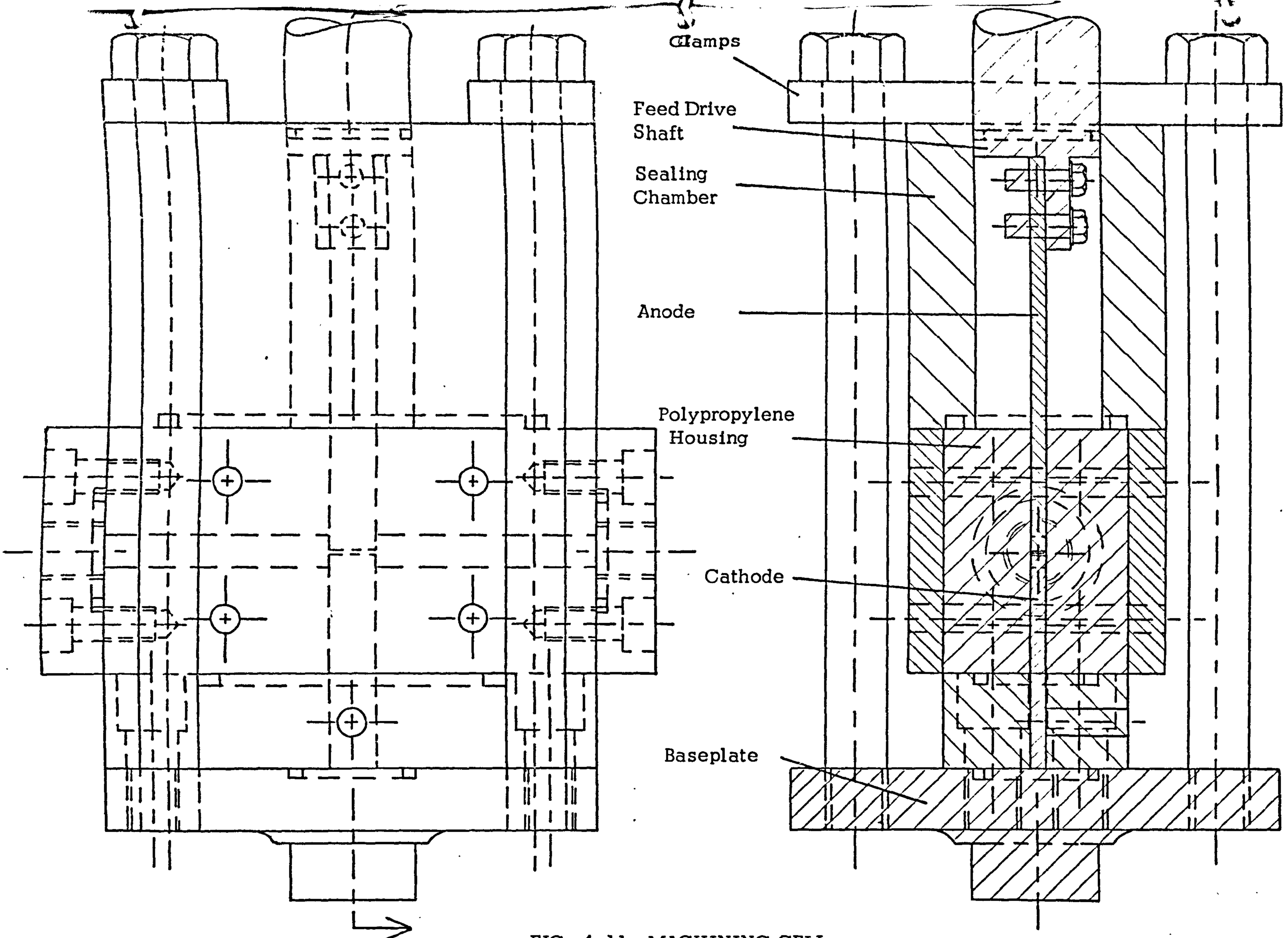

FIG. 4.11 MACHINING CELL

thermometer situated in the 0.1 m^3 capacity tank. A 10% solution of sodium chloride was used at a temperature of 30°C.

The suction line of the pump drew from the top of the tank to minimise recirculation of metal precipitate. A filter unit on the delivery side prevented small particles from entering the machining cell. A by-pass valve in the flow circuit allowed variable electrolyte flowrate and outlet pressure was controlled by a needle valve. Stainless steel piping was used in the circuit due to the high pressures developed by the pump.

The electrolyte flowrate was measured with a Rhodes flowmeter suitable for flowrates up to 40×10^{-5} m^3 s^{-1}. This was a rotating vane flowmeter and operated from a transistorised frequency to indicating meter convertor with input from a reed switch transmitter. The output was displayed on the Rikdenki pen-recorder. The flowmeter was calibrated before use with a weighing tank. At flowrates less than 5×10^{-5} m^3 s^{-1} the meter was inaccurate and the flowrate was measured by discharging the electrolyte from the machining cell into a measuring jar for a known time interval during each test.

Machining current, voltage, feedrate and electrolyte inlet and outlet temperatures and pressures were measured by the methods used in the previous work. Gap measurement was attempted using the electric contact method but was not reliable and the theoretical values were assumed. The anode profiles were measured with a Nikon optical projector with a 50x magnification. The rags on the sides of the workpieces were removed prior to measurement of the profile.

4.2.3 Experimental Results

Tests were carried out with the by-pass valve closed so that the pump delivered at maximum capability. A test series consisted of a set voltage and increasing the feedrate in successive tests by 1.0 mm min^{-1} until machining failure occurred.

The first test series is shown in Table 8. At a voltage of 32 V the feedrate was increased from 1 to 8 mm min^{-1} (the maximum available) without machining failure. At each increment in feedrate the inlet pressure increased with consequent reduction in flowrate.

To obtain smaller electrode gaps and higher electrolyte velocities the machining voltage was reduced to 16 V (Table 9). The maximum feedrate obtainable was 6 mm min^{-1}. At a feedrate of 7 mm min^{-1} sparking across the electrode gap terminated the test. The characteristics of machining failure, observed in Chapter 3, occurred instantaneously since the time required for the workpiece to traverse the electrode gap was small. The heat generated by sparking melted the tool and workpiece and they were replaced.

For choking to represent a limitation on electrolyte flow velocity at inlet then if the feedrate is maintained the flow velocity should be reduced. Further tests at 7 mm min^{-1}, with the by-pass valve opened slightly, to reduce the electrolyte flowrate, were carried out but machining failure and sparking were again observed.

In Fig. 4.12 the electrolyte flow velocities for the tests in Table 9 are plotted against feedrate. The theoretical limits on feedrate and flow velocity are shown, acceptable values lie to the left of the

Operating Conditions : Machining Voltage - 32 V
Outlet Pressure - 170 kN m^{-2}
Inlet Temperature - 30°C
Electrode Area - .304 cm^2

Test	Feedrate (mm min^{-1})	Machining Current (A)	Flowrate ($m^3 s^{-1}$ x 10^{-5})	Temperature Increase (K)	Inlet Pressure (kN m^{-2})	Electrode Gap at Inlet (mm)
C1	1	14.7	9.1	4.0	1240	.92
C2	2	31.4	7.3	7.0	2270	.46
C3	3	39.2	5.8	10.0	2800	.31
C4	4	54.0	3.8	15.5	3070	.23
C5	5	68.5	3.3	17.2	3440	.185
C6	6	81.5	3.1	23.3	3800	.154
C7	7	95.0	2.5	31.0	4000	.132
C8	8	107	2.1	38.4	4400	.077 .115

TABLE 8

Operating Conditions : Machining Voltage - 16 V
Outlet Pressure - 170 kN m^{-2}
Inlet Temperature - 30°C
Electrode Area - .304 cm^2

Test	Feedrate (mm min^{-1})	Machining Current (A)	Flowrate ($m^3 s^{-1}$ x 10^{-5})	Temperature Increase (K)	Inlet Pressure (kN m^{-2})	Electrode Gap at Inlet (mm)
C12	2	29.2	2.9	7.5	3440	.22
C13	3	42.1	2.3	14.0	3920	.158
C14	4	55.0	1.7	16.0	4480	.117
C15	5	73.8	1.5	24.2	4540	.094
C16	6	83.2	1.1	26.1	4960	.079
C17	7	Machining Failure Conditions				

TABLE 9

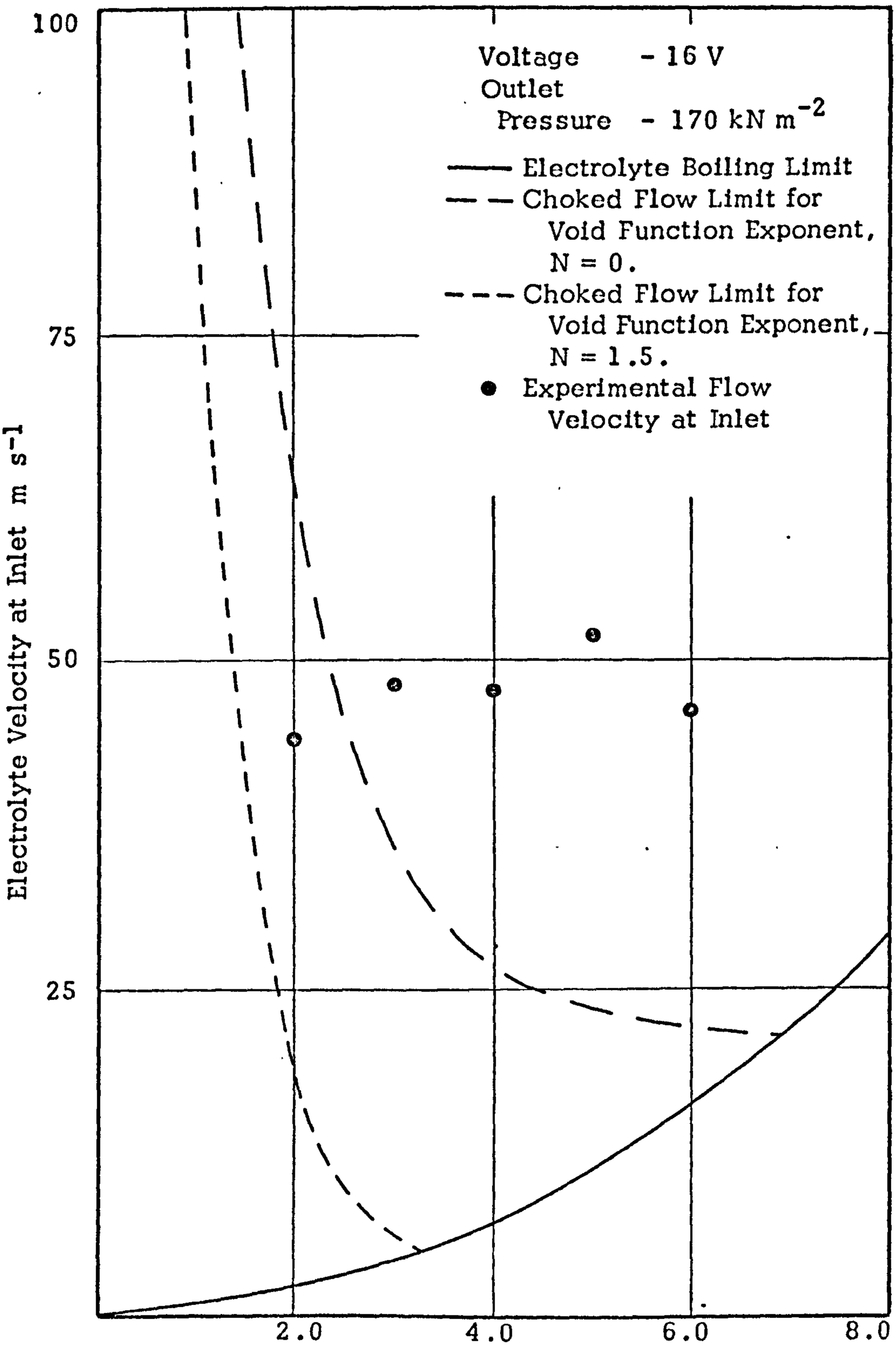

FIG. 4.12 COMPARISON OF EXPERIMENTAL FLOW VELOCITY WITH THEORETICAL LIMITS ON ELECTROLYTE VELOCITY AT INLET

curves. The lower limit is taken to be electrolyte boiling in the exit plane. The upper limits on velocity are calculated from the choked flow equation (52) for void function exponents of 1.5 and 0. The experimental flow velocities are considerably greater than the choked flow limits.

Further tests were performed at 8 V (Table 10). Machining failure and sparking terminated the test at 5 mm min^{-1}. At a feedrate of 4 mm min^{-1} the pump is operating close to shut-off. Further increase in feedrate and the flowrate becomes less and is not sufficient to prevent boiling within the bubble-electrolyte layer. This also applies to Test 17 in Table 9. At the maximum safe feedrates in Tables 9 and 10 there is no indication of the electrolyte outlet temperature approaching the boiling point of the electrolyte.

The characteristics of the anode profile at high feedrates and flow velocities are shown in Table 11. The degree of scatter in the anode profiles indicates that the workpiece alignment procedure was not accurate. Moreover visual examination of the workpieces showed undulations on the machined surface which also affected the profile measurements. For this reason no attempt was made to match the profile with the theoretical model. The assumption of a void exponent of zero in Fig. 4.12 represents the upper limit of choked flow velocities and the frictional multiplier does not affect these values.

The tests in Table 11 also show that, for short flow path lengths, the lower bound to the electrolyte velocity is where boiling occurs within the gap and the outlet temperature is well below boiling point.

Operating Conditions : Machining Voltage - 8 V
Outlet Pressure - 170 kN m^{-2}
Inlet Temperature - 30°C
Electrode Area - .304 cm^2

Test	Feedrate (mm min^{-1})	Machining Current (A)	Flowrate ($m^3 s^{-1} \times 10^{-5}$)	Temperature Increase (K)	Inlet Pressure (kN m^{-2})	Electrode Gap at Inlet (mm)
C20	2	28.0	3.7	8.5	2480	.102
C21	3	42.5	1.2	11.0	4820	.065
C22	4	57.0	0.5	16.8	5200	.048
C23	5	Machining Failure Conditions				

TABLE 10

Operating Conditions : Machining Voltage - 32 V
Feedrate - 6 mm mm^{-1}
Outlet Pressure - 170 kN m^{-2}
Inlet Temperature - 30°C
Electrode Area - .304 cm^2

Test	Machining Current (A)	Flowrate ($m^3 s^{-1} \times 10^{-5}$)	Temperature Increase (K)	Inlet Pressure (kN m^{-2})	Electrode Gap at Inlet (mm)
C6	82.5	3.1	23.3	3800	.167
C25	82.0	2.9	24.0	3020	.167
C26	83.0	2.3	30.0	2070	.167
C27	84.0	2.1	34.2	1700	.167
C28	83.0	1.7	41.5	1350	.167
C29	Machining Failure Conditions				

Distance along anode surface from inlet (mm)

Test	0	2.5	5.0	7.5	10.0
C6	0	+.14	+.125	+.095	+.105
C25	Profile 0	+.03	+.075	-.035	-.020
C26	Deviat-0	+.185	+.050	+.030	+.010
C27	ion mm 0	+.028	+.011	-.065	-.095
C28	0	+.060	+.010	-.035	+.015

TABLE 11

To summarise, the upper limit to the electrolyte velocity is determined by the performance characteristics of the pump and the theoretical choked flow condition does not occur for the conditions of machining used.

5.0 DISCUSSION

5.1 The Theoretical Model

The theoretical model developed by Thorpe and Zerkle (16,17,18) for the prediction of the equilibrium electrode gap, shows good agreement with experimental anode profiles if empirical model parameters are used. The model parameters, the frictional multiplier and the void function exponent, are dependent on the electrolyte flow velocity and the outlet pressure but show little variation with current density and machining voltage.

The frictional multipliers, required to match the experimental pressure loss in tests, range from 1.2 to 3.2 which indicates an increase in shear stress at the surfaces of the electrodes due to gas bubble nucleation. The frictional multipliers become less with increase in flow velocity and outlet pressure. Landolt et al (22) found, from photographic observations, that bubble size decreased with approximately the square of the flow velocity. A small increase in bubble size with current density was observed. The frictional multiplier may be related to the size of bubbles evolving on the cathode surface. Nikuradse (52) found that the friction factor for turbulent flow in pipes increased with increase in surface roughness. Surface roughness was described in terms of the ratio of the diameter of sand grains on the pipe wall to the pipe diameter. In electrochemical machining the gas bubbles, nucleating on the surfaces of the electrodes may act as small roughness protrusions. Nikuradse (52) also found that the friction factor in rough pipes was complexly related to the

Reynolds Number of the flow but a similar relationship was not observed in this work within the relatively limited range of flowrates used. As an alternative to formulating empirical correlations, such as are available for steam-water flow, frictional multipliers are reported in Chapter 3 for operating conditions similar to those used in practice for die-sinking and forming operations.

The void function exponent, n, is a generalisation of heterogeneous conduction mechanisms to account for the effect of gas bubbles on the electrolyte conductivity. De la Rue and Tobias (21) found that n = 1.5 described experimental data for non-conducting particles in a static electrolyte. The void function exponent in the theoretical model also accounts for the assumptions of no relative motion between bubbles and electrolyte and that of homogeneous bubbly flow between the electrodes. In general the slip ratio in two-phase systems is dependent on the void fraction and density of the gas bubbles, and the flowrate and has to be determined experimentally. Photographic observations (22) have shown that the bubbles are concentrated in a layer close to the cathode so that the flow is not homogeneous. However, the assumptions are required to allow solution of the equations.

The void function exponents required to match the experimental anode profiles in Chapter 3 are lower than 1.5 and decrease with increase in outlet pressure and increase in flow velocity. The marked difference from the value of 1.5, used by Thorpe and Zerkle (16,17,18) and by Hopenfield and Cole (15), indicates that the above assumptions

are in error and that the bubbles may also be partially dissolved in the electrolyte. This has been shown in low current density experiments (53). The solubility of a gas in a liquid is a function of temperature, pressure and time (54). The solubility of hydrogen in sodium chloride solution decreases slowly with increase in temperature and is directly proportional to pressure. An alternative explanation is that the residence time of the hydrogen within the gap is so short that the atomic hydrogen is not all combined to form molecular hydrogen. However, Landolt (22) found that very small bubbles, less than 20μm, were formed at a current density of 100 A cm^{-2} and at flow velocities above 10 m s^{-1} which are of the order of the conditions used in Chapter 3.

The influence of the hydrogen bubbles on the anode profile only becomes apparent towards outlet and at low flowrates where the local pressure is low. It is important to note that, in Chapter 3, the anode profiles obtained at an outlet pressure of 800 kN m^{-2} would be accurately predicted by the constant gas density model and by neglecting the effect of gas bubbles on the electrolyte conductivity.

In the experimental work with the sodium nitrate electrolyte the gas bubbles appear to have very little effect on the electrolyte conductivity. The anode profiles also differ in shape from those in tests using sodium chloride electrolyte. Landolt (22) observed less gas evolved at the cathode with sodium nitrate electrolyte relative to that with sodium chloride electrolyte. Mao (48) found that no

hydrogen was evolved at the cathode but that the nitrate was reduced to ammonia and hydroxylamine. However, the change in gap width for the tests at high flowrates is greater than that predicted assuming the gas bubbles have no effect on the electrolyte conductivity. Freer (30) has shown that a resistive film is formed on mild steel anodes machined using sodium nitrate electrolyte. The present work indicates that the resistance of the film becomes less along the electrode length or that some factor influences the anode profile other than electrolyte conductivity.

5.2 The Lower Bound to the Electrolyte Velocity

The experimental work with the thermistors set into the cathode (Section 4.1) demonstrates that the lower bound to the electrolyte velocity or flowrate is where boiling occurs within the bubble-electrolyte layer close to the cathode. The electrolyte boils due to the reduction in area available, by the bubbles, for the passage of machining current such that high temperatures are generated in the electrolyte around the bubbles. The temperatures measured down-stream of the electrodes represent the 'mixed cup' temperature of the electrolyte and are considerably lower than those in the bubble electrolyte layer particularly at low machining voltages. The resistance of the electrolyte increases due to the formation of steam bubbles and the anode converges towards the cathode at outlet so that sparking or arcing occurs across the gap. Machining current fluctuations are observed at flowrates corresponding to boiling within the gap. This

may be caused by steam bubbles moving into the cooler bulk electrolyte flow, collapsing due to condensation, and causing a sudden change in the resistance of the electrolyte.

The results may be considered in relation to those obtained in other investigations as it is important that the cause of machining failure is clearly defined to provide a basis for the selection of operating conditions. Landolt et al (22), using a constant current method, report cell voltage oscillations at low electrolyte flowrates. The oscillations coincided with the appearance of large bubbles of different size and shape to that of the hydrogen bubbles. In the context of the results reported here these bubbles may be steam bubbles. Landolt (22) also observed bubbles sticking to the cathode and proposed that sparking is the result of complete instantaneous coverage of the cathode with bubbles although this could not be photographed.

Bubbles may be assumed to detach from a surface when buoyancy and inertia forces on the bubbles become larger than the normal component of surface tension (55). To determine experimentally if the hydrogen bubbles were remaining on the cathode surface, tests were carried out, (as described in Section 4.1), with a surfactant added to the electrolyte. A concentration of 0.2% of the surfactant, Lissapol-n, was added to reduce the surface tension by almost 50%. This was determined experimentally by the Du Nuoy method using a Cambridge Tensiometer. Initial tests using this electrolyte produced results which were not repeatable. However, impurities have a marked

effect on surface tension (18) and further work was carried out with a freshly prepared, clean electrolyte. For this case, the results were repeatable and were similar to those in Fig. 4.2. Thus it is concluded that machining failure is not the result of bubbles adhering to the cathode surface.

Kellogg (56) investigated the formation of gas bubble layers on wire electrodes at low current densities. The formation of the layer coincided with a drastic increase in the surface temperature of the electrodes. This is analogous to critical burnout which limits the heat transfer rate in boiler tubes. However care was taken, at the assembly stage, to prevent the thermistors measuring the cathode surface temperature and no drastic temperature increase was observed.

when machining copper with phosphoric acid electrolyte
Baxter (28) observed that, at the maximum or limiting current density, the resistance of the electrolyte close to the cathode increased, the current density became less towards outlet and that the limiting current density was directly proportional to (outlet pressure)$^{\frac{1}{3}}$. These results are consistent with boiling of the electrolyte within the bubble layer.

In the experimental work in Section 4.1 the machining current was maintained at a constant level by close control of the electrolyte flowrate and outlet pressure. In the tests at machining failure conditions on the Anocut machine the coverging gap at outlet restricts the electrolyte flowrate so that the outlet temperature increases. Boiling within the bubble layer spreads from outlet towards inlet. The electrode gap cannot change at the same rate as the electrolyte

conductivity and the machining current becomes less. Increase in outlet pressure increases the boiling point of the electrolyte and reduces the volume of gas bubbles in the gap so that lower flowrates are possible (Fig. 3.15).

Machining failure, in tests using sodium nitrate electrolyte, is similar in most respects to that with the sodium chloride electrolyte. The reduced current efficiency in those tests (Table 7) is due to the low current density in the outlet region as a result of boiling in the bubble layer. Low current efficiencies and passivation are observed at a current density of 16 A cm^{-2} in Fig. 4.8. The distinctive shiny strip on the machined surface (Fig. 3.14) may be due to values of the current density and anode potential corresponding to the polishing region of the polarisation curve.

Landolt (22) and Mao (48) have noted that less gas is evolved at the cathode with nitrate solution relative to that with chloride solution. As a result it would be expected that machining failure would occur at lower flowrates with the nitrate solution and this was, indeed, observed by Landolt. However, this is not substantiated in the present work and the lowest flowrate in Table 6 is greater than corresponding values, under all test conditions, with the sodium chloride solution. A tendency to machining failure and sparking with nitrate electrolyte has also been noted by Flett (10). The only apparent explanation of this result is the age or the purity of the electrolyte used in the tests. The initial test series using the Anocut machine was carried out with a sodium chloride solution which had been used for

some time in other work whereas a fresh solution of sodium nitrate was prepared for the second test series. An improvement in electrolyte performance with age is well known although the cause is not established.

The lower bound to the electrolyte velocity with the sodium nitrate solution at low current densities (Fig. 4.8) is the result of passivation of the anode surface. Passivation at low current densities has an important effect on the accuracy of the process as it prevents metal removal at areas remote from the tool cutting face. Landolt, Muller and Tobias (35) obtained order of magnitude agreement between experimental and predicted passivation current densities from known hydrodynamic equations for mass transfer. The equations are not in agreement with experimental data for a machining cell similar to those used in practice (29). For this reason no attempt was made to relate these equations with the results reported in this work. In addition an order of magnitude estimate of the lower bound to the electrolyte flowrate is of limited value in relation to the selection of operating conditions.

5.3 The Theoretical Choked Flow Condition

Under certain operating conditions the theoretical model predicts a choked flow condition similar to that occurring in compressible and two-phase flows. The theoretical choked flow condition in electrochemical machining corresponds to an upper bound to the electrolyte velocity and a limiting value of the tool feedrate.

However, the theoretical model is not verified in this respect. In the tests specifically designed to investigate the choked flow condition, flow velocities are obtained which are much greater than those corresponding to choking (Fig. 4.12). The upper limit of choked flow velocities were calculated on the assumption of a void exponent function of zero which appears probable due to the low values obtained at high flow velocities in Chapter 3. The current densities and flow velocities, used in Section 4.2, are much greater than those likely to be encountered in practice.

Choking appears to be a consequence of the assumption of homogeneous bubbly flow, in the theoretical analysis, which is required for a solution to the equations. In a stratified or separated flow, which appears to be the case in the electrode gap (22), choking can only occur when the velocity of either the bubble layer or the bulk electrolyte flow attains the velocity of sound of the pure phase (19). Typical values of the velocity of sound of hydrogen and water are of the order of 1000 m s^{-1} and are far outwith the capabilities of pumps used in electrochemical machining. Thus it is considered that operating conditions of machining should not be based on the maximum tool feedrate predicted from the choked flow condition.

The frictional multipliers and void function exponents could not be determined for the tests in section 4.2 due to inaccuracy in the workpiece alignment arrangement and the undulations on the machined surfaces which became apparent at machining gap widths of less than 0.1 mm. However, in machining operations with short flow path

lengths and high flow velocities the frictional pressure loss is small relative to the velocity head loss at inlet so that suitable values of the frictional multiplier are not essential to the selection of operating conditions.

5.4 Correlation of Results

A method of prediction of the lower bound to the electrolyte velocity is required to provide a basis for the selection of operating conditions. The lower bound is where boiling occurs within the bubble-electrolyte layer close to the cathode. To attempt to describe this situation mathematically would require a separated flow model in which the equations of continuity of mass, motion, energy and charge are derived for the bulk electrolyte flow, the gas bubble phase and the electrolyte surrounding the bubbles. Such analyses are very complex (58) and the number of variables generally exceeds the number of equations such that simplifying assumptions and additional model parameters are required.

The value of the model developed by Thorpe and Zerkle (16,17,18) is that the describing system of coupled, non-linear differential equations was solved to obtain simple algebraic expressions for the variation in gap width, void fraction, electrolyte velocity and temperature which serve as convenient rules for the tool and production engineer concerned with electrochemical machining. As an alternative to formulating a more complex model, which may not

reduce to simple equations, a semi-theoretical correlation is introduced.

The energy equation derived by Thorpe and Zerkle (16, 17) is:

$$\rho_f V_f \frac{dT}{dx} = \frac{V \phi}{C_f (1 - \alpha) y} \tag{28}$$

Substituting for yV_f from equation (26) (Appendix I)

$$\frac{dT}{dx^*} = \frac{T_r}{\eta x^* + 1} \tag{36}$$

This is an explicit equation having the solution:

$$T = T_o + \frac{T_r}{\eta} \ln (1 + \eta x^*) \tag{38}$$

The co-ordinate x^* is of order 10^{-3} or less and η is less than unity.

Thus equation (38) reduces to:

$$T = T_o + T_r x^* \tag{48}$$

$$\therefore T - T_o = \frac{V}{\varepsilon \lambda_a C_f} \cdot \frac{x \rho_a V_c}{\rho_o V_o y_o} \tag{61}$$

The current density, $\phi = \frac{\rho_a V_c}{\varepsilon \lambda_a}$ (9)

$$\therefore T - T_o = \frac{V \phi x}{C_f \rho_o V_o y_o} \tag{62}$$

This is the equation for the temperature increase, from inlet to outlet, of the bulk electrolyte flow. The temperature of the electrolyte around the bubbles is greater due to the reduction in area available for the passage of current. If the bubbles are assumed to be spherical and in contact with each other then the most open packing of spheres is where each layer lies immediately above the other on a square base. This arrangement has a void of approximately 50% (59) where void is

the ratio of open space volume to the combined open space volume and sphere volume in the packing. The effective area available for the passage of current is $d^2 - \pi/4\ d^2$ where d is the diameter of the bubbles. The resistance of the bubble-electrolyte layer is then:

$$R_l = \frac{y_l}{k_f\ d^2\ (1 - \pi/4)} \tag{63}$$

Similarly the resistance of the electrolyte layer close to the anode is:

$$R_f = \frac{y_f}{k_f \cdot A} \tag{64}$$

Since the volume of bubbles and electrolyte in the bubble-electrolyte layer is assumed equal, the ratio of the thickness of this layer to the electrolyte layer is:

$$\frac{y_l}{y_f} = \frac{2\alpha}{1 - 2\alpha} \tag{65}$$

Applying Ohm's law across the electrode gap:

$$I = \frac{V_f}{R_f} = \frac{V_l}{R_l}$$

$$\therefore\ \frac{V_l}{V_f} = \frac{R_l}{R_f} \tag{66}$$

Substituting equations 63 and 64 then:

$$\frac{V_l}{V_f} = \frac{y_l}{y_f\ (1 - \pi/4)} \tag{67}$$

From equation 65

$$\frac{V_l}{V_f} = \frac{2\alpha}{(1 - 2\alpha)(1 - \pi/4)} \tag{68}$$

Thus the potential drop in the bubble-electrolyte layer is

$$V_l = \frac{V_f \cdot 2\alpha}{(1 - 2\alpha)(1 - \pi/4)} \tag{69}$$

Also $$V = V_l + V_f \tag{70}$$

Substituting for V_f from equation 69

$$V = V_1 + \frac{V_1 (1 - 2\alpha) (1 - \pi/4)}{2\alpha}$$

$$= V_1 \left[1 + \frac{(1 - 2\alpha)(1 - \pi/4)}{2\alpha}\right] \quad (71)$$

$$\therefore V_1 = \frac{V}{\left[1 + \frac{(1 - 2\alpha)(1 - \pi/4)}{2\alpha}\right]} \quad (72)$$

On the basis of the assumption of cubic packing of the hydrogen bubbles then the mass of electrolyte within the bubble-electrolyte layer is $\rho_o V_o y_o \alpha$ and the maximum current density in this layer is $I/A (1 - \pi/4)$. The equation for the temperature increase within the layer is

$$T_1 - T_o = \frac{V_1 \; I \; x}{C_f \rho_o \; V_o \; y_o \alpha \; A(1 - \pi/4)} \quad (73)$$

Substituting from equation 72

$$T_1 - T_o = \frac{VI\,x}{\left[1 + \frac{(1 - 2\alpha)(1 - \pi/4)}{2\alpha}\right] C_f \rho_o \; V_o \; y_o \alpha \; A \; (1 - \pi/4)}$$

$$\frac{V\phi x}{C_f \rho_o \; y_o \; V_o \alpha \; . \; 215} \left[1 + \frac{(1 - 2\alpha) . \; 215}{2\alpha}\right] \quad (74)$$

The equation predicts temperatures (at outlet within the bubble-layer) much greater than those compatible with experimental results; for instance for a volume fraction of gas at outlet of 0.3 the predicted temperature increase is 13.6 times greater than the temperature increase of the bulk electrolyte flow (equation 62). The equation may be modified by assuming the minimum current density on the plane of bubble contact:

$$T_1 - T_o = \frac{V\phi x}{C_f \rho_o \; y_o \; V_o \alpha \left[1 + \frac{(1-2\alpha) . \; 215}{2\alpha}\right]} \quad (75)$$

Equation 75 is calculated for tests close to the point of machining failure (Table 12) but shows poor agreement with the boiling point of the electrolyte

Test No.	Feedrate mm min^{-1}	Voltage V	Flowrate $m^3 s^{-1} \times 10^{-5}$	Outlet Pressure kN m^{-2}	Temperature Increase ^oC	Void Fraction at Outlet	T_1 (Eqn.75) ^oC	Boiling Point at Outlet ^oC
4	.55	16	5.0	170	24	.341	84	119
9	.78	16	6.0	150	27	.389	85	116
1-08	1.0	20	30.0	170	23	.277	111	119
1-16	1.0	20	18.0	800	43	.121	252	177
1-24	2.0	20	27.0	170	49	.438	149	119
1-28	2.25	20	32.0	180	46	.426	144	121
1-37	1.0	10	18.0	170	19	.377	87	119
1-40	1.25	10	19.0	170	21	.418	78	119
2-17	1.0	20	36.0	170	21	.290	103	129
2-25	1.5	20	37.0	190	29	.342	117	134
C16	6.0	16	1.1	170	26	.388	93	119
C22	4.0	8	0.5	170	17	.467	66	119

TABLE 12

at the corresponding outlet pressure. In addition the inclusion of the void fraction in the denominator of the equation implies that increase in pressure increases the temperature within the bubble-electrolyte layer which is the converse of the result obtained experimentally (Fig. 4.6).

However, with the exception of the tests culminating with Test 1-16 (Table 12) which were discontinued due to the temperature and pressure limitations of the nylon piping and Tests 2-17 and 2-24 with the sodium nitrate electrolyte, the average value of the void fraction of gas bubbles at outlet is .391. The variation in values of the void fraction may be due to the difficulty in the experimental work in determining the flowrate just above that at which machining failure occurred. The Production Engineering Research Association (9) found that the criterion of void fraction at outlet equal to 0.4 correlated with observed maximum safe feedrates for drilling operations although only three results were presented. Landolt et al (22) found, from photographic estimates of the void fraction, that voltage fluctuations preceeding a spark, occurred at a void fraction of approximately 0.2. The expression for void fraction (equation 45) does not allow for the effects of bubble dissolution in the electrolyte which may be significant as discussed previously.

The void fraction at outlet is determined from the simple relationship:

$$\alpha = \frac{Ax^*}{1 + Ax^*} \qquad (45)$$

and is independent of the model parameters. The observed correlation of void fraction, at outlet, close to 0.4 with experimental data for flowrates just above the machining failure condition in the tests with relatively long electrodes, the extreme conditions of machining in Section 4.2 and for drilling electrodes (9) provides a suitable means of determining the lower bound to the electrolyte flowrate. The results indicate that boiling occurs within the bubble-electrolyte layer when the void fraction at outlet approaches this value.

5.5 The Operating Characteristics of Electrochemical Machining

The operating conditions of electrochemical machining are the tool feedrate, the applied voltage, the electrolyte flowrates and the inlet and outlet pressure of flow in the tooling fixture. The workpiece material and required dimensions are known. The type of electrolyte to be used is affected by the workpiece material and is discussed at length in other work (6, 8). In practice solutions of sodium chloride and sodium nitrate, or mixtures of both, are often used. The limits on electrolyte concentration and inlet temperature, which control the conductivity, are discussed in Section 1.3.

The tool feedrate is the most important operating condition on economic considerations. If the feedrate is limited by the maximum current from available power supplies then the minimum machining voltage should be established. This limit is unlikely to be due to the present trend towards machines built for specific applications which also emphasises the need for a method of prediction of operating conditions.

The inlet pressure and flowrate are limited by the performance capability of the electrolyte pump since choking does not occur in electrochemical machining at conditions used at present. An additional lower limit on electrolyte flowrate, to that discussed previously, is where the temperature of the electrolyte flow, at outlet from the tooling fixture, exceeds the boiling point at atmospheric pressure. If the outlet temperature is greater than this limit, the electrolyte will boil as it is reduced to atmospheric pressure in the control valve or flow restrictor. This can cause unstable flow or a critical flow condition in the valve such that the flowrate cannot be increased by further increase of the pressure differential. The discharge of saturated water from short nozzles and orifices has been investigated by Fauske (60). A maximum flowrate occurs which depends

on the velocity, pressure differential and nozzle length. This was not investigated in relation to electrochemical machining since temperatures greater than the electrolyte boiling point at atmospheric pressure can also result in thermal expansion of the tool and instability of the insulating materials used in the tool fixture. Boiling electrolyte is also a hazard to the machine operator in the event of an accidental pipe burst.

Within the above limitations, the operating characteristics of electrochemical machining are shown in Fig. 5.1 for the tests in Tables 2 and 4. The inlet pressure-flowrate curve was obtained from the computer program output data. Average values of the model parameters for the tests in Tables 2, 4 and 5 at an outlet pressure of 170 kN m^{-2} are assumed. Increase in feedrate from 1.0 to 2.0 mm min^{-1} reduces the gap width and a greater pressure is required to force a given electrolyte flowrate through the gap. Thus the flowrate-pressure curve moves towards the limit on flowrate. The point of intersection of the pump performance curve and the limit on void fraction at outlet determines the maximum feedrate. Operation close to the left of the pump performance curve also reduces the power required to drive the pump. For the pump in the Anocut installation the maximum load of 56 kW is greater than the power consumed in most of the tests in Fig. 5.1.

Reducing the machining voltage from 20 to 10 V (Fig. 5.2) approximately halves the electrode gap. The maximum feedrate is reduced from 2.25 to 1.25 mm min^{-1}. The limit on void fraction at

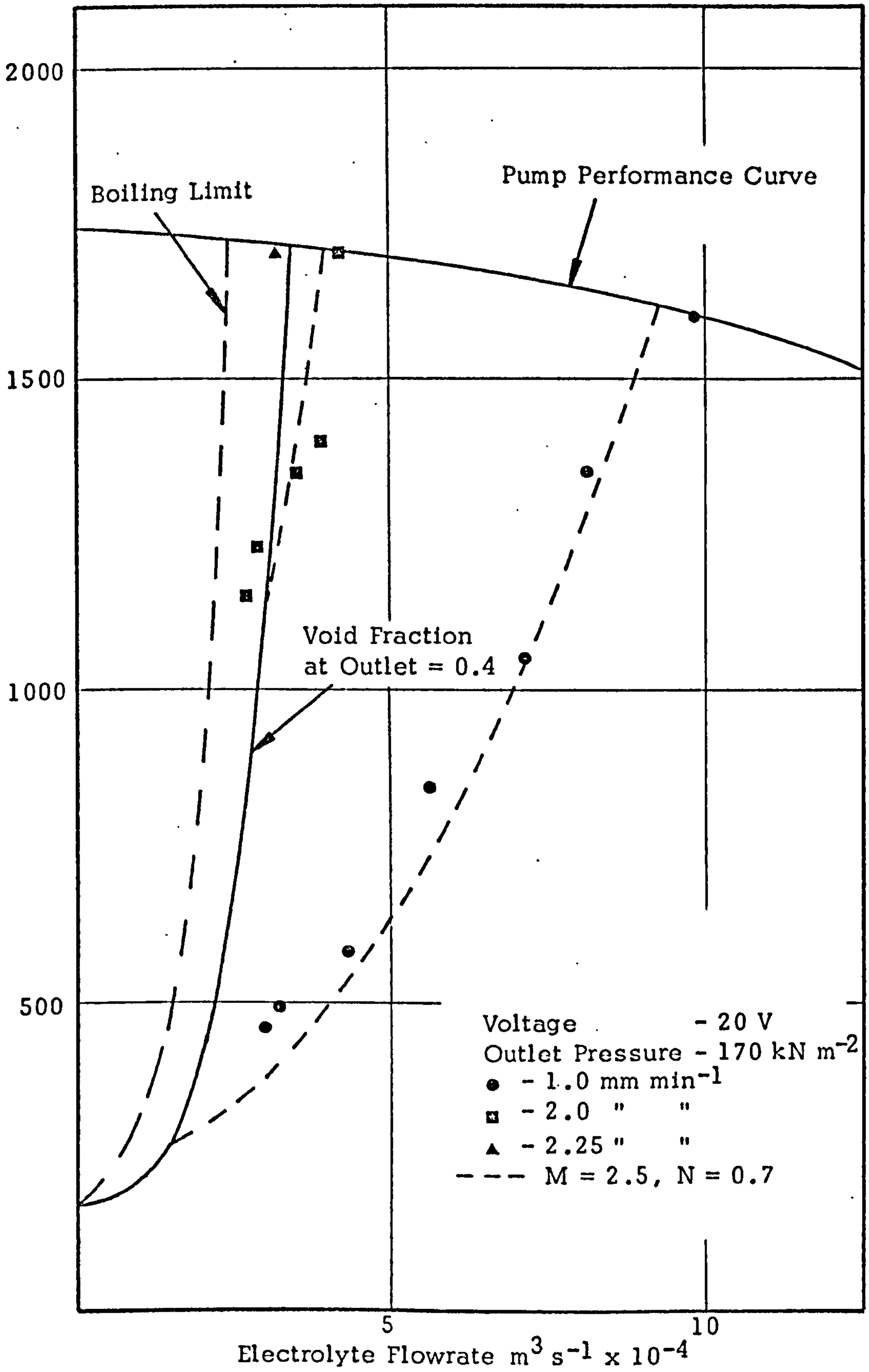

FIG. 5.1 OPERATING CHARACTERISTICS OF ELECTROCHEMICAL MACHINING

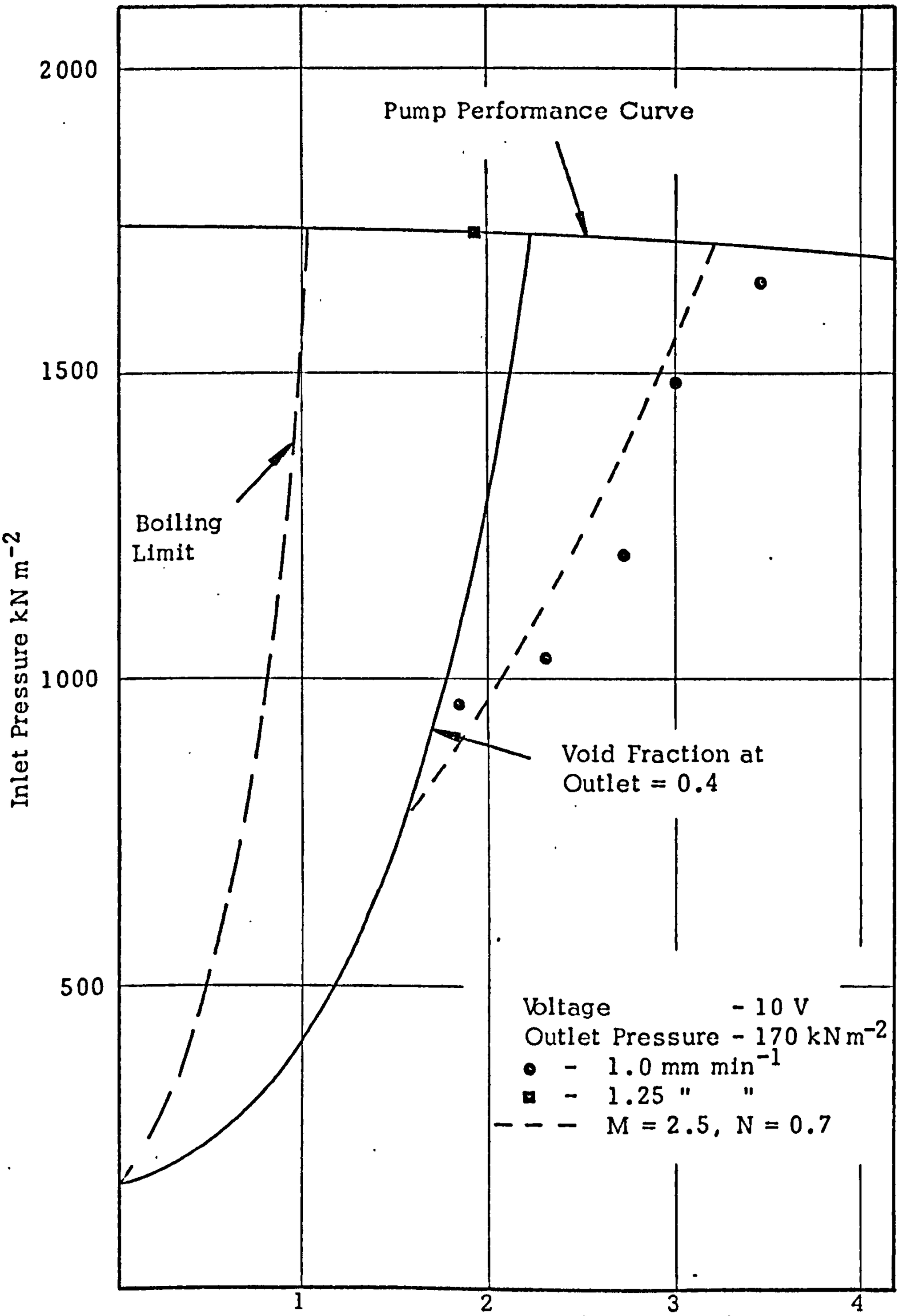

FIG. 5.2 OPERATING CHARACTERISTICS FOR MACHINING AT A LOW VOLTAGE

outlet is unchanged for a given feedrate and flowrate but the boiling limit moves to the left since less heat is dissipated in the electrolyte within the gap.

Increase in outlet pressure to 800 kN m^{-2} (Fig. 5.3) has two important effects:

(a) Electrolyte boiling at atmospheric pressure becomes the restraint on flowrate since the void fraction at outlet is inversely proportional to pressure.

(b) The inlet pressure-flowrate curve, based on average values of the model parameters for the tests in Table 3, moves towards the limiting curve. Although the increase in outlet pressure reduces the pressure differential for a given flowrate, the available differential is reduced by 630 kN m^{-2}. An inlet pressure-flowrate curve could be plotted, to the right of the boiling limit, for a feedrate of 2.5 mm min^{-1} which is only a marginal increase in feedrate from 2.25 mm min^{-1} at the lower outlet pressure.

The operating characteristics of machining using sodium nitrate electrolyte, at the same conductivity as that of the sodium chloride electrolyte, are shown in Fig. 5.4. The greater density of the sodium nitrate electrolyte raises the pump performance curve. As a result of the lower current efficiency of machining with this electrolyte the gap widths are smaller and the currents are greater than those with sodium chloride at the same feedrate and voltage. The results also show poor agreement with the correlation of void fraction at outlet equal to 0.4. However, as discussed previously, this may be due to the use

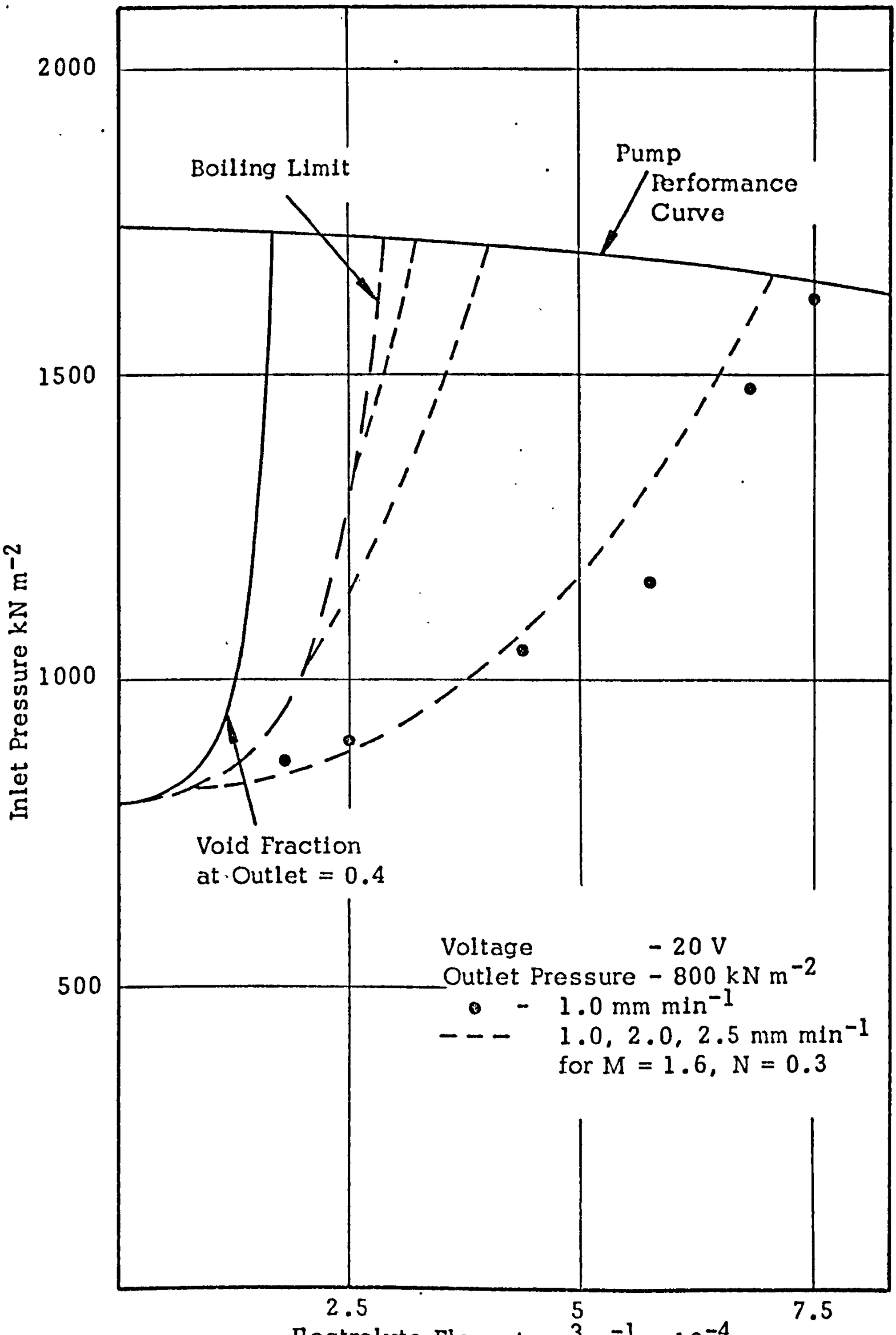

FIG. 5.3 OPERATING CHARACTERISTICS FOR MACHINING AT A HIGH OUTLET PRESSURE

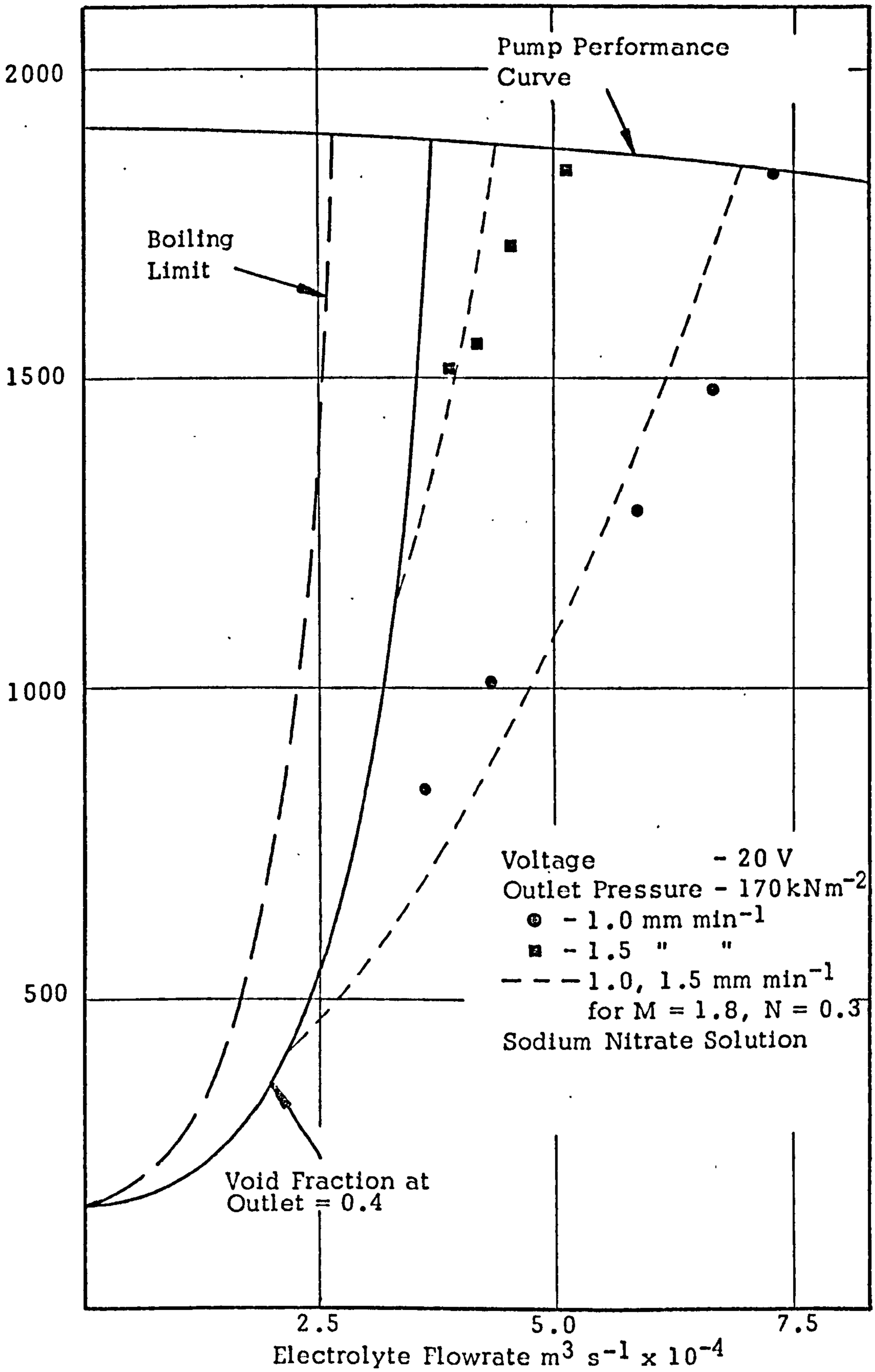

FIG. 5.4 OPERATING CHARACTERISTICS FOR MACHINING WITH SODIUM NITRATE SOLUTION

of a fresh electrolyte in the experimental tests.

Figs. 5.1 and 5.3 indicate that an optimum outlet pressure exists which can be obtained from the limits on equations (45) and (48). The void fraction af gas at outlet from the gap is

$$\alpha_e = \frac{A_e x^*}{1 + A_e x^*} \tag{45}$$

$$\text{For } \alpha_e = 0.4$$

$$A_e x^* = .667 \tag{76}$$

The temperature increase from inlet to exit is

$$T_e - T_o = Tr\, x^* = \frac{V}{\lambda_a C_f}\, x^* \tag{48}$$

For T_e equal to the electrolyte boiling point at atmospheric pressure then:

$$T_b - T_o = \frac{V}{\lambda_a C_f}\, x^* \tag{77}$$

Substituting equation (76) in (77):

$$T_b - T_o = \frac{V}{\lambda_a C_f} \cdot \frac{.667}{A_e} \tag{78}$$

$$\text{where } A_e = \frac{\rho_o \lambda_g}{\rho_g \lambda_a} \tag{35}$$

The density of the gas at outlet is determined from:

$$\rho_g = \frac{p_e}{R_g T_e} \tag{29}$$

Substituting equations (29) and (35) in equation (78) then:

$$p_e = \frac{(T_b - T_o)\, C_f \rho_o \lambda_g R_g T_b}{V\ .667} \tag{79}$$

Thus the optimum outlet pressure is inversely proportional to the voltage drop in the gap and shows small variation with electrolyte

properties. The optimum outlet pressure moves the correlation of void fraction at outlet equal to 0.4 onto the boiling limit curve (Fig. 5.5). The inlet pressure-flowrate curve for a feedrate of 2.0 mm min^{-1} could be plotted to the right of the limiting curve which is a substantial increase from 1.25 mm min^{-1} in Fig. 5.2.

However turbulent electrolyte flow in the gap is a requirement for the effective removal of dissolved metal. Freer et al (30) have shown that Reynolds Number is important in relation to the polarisation characteristics of a metal and that striations on the anode surface can be avoided by using high flow velocities to remove weak anodic films. In addition the concentration overvoltage at the electrode surface is minimised. The criterion for turbulence along the gap is:

$$Re_o > 4000 \qquad (80)$$

The Reynolds Number is directly proportional to flowrate for a given workpiece-tool configuration. Equation 80 corresponds to a minimum flowrate of about 0.6×10^{-4} m^3 s^{-1} in Fig. 5.5. Thus operating conditions may be selected such that the limiting curve intersects the pump performance curve at a flowrate of this order allowing further increase in tool feedrate.

5.6 A Procedure for the Prediction of Operating Conditions

The high capital cost of large electrochemical machines is such that the machine hour rate is much greater than that for conventional machine tools (61). To reduce the machining cost going onto each part or component the selection of operating conditions should be directed

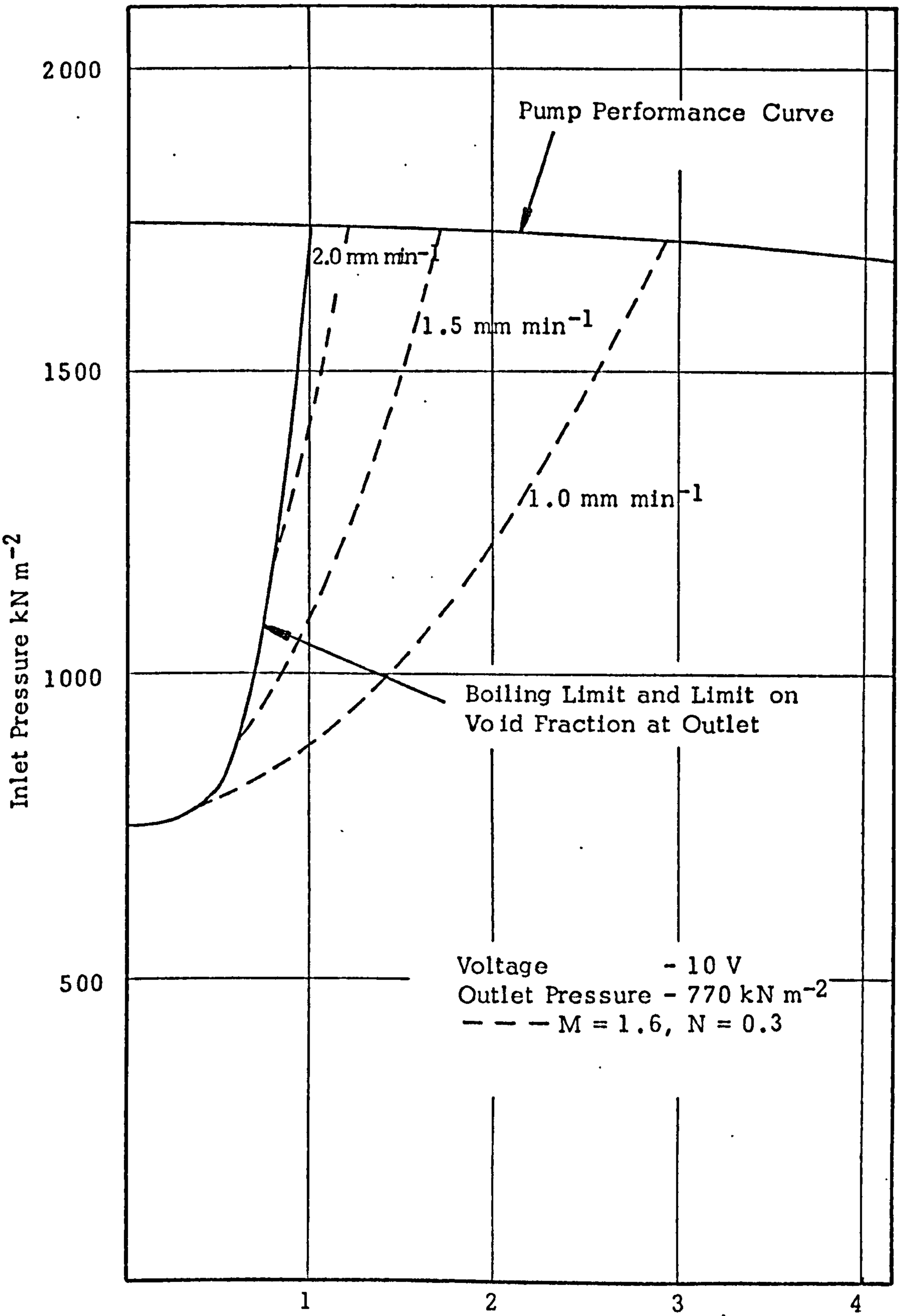

FIG. 5.5 OPERATING CHARACTERISTICS FOR MACHINING AT 10 VOLTS AT THE OPTIMUM OUTLET PRESSURE

towards attaining the maximum reliable feedrate consistent with repeatable work within the required tolerances.

Consideration should first be given to the gap size between the electrodes. A small gap reduces the size of machining inaccuracies, due to process fluctuations,such as electrolyte conductivity, and allows improved tool reproduction on the workpiece. The undulations on the machined surfaces, in the tests in Section 4.2, at gap widths less than about 0.1 mm may indicate that this is a suitable lower limit. A larger gap will usually be required for diesinking and forming operations. The mesh size of the filters in the electrolyte system and the stability of the ram drive and tooling fixture should also be considered in this respect.

The selection of operating conditions can be affected by the polarisation characteristics of the metal-electrolyte combination. For accurate reproduction of sharp detail machining should be at the highest current density before the transition from activation to diffusion control. The transition current density is obtained from a plot of machining characteristics in a form of polarisation curve such as that developed by Larsson (29). At the higher current densities in the diffusion region the dependence of current density on flowrate may be obtained empirically from this type of plot. The mode of dissolution control is also important if good surface finish and selective metal removal are required on the workpiece (5, 29, 35, 39).

The theoretical model was developed for an initially plane and parallel electrode configuration. Thus the model is directly applicable

to cross flow tools with approximately constant width such as those used to machine turbine blades. The model has also been developed for rectilinear and radial electrolyte flow with curved electrodes (17). In a complex shaped tool with internal supply ducts, a complete theoretical description is extremely complicated. A simpler approach is to evaluate the pressure-flowrate curve for a rectangular section of the tool extending from the supply duct to the tool perimeter for the longest electrolyte flow path length.

The minimum electrolyte flowrate can be calculated on the basis of Reynolds Number just greater than 4000. The tool feedrate, machining voltage and outlet pressure have to be obtained by an iterative procedure using a plot similar to that in Fig. 5. . Machining voltages of from 10 to 14 V are often used in die-sinking operations and, from equation (79), correspond to outlet pressures of 600 and 440 kN m^{-2} respectively. These values are suitable starting points. Application of an outlet pressure also suppresses any tendency towards cavitation in the gap. Approximate values of the frictional multiplier and void function exponent at a given pressure have to be obtained by interpolation of the experimental data in Figs. 5.1 to 5.3. At high outlet pressures the acceleration term in the pressure drop equation (50) becomes small such that integration of this equation is unnecessary. The maximum tool feedrate is obtained from the point of intersection of the limiting curve, from equations (76) and (77), with the pump performance curve. It may be necessary to further restrict the temperature increase to give a more uniform gap along the electrode

length. Some margin of error , to the right of the limiting curve, should be allowed for as the electrolyte flow may not be uniformly distributed within the gap.

With the operating conditions of machining specified the tool shape for a given workpiece shape can be calculated. At high outlet pressures and flow velocities the void exponent function, $n \rightarrow 0$ such that the gap variation along the electrode length can be predicted from the algebraic relation, equation (46). Corrections due to conducitivity variation can then be incorporated in design procedures and computer programs for curved electrodes such as those described by Wilson (6) and Tipton (11).

6.0 CONCLUSIONS

A model, developed by Thorpe and Zerkle (16, 17, 18), is used for the prediction of the one-dimensional equilibrium electrode gap in electrochemical machining. The model has been found to show good agreement with experimental results for sodium chloride electrolyte but empirical parameters are required. The parameters, the frictional multiplier, M, and the void function exponent, n, are dependent on the electrolyte flow velocity and outlet pressure and show little variation with machining voltage and current density. The frictional multiplier ranges from 1.2 to 3.2 which indicates an increase in shear stress at the electrode surfaces due to the evolution of gas bubbles. The void function exponent, n, is significantly lower than previously assumed values; at high electrolyte flow velocities and outlet pressure $n \rightarrow 0$ such that the effect of gas bubbles on the electrolyte conductivity is negligible and the equilibrium gap may be predicted by a simple algebraic relationship.

At operating conditions most favourable to economic and accurate machining the model predicts an upper bound to the electrolyte velocity which corresponds to a limiting value of the tool feedrate. However, the model is not verified in this respect and experimental conditions are obtained which exceed those predicted theoretically. The upper bound to the electrolyte velocity is the hydraulic characteristic of the electrolyte pump.

The cause of machining failure has been found to be boiling within the bubble-electrolyte layer close to the cathode. The electrolyte boils due to the reduction in area available, by the bubbles, for the passage of machining

current such that high temperatures are generated in the electrolyte. The temperatures measured downstream of the electrode gap are considerably lower than those measured close to the cathode. The formation of steam bubbles increases the resistivity of the electrolyte and the anode converges towards the cathode at outlet so that sparking and machining failure occur. Increase in outlet pressure increases the electrolyte boiling point and reduces the volume of gas bubbles so that a lower flowrate is sufficient to maintain equilibrium machining. The experimental results are consistent with machining failure tests at operating conditions similar to those in practice for both sodium chloride and sodium nitrate electrolytes.

A semi-theoretical model is introduced to allow prediction of the boiling condition but fails to agree with experimental results of tests close to machining failure. However, the criterion of void fraction of gas bubbles, at outlet, equal to 0.4 correlates quite well with these tests at high feedrates. Additional limitations on the process are that the electrolyte temperature within the gap is less than the boiling point at atmospheric pressure and that the flow is turbulent at inlet to the gap. The limitations allow prediction of operating conditions for given workpiece-tool configuration and electrolyte pump performance capability.

ACKNOWLEDGEMENTS

The author wishes to express his gratitude to Professor D. S. Ross, B.Sc., Ph.D., A.R.C.S.T., C.Eng., F.I.Mech.E., F.I.Prod.E., M.B.I.M., F.R.S.A. for the use of workshop and laboratory facilities; to Dr. J. A. McGeough, B.Sc. Ph.D., A.Inst.P., who initiated this work; to Dr. C. N. Larsson, B.Sc., Ph.D., A.I.M.F. for advice pertaining to this work.

The author also wishes to thank the laboratory staff for some assistance with the construction of the experimental apparatus.

SUGGESTIONS FOR FURTHER WORK

1. An extension of the present work would be an investigation of the equilibrium gap width variation for complex tool geometries such as those used to machine turbine blades.

2. In some applications the electrolyte is supplied through slots in the tool face. Further work is required to establish the position, shape and size of such slots to give uniform electrolyte flow over the tool face.

3. Much of the electrochemical machining literature is in a form not readily understood by the personnel using the process in industry. A handbook or standard is necessary to describe operating and design procedures and to provide sample calculations and computer programs such as that developed by Tipton (11).

BIBLIOGRAPHY

1. GLASSTONE, S., 'Introduction to Electrochemistry', D. Van Nostrand Co., (1964).

2. PITSCHKE, F. A., 'Picking an E.C.M. Electrolyte to Fit the Job', A.S.M.E. Technical Paper No. 706, (1965).

3. ALLISON , C. R., 'How Electrolytes Influence the E.C.M. Process', A.S.T.M.E. Paper No. SP64-79, (1964).

4. BERGSMA, F., 'The Role of the Electrolyte in Electrochemical Machining of Metal', I.S.E.M. Conf., Vienna, (1970).

5. LABODA, M. A. and MACMILLAN, M. L., 'A New Electrolyte for Electrochemical Machining', Jour. Electrochem. Soc., Vol. 116, 199 (1969).

6. WILSON, J. F., 'Practice and Theory of Electrochemical Machining', Wiley Interscience, (1971).

7. TIPTON, H., 'The Dynamics of Electrochemical Machining', Proc. 5th Int. Conf. Machine Tool Des. Res. Conf., Birmingham, pp. 509-522, (1964).

8. DE BARR, A. R. and OLIVER, D. A., 'Electrochemical Machining', Macdonald and Co. Ltd., London, (1968).

9. PRODUCTION ENGINEERING RESEARCH ASSOCIATION, 'Electro-chemical Machining Equipment and Techniques', Report 145, (1965).

10. FLETT, D., 'Production Capabilities of Electrochemical Machining' M.Sc. Thesis, University of Strathclyde, Glasgow (1971).

11. TIPTON, H., 'The Determination of the Shape of Tools for Use in E.C.M.', Machine Tool Industry Research Association Report 40.

12. KRYLOV, A. R., Jour. Mathematical Physics, Vol. 13, No. 15 (1969).

13. COLLETT, D. E., Hewson-Browne, R.C. and WINDLE, D.W., Jour. Eng. Maths., Vol. 4, No. 29 (1970).

14. THORPE, J. F., 'On the Kinematics of Electrochemical Machining', A.S.M.E. Paper 68-WA/Prod.-22, (1968).

15. HOPENFIELD, J. and COLE, R. R., 'Prediction of the One Dimensional Equilibrium Gap in Electrochemical Machining', Trans. A.S.M.E. Jour. Eng. Ind., pp. 755-765, (1969).

16. THORPE, J. F. and ZERKLE, R. D., 'Analytical Determination of the Equilibrium Electrode Gap in Electrochemical Machining', Int. J. Mach. Tool Des. Res., Vol. 9, pp. 131-144, (1969).

17. THORPE, J. F. and ZERKLE, R. D., 'A Theoretical Analysis of The Equilibrium Sinking of Shallow, Axially Symmetric Cavities by Electrochemical Machining' from 'Fundamentals of Electrochemical Machining' edited by Faust, C. L., The Electrochemical Society, Princeton, (1971).

18. THORPE, J. F. and ZERKLE, R.D., 'Development of Techniques for the Utilisation of Electrochemical Machining' Report No. MT-019, Naval Ordnance Systems Command, Louisville, Kentucky (1973).

19. WALLIS, G. B., 'One-Dimensional Two-Phase Flow', McGraw-Hill Co., New York, (1971).

20. MARTINELLI, R. F. and NELSON, D. B., 'Prediction of Pressure Drops in Forced Circulation of Boiling Water', Trans. A.S.M.E. 70, pp. 695-702, (1948).

21. DE LA RUE, A. E. and TOBIAS, C. W., 'On the Conductivity of Dispersions', Jour. Electrochem. Soc., Vol. 106, pp. 827-833, (1959).

22. LANDOLT, D et al, 'An Optical Study of Cathodic Hydrogen Evolution in High Rate Electrolysis', Jour. Electrochem. Soc. Vol. 117, No. 6 (1970).

23. WILLIAMS, L. A., 'Sparks in E.C.M. - Their Causes and Cures' Anocut Shaped Electrode Machine Manual, Anocut Engineering Co., Illinois, U.S.A.

24. BALDWIN, G. L., 'Electrochemical Machining', Ph.D. Thesis, Rugby Coll. of Technology, (1968).

25. KAWAFUNE, K. and MIKOSHIBA, T., 'Accuracy in Cavity Sinking by Electrochemical Machining', Ann. C.I.R.P. Vol. 15, pp. 443-455, (1967).

26. CHIKAMORI, K. et al, 'Flow of Electrolyte in Electrochemical Die-Sinking', Bull. Japanese Soc. Prec. Eng., Vol. 2, No. 4, (1968).

27. ITO, S. and SEIMIYA, K. 'Hydraulic Approach to Electrolyte Flow in Electrochemical Machining', Proc. Int. Machine Tool Des. Res. Conf., (1972).

28. BAXTER, A. C., 'Electrochemical Machining', Ph.D. Thesis, University of Warwick, (1969).

29. LARSSON, C. N., 'Rates of Anodic Dissolution in E.C.M.', Ph.D. Thesis, C.N.A.A., Lanchester College, Coventry, (1968).

30. FREER, H. E., HANLEY, J. B. and MACLELLAN, G. D. S., 'Electrochemical Machining of Plain Carbon Steels' from 'Fundamentals of Electrochemical Machining' edited by Faust, C.L., The Electrochemical Society, Princeton, (1971).

31. HOAR, T. P., Proc. 3rd Meeting C.I.I.C.E., Milan (1950).

32. McGEOUGH, J. A., Ph.D. Thesis, University of Glasgow (1966).

33. FAUST, C. L., 'Electrochemical Machining of Metals', Trans. Int. Metal Finishing Conf., Vol. 41, (1964).

34. TURNER, T. S. and CUTHERBERTSON, J. W., 'Electrochemical Machining - A Study of the Effects of Some Variables', The Production Engineer, pp. 270-281, (1966).

35. LANDOLT, D., 'High Rate Anodic Dissolution of Copper', Jour. Electrochem. Soc., Vol. 116, No. 10, (1969).

36. HOARE, J. P., 'Oxide Film Studies on Iron in Electrochemical Machining Electrolytes, Jour. Electrochem. Soc., Vol. 117, No. 1, (1970).

37. COOK, N. H. et al, 'Increasing Electrochemical Machining Rates', Massachusetts Inst. of Technology, (1967).

38. POWERS, R. W. and WILFORE, W.G., 'Some Observations on the Anodic Dissolution of Titanium at High Current Densities' from 'Fundamentals of Electrochemical Machining' edited by Faust, C.L., The Electrochemical Societry, Princeton, (1971).

39. HOARE, J. D., 'Oxide Film Studies on Iron in Electrochemical Machining Electrolytes', Jour. Electrochem. Soc, Vol. 117, No. 1 (1970).

40. CHIN, D. T., 'Anodic Films in E.C.M. Electrolytes: Onset of Passivation of Mild Steel in Nitrate Solution', Jour. Electrochem. Soc., Vol. 119, No. 9, (1972).

41. MAO, K. W., LABODA, M. A. and HOARE, J. P., 'Anodic Film Studies on Steel in Nitrate-Based Electrolytes for E.C.M.', Jour. Electrochem. Soc., Vol. 119, No. 4 (1972).

42. FLEURY, J., First International Conference on Electrochemical Machining, Leicester University (1973).

43. CHIKAMORI, K., 'Electrolytic Dissolution of Mild Steel in High Current Density Region', Research Paper, Government Mechanical Engineering Laboratory, Tokyo, Japan.

44. PERSONAL COMMUNICATION, Healy's of Leicester Limited.

45. HARTNETT, J. P., KOH, J. C. Y. and McCOMAS, S. T. 'A Comparison of Predicted and Measured Friction Factors for Turbulent Flow Through Rectangular Ducts', A.S.M.E. Journal of Heat Transfer pp. 82-88 (1962).

46. VENNARD, J. K., 'Elementary Fluid Mechanics', Wiley, New York (1961).

47. ROHSENOW, W. M. and CHOI, H. Y., 'Heat, Mass and Momentum Transfer' P. 72, Prentice-Hall (1961).

48. MAO, K. W., 'E.C.M. Study in a Closed Cell Ststem', Jour. Electrochem. Soc., Vol. 118, No. 11 (1971).

49. KONIG, W. and DEGENHARDT, H. in 'Fundamentals of Electro-chemical Machining' edited by Faust, C. L., The Electrochemical Society, Princeton (1971).

50. BAKER, H. D., RYDER, E. A. and BAKER, N. H., 'Temperature Measurement in Engineering', Vol. 1, p. 38, Chapman and Hall (1953).

51. LEONG, K., 'The Overcut in Electrochemical Machining', M.Sc. Thesis, University of Strathclyde, Glasgow (1970).

52. NIKURADSE, J., 'Stromungsgesetz in rauhen Rohren', V.D.I. - Forschungsheft, 361 (1933) N.A.C.A. Transl. TM 1292.

53. TOBIAS, C. W., 'Mass Transport Processes in E.C.M.', First Int. Conf. on E.C.M., Leicester University (1973).

54. SEIDALL, A., 'Solubilities of Inorganic and Metal Organic Compounds', p. 553-560, Van Nostrand (1940).

55. TONG, L. S., 'Boiling Heat Transfer and Two Phase Flow', Wiley, New York (1965).

56. KELLOG, H. H., Jour. Electrochem. Soc., Vol. 99, No. 133 (1930).

57. BAYER, J., CUMMINGS, M. A. and JOLLIS, A. V., 'Final Report on Electrolytic Machining Development,' Technical Report ML-TDR-64-313, (1964).

58. HEWITT, G. F. and HALL-TAYLOR, N. S., 'Annular Two-Phase Flow', Pergamon Press, Oxford (1970).

59. DALLAVALLE, J. M., 'Micromeretics', Pitman Publishing Co., New York (1943).

60. FAUSKE, H. K., 'The Discharge of Saturated Water Through Short Tubes,' Chem. Eng. Progress Sym. Series, No. 59, Vol. 61 (1964).

61. LARSSON, C. N., 'Electrochemical Machining Outwith the Aero-Space Industry', Trans. Institution of Engineers and Shipbuilders in Scotland, Paper No. 1369 (1972).

62. McGEOUGH, J. A., 'Principles of Electrochemical Machining', Chapman and Hall, London (1974).

63. WOLOSEWICZ, R. M., 'E.C.M. Electrolyte Properties', S.M.E. Technical Paper MR 70-220 (1970).

64. 'International Critical Tables', McGraw-Hill Publishing Co., New York (1929).

65. PERRY, J. H., Chemical Engineers' Handbook, McGraw-Hill Publishing Co., New York (1950).

APPENDIX I

Theoretical Model

The theoretical model was developed by Thorpe and Zerkle (16, 17, 18) for the determination of the equilibrium electrode gap in electrochemical machining.

Consider the electrode configuration shown in Fig. A1. The gap is of local thickness y and of length L with $y \ll L$. The cathode or tool moves towards the anode or workpiece with local velocity V_c. At a point opposite the cathode the workpiece is dissolved with local velocity V_a. The current density, ϕ, is a function of position x and time t. The hydrogen gas is evolved at the cathode surface with local mass flux $\dot{m}_g$ and moves with the electrolyte with average velocity V_g in some equivalent area proportional to the dimension y_g. The gas is distributed in the form of bubbles within an electrolyte layer close to the cathode; this layer is known as the bubble layer of thickness δ. The consideration of gas and liquid as separate phases simplifies the derivation of the transport equations for mass, momentum and energy which do not depend on the gas distribution.

The electrolyte flows with velocity V_f in an area proportional to the dimension y_f. The anode dissolves with local mass flux $\dot{m}_a$. The area occupied by the metal hydroxide precipitate is considered negligible. Bayer et al (57) have found that the precipitate has no significant effect on electrolyte conductivity. Thus electrolyte and precipitate may be treated as a liquid phase with velocity V_f and area proportional to y_f. Then

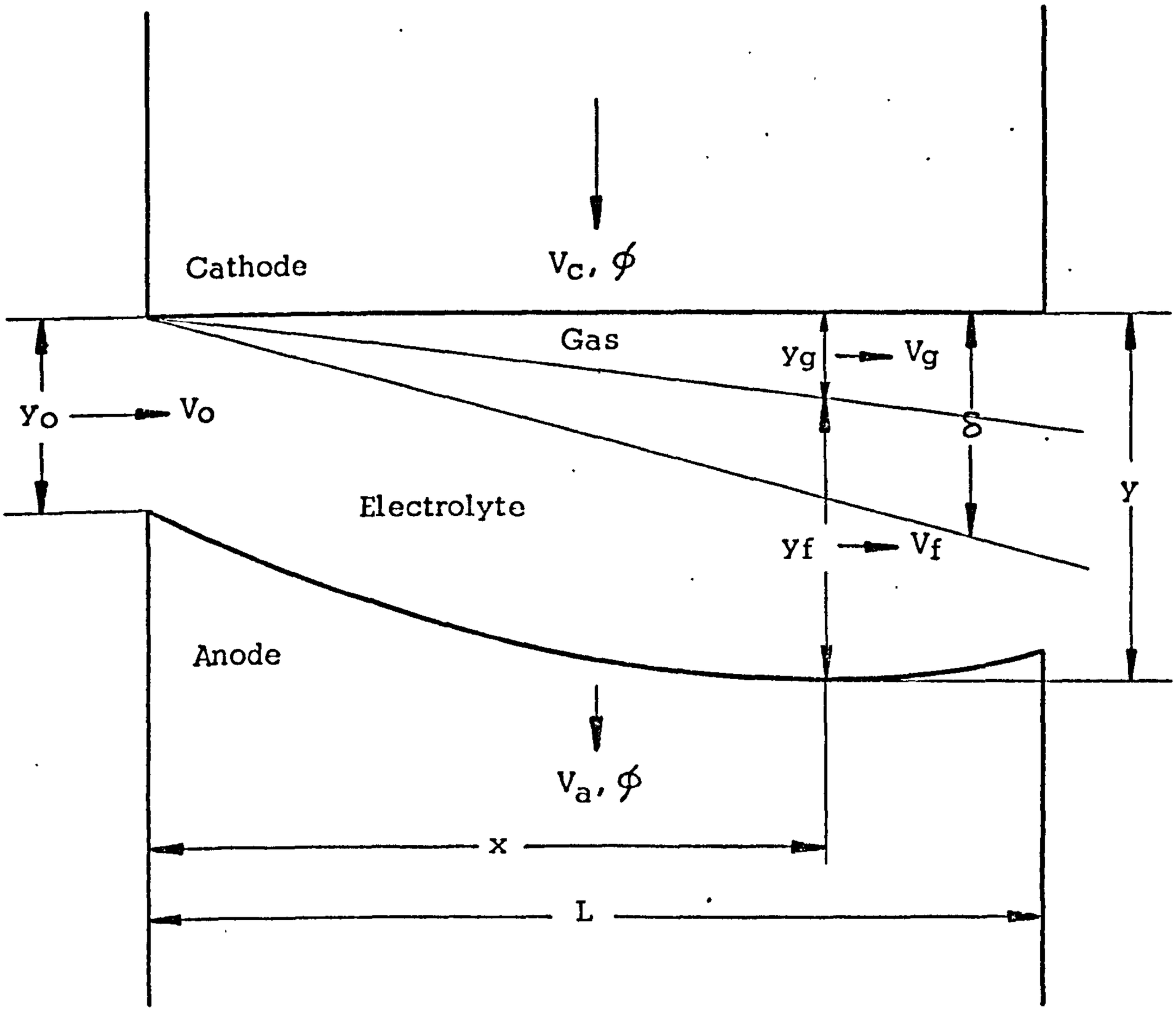

FIG. A1 PHYSICAL MODEL

$$y = y_g + y_f \tag{1}$$

The void fraction of hydrogen and the slip ratio are defined by

$$\alpha = y_g/y \tag{2}$$

$$\sigma = V_g/V_f \tag{3}$$

The slip ratio, σ , depends on the void fraction, the ratio of gas density to liquid density and the electrolyte flowrate and, in the absence of theoretical relations and experimental data, is assumed to be unity.

Fundamental Kinematic Equation of Electrochemical Machining

The fundamental equation is

$$\frac{\partial y}{\partial t} = V_a - V_c \tag{4}$$

where t is time. V_a is related to the anode density ρ_a and the mass flux rate $\dot{m}_a$ by

$$\dot{m}_a = \rho_a V_a \tag{5}$$

The mass flux rate is in turn related to the current density from Faraday's law:

$$\dot{m}_a = \lambda_a \phi \tag{6}$$

where λ_a is the electrochemical equivalent weight of the anode metal in units mass per Faraday. The mass flux rate may also be determined for alloy metals (29). However, the current efficiency may be defined (11):

$$\varepsilon = \frac{\text{actual amount of metal removed}}{\text{theoretical amount of metal removed}}$$

$$\therefore \varepsilon = \frac{\rho_a V_c}{\phi \lambda_a} \tag{7}$$

The current efficiency is dependent on the metal-electrolyte combination and other factors and may be determined experimentally from weight loss measurements. Substituting equation (7) into (4):

$$\frac{\partial y}{\partial t} = \frac{\varepsilon \lambda_a \phi}{\rho_a} - V_c \qquad (8)$$

Under equilibrium conditions of machining the local feedrate, V_c, equals the workpiece dissolution rate, V_a. Thus current density,

$$\phi = \frac{\rho_a V_c}{\varepsilon \lambda_a} \qquad (9)$$

The current density becomes constant under these conditions and is independent of position along the gap.

Derivation of Electrical Equations

When an electrode is immersed in an electrolyte, atoms leave its surface to become ions and ions are deposited as atoms in a continuous, balanced exchange. A potential called the electrode potential then exists between a point just inside the surface of the electrode to a point just inside the electrolyte. Different electrode materials exhibit different electrode potentials. For the iron work-pieces used in the experimental work the electrode or reversible potential is 0.44 V. Since hydrogen is evolved at the stainless steel cathode the electrode potential is taken to be zero (62).

As the current flows between the electrodes, phenomena occur at the electrode surfaces which oppose the flow of current. They are termed the anode and cathode over-voltages and include activation polarisation, concentration polarisation and ohmic over-voltage (6).

The additional energy for the discharge of ions is the activation over-voltage and is determined from Tafel's equation:

$$\eta_a = a + b \log J$$

$$\text{where } a = \frac{2.303\ RT}{z \alpha F} \log J_o$$

$$\text{and } b = \frac{2.303\ RT}{z \alpha F} \text{ where } \alpha \text{ is the transfer coefficient}$$

The activation over-voltage increases slowly with current density. For the conditions used in this work the sum of the activation over-voltages at each electrode is about 1.5 volts.

The concentration over-voltage is a measure of the energy required for migration of ions through a concentration layer close to the electrodes. In the highly turbulent flow at the electrodes the concentration over-voltage is assumed negligible.

The ohmic over-voltage may be caused by solid films on the anode and cathode surfaces. Such films did form on the cathode in this work, but were easily removed. An oxide film formed on the anode surface in tests using sodium nitrate solution. However in the absence of information regarding the resistance of oxide films, which vary widely with different metal-electrolyte combinations, the anode ohmic over-voltage is assumed to be negligible.

Apart from the voltage losses at the surfaces of the electrodes, the resistance of the electrolyte in the gap may be represented by a simple form of Ohm's law. Let the sum of the overvoltages at the surfaces of the electrodes be represented by Epol. Similarly the reversible electrode potential is Erev. The applied potential or voltage across the electrodes is E and the voltage V, for overcoming the ohmic resistance

of the electrolyte is

$$V = E - \Delta E \tag{10}$$

where $\Delta E = Epol + E_{rev}$ (11)

From Ohm's law

$$V = \phi R \quad \text{where } R = \text{resistance x area} \tag{12}$$

where the electrode gap resistance is given by

$$R = r\,y \tag{13}$$

where r is the specific resistance of the electrolyte. The area resistance product, R, of the electrode gap is a function of the resistance properties of the pure liquid electrolyte, the void fraction α and the temperature of the phases.

The cross-section occupied by hydrogen at position x along the gap is proportional to y_g (Fig. A1). The void is distributed within a bubble layer of thickness δ. Thus the void fraction within the bubble layer can be defined by

$$\alpha' = y_g/\delta \tag{14}$$

The total transverse resistance, per unit cross-sectional area perpendicular to y, is

$$R = r_{tp}\delta + r_f (y - \delta) \tag{15}$$

where r_{tp} is the two-phase resistivity in the bubble layer and r_f is the liquid electrolyte resistivity. The two-phase resistivity in the bubble layer is a function of α':

$$r_{tp} = r_f \; f(\alpha') \tag{16}$$

It is assumed that the bubbles are randomly distributed in the bubble layer. For a random dispersion of non-conducting spheres in a conducting medium then :

$$f(\alpha') = (1 - \alpha')^{-1.5} \tag{17}$$

De la Rue and Tobias (21) have shown experimentally that up to a void fraction of 40% this relation adequately describes the resistivity variation due to the uniform dispersion of non-conducting particles of different shapes and sizes in a static electrolyte. However, the bubbles may be concentrated close to the cathode surface (22) and it is convenient to introduce a generalised void function exponent, n, which has to be determined experimentally. Equation (17) becomes

$$f(\alpha') = (1 - \alpha')^{-n} \tag{18}$$

Combining equations (14) and (2):

$$\alpha' = \frac{Y}{\delta}\alpha \tag{19}$$

Equation (15) can then be written as

$$R = r_f\left[(y - \delta) + \delta(1 - \frac{Y}{\delta}\alpha)^{-n}\right] \tag{20}$$

The specific conductance, k_f, of the electrolyte increases with temperature and a linear relation with temperature may be assumed for most electrolytes:

$$k_f = \frac{1}{r_f} = k_o\ [1 + \gamma(T - T_o)] \tag{21}$$

where k_o and T_o are conductivity and temperature respectively, at the gap entrance, and γ is the conductivity coefficient.

Combining equations (12), (20) and (21)

$$(y - \delta) + \delta(1 - \frac{Y}{\delta}\alpha)^{-n} = \frac{Vk_o[1 + \gamma(T - T_o)]}{\phi} \tag{22}$$

To relate equation (22) to the gap width it is assumed that $y = \delta$

similar to the approach used by Hopenfield and Cole (15). The effects of this assumption are taken into account by the experimentally determined void function exponent, n. Equation (22) becomes

$$y = \frac{Vk_o}{\phi} \left[1 + \gamma (T - T_o) \right] \quad (1 - \alpha)^n \tag{23}$$

This equation shows the dependence of gap width on electrolyte temperature and void fraction of hydrogen bubbles. The gap width at inlet to the electrodes is obtained by combining equations (9) and (23).

$$y_o = \frac{Vk_o \varepsilon \lambda_a}{\rho_a V_c} \tag{24}$$

Transport Equations

The transport equations of continuity, motion, energy and state may be derived (16) from consideration of an elemental control volume at some position, x, along the electrode gap.

(a) Continuity of Mass

For the gas phase

$$\frac{d}{dx} (\rho_g \alpha \sigma \; y \; V_f) = \lambda_g \phi \tag{25}$$

For the liquid phase

$$\frac{d}{dx} \left[\rho_f (1 - \alpha) y \; V_f \right] = (\varepsilon \lambda_a - \lambda_g) \phi \tag{26}$$

(b) Motion

$$\rho_g \alpha \frac{d}{dx} \left(\frac{\sigma^2 V_f^2}{2} \right) + \rho_f (1 - \alpha) \frac{d}{dx} \left(\frac{V_f^2}{2} \right)$$

$$= - \frac{dP}{dx} - \frac{2\tau}{y} - \left[\varepsilon \lambda_a + \sigma \lambda_g \right] \frac{\phi V_f}{y} \tag{27}$$

This is a familiar form of the equation of motion (19). The terms on the left side represent acceleration of the gas and liquid phases; the terms on the right side represent static pressure gradient, friction losses and transverse momentum flux.

(c) Energy

The energy transport of the gas phase is assumed negligible due to the low heat capacity of the gas relative to that of the electrolyte. The power dissipated as heat in the electrolyte is considered to be entirely removed by electrolyte flow. Thus

$$\rho_f V_f c_f (1-\alpha) y \frac{dT}{dx} = V \phi \qquad (28)$$

Viscous heat dissipation in the electrolyte has been shown (15) to be negligible.

(d) State

A relation between pressure, temperature and density of the gas phase is obtained from the equation of state for an ideal gas:

$$\rho_g = \frac{P}{R_g T} \qquad (29)$$

The electrolyte density, ρ_f, is assumed constant with temperature and pressure:

$$\rho_f = \rho_o \qquad (30)$$

where subscript o denotes the inlet value.

Solution of Equations

Integrating equations (25) and (26) and eliminating $y V_f$, an algebraic equation is obtained for the void fraction.

$$\alpha = \frac{Ax^*}{1 + (A + \eta)\, x^*} \tag{31}$$

$$\text{where } x^* = \frac{x^o}{\varsigma} \quad ; \quad x^o = \frac{x}{L} \tag{32}$$

$$\varsigma = \frac{\rho_o\, y_o\, V_o}{\rho_a\, L\, V_c} \tag{33}$$

$$\eta = \frac{\varepsilon \lambda_a - \lambda_g}{\varepsilon \lambda_a} \tag{34}$$

$$A = \frac{\rho_o \lambda_g}{\sigma \varepsilon \lambda_a \rho_g} \tag{35}$$

A is a function of gas density, ρ_g, which, in turn, is a function of position x^*.

Substituting y V_f from equation (26) into equation (28) then

$$\frac{dT}{dx^*} = \frac{T_r}{\eta\, x^* + 1} \tag{36}$$

where T_r is a reference temperature

$$Tr = \frac{V}{C_f \varepsilon \lambda_a} \tag{37}$$

Equation (36) is an explicit relation having the solution

$$T = T_o + \frac{T_r}{\eta} \ln\, (1 + \eta\, x^*) \tag{38}$$

Substituting equation (38) into (21)

$$\frac{1}{r_f} = k_f = k_o \left[1 + \frac{B}{\eta} \ln\, (1 + \eta\, x^*) \right] \tag{39}$$

where $B = \gamma\ T_r$.

By substituting equations (31) and (39) into (23), the ratio of the local gap width to that at inlet may be obtained.

$$\frac{y}{y_o} = \left[\frac{1 + \eta x^*}{1 + (\eta + A)\, x^*} \right]^n \left[1 + \frac{B}{\eta} \ln\, (1 + \eta\, x^*) \right] \tag{40}$$

The ratio of the electrolyte flow velocity, V_f, to that at inlet may be determined from equations (26), (31) and (40).

$$\frac{V_f}{V_o} = \frac{\left[1 + (h + A)\, x^*\right]^{n+1}}{(1 + \eta\, x^*)^n \left[1 + \frac{B}{\eta} \ln (1 + \eta\, x^*)\right]} \tag{41}$$

The dimensionless form of the pressure gradient is obtained from the equation of motion (27).

$$\frac{dp^o}{dx^*} = -2\,\frac{y_o}{y}\left\{\frac{d}{dx^*}\left[\left\{1 + x^*\left[\sigma(1-\eta) + 1\right]\right\} V_f^o\right]\right.$$
$$\left. -(1-\eta)\, x^*\,\frac{dV_f^o}{dx^*} + \frac{\zeta M k_o V_f^{o\,2}}{4}\right\} \tag{42}$$

where M is the two-phase frictional multiplier defined by $M = \frac{f}{fo}$

and Ko is the pressure loss coefficient at inlet, $K_o = \frac{fo\,L}{y_o}$

The equation of state (29) for the gas phase becomes

$$p^o = \frac{C}{A}\left[1 + \frac{T_r^o}{\eta} \ln (1 + \eta\, x^*)\right] \tag{43}$$

where $T_r^o = \frac{T_r}{T_o}$

and $C = \frac{2\,\lambda_g\, R_g\, T_o}{\sigma\, \varepsilon\, \lambda_a\, V_o^2}$ (44)

Approximate Equations

The equations may be simplified by approximations. The co-ordinate

$x^* = \frac{x\,\rho_a\, V_c}{\rho_o\, y_o\, V_o}$ is of order of magnitude 10^{-2} or less

since the velocity of the cathode is small relative to the velocity of electrolyte flow. Thus $\eta\, x^*$ is negligible compared to unity since

$\eta \approx 1$. The equations become

$$\alpha = \frac{Ax^*}{1 + Ax^*} \tag{45}$$

$$y^o = \frac{y}{y_o} = \frac{1 + Bx^*}{(1 + Ax^*)^n} \tag{46}$$

$$V_f{}^o = \frac{V_f}{V_o} = \frac{(1 + Ax^*)^{n+1}}{1 + Bx^*} \tag{47}$$

$$T^o = \frac{T}{T_o} = 1 + T_r{}^o x^* \tag{48}$$

$$p^o = \frac{p}{\rho_o V_o{}^2/2} = \frac{C}{A} T^o \tag{49}$$

$$\frac{dp^o}{dx^*} = -\frac{2}{y^o}\left[\frac{d V_f{}^o}{dx^*} + \frac{M K_o}{4} V_f{}^{o\ 2}\right] \tag{50}$$

At high pressure drops across the electrode gap, the gas density function, A, varies appreciably and the equations must be solved simultaneously.

The differential $\frac{dV_f{}^o}{dx^*}$ may be expressed as:

$$\frac{d V_f{}^o}{dx^*} = \frac{\partial V_f{}^o}{\partial x^*} + \frac{\partial V_f}{\partial T^o}\frac{dT}{dx^*} + \frac{\partial V_f{}^o}{\partial p^o} \cdot \frac{dp^o}{dx^*} \tag{51}$$

Within the operating conditions typical of electrochemical machining the variation in density, and hence velocity, of the electrolyte with temperature is negligible:-

$$\therefore \quad \frac{\partial V_f{}^o}{\partial T^o} \cdot \frac{dT}{dx^*} = 0$$

Thus equation (50) becomes:-

$$\frac{dp^o}{dx^*} = \frac{-2}{y^o}\left[\frac{\partial V_f^o}{\partial x^*} + \frac{V_f{}^o}{p^o} \cdot \frac{dp^o}{dx^*} + \frac{\rho M . K_o}{4} V_f^{o\ 2}\right] \tag{52}$$

$$\frac{dp^o}{dx^*} + \frac{2}{y^o} \frac{\delta V_f^o}{\delta p^o} \cdot \frac{dp^o}{dx^*}$$

$$= - \frac{2}{y^o} \left[\frac{\delta V^o_f}{\delta x^*} + \frac{\rho M . K_o V_f^{o\,2}}{4} \right] \tag{53}$$

$$\frac{dp^o}{dx^*} = \frac{- \frac{2}{y^o} \left[\frac{\delta V^o_f}{\delta x^*} + \rho \frac{M . K_o V_f^{o\,2}}{4} \right]}{1 + \frac{2}{y^o} \frac{\delta V^o_f}{\delta p^o}} \tag{54}$$

Differentiating equation (47) by quotient rule:

$$\frac{\delta V^o_f}{\delta x^*} = \frac{(1 + Bx^*)\ (n+1)\ (1+Ax^*)^n \left(A + \frac{CT_r^o}{p^o} . x^*\right) - (1+Ax)^{n+1} . B}{(1 + Bx^*)^2} \tag{55}$$

Also:-

$$\frac{\delta V_f^o}{\delta p^o} = \frac{(n+1)\,u^n}{1 + Bx^*} \frac{\delta u}{\delta p^o} \quad \text{where} \quad u = 1 + Ax^*$$

From equation (49)

$$A = \frac{C}{p^o} . T^o$$

$$\therefore u = 1 + \frac{C}{p^o} . T^o . x^*$$

$$\therefore \frac{\delta u}{\delta p^o} = - \frac{C\,T^o\,x^*}{p^{o\,2}}$$

$$\therefore \frac{\delta V_f^o}{\delta p^o} = \frac{- (n+1)\ (1 + Ax^*)^n\ C\,T^o\ x^*}{(1 + Bx^*)\ p^{o\,2}} \tag{56}$$

Substituting equations (55) and (56) in (54).

$$\frac{dp^o}{dx^*} = - \frac{2}{y_o} \left[\frac{(1 + Bx^*)\ (n+1)\ (1+Ax^*)^n \left(A + \frac{CT_r^o}{p^o} . x^*\right) - (1+Ax^*)^{n+1} . B}{(1 + B . x^*)^2} + \rho \frac{M . K_o}{4} \frac{(1+Ax^*)^{2n+2}}{(1+Bx^*)^2} \right]$$

$$\div \left(1 - \frac{2}{y_o} . \frac{(n+1)\ (1+Ax^*)^n\ CT^o\ x^*}{(1 + Bx^*)\ p^{o\,2}}\right) \tag{57}$$

Substituting for y_o from equation (46)

$$\frac{dp^o}{dx^*} = -2\frac{(1+Ax^*)^n}{1+Bx^*}\left[\frac{(1+Bx^*)(n+1)(1+Ax^*)^n\left(A+\frac{CT_r{}^o x^*}{p^o}\right)-(1+Ax^*)^{n+1}B}{(1+B.x^*)^2}\right.$$

$$\left.+\frac{\rho_m K_o}{4}\frac{(1+Ax^*)^{2n+2}}{(1+Bx^*)^2}\right]$$

$$\div\left(1-2\frac{(1+Ax^*)^n,(n+1)(1+Ax^*)^n\ CT^o\ x^*}{(1+Bx^*)\quad(1+Bx^*)\ p^{o\,2}}\right) \tag{58}$$

$$= -2\frac{(1+Ax^*)^{2n}}{(1+Bx^*)^2}\left[(n+1)\left(A+\frac{CT_r{}^o\ x^*}{p^o}-B\frac{(1+Ax^*)}{(1+Bx^*)}\right.\right.$$

$$\left.\left.+\frac{\rho M K_o}{4}\frac{(1+Ax^*)^{n+2}}{(1+Bx^*)}\right]\right.$$

$$\div\left(1-2(n+1)\frac{(1+Ax^*)^{2n}}{(1+Bx^*)^2}\quad\frac{CT^o\ x^*}{p^{o\,2}}\right) \tag{59}$$

It is important to note that equation (59) has a singularity i.e. as x* increases from a value of zero at inlet, eventually the denominator will become zero. Thorpe and Zerkle (16, 17,18) consider that this situation represents a choking condition similar to that occurring in compressible flow and two-phase flow. In electrochemical machining this situation should be avoided to prevent machining failure. If the feedrate, V_c, is maintained then the inlet flow velocity must be reduced.

APPENDIX II

Computer Program

The author is extremely grateful to Professor J. F. Thorpe of the University of Cincinnati for the use of a computer program developed to allow a numerical solution to equation (59). The method of solution is Milne's predictor-corrector.

The symbols and units for the program input data are:

E	Applied Voltage, E	Volts
VC	Feedrate, V_C	in. min^{-1}
PRE	Outlet Pressure, Pe	lb. in^{-2}a.
QO	Electrolyte Flowrate, Q_o	U.S.gal.min^{-1}
CEA	Electrochemical Equivalent of Anode, λa	g F^{-1}
DENA	Density of Anode, ρ a	lb. ft^{-3}
EL	Electrode length, L	in.
W	Electrode Width, w	in.
TO	Electrolyte Inlet Temperature, To	^oF
VIS	Electrolyte Kinematic Viscosity, ν	ft^2 hr^{-1}
DENO	Electrolyte Density, ρ o	lb. ft^{-3}
ECO	Electrolyte Conductivity at Inlet, k_o	Ω^{-1} cm^{-1}
GAM	Electrolyte Conductivity Coefficient, γ	$^oF^{-1}$
CF	Electrolyte Specific Heat, C_f	BTU lb^{-1} $^oF^{-1}$
EREV	Reversible Potential, Erev	volts
EPOT	Activation Potential, Epol	volts
EFF	Current Efficiency, ε	none

EM	Frictional Multiplier, M	none
EN	Void Function Exponent, n	none
CLC	Contraction Loss Coefficient at Inlet, Ko	none

The program is in FORTRAN language. The input data cards are:

```
READ (5,5) E, VC, PRE, QO
READ (5,5) CEA, DENA, EL, W
READ (5,5) TO, VIS, DENO, ECO, GAM, CF
READ (5,5) EREV, EPOL, EFF
READ (5,5) EM, EN, CLC
5 FORMAT (4F10.4, 2F10.5)
```

The output data consists of the input data and the output parameters which are:

Supply Pressure, Po	lb. in^2a
Electrolyte Inlet Velocity, Vo	ft. sec^{-1}
Reynolds Number, Re	none
Electrolyte Outlet Temperature, Te	^oF
Current Density, ϕ	amp in^{-2}
Friction factor, f	none
Mach number at outlet, Mae	none

The output variables are printed out at locations along the gap. In the present form of the program 11 equally spaced locations are used for the output variables which are:

Position, $^{x}/L$	none
Pressure, P	lb. in^2 a
Void Fraction, α	none
Gap Thickness, y	in
Electrolyte Velocity, V_f	ft. sec^{-1}

Equations (45), (46), (47) and (48) were evaluated, at the outlet from the gap and the calculations gave agreement with the corresponding computed output variables.

```
C
C                                   PROGRAM  LISTING
C
C                                 INPUT DATA FOR TEST 01
C
      DIMENSION P(105),DPDX(105)
      READ (5,2) I
      DO 600 J=1,I
    2 FORMAT(I2)
      READ(5,5,END=700) E,VC,PRE,QO
      READ(5,5,END=700) CEA,DENA,EL,W
      READ(5,5,END=700) TO,VIS,DENO,ECO,GAM,CF
      READ(5,5,END=700) EREV,EPOL,EFF
      READ(5,5,END=700) EM,EN,CLC
C
      XSTEPS=100.
      IDELX=10
C
    1 FORMAT(1H1)
    5 FORMAT(4F10.4,2F10.5)
   10 FORMAT(5X,4F12.4,2F12.5)
   12 FORMAT(53H                         E           VC          PRE          QO
   14 FORMAT(5X,48H          VOLT          IPM         PSIA         GPM)
   16 FORMAT(53HO              CEA          DENA           EL            W
   18 FORMAT(5X,48H   G/FARADAY   LBM/FT**3          INCH         INCH)
   20 FORMAT(77HO                TO          VIS         DENO          ECO
     1       GAM          CF)
   22 FORMAT(5X,72H               F     FT**2/HR    LBM/FT**3     1/OHM-CM
     1    1/F    BTU/LBM-F)
   24 FORMAT(41HO                EREV          EPOL          EFF)
   26 FORMAT(5X,36H          VOLT          VOLT          -)
   28 FORMAT(41HO                EM            EN          CLC)
   30 FORMAT(5X,36H              -             -           -)
   32 FORMAT(//15X,19H SUPPLY PRESSURE = ,F6.1,5H PSIA/)
   34 FORMAT(15X,30H ELECTROLYTE INLET VELOCITY = ,F6.1,4H FPS/)
   36 FORMAT(15X,19H REYNOLDS NUMBER = ,F8.0/)
   38 FORMAT(15X,20H EXIT TEMPERATURE = ,F6.1,2H F/)
   40 FORMAT(15X,19H CURRENT DENSITY = ,F6.1,10H AMP/IN**2/)
   42 FORMAT(15X,27H FRICTION FACTOR (EM*FO) = ,F6.4/)
   44 FORMAT(15X,20H EXIT MACH NUMBER = ,F5.2///)
   46 FORMAT(60HO          X/L           P          ALPHA           Y
     1  VF)
   48 FORMAT(60H             -           PSIA           -           INCH
     1 FPS/)
   50 FORMAT(F12.2,F12.1,F12.3,F12.4,F12.1)
   52 FORMAT(12X,27H *****INPUT PARAMETERS*****//)
   54 FORMAT(12X,28H *****OUTPUT PARAMETERS*****/)
   56 FORMAT(12X,27H *****OUTPUT VARIABLES*****/)
   60 FORMAT(//10X,37H INLET PRESSURE GREATER THAN 500 PSIA)
C
C          WRITE INPUT PARAMETERS
      WRITE (6,52)
      WRITE (6,12)
      WRITE (6,14)
```

```
      WRITE (6,10) E,VC,PRE,QO
      WRITE (6,16)
      WRITE (6,18)
      WRITE (6,10) CEA,DENA,EL,W
      WRITE (6,20)
      WRITE (6,22)
      WRITE (6,10) TO,VIS,DENO,ECO,GAM,CF
      WRITE (6,24)
      WRITE (6,26)
      WRITE (6,10) EREV,EPOL,EFF
      WRITE (6,28)
      WRITE (6,30)
      WRITE (6,10) EM,EN,CLC
      WRITE (6,1)
C
C         CALCULATE AUXILIARY QUANTITIES
      CEG=1.003
      RG=766.4
      SR=1.
      V=E-EREV-EPOL
      TR=41490.*V/(EFF*CEA*CF)
      TRO=TR/(TO+460.)
      B=GAM*TR
      ETA2=(SR+CEG+EFF*CEA)/(EFF*CEA)
      YO=.006014*EFF*CEA*V*ECO/(DENA*VC)
      VO=QO/(3.117*YO*W)
      C=64.4*(CEG*RG*(TO+460.))/(SR*EFF*CEA*VO**2)
      ZETA=720.*DENO*YO*VO/(DENA*EL*VC)
      ELDL=1./ZETA
      RE=600.*VO*YO/VIS
      TE=TO+TR*ELDL
      PHI=2.54*V*ECO/YO
      FO=1./(.86859*ALOG(RE/(1.964*ALOG(RE)-3.8215)))**2
      IF (RE.LT.3000.) FO=64./RE
      ENFO=EM*FO
      EKO=FO*EL/YO
      D=ZETA*EM*EKO/4.
C
      LS=XSTEPS+1.1
      PES=PRE
      P(LS)=9274.*PES/(DENO*VO**2)
      A=C*(1.+TRO*ELDL)/P(LS)
      G=1.+A*ELDL
      F=1.+B*ELDL
      VD1=1.-2.*(EN+1.)*G**(2.*EN)/F**2*A*ELDL/P(LS)
      KONE=1
      IF (VD1.GT.0.) KONE=2
      H=ELDL/XSTEPS
      PO=50.
      NN=0
      K3=0
      K4=0
  10  P(1)=9274.*PO/(DENO*VO**2)
      X=0.
```

```
      NN=NN+1
C
      DO 120 L=1,4
      LD=L
      IF (L.EQ.1) GO TO 115
      X=X+H
      P(L)=P(L-1)+H*PDE
      IF (P(L).LE.0.) GO TO 180
  115 A=C*(1.+TRO*X)/P(L)
      G=1.+A*X
      F=1.+B*X
      VD1=1.-2.*(EN+1.)*G**(2.*EN)/F**2*A*X/P(L)
      IF (VD1.LE.0.) GO TO 180
      VN1=-2.*G**(2.*EN+1.)/F**2*((EN+1.)/G*(A+C*TRO/P(L)*X)-B/F+
     1D*G**(EN+1.)/F+ETA2)
      DPDX(L)=VN1/VD1
      P2=P(L)+H*DPDX(L)
      IF (P2.LE.0.) GO TO 180
      X1=X+H
      A=C*(1.+TRO*X1)/P2
      G=1.+A*X1
      F=1.+B*X1
      VD2=1.-2.*(EN+1.)*G**(2.*EN)/F**2*A*X1/P2
      IF (VD2.LE.0.) GO TO 180
      VN2=-2.*G**(2.*EN+1.)/F**2*((EN+1.)/G*(A+C*TRO/P2*X1)-B/F+
     1D*G**(EN+1.)/F+ETA2)
  120 PDE=.5*(DPDX(L)+VN2/VD2)
C
C         PROCEED WITH INTEGRATION
      DO 125 L=5,LS
      LD=L
      P(L)=P(L-4)+4.*H/3.*(2.*DPDX(L-3)-DPDX(L-2)+2.*DPDX(L-1))
      IF (P(L).LE.0.) GO TO 180
      EL1=L-1
      X=EL1*H
      A=C*(1.+TRO*X)/P(L)
      G=1.+A*X
      F=1.+B*X
      VD1=1.-2.*(EN+1.)*G**(2.*EN)/F**2*A*X/P(L)
      IF (VD1.LE.0.) GO TO 180
      VN1=-2.*G**(2.*EN+1.)/F**2*((EN+1.)/G*(A+C*TRO/P(L)*X)-B/F+
     1D*G**(EN+1.)/F+ETA2)
      DPDX(L)=VN1/VD1
      P(L)=P(L-2)+H/3.*(DPDX(L-2)+4.*DPDX(L-1)+DPDX(L))
      IF (P(L).LE.0.) GO TO 180
  125 CONTINUE
C
  180 IF (NN.GT.25) GO TO 330
      GO TO (300,310,600),KONE
C
  300 IF (LD.LT.LS.OR.VD1.LE..0) GO TO 302
      IF (VD1.LT..01) GO TO 330
      P03=P0
      K3=1
```

```
      K34=K3*K4
      IF (K34.EQ.1) GO TO 304
      PO=PO3-30
      IF (PO.LT.PES) PO=PES
      GO TO 110
  302 PO4=PO
      K4=1
      K34=K3*K4
      IF (K34.EQ.1) GO TO 304
      PO=PO4+50.
      IF (PO.GT.901.) GO TO  500
      GO TO 110
  304 PO34=(PO3+PO4)/2.
      IF (ABS(PO-PO34).LE..01) GO TO 330
      PO=PO34
      GO TO 110
C
C          FIND INLET PRESSURE
  310 IF (LD.LT.LS) GO TO 314
      PE=P(99)*DENO*VO**2/9274.
      IF (PE.LT.(PES-.1)) GO TO 314
      IF (PE.GT.(PES+.1)) GO TO 312
      GO TO 330
  312 PO3=PO
      K3=1
      K34=K3*K4
      IF (K34.EQ.1) GO TO 316
      PO=PO3-30.
      IF (PO.LT.PES) PO=PES
      GO TO 110
  314 PO4=PO
      K4=1
      K34=K3*K4
      IF (K34.EQ.1) GO TO 316
      PO=PO4+50.
      IF (PO.GT.501.) GO TO 500
      GO TO 110
  316 PO34=(PO3+PO4)/2.
      IF (ABS(PO-PO34).LE..01) GO TO 330
      PO=PO34
      GO TO 110
C
C          WRITE OUTPUT PARAMETERS
  330 PRO=PO+DENO*VO**2*(1.+CLC)/9274.
      EMA=SQRT(1.-VD1)
      IF (KONE.EQ.1) EMA=1.00
      WRITE (6,54)
      WRITE (6,32) PRO
      WRITE (6,34) VO
      WRITE (6,36) RE
      WRITE (6,38) TE
      WRITE (6,40) PHI
      WRITE (6,42) EMFO
      WRITE (6,44) EMA
```

```
      WRITE (6,56)
      WRITE (6,46)
      WRITE (6,48)
C
C        WRITE OUTPUT VARIABLES
      LAST=LS
      IF (KONE.EQ.1) LAST=LS-1
      DO 400 L=1,LAST,IDELX
      EL1=L-1
      X=EL1*H
      A=C*(1.+TRO*X)/P(L)
      G=1.+A*X
      F=1.+B*X
      XOL=EL1/XSTEPS
      PR=P(L)*DENO*VO**2/9274.
      AL=A*X/G
      YY=F/(G**EN)
      VV =G**(EN+1.)/F
      Y=YY*YO
      VF=VV*VO
  400 WRITE (6,50) XOL,PR,AL,Y,VF
C
      IF (KONE.EQ.2) GO TO 600
      K2=1
      NR=0
      P(LS)=9274.*PES/(DENO*VO**2)
  340 NR=NR+1
      IF (NR.GT.25) GO TO 350
      A=C*(1.+TRO*ELDL)/P(LS)
      G=1.+A*ELDL
      F=1.+B*ELDL
      VD1=1.-2.*(EN+1.)*G**(2.*EN)/F**2*A*ELDL/P(LS)
      IF (ABS(VD1).LT..01) GO TO 350
      IF (K2.EQ.2) GO TO 342
      IF (VD1.GT..0) GO TO 342
      PLS1=P(LS)
      P(LS)=P(LS)+.1*P(1)
      GO TO 340
  342 IF (VD1.GT..0) PLS2=P(LS)
      IF (VD1.LT..0) PLS1=P(LS)
      P(LS)=(PLS1+PLS2)/2.
      K2=2
      GO TO 340
  350 XOL=1.
      PR=P(LS)*DENO*VO**2/9274.
      AL=A*ELDL/G
      YY=F/(G**EN)
      VV =G**(EN+1.)/F
      Y=YY*YO
      VF=VV*VO
      WRITE (6,50) XOL,PR,AL,Y,VF
      GO TO 600
C
  500 WRITE (6,60)
  600 CONTINUE
      GOTO 800
  700 WRITE (6,701)
  701 FORMAT (' INSUFFICIENT DATA')
  800 STOP
      END
```

*****INPUT PARAMETERS*****

E	VC	PRE	QO
VOLT	IPM	PSIA	GPM
16.0000	0.0220	22.7000	1.5100

CEA	DENA	EL	W
G/FARADAY	LBM/FT**3	INCH	INCH
28.0000	487.0000	3.9900	0.4700

TO	VIS	DENO	ECO	GAM	CF
F	FT**2/HR	LBM/FT**3	1/OHM-CM	1/F	BTU/LBM-F
68.0000	0.0370	66.8000	0.1260	0.01250	0.89000

EREV	EPOL	EFF
VOLT	VOLT	-
0.4400	1.4800	1.0000

EM	EN	CLC
-	-	-
1.4000	1.2000	0.3600

*****OUTPUT PARAMETERS*****

SUPPLY PRESSURE = 70.8 PSIA

ELECTROLYTE INLET VELOCITY = 37.2 FPS

REYNOLDS NUMBER = 16670.

EXIT TEMPERATURE = 89.9 F

CURRENT DENSITY = 157.9 AMP/IN**2

FRICTION FACTOR (EM*FO) = 0.0379

EXIT MACH NUMBER = 0.73

*****OUTPUT VARIABLES*****

X/L	P	ALPHA	Y	VF
-	PSIA	-	INCH	FPS
0.00	57.3	0.000	0.0276	37.2
0.10	54.7	0.010	0.0281	37.0
0.20	52.1	0.022	0.0284	37.0
0.30	49.5	0.034	0.0288	37.0
0.40	46.8	0.047	0.0290	37.2
0.50	44.0	0.062	0.0292	37.5
0.60	41.0	0.079	0.0293	38.1
0.70	37.8	0.098	0.0292	39.0
0.80	34.2	0.121	0.0290	40.3
0.90	29.8	0.152	0.0284	42.6
1.00	22.8	0.207	0.0268	48.3

APPENDIX III

Electrolyte Properties

Sodium chloride and sodium nitrate solutions were used as the electrolytes in the experimental work. The properties of an electrolyte can be determined from the temperature and the density which are easily measured with a thermometer and a hydrometer, respectively. It is convenient in this work to define concentration percentage as 100 × mass of salt/mass of solution. The concentration can be obtained from the electrolyte temperature and density. The data for the density, conductivity, viscosity, specific heat and boiling point of the electrolytes was obtained from references (63, 64, 65) and is presented in Figs. A2 to A10.

The calibrations for the thermistors, at outlet from thegap in the work in Chapter 3, at outlet from the gap and at 6 mm from outlet within the electrode in the work in Chapter 4, Section 1, are also presented.

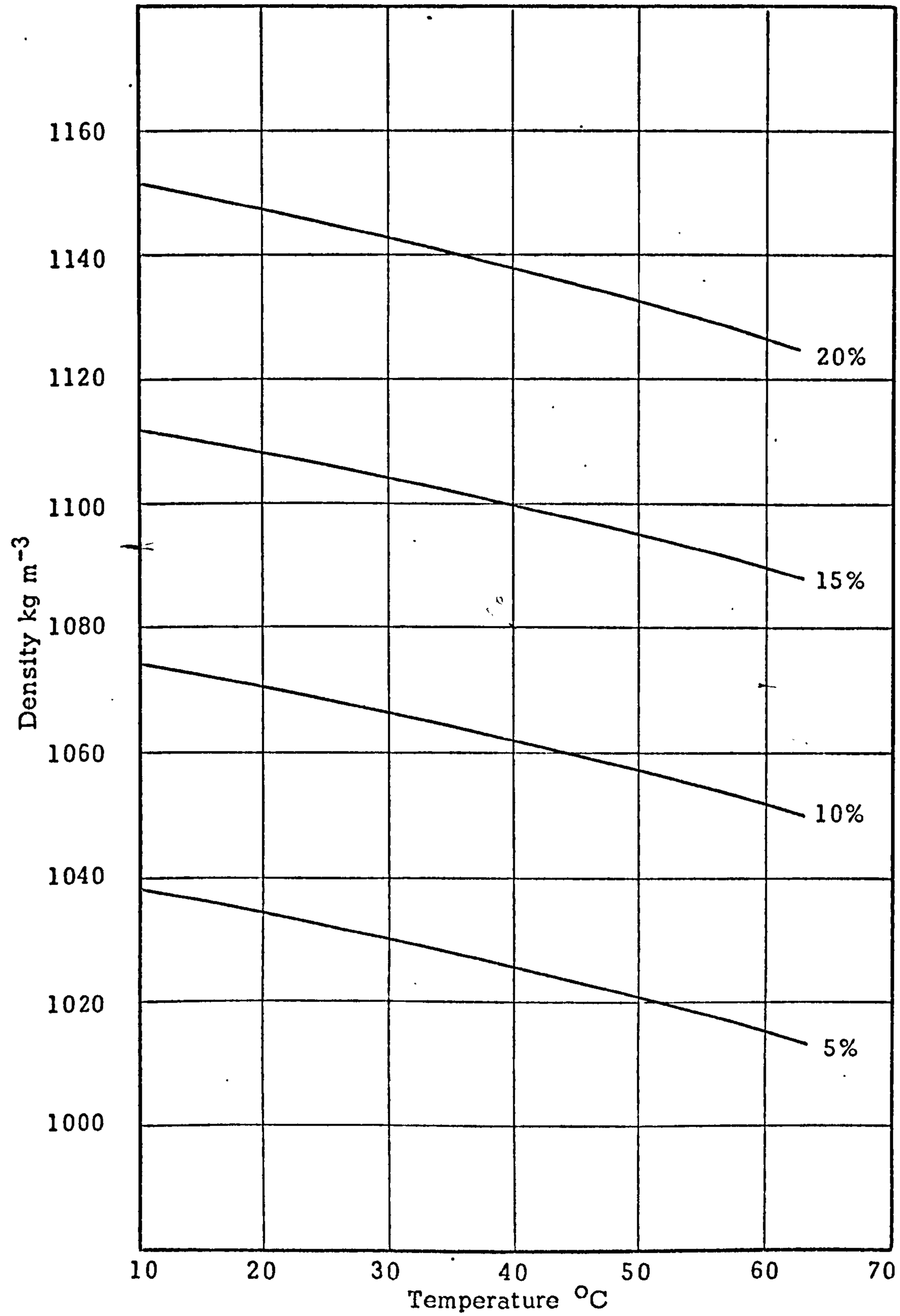

FIG. A2 DENSITY OF SODIUM CHLORIDE SOLUTIONS

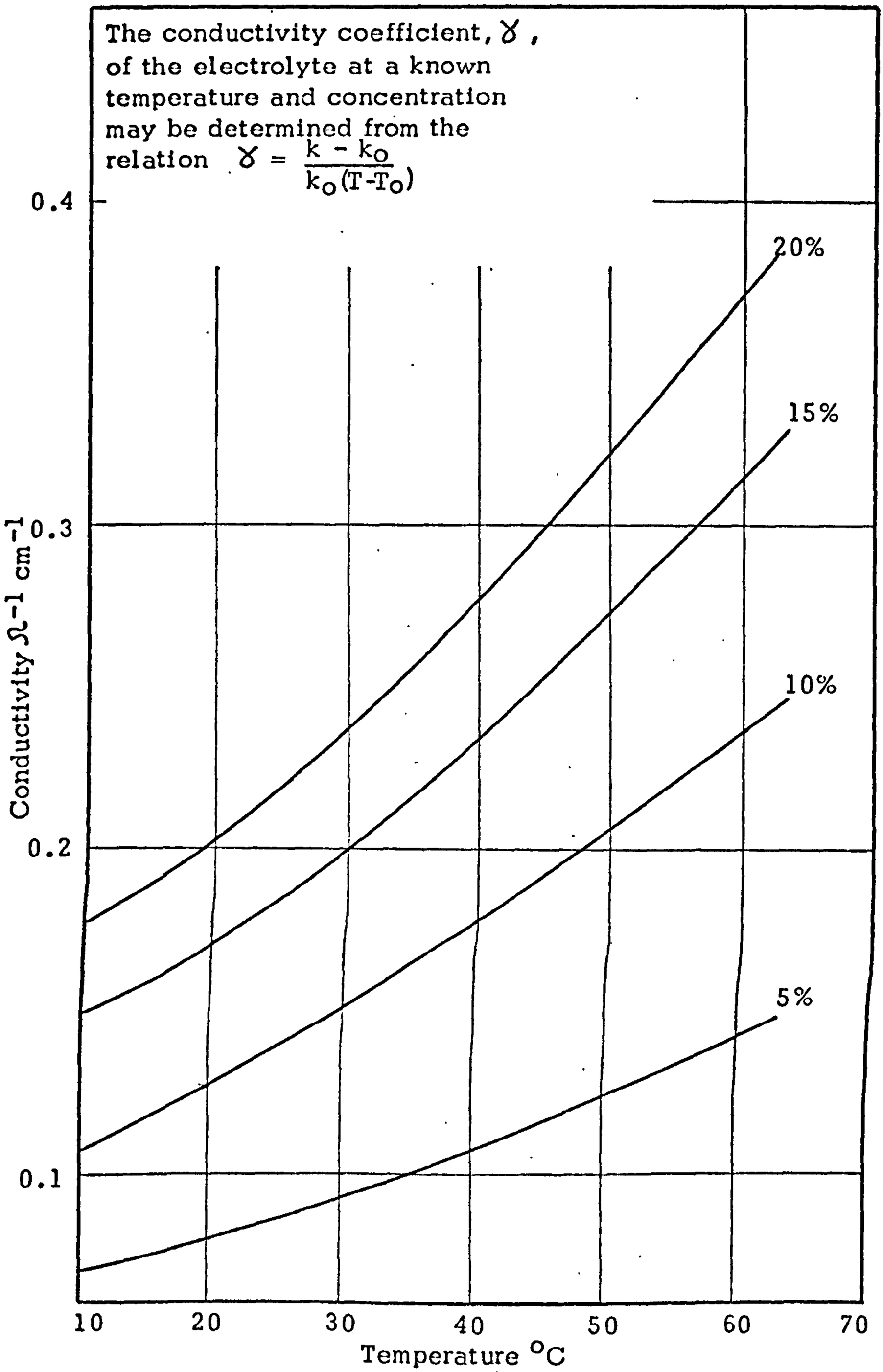

FIG. A3 CONDUCTIVITY OF SODIUM CHLORIDE SOLUTIONS

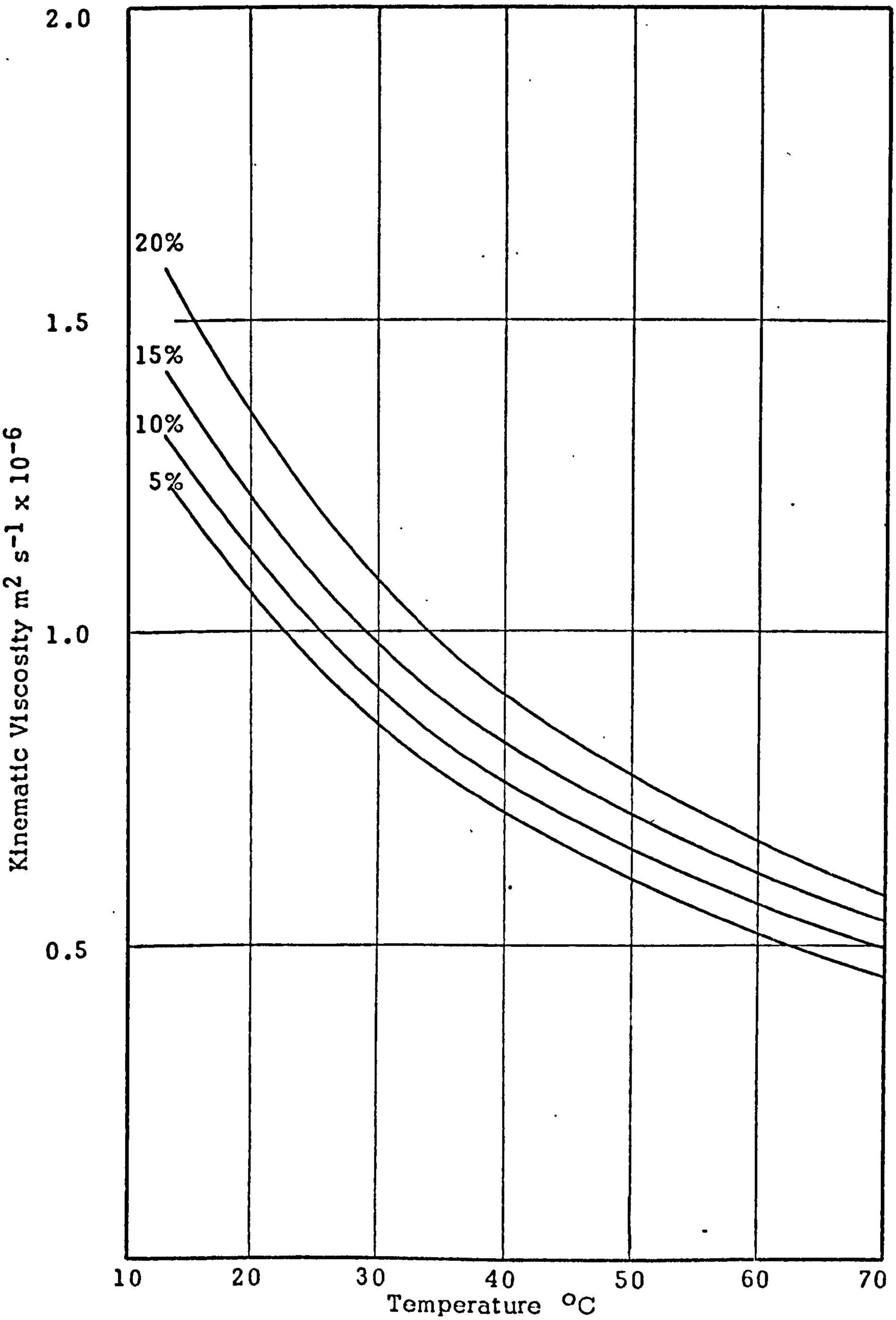

FIG. A4 KINEMATIC VISCOSITY OF SODIUM CHLORIDE SOLUTIONS

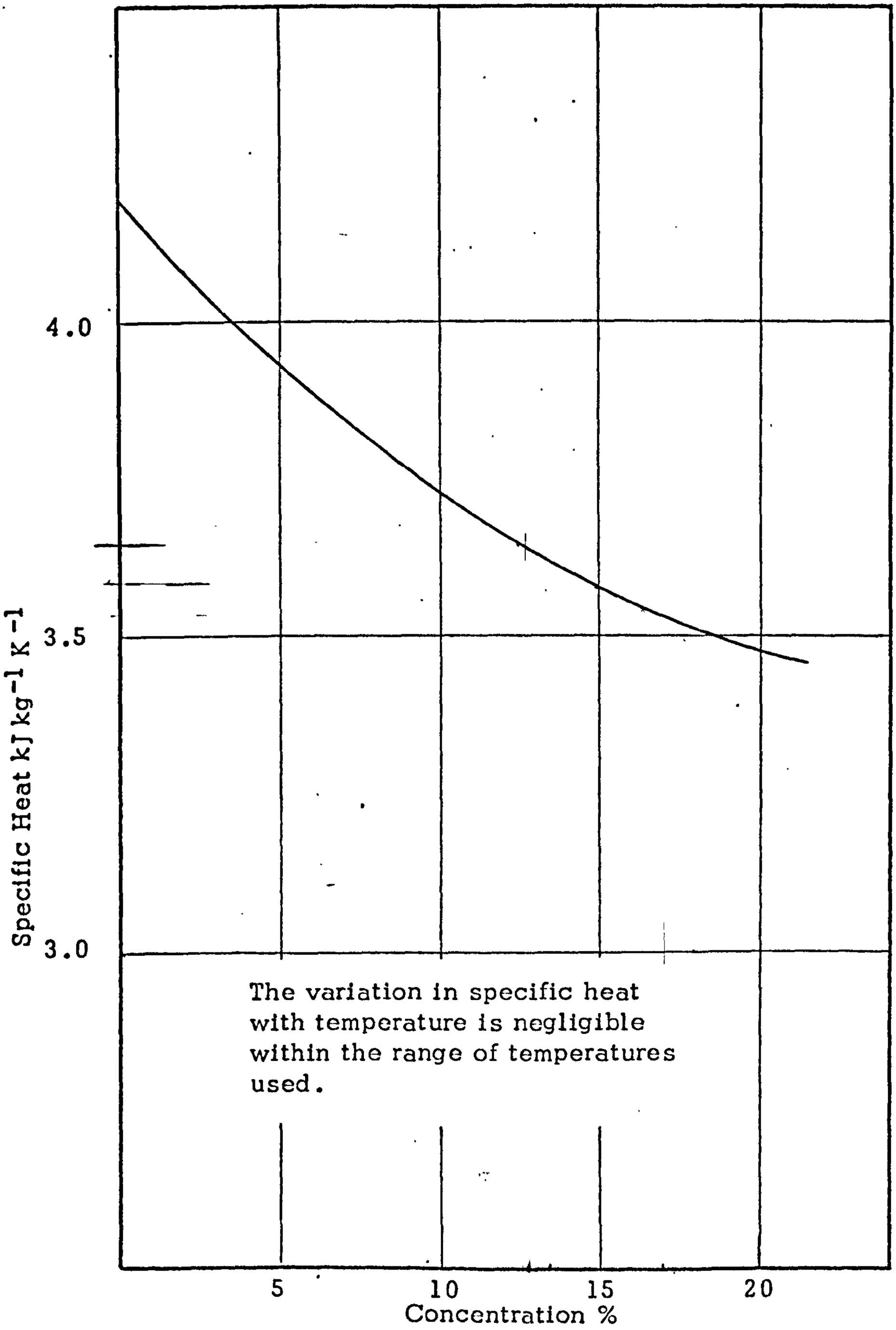

FIG. A5 SPECIFIC HEAT OF SODIUM CHLORIDE SOLUTIONS

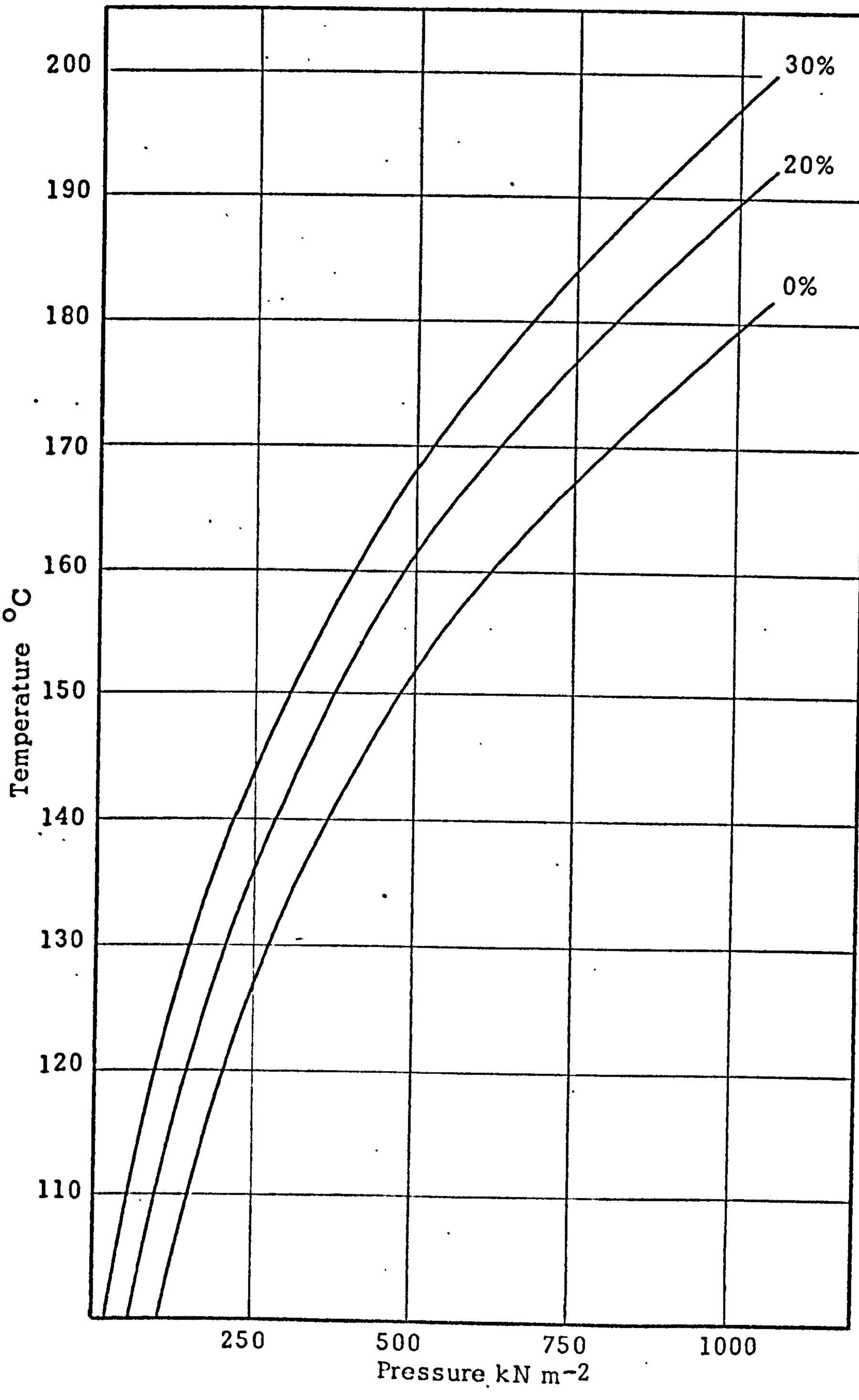

FIG. A6 BOILING POINT OF SODIUM CHLORIDE SOLUTIONS

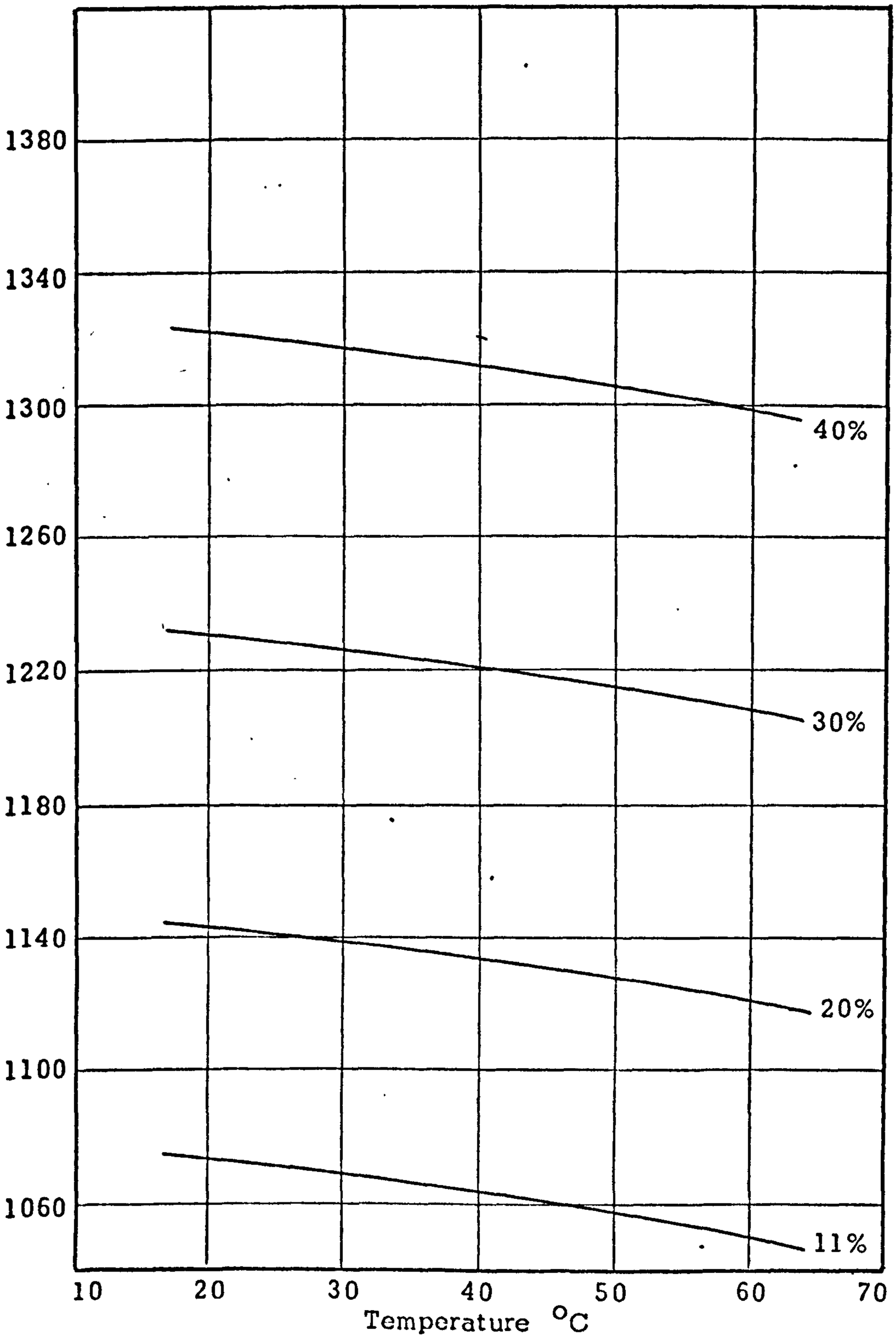

FIG. A7 DENSITY OF SODIUM NITRATE SOLUTIONS

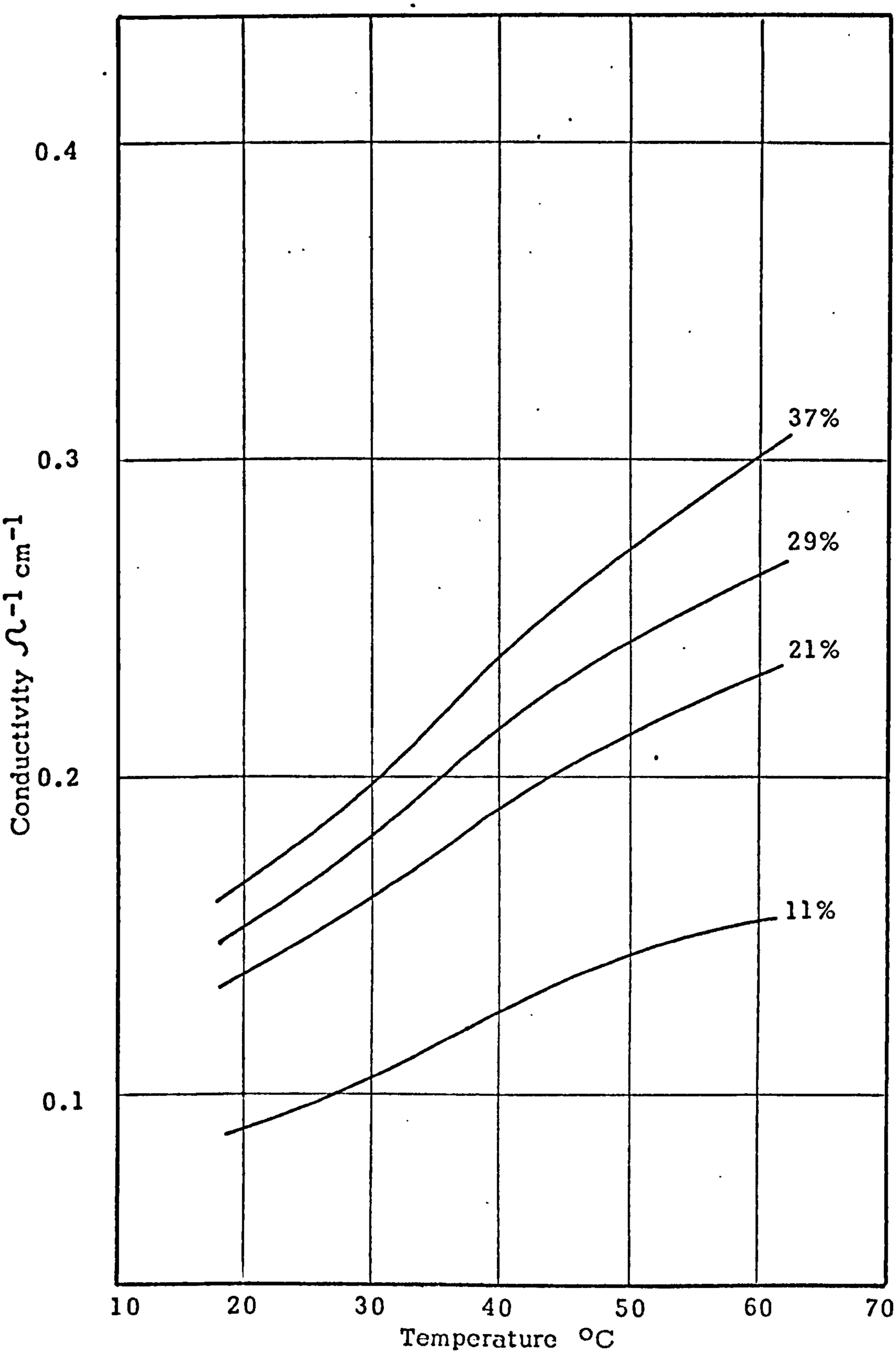

FIG. A8 CONDUCTIVITY OF SODIUM NITRATE SOLUTIONS

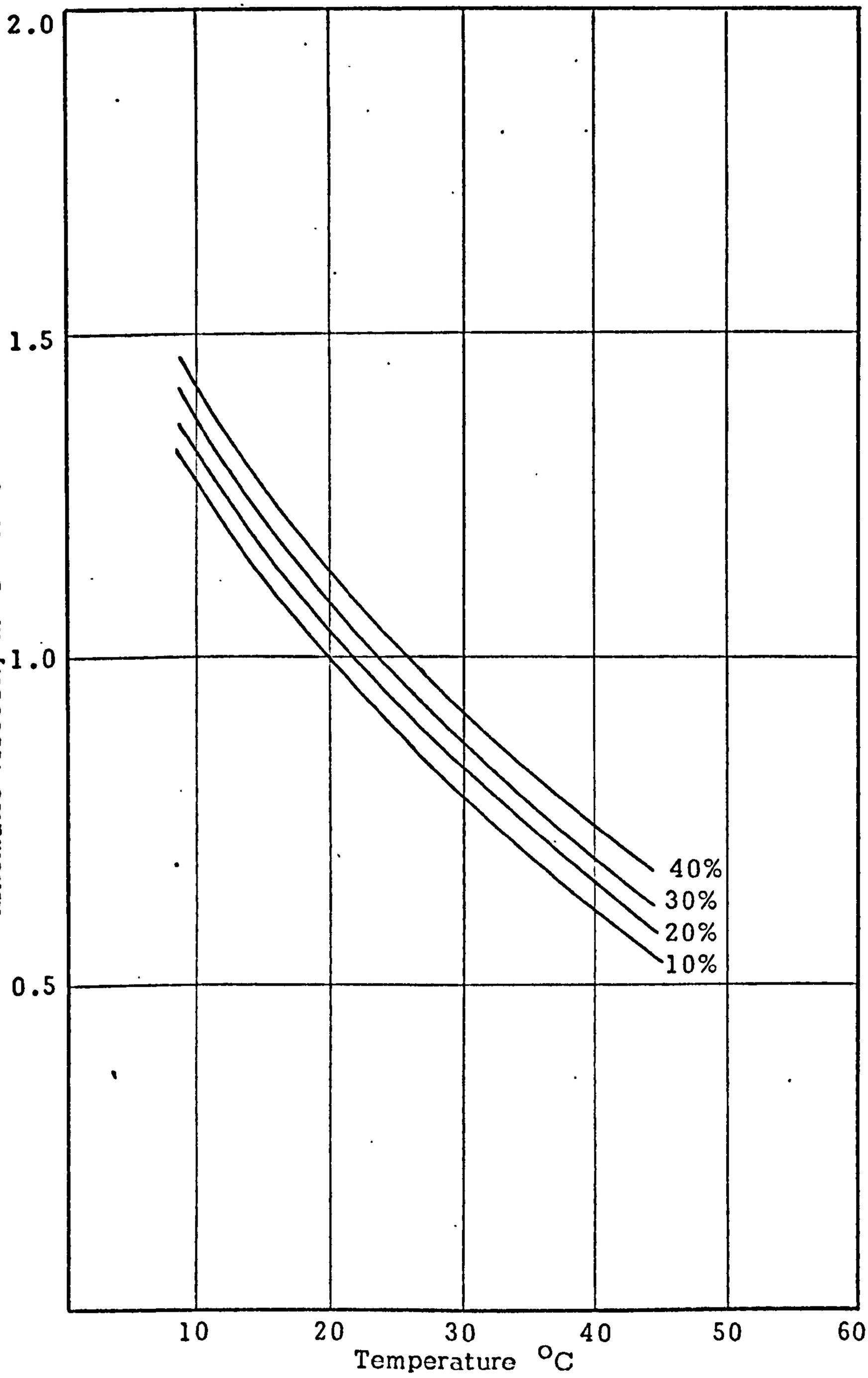

FIG. A9 KINEMATIC VISCOSITY OF SODIUM NITRATE SOLUTIONS

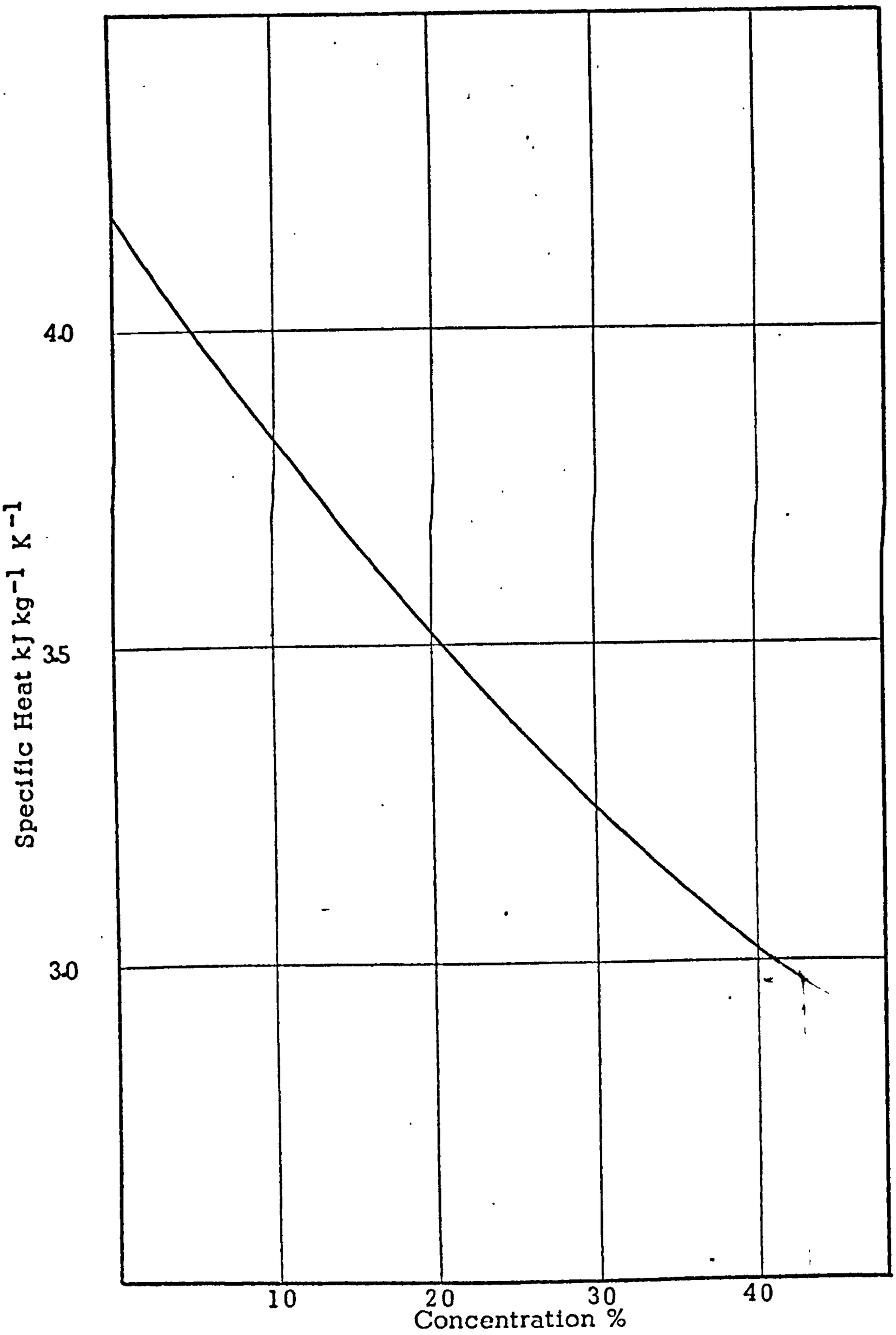

FIG. A10 SPECIFIC HEAT OF SODIUM NITRATE SOLUTIONS

FIG. A11 CALIBRATION FOR THERMISTOR AT OUTLET (3.5)

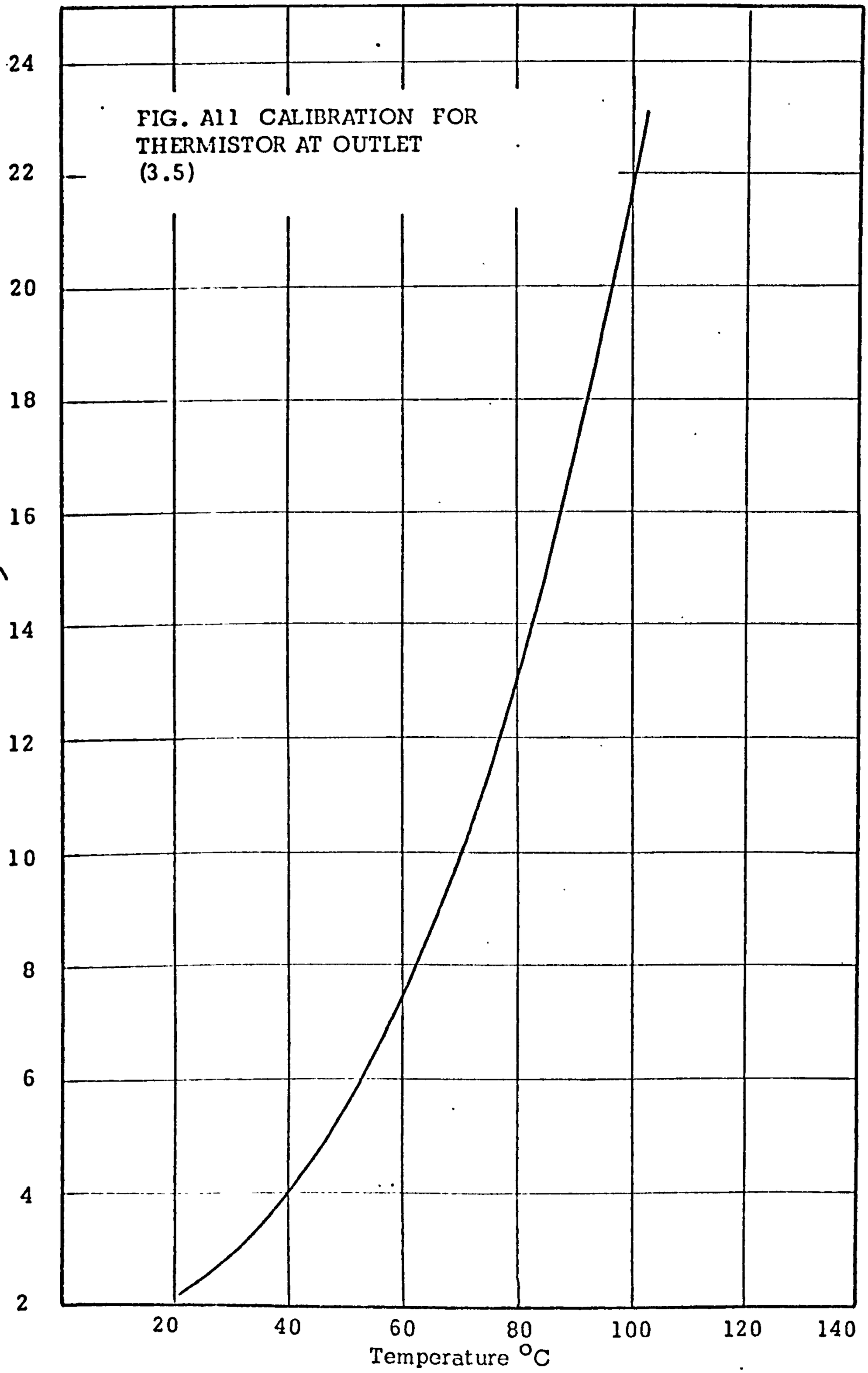

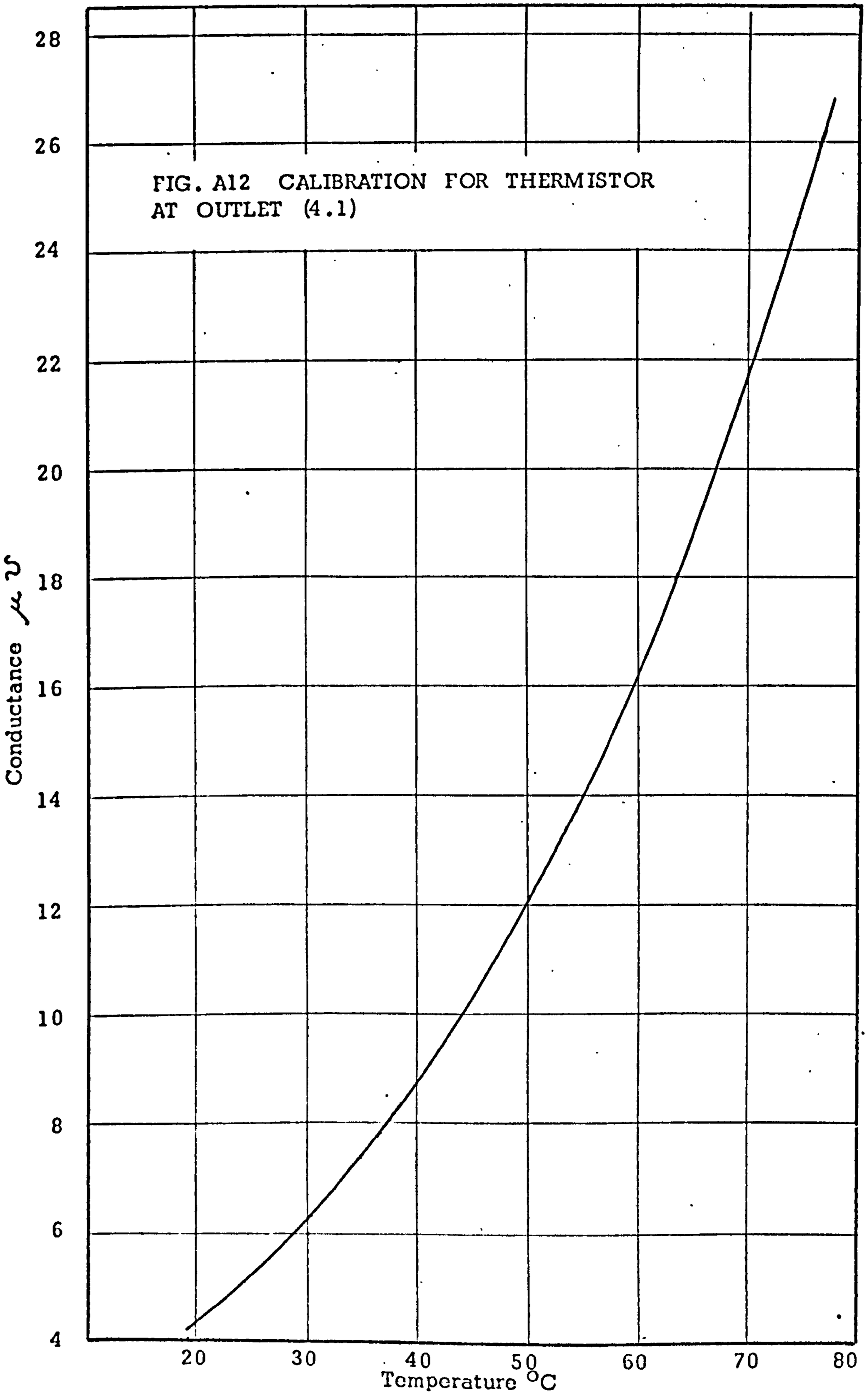

FIG. A12 CALIBRATION FOR THERMISTOR AT OUTLET (4.1)

FIG. A13 CALIBRATION FOR THERMISTOR IN CATHODE 6 mm FROM OUTLET